EVALUATION AND PARAMETRIC MODELING OF 50 KW ORGANIC RANKINE CYCLE FOR WASTE HEAT RECOVERY FROM RURAL ALASKA DIESEL GENERATOR POWER PLANTS

By

Vamshi Krishna Avadhanula

RECOMMENDED:

Dr. Sunwoo Kim

Dr. Harold E. Bargar

Dr. Debendra K. Das

Dr. Chuen-Sen Lin
Advisory Committee Chair

Dr. Rorik A. Peterson
Chair, Department of Mechanical Engineering

APPROVED:

Dr. Douglas J. Goering
Dean, College of Engineering and Mines

Dr. John C. Eichelberger
Dean of the Graduate School

11 August 2015
Date

EVALUATION AND PARAMETRIC MODELING OF 50 KW ORGANIC RANKINE CYCLE FOR WASTE HEAT RECOVERY FROM RURAL ALASKA DIESEL GENERATOR POWER PLANTS

A

DISSERTATION

Presented to the Faculty

of the University of Alaska Fairbanks

in Partial Fulfillment of the Requirements

for the Degree of

DOCTOR OF PHILOSOPHY

By

Vamshi Krishna Avadhanula, M.S.

Fairbanks, Alaska

August 2015

Abstract

In rural Alaska, there are about 180 villages that run independent electrical power systems using diesel generator sets. A diesel engine generator loses fuel energy in the form of waste heat through the charge air cooler (after cooler), the jacket water cooler, friction, and exhaust. Diesel engine jacket water and exhaust account for about 20% and 30% of the total fuel energy, respectively. In previous studies it has been demonstrated that about 80% of the heat present in jacket water and 50% of the heat from exhaust gases can be recovered for useful purposes such as heating, power generation, refrigeration, and desalination. In this study, the diesel engine waste heat application selected was power generation using an organic Rankine cycle (ORC) heat engine.

The basic principle of an ORC system is similar to that of the traditional steam Rankine cycle; the only difference is the working fluid. The working fluids generally used in an ORC are refrigerants, such as R11, R113, R123, R134a, R245fa, and HFE-7000. The working fluid in the ORC system under study is R245fa. A typical ORC consists of a pump, preheater, evaporator, expansion machine (expander), and condenser. The working fluid is pressurized through the pump and supplied to the preheater and evaporator, where it is heated by the heat source. The working fluid exits the evaporator as vapor or liquid/vapor. It expands in the expander, generating power. The low-pressure working fluid exiting the expansion machine is liquefied in the condenser by a cooling source, returned to the pump, and the cycle repeats.

At the University of Alaska Fairbanks (UAF) power plant, a lab experimental setup was designed: a hot water loop (heat source) and cold water loop (heat sink) for testing the 50 kW ORC power unit. Different diesel engine waste heat recovery conditions were simulated to study the unit's reliability and performance. After lab testing, the ORC system was installed permanently on a 2 MW Caterpillar diesel engine for jacket water heat recovery in Tok, Alaska, and tested further. These two tests provide for the goals of the present dissertation which are: (i) testing of a 50 kW ORC system for different heat source and heat sink supply conditions, (ii) develop guidelines on applying the present 50 kW ORC system for individual rural Alaska diesel gen-sets, (iii) develop empirical models for the screw expander, (iv) develop heat transfer correlations for single-phase and two-phase evaporation, and two-phase condensation for refrigerant R245fa in the preheater, evaporator and condenser, respectively, and (v) parametric modeling and validation of the present ORC system using the empirical correlations developed

for a screw expander and R245fa in heat exchangers to predict the performance of the ORC system for individual diesel generator sets.

The lab experimental data were used to plot performance maps for the power unit. These maps were plotted with respect to hot water supply temperature for different ORC parameters, such as heat input to power unit in evaporator and preheater, heat rejection by power unit in condenser, operating power output, payback period, and emissions. An example of how performance maps can be used is included in this dissertation.

As detailed in this dissertation, the resulting lab experimental data were used to develop guidelines for independent diesel power plant personnel installing this ORC power unit. The factors influencing selection of a waste heat recovery application (heating or power) are also discussed. A procedure to find a match between the ORC system and any rural diesel generator set is presented. Based on annual electrical load information published in Power Cost Equalization data for individual villages, a list of villages where this ORC system could potentially be beneficial is included.

During lab work at the UAF power plant, experimental data were also collected on the refrigerant side (R245fa) of the ORC system. Inlet and outlet pressures and temperatures of each component (evaporator, pump, and expander) of the ORC were measured. Two empirical models to predict screw expander power output were developed. The first model was based on polytropic work output, and the second was based on isentropic work output. Both models predicted screw expander power output within ±10% error limits.

Experimental data pertaining to the preheater, evaporator, and condenser were used to develop R245fa heat transfer correlations for single-phase and two-phase evaporation and two-phase condensation in respective heat exchangers. For this study the preheater, evaporator, and condenser were brazed plate heat exchangers (BPHEs). For single-phase heat transfer in the preheater, a Dittus-Boelter type of correlation was developed for R245fa and hot water. For R245fa evaporation in the evaporator, two heat transfer correlations were proposed based on two-phase equation formats given in the literature. For condensation of R245fa in the condenser, one heat transfer correlation was proposed based on a format given in the literature. All the proposed heat transfer correlations were observed to have good agreement with experimental data.

Finally, an ORC parametric model for predicting power unit performance (such as power output, heat input, and heat rejection) was developed using the screw expander model and proposed heat transfer correlations for R245fa in heat exchangers. The inputs for the parametric model are heating fluid supply conditions (flow rate and temperature) and cooling fluid supply conditions, generally the only information available in rural Alaska power plant locations. The developed ORC parametric model was validated using both lab experimental data and field installation data. Validation has shown that the ORC computation model is acceptable for predicting ORC performance for different individual diesel gen-sets.

Table of Contents

Page

Page

Page

Page

List of Figures

Page

Page

Page

List of Tables

Page

Page

Acknowledgments

I take it as a great pleasure to express my heartfelt gratitude to my principal advisor, Dr. Chuen-Sen Lin, for his constant support, invaluable guidance, encouragement, and kindness throughout this project. I would also like to thank my advisory committee members Dr. Debendra K. Das, Dr. Harold E. Bargar and Dr. Sunwoo Kim for their valuable suggestions in completing this thesis.

I gratefully acknowledge the financial support provided by Alaska Energy Authority, Denali Commission, and Alaska Department of Environmental Conservation. I would also like to thank Ms. Gwen Holdmann, Mr. Brent Sheets and Mr. Ross Coen from the Alaska Center for Energy and Power (ACEP) for providing managerial assistance to complete this project on time. I acknowledge ACEP for providing tools and equipment for installation, The UAF Power Plant for providing lab space for performing the experiment and UAF Facilities Services for providing personnel during installation of tough and heavy components.

I remain grateful to my late father, Mr. Narahari. It was his dream to see me as a Ph.D. scholar. I remain indebted to my family members Mrs. Sudha Rani (mother), Mrs. Laxmi Roshini (wife), Mr. Karteek Kumar (brother) and Mrs. Shruti on whose constant encouragement and love I have relied throughout my entire time at the academia. I would like to thank my best friend Mr. Ravikanth S. Vajjha and other friends at UAF for their support and comments about my work.

Chapter 1. Introduction

Internal combustion engines convert fuel energy into power using thermodynamic processes. During this conversion a considerable amount of fuel energy is lost. A diesel engine loses this fuel energy in the form of waste heat through the charge air cooler (after cooler), the jacket water cooler, friction and exhaust. Diesel engine jacket water and exhaust account for about 20% and 30% of the total fuel energy, respectively. The charge air cooler and friction account for another 12%. Rather than being lost to the atmosphere, the energy present in diesel engine jacket water and exhaust can be recovered for useful applications, such as heating (space heating, domestic water heating, or warming of municipal water supplies to prevent freezing), power generation, refrigeration, and desalination.

In rural Alaska there are about 180 villages that run independent electrical power systems using diesel generators. In 2007 their electrical consumption was 370,000 MWh [1]. Taking into account the 38% fuel efficiency of a diesel engine, nearly 486,800 MWh of heat energy at an elevated temperature was lost to the atmosphere from engine jacket liquid and exhaust.

In rural Alaska, jacket water heat recovery is a well-established technology and about half of rural villages are equipped with jacket water heat recovery systems for heating purposes. Among them many are equipped with combined jacket water and charge air heat recovery systems.

Due to concerns of cost, reliability, and possible maintenance problems, rarely has exhaust heat been recovered for useful application at any village diesel power system. However, the fuel price surge in recent years has led to a re-evaluation of exhaust heat recovery for improved village fuel-energy efficiency.

Applications for recovered heat from diesel engines may include desalination, refrigeration, space heating, and power generation. A brief description of these heat recovery applications and reasons for selecting or not selecting a particular one follows with a short literature survey. With geographical location and diesel consumption in mind, we can choose a reliable, economical heat recovery application for Alaska villages. The selection of the most desirable application, one with good potential for many years, is based on need, availability, feasibility, and benefit for rural Alaskans.

1.1 Desalination

Waste heat from diesel engines (both jacket water and exhaust gas) can be used for the purification of seawater (desalination) for household or industrial use. Water desalination using industrial waste heat (such as power plant waste heat or gas-turbine exhaust) and diesel engine waste heat is a well-established technology. The two major processes used in seawater desalination are Multi-Stage Flash desalination (MSF) and Multi-Effect Distillation desalination (MED). Examples of both methods are given in literature citation [2] and [3].

Diesel engine waste heat could be used to purify underground water for drinking purposes in much the same way that seawater is desalinated. But according to the Alaska Department of Environmental Conservation in March 2005, the mineral content of groundwater for most Alaska villages is well within acceptable limits [4]. Using diesel engine waste heat for water purification purposes is not justifiable.

1.2 Refrigeration

Heat present in exhaust can be used for refrigeration purposes, for ice-making for the local fishing industry or for air conditioning in vehicles. The cycles used for this purpose may be vapor absorption refrigeration systems (e.g., ammonia-water, water-lithium bromide based systems) or solid adsorption refrigeration systems (e.g., zeolite-water systems). Some examples of research conducted on the use of a low-grade heat source for cooling are presented in literature citations [5], [6], and [7].

The application of exhaust heat for refrigeration is a viable industry. Much research has been done in this area, and ice-making has been demonstrated in Kotzebue, Alaska. But unless a large commercial user of ice exists, such as a local fishing industry in the summer, the costs are not justifiable. A small portion of village power plant waste heat is enough to produce the ice needed, and in Alaska it is needed locally (e.g., in coastal villages) only from May to mid-September. These are the reasons for not selecting refrigeration as the best power plant waste heat application.

1.3 Diesel Engine Waste Heat for Heating

Heating is crucial for six to eight months of the year for all village residents in Alaska. Recovered heat can be used for space heating, domestic water heating, or for warming municipal water supplies to prevent freezing. Of all applications, net heat energy recovered is highest for heating. In general, about 50% or more of the heat present in exhaust may be recoverable for

heating. These factors led to heating as the diesel engine exhaust heat recovery application of choice in previous work, where the same research team at the UAF Energy Center successfully demonstrated the experimental and economic analysis of exhaust heat recovery for heating [1, 8, 9].

1.4 Diesel Engine Waste Heat to Power Conversion

Basically, diesel engine waste can be converted to power by two methods:

(i) Thermoelectric generators (TEG)

(ii) Thermodynamic cycles (ORC, ammonia-water vapor absorption power cycle)

1.4.1 Thermoelectric Generators

A TEG works on the principle of the Seebeck effect. The simplest TEG consists of a thermocouple, comprising a p-type and n-type thermo-element connected electrically in series and thermally in parallel. Heat is pumped into one side of the couple junction and rejected from the opposite side. An electrical current is produced, proportional to the temperature gradient between the hot and cold junctions. Some examples of research conducted on using an IC engine waste heat source for TEGs is presented in literature citations [10] and [11].

In industry, exhaust heat recovery using TEGs is still in the research stage. (Please refer to DEER conference proceedings in 2009, 2010, and 2011 for the section "*Thermoelectrics for Vehicle Applications*" [12].) The main drawback of a TEG is its temperature dependence. TEGs have better performance in a specified temperature range, and their efficiency falls off rapidly if temperature is below or above that range. Exhaust temperature varies as engine load varies. It is expected that with use of a TEG, a 3%–5% improvement in fuel consumption could be achieved, but this has not yet been proven [12]. Cost of an efficient TEG, one that works well over a varying temperature range, is prohibitively high. Maintenance of TEG units is also very high, making them unsuitable for remote Alaska village generators with large load fluctuations between day and night, summer and winter usages.

1.4.2 Thermodynamic Cycles

Diesel engine waste heat for power conversion using thermodynamic cycles such as organic Rankine cycle (ORC) or ammonia-water vapor absorption power cycle (e.g., Kalina Cycle) is a promising possibility for increasing the efficiency of Alaska village power plants. Industry scale waste heat recovery ORC has been implemented and 8% to 18% recovery of waste heat has been achieved (Table 1.2). This is a considerable amount. The thermodynamic efficiency of the

ammonia-water absorption cycle for waste heat recovery was reported to be 11% to 26% (Table 1.4). Tables 1.1 to 1.4 list the literature review (both analytical and physical system) for the organic Rankine cycle and ammonia-water vapor absorption power cycle. The reason for selecting the ORC is explained below.

In Tables 1.1 to 1.4, the analytical system literature review is based on thermodynamic, energy balance, and heat transfer equations. No physical system is present. The physical system literature review is the one based on published installed-or-working-prototype system data.

Table 1.1 Analytical system literature review for ORC power systems

Literature Citation	Heat source	Heat source Temperature	Heat Sink Temperature	Working fluid	Power output	Efficiency
[13]	Engine exhaust and jacket water from turbocharged, Mercedes-Benz OM422A, 243 kW, direct injection, water-cooled 6-cylinder, Vee engine	Jacket water at 88°C and Exhaust gas at 470°C	Ambient temperature at 30°C for R-12 and Water cooled condenser for "Water" as working fluid	R-12 and water	38.5kW (R-12); 37.2kW (water)	16% (R-12) and 15.3% (water) boost in engine efficiency
[14]	Biomass, industrial waste and solar thermal	90°C to 110°C (at inlet to expander)	25°C	R134a, Water, R227ea, R245fa, Toluene, Iso-Butane, Acetone, Iso-Pentane, n-pentane, Dimethylether	9.9W (Toluene) to 282W (Dimethyl-ether)	2.04% (Water) to 2.86% (Iso-butane)
[15]	275kW turbo-charged heavy duty diesel engine	95°C (Jacket water); 184°C (Charge air cooler); 688°C (EGR)	20°C	A dry fluid with critical pressure <65bar (No specific fluid)	55kW	18% thermal efficiency
[16]	Engine waste heat	260°C	9°C (air cooled)	Isobutane and Isopentane	1650kW to 1750kW	7% to 9% thermal efficiency
[17]	Geothermal sources	90°C	30°C (Water)	Ammonia, R123, n-pentane, PF5050	10MW	5.7% to 7.4% thermal efficiency
[18]	2 X 8.9MW diesel engine exhaust	346°C exhaust gases	25°C Water	Hexamethyldisiloxane	1603kW	17.3%

Table 1.2 Physical system literature review for ORC power systems

Literature Citation	Heat source	Heat source Temperature	Heat Sink Temperature	Working fluid	Power output	Efficiency
[19]	20 kW electric heaters (2 X 10 kW)	45°C to 70°C (HCFC-123) and 115°C to 125°C (water) (measurement at inlet to turbine)	Not available	HCFC-123 and water	20W to 150W (HCFC-123) and 60W to 150W (water)	0.2% to 1.25% (HCFC-123) and 0.36% to 0.75% (water) (heat conversion efficiency)
[20]	Hot air source	172.6°C to 182.3°C	13.2°C to 15°C	HCFC-123	0.67kW to 1.03kW	4% to 6.1% cycle efficiency
[21]	Hot water heater	100°C	26.67°F (Water)	HFE-7000	937W	3.1% thermal efficiency
[22]	Hot water from a geothermal well	73.33°C	4.44°C	R-134a	210 kW	8.2% heat conversion efficiency
[23]	Exhaust from a 27MW gas turbine driving a natural gas pipeline compressor	480°C	–18°C to 35°C (Air cooled condenser)	Pentane	5.5MW	15% heat conversion efficiency
[24]	Hot water from a geothermal well	106°C	10°C	Fluorocarbons	500kW	8.13% heat conversion efficiency
[25]	Solar energy	300°C	Not available	n-pentane	1.0MW	12.1% design point efficiency
[26]	Exhaust gas from cryogenic gas turbine	260°C (Hot oil temperature)	21.11°C (Air cooled)	n-pentane	3.05MW	13% thermal efficiency
[27]	Biomass CHP plant	250°C to 300°C (thermal oil temperature)	60°C	Not available	1.1MW	18% thermal efficiency
[28]	Biomass CHP plant	300°C (thermal oil temperature)	60°C (Water)	Silicon oil	1.0MW	18% thermal efficiency
[29]	7MW -8MW stationary diesel engine	240°C to 310°C (thermal oil temperature)	25°C	Not available	0.6MW	16% to 20% thermal efficiency

Table 1.3 Analytical system literature review for ammonia-water vapor absorption power systems

Literature Citation	Heat source	Heat source Temperature	Heat Sink Temperature	Power output	Efficiency
[30]	Low temperature heat source	90°C	30°C	Not available	2.3% to 10%
[31]	Hybrid system for power and refrigeration	Dry Saturated steam at 0.69MPa (164.37°C)	32°C	115kW	58% Coefficient of performance
[18]	2 X 8.9MW diesel engine exhaust	346°C exhaust gases	25°C Water	1615kW	17.5%

Table 1.4 Physical system literature review for ammonia-water vapor absorption power systems

Literature Citation	Heat source	Heat source Temperature	Heat Sink Temperature	Power output	Efficiency
[32]	Solar Centaur 50 natural gas turbine	475°C to 520°C	11°C Water	1.6MW to 2.7MW	22.5% to 26.5%
[33]	Hot water from geothermal well	125°C	4°C	2MW	11.8%
[34]	Hot water from geothermal well	120°C	Not available	3.4MW	11% thermal efficiency (Calculated)
[35]	Hot water from geothermal well	100°C	Not available	50kW	Not available

From the above literature review for ORC and ammonia-water absorption power cycles (Tables 1.1 to Table 1.4), it can be observed that no physical system proven for reliability and performance existed (at the beginning of this project) for low-grade heat (less than 1 MW of heat input, i.e., less than 100 kW power systems at 10% thermal efficiency). If systems exist for low-grade heat, they are only lab experimental setups [19, 20, 21] not proven for long-term reliability and not readily available for installation to recover heat from stationary diesel engines. This led the research team to search for a semi-commercially available waste heat recovery unit that could be used to recover heat from rural Alaska village diesel gen-sets. A semi-commercial unit is a ready-to-deliver working or prototype unit lacking field test data on performance, verification, and system improvement. Results of our search are given in the literature [36]. ElectraTherm® was the only company manufacturing a 50 kW ORC unit, and they readily agreed to deliver a

power unit to us. But there were no published reliability and performance results for this 50 kW ORC system in the open literature that could be used to evaluate the performance (i.e., power output, efficiency, fuel savings, emissions reductions) of the power system for rural Alaska conditions.

1.5 Present Research

In the work presented in this study, ElectraTherm's® 50 kW ORC power unit was tested in a lab environment at the University of Alaska Fairbanks (UAF) power plant for reliability and performance. After lab testing, the same ORC power unit was put on a 2 MW Caterpillar diesel engine for jacket water heat recovery in Tok, Alaska, as part of field installation and tested further. Experimental data collected from these ORC system setups were used to meet the goals of the project described in this dissertation:

1. to determine 50 kW ORC system performance and reliability for different heat source and heat sink supply conditions,
2. to develop 50 kW ORC system application guidelines for individual rural Alaska diesel gen-sets,
3. to develop empirical models for the screw expander,
4. to develop heat transfer correlations for single-phase and two-phase evaporation, and two-phase condensation for refrigerant R245fa in the preheater, evaporator, and condenser, respectively, and
5. to parametrically model and to validate this ORC system using the empirical correlations developed for the screw expander and R245fa in heat exchangers to predict ORC system performance for individual diesel generator sets.

1.6 Organic Rankine Cycle

The basic principle of the ORC system is similar to that of the traditional steam Rankine cycle; the only difference is the working fluid. The working fluids generally used in an ORC are refrigerants, such as R11, R113, R123, R134a, R245fa, and HFE-7000. As shown in Figure 1.1, a typical ORC consists of a pump, preheater, evaporator, expansion machine (expander), and condenser. The working fluid is pressurized through the pump and supplied to the preheater and evaporator, where it is heated by the heat source (heating fluid loop in Figure 1.1). The working fluid exiting the evaporator is in a vapor or liquid/vapor condition. It is expanded in the expander while power is generated. The low-pressure working fluid exiting the expansion machine is

liquefied in the condenser by a cooling source (cooling fluid loop in Figure 1.1) and returned to the pump. In a diesel engine waste heat application of the ORC, the heat source may be engine jacket water, exhaust gases, or a combination of the two. The cooling source could be a lake, a river, an underground well, air-cooled radiator, or a cooling tower. It depends on the ORC installation's location and the economic viability of the cooling source.

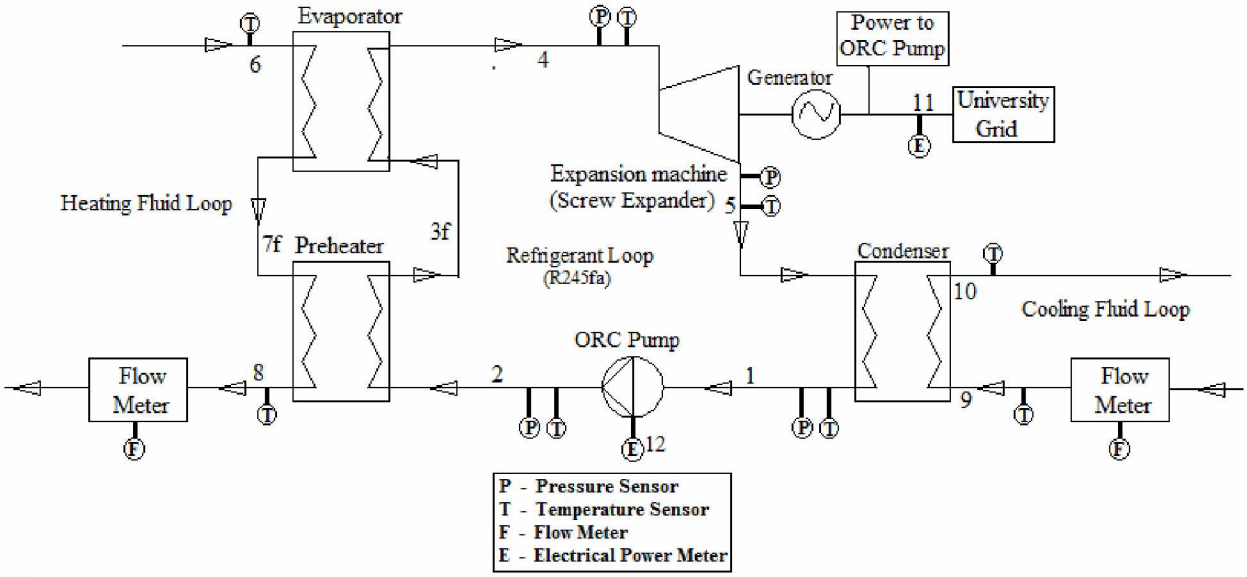

Note:
1. Heating fluid was hot water in experimental setup at UAF and 60/40 propylene glycol/water mixture in field installation.
2. Cooling fluid was cold water in both the installations.

Figure 1.1 Schematic of organic Rankine cycle system under consideration

In this ORC process the preheater, evaporator, and condenser are heat exchangers. Brazed plate heat exchangers (BPHEs) are used in this ORC system. Refrigerant R245fa is the working fluid. The working fluid pump is a vane-type feed pump with variable frequency drive (VFD) capability. The expansion device converts the high enthalpy working fluid exiting the evaporator to mechanical energy. For low-grade heat applications it should be able to admit two-phase mixtures. Some of the expansion devices used in low-grade heat applications are screw expanders and scroll expanders. A screw expander is the expansion device in the 50 kW ORC machine under discussion.

1.7 Summary of Chapters

This thesis has been written in manuscript format. Chapter 1 is a general introduction with a brief literature review. Chapters 2 and 3 have been published in journals. Chapters 4 and 5 will be submitted to journals for review soon. Chapter 6 presents general conclusions reached at the

end of this project. Appendix A is additional publication based on the outcome of present research.

Chapter 2 discusses the experimental setup for testing the 50 kW ORC power unit, the reliability and performance tests conducted on the unit, and test results. The experimental setup includes the heat source loop, heat sink loop, electrical system, and instrumentation. Experimental results from the reliability and performance tests are discussed using parameters such as screw expander power output, efficiencies of screw expander and power unit, effect of parasitic pump power consumption, diesel fuel saved, emissions reductions and payback period estimations.

When the available heat is less than 1 MW, the heat-to-power conversion using thermodynamic cycles is still in the research stage due to non-availability of an expansion device. For low-value heat, in some cases the working fluid is still in the two-phase region (on the higher-quality side) at the evaporator exit (state-4 in Figure 1.1). Due to erosion problems, traditional turbines cannot admit two-phase "wet" mixtures at the inlet and the turbine exit quality of the two-phase mixture should be as high as possible. In this regard, researchers are studying other types of expansion devices, the most important of these being scroll expanders [20, 21, 37, 38], and screw expanders [39, 40, 41, 42, 43]. In the 50 kW ORC system discussed here, a screw expander was the expansion device, with R245fa as the working fluid.

Chapter 3 gives two empirical models for performance estimation of screw expanders. These empirical models were developed based on lab experimental data. The first is based on a polytropic expansion process, and the second one is based on isentropic work.

Chapter 4 presents the developed heat transfer correlations for R245fa in the preheater, evaporator, and condenser (Figure 1.1). In the preheater, it is single-phase heat transfer from hot fluid to R245fa. In the evaporator it is two-phase evaporation heat transfer from hot fluid to R245fa, and in the condenser it is two-phase condensation heat transfer from R245fa to cold fluid. These heat transfer correlations for R245fa were developed based on lab experimental data.

Chapter 5 presents a calculation procedure developed to model the present 50 kW ORC system to estimate performance parameters such as heat input, power output, heat rejection, and working fluid pump power consumption. The model was developed using the empirical relations

for the screw expander in Chapter 3 and heat transfer correlations for R245fa in Chapter 4. The developed model was verified using both lab experimental data and field installation data.

Appendix A gives guidelines for installing this ORC system on individual village diesel engines. This chapter also presents a brief comparison of the effect of applying waste heat for heating and waste heat to power.

1.8 References

[1] Lin, C.S., "Capture of heat energy from diesel engine exhaust," Final report prepared for National Energy Technology Laboratory, DOE Award # DE-FC26-01NT41248, November 2008.

[2] Williams, J.S. and Hodgson, A.S., "Multistage flash desalination utilizing diesel generator waste heat," Journal of Industrial and Engineering Chemical Process Design and Development, Vol.10(4), pp.460-466, 1971.

[3] Kronenberg, G. and Lokiec, F., "Low-temperature distillation processes in single- and dual-purpose plants," Journal of Desalination, Vol.136, pp.189-197, 2001.

[4] Alaska Department of Environmental Conservation, "Ground Water in Alaska," March 2005.

[5] Lu, Y.Z., Wang, R.Z., Jianzhou, S., Xu, Y.X., and Wu, J.Y., "Practical experiments on an adsorption air conditioner powered by exhausted heat from a diesel locomotive," Journal of Applied Thermal Engineering, Vol.24, pp.1051-1059, 2004.

[6] Wang, L.W., Wang, R.Z., Wu, J.Y., Wang, K., and Wang, S.G., "Adsorption ice makers for fishing boats driven by the exhaust heat from diesel engine: choice of adsorption pair," Journal of Energy Conservation and Management, Vol.45, pp.2043-2057, 2004.

[7] Talom, H.L. and Beyene, A., "Heat recovery from automotive engine," Journal of Applied Thermal Engineering, Vol.29, pp.439-444, 2009.

[8] Raghupatruni, P., "Performance analysis of capture of heat energy from diesel engine exhaust," Master's Thesis, University of Alaska Fairbanks, 2007.

[9] Raghupatruni, P., Lin, C.S., Witmer, D., Bargar, E., Schmid, J., Johnson, T., and Avadhanula, V.K., "An experimental feasibility study of using diesel exhaust for space heating in Alaskan villages," Proceedings of the Tenth International Conference on Advanced Computational Methods and Experiments in Heat Transfer, Maribor, Slovenia, WIT Press, Vol.61, pp.93-104, July 2008.

[10] Fairbanks, J.W., "Thermoelectric applications in vehicles status 2008," Proceedings of the 6th European Conference on Thermoelectrics, Paris, France, July 2008.

[11] Wojciechowski, K., Merkisz, J., Fuć, P., Lijewski, P., and Schmidt, M., "Study of recovery of waste heat from the exhaust of automotive engine," Proceedings of the 5th European Conference on Thermoelectrics, Odessa, Ukraine, September 2007.

[12] Directions in Engine-Efficiency and Emissions Research (DEER) Conference Presentations, http://www1.eere.energy.gov/vehiclesandfuels/resources/proceedings/index.html. Accessed July 16th 2012.

[13] Aly, S.E., "Diesel engine waste-heat power cycle," Journal of Applied Energy, Vol.29(3), pp.179-189, 1988.

[14] Paolo, C., "Exergoeconomic analysis and optimization of organic Rankine cycles," Master's Thesis, University of Ontario Institute of Technology, 2012.

[15] Teng, H., Regner, G., and Cowland, C., "Waste heat recovery of heavy-duty diesel engines by organic Rankine cycle Part I: Hybrid energy system of diesel and Rankine engines," SAE technical paper # 2007-01-0537, World congress, Detroit, Michigan, April 16-19, 2007.

[16] Grabinski, P., "Optimization of the performance of an organic Rankine cycle used as waste heat recovery system in a bio-liquid diesel engine power plant," Master's Thesis, University of Iceland, February 2011.

[17] Madhawa, H.H.D., Golubovic, M., Worek, W.M., and Ikegami, Y., "Optimum design criteria for an organic Rankine cycle using low-temperature geothermal heat source," Journal of Energy, Vol.32, pp.1698-1706, 2007.

[18] Bombarda, P., Invernizzi, C.M., and Pietra, C., "Heat recovery from diesel engines: A thermodynamic comparison between Kalina and ORC cycles," Journal of Applied Thermal Engineering, Vol.30, pp.212-219, 2010.

[19] Yamamoto, T., Furuhata, T., Arai, N., and Mori, K., "Design and testing of the organic Rankine cycle," Journal of Energy, Vol.26, pp.239-251, 2001.

[20] Quoilin, S., "Experimental study and modeling of a low temperature Rankine cycle for small scale cogeneration," Master's Thesis, University of Liege, May 2007.

[21] Reid, A.D., "Low temperature power generation using HFE-7000 in a Rankine cycle," Master's Thesis, San Diego State University, July 2010.

[22] Holdmann, G., "The Chena Hot Springs 400 kW Geothermal Power Plant: Experience Gained During the First Year of Operation," Transactions of the Geothermal Resource Council, Vol.31, pp.509-514, Davis, CA, September 2007.

[23] Leslie, N.P., Zimron, O., Sweetser, R.S., and Stovall, T.K., "Recovered energy generation using an Organic Rankine Cycle system," ASHRAE Transactions # CH-09-024, Vol.115, Part 1, ASHRAE Winter Conference, Chicago, 2009.

[24] Pernecker, G. and Uhlig, S., "Low-enthalpy power generation with ORC-Turbogenerator: The Altheim project, Upper Austria," GHC Bulletin, March 2002.

[25] Canada, S., Cohen, G., Cable, R., Brosseau, D., and Price, H., "Parabolic trough Organic Rankine Cycle solar power plant," Presented at the 2004 DOE Solar Energy Technologies Program Review Meeting, Denver, Colorado, October 25-28, 2004.

[26] Nasir, P., Jones, S., Schochet, D., and Posner, D., "Utilization of turbine waste heat to generate electric power at Neptune plant," Proceedings of 83rd Gas Processors Association Annual Convention, New Orleans, LA, March 2004.

[27] Bini, R., Schwarz, D.A., Gaia, M., Bertuzzi, P., and Righini, W., "Operational results of the first biomass CHP plant in Italy based on an Organic Rankine Cycle turbogenerator and overview of a number of plants in operation in Europe since 1998," Proceedings of the 2nd World Conference on Biomass for Energy, Industry and Climate Protection, Rome, Italy, pp.1716-1721, May10-14, 2004.

[28] Obernberger, I., Thonhofer, P., and Reisenhofer, E., "Description and evaluation of the new 1,000kWe Organic Rankine Cycle process integrated in the biomass CHP plant in Lienz, Austria," Euroheat & Power, Vol.10, pp.18-25, 2002.

[29] Turboden ORC plants for Industrial Heat Recovery. Turboden press release URL: http://www.turboden.eu/it/public/downloads/11-COM.P-18-rev.4_HR_ENG.pdf. Accessed July 17th 2012.

[30] Madhawa, H.H.D., Golubovic, M., Worek, W.M., and Ikegami, Y., "The performance of the Kalina cycle system 11 (KCS-11) with low-temperature heat sources," Journal of Energy Resources Technology, Vol.129, pp.243-247, 2007.

[31] Amano, Y., Suzuki, T., Hashizume, T., Akiba, M., Tanzawa, Y., and Usui, A., "A hybrid power generation and refrigeration cycle with ammonia-water mixture," Proceedings of

ASME International Joint Power Generation Conference, Miami Beach, Florida, July 23-26, 2000.

[32] Leibowitz, H. and Mirolli, M., "First Kalina combined-cycle plant tested successfully," Power Engineering, Vol. 101(5), pp.45-48, 1997.

[33] Valdimarsson, P., "The Kalina power plant in Husavik – Why Kalina and what has been learned," Workshop on Electricity Generation from Enhanced Geothermal Systems, Strasbourg, France, September 14-16, 2006.

[34] Knapek, E. and Kittl, G., "Unterhaching power plant and overall system," Proceedings of the European Geothermal Congress, Unterhaching, Germany, May 30 - June 1, 2007.

[35] Yanagisawa, N., Muraoka, H., Sasaki, M., Sugita, H., Ioka, S., Sato, M., and Osato, K., "Starting field test of Kalina system using hot springs fluid in Japan," Proceedings of 37th Workshop on Geothermal Reservoir Engineering, Stanford University, Stanford, California, January 30 - February 1, 2012.

[36] Alaska Energy Authority, "Task one final report: Test evaluation of organic Rankine cycle engines operating on recovered heat from diesel engine exhaust," http://www.akenergyauthority.org/Content/Programs/AEEE/PDF%20files/8-27-09_AEA-RSA0925TaskOneFinalReport.pdf, August 2009. Accessed July 17th 2012.

[37] Johnston, J.R., "Evaluation of expanders for use in a solar-powered Rankine cycle heat engine," Master's Thesis, The Ohio State University, 2001.

[38] Aoun, B. and Clodic, D.F., "Theoretical and experimental study of an oil-free scroll vapor expander," International Compressor Engineering Conference, Purdue, July 14-17, 2008.

[39] Smith, I.K., Stosic, N., and Kovacevic, A., "Screw expanders increase output and decrease the cost of geothermal binary power plant systems," Transactions of Geothermal Resource Council, 2005.

[40] Smith, I.K., Stosic, N., and Aldis, C., "Trilateral flash cycle system – A high efficiency power plant for liquid resources," Proceedings of World Geothermal Congress, 1995.

[41] Kaneko, T. and Hirayama, N., "Study of fundamental performance of helical screw expanders," The Japan Society of Mechanical Engineers, Vol.28 (243), pp.1970-1976, 1985.

[42] Ng, K.C., Lim, T.B., and Bong, T.Y., "Analysis of screw-expander performance," Proceedings of the Institution of Mechanical Engineers, Part E, Journal of Process Mechanical Engineering, Vol.203(E1), pp.15-20, 1989.

[43] Ng, K.C., Bong, T.Y., and Lim, T.B., "A thermodynamic model for the analysis of screw expander performance," Journal of Heat Recovery Systems & CHP, Vol.10(2), pp.119-133, 1990.

Chapter 2. Testing a 50kW ORC at Different Heating and Cooling Source Conditions to Map Performance Characteristics*

2.1 Abstract

In 2007 the electrical power consumption of 180 rural Alaska villages was 370,000 MWh generated using isolated diesel gen-sets. From a stationary diesel engine, a considerable amount of heat energy at an elevated temperature is released into the atmosphere from engine jacket liquid and exhaust gases. In rural Alaska, due to infrastructure, economic impact, and village need, heat recovery applications for purposes other than power generation may not be appropriate. Other appropriate types of heat recovery applications in Alaska include desalination, refrigeration, and local heating. Also, due to the varying sizes and electrical loads of most of these diesel gen-sets (from 100 kW to 1 MW), small heat recovery power systems (80kW or less) are preferred over industrial-scale systems. In a typical village diesel genset application, hot liquid from the engine jacket and/or from the exhaust-to-liquid heat exchanger would most likely be the waste heat source. In this study a performance test was conducted under different heating and cooling conditions on a 50kW ORC power unit. The experimental setup for testing the ORC power unit consisted of a heat source loop, heat sink loop, electrical system, and instrumentation (for data collection). The ORC power unit was tested for hot water supply (heat source) temperatures varying from 68.3°C (155°F) to 107.2°C (225°F) and flow rate varying from 27.2m^3/hr (120gpm) to 68.1m^3/hr (300gpm) and for cold water supply (heat sink) temperatures of 10°C (50°F) and 20°C (68°F) and flow rate varying from 27.2m^3/hr (120gpm) to 45.4m^3/hr (200gpm). The performance test results will be used to make performance maps for the ORC system. These maps are in the form of system-characteristic plots for efficiency, operating power output, and parasitic pump power consumption with respect to different heating and cooling conditions. The data can be used in predicting long-term electrical power generation, efficiency, fuel savings, and economic benefit (i.e., payback period) for given heating and electrical load patterns. In addition, emissions and CO_2 or greenhouse gas (GHG) reductions can also be estimated based on ORC electrical energy generation and fuel savings. If the ORC power unit is to be installed to recover waste heat from village diesel engines, note that power unit performance will vary from village to village due to electrical load pattern, heat energy pattern,

---

* Avadhanula, V.K., Lin, C.S., and Johnson, T., "Testing a 50kW ORC at Different Heating and Cooling Source Conditions to Map the Performance Characteristics", SAE Technical Paper # 2013-01-1649, April 2013.

environmental conditions (e.g., for cooling source), and infrastructure availability. The performance maps also provide power-plant personnel with information that may be used in heat distribution for different heating and cooling conditions to optimize the benefit obtainable from diesel power plant waste heat. Different waste heat distribution applications may include heating, power, and refrigeration. With use of village power plant data, an example is given in this paper for how to predict electrical power generation, efficiency, and economic benefit using the developed performance maps.

2.2 Introduction and Literature Review

From a stationary diesel engine generator, the main source of electricity in circumpolar regions, about 60% of fuel energy is lost in the form of waste heat through the charge air cooler (after cooler), the jacket liquid cooler, friction, and exhaust. This waste heat has a low heat flux value (amount of heat rate) and a low-grade (i.e., low temperature) form of heat energy. Of the total fuel energy, diesel engine jacket liquid and exhaust account for about 20% and 30%, respectively. If this low-grade heat is recovered for useful application rather than being lost to the atmosphere, considerable annual savings in diesel fuel and an increase in power plant efficiency as a whole could be achieved. Waste heat recovery applications may include heating (space heating, domestic water heating, or warming of municipal water supplies to prevent freezing), power generation, refrigeration, and desalination.

In rural Alaska there are about 180 villages that run independent electrical power systems using diesel generators. In 2007 their electrical consumption was 370,000 MWh [1]. Taking into account the 38% fuel efficiency of diesel engines, nearly 486,800 MWh of heat energy at an elevated temperature was lost to the atmosphere from engine jacket liquid and exhaust. Here it should be noted that the electrical capacity of diesel gen-sets varies from about 100kW to 1MW. Jacket liquid heat recovery for heating is a well-established technology in rural Alaska, and about half of rural villages in Alaska are equipped with jacket water heat recovery systems. Many are equipped with combined jacket water and charge air heat recovery systems for heating purposes. But rarely has exhaust heat been recovered for useful application at a village diesel power system, due to concerns about cost, reliability, and possible maintenance problems.

As stated earlier, applications of recovered heat from diesel engines may include desalination, refrigeration, space heating, and power generation. According to the Alaska Department of Environmental Conservation in March 2005, the mineral content of groundwater

for most Alaska villages is well within acceptable limits [2]. Therefore, using diesel engine waste heat for desalination in rural Alaska is not justifiable. Applying diesel gen-set waste heat for refrigeration is not economical in Alaska. Ice may be needed locally, such as in coastal villages with a fishing industry, but only seasonally (from May to mid-September) and only if a large commercial user of ice exists. Otherwise, the application is not justifiable.

Heating is crucial for six to eight months of the year for all village residents in Alaska. Recovered heat can be used for space heating, domestic water heating, or for warming municipal water supplies to prevent freezing. Of all applications, net heat energy recovered is highest for heating. Generally, about 50% or more of heat present in exhaust may be recoverable for heating. These factors led to heating as the diesel engine exhaust heat recovery application of choice in previous work [1, 3, and 4]. But due to high cost of arctic piping, high installation cost, long distance between diesel power house and nearby buildings; the application of heat recovery for heating is not a viable option for every village.

A diesel engine waste heat to power conversion system may include thermodynamic systems or direct heat to electricity conversion systems. Examples of thermodynamic systems are organic Rankine cycle (ORC) systems or ammonia-water vapor absorption power systems (e.g., Kalina cycle). An example of direct heat-to-electricity is the thermoelectric generator (TEG). In industry, exhaust heat recovery using thermoelectric generators (TEGs) is still in the research stage [5]. The main drawback of a TEG is its temperature dependence. TEGs have better performance in a specified temperature range, and their efficiency falls off rapidly if temperature is below or above that range. Cost of an efficient TEG, one that works well over a varying temperature range, is prohibitively high. Maintenance of TEG units is also very high, making them unsuitable for remote Alaska village generators with large load fluctuations between day and night, summer and winter usages.

Diesel engine waste heat for power conversions using thermodynamic cycles is a promising possibility for increasing the efficiency of Alaska village power plants. At industry level ORC has been implemented, and 8% to 18% recovery of heat has been achieved [6, 7, 8, 9, and 10] depending on heat source temperature, heat source type, and heat flux rate. This is a considerable amount. The thermodynamic efficiency of the ammonia-water absorption cycle at industry level was reported to be 11% to 26% [11, 12, and 13]. Industry-level power systems have power output greater than 100 kW, and at 10% thermal efficiency (heat-to-power conversion efficiency)

of the heat recovery system they would require 1MW of heat input or more. Therefore, for this study the stationary diesel engine gen-set waste heat recovery application selected was power generation using thermodynamic systems.

As seen from the authors' literature review for ORC and ammonia-water absorption power cycles, no physical systems proven for reliability and performance existed for low-grade (low temperature) and low heat flux value (less than 800kW of heat input, i.e., less than 80kW diesel waste heat for power systems at 10% thermal efficiency) when this project began. If such systems exist, they are only experimental [14, 15, and 16] and not proven for long-term reliability test and readily available for installation (e.g., to recover heat from stationary diesel engines). Due to isolation of most of the villages in rural Alaska, no highly trained operation and maintenance personnel are available and shipping fees (by air year round or by barge in summer) and travel costs are extremely expensive. Reliability and ease of operation, and minimal fabrication, installation, and maintenance requirements become critical factors in selecting heat recovery application units. A retrofit unit with fewer requirements in fabrication of supporting systems is preferable. This led the research team to look for a semi-commercial waste heat recovery unit that could be used with diesel gen-sets in rural Alaska villages. A semi-commercial unit is a working or prototype unit lacking field testing data for performance, verification, and system improvement. Table 2.1 details our search results. Of all companies with waste heat to power conversion units available, ElectraTherm® was the only one manufacturing a 50kW ORC unit, which they readily agreed to deliver. But there were no published reliability and performance results for the 50kW ORC system in the open literature that could be used to evaluate the system's performance (i.e., power output, efficiency, fuel savings, emissions reductions) for rural Alaska conditions.

The main goal of this paper is to give performance test results in the form of maps and a method to predict the long-term outcome of installing this 50kW power unit on a village diesel engine for waste heat recovery. With village power plant data, an example is given in this paper for how to predict electrical power generation, efficiency, and economic benefit using the developed performance maps. This paper also gives a brief description of the experimental setup used for testing a 50kW ORC power unit for reliability and performance. Reliability testing was conducted at full load gross power output of the power unit (i.e., 50kW screw expander power output) for 600 hrs to evaluate the long-term performance of the machine and the whole system.

A performance test on the power unit was conducted mainly to learn how the power unit and its individual components (expander, evaporator, preheater, condenser, and pump) perform, particularly at different hot water and cold water flow rates and temperatures. The power unit was tested at 5 different hot water flow rates, 5 different hot water temperatures, 3 different cold water flow rates and 2 different cold water temperatures. Rates and temperatures are given in Table 2.2. Approximately 150 performance tests were conducted on the ORC power unit. Results were used to make performance maps in the form of contour plots for efficiency, operating power output, and parasitic pump power consumption with respect to different heating and cooling conditions. This data can be used in predicting long-term electrical power generation, efficiency, fuel savings, and economic benefit (i.e., payback period) for given village heating and electrical load patterns.

2.3 Experimental Setup

With the help of line diagrams, this section briefly describes the experimental setup. Components used to control heat source and heat sink flow rates and temperatures to the power unit, a method of uploading electrical power to grid, and instrumentation for data collection are also given. Here it should be noted that the experimental setup was located in the University of Alaska Fairbanks (UAF) power plant, a coal-fired CHP plant. As abundant low-pressure saturated steam (205.7kPa) was readily available, it was used as the heat source for the ORC power unit.

The basic principle of the ORC system is similar to that of the steam Rankine cycle system except that the working fluid is organic (such as R134a, R245fa, R123, ammonia) instead of steam. The basic components of the ORC are pump, evaporator, expander, and condenser. The liquid refrigerant from the condenser is pumped at high pressure to the evaporator. In the evaporator, the refrigerant is heated to the required superheated or saturated condition. This high pressure working fluid is converted to low-pressure liquid or vapor/liquid mixture (to the condenser pressure) using an expander that is connected to the generator to produce power. The low-pressure refrigerant from the expander is cooled to the desired state in the condenser. The liquid portion is again pumped to the evaporator, and the cycle continues. In a diesel generator waste heat application, the heating fluid used to heat the ORC working fluid in the evaporator may be from engine jacket liquid or 50/50 glycol/water mixture exiting the exhaust heat exchanger or both combined, and it is called heat source loop. In the condenser the ORC working

fluid rejects heat to the cooling fluid (usually water). The cooling fluid may be from the cooling tower, radiator, a large water body (a nearby river or lake), or underground well; and is called the heat sink loop.

In our ORC system, the working fluid was R245fa, a non-flammable fluid with ozone depletion potential of zero and no listed phase-out year. R245fa was used due to the match of refrigerant properties, range of operation temperature, and temperature range of available heat sources.

Figure 2.1 shows the experimental setup for testing the 50kW ORC power unit. The experimental setup consists of four major components: (i) heat source loop, (ii) heat sink loop, (iii) electrical system (shown in Figure 2.1), and (iv) instrumentation (not shown in figures). In this experiment, the heat source loop was further divided into a steam supply loop and a hot water loop. Hot water, which exchanges heat with steam in the steam-to-hot water heat exchanger, was supplied to the evaporator of the power unit as heating fluid (explained in Section 2.3.1). Cold water from a fire hydrant was used in the heat sink loop. The electrical system is the wiring required to upload power to the grid and to wire various power-consuming components. Instrumentation includes various data collection components, such as flow meters, thermocouples, and electrical meters.

2.3.1 Heat Source Loop

In testing the 50kW power unit, the heat source was low-pressure steam instead of waste heat from a diesel generator set. The reason for using steam as the heat source was that it was easy to design the heat source loop and control heat source temperatures to mimic the temperatures and flow rates of engine jacket water when testing the power unit. For the performance test, we needed to test the power unit at different heat source conditions (i.e., hot water flow rates and temperatures). This would not be possible using field engine waste heat, since a village field diesel generator set constantly needs to meet the village electrical load demand which may not cover the wide ranges of flow rate and temperature spectrum desired for the present testing (Table 2.2).

Figure 2.1 shows the heat source loop, which is further divided into a steam supply loop and a hot water loop. The major components used to build the heat source loop included (on the steam supply loop) a steam-to-hot water heat exchanger, a steam-flow control valve with

actuator and steam trap, and (on the hot water loop) 4" SCH40 black iron piping with Gruvlok fittings, a hot water VFD pump, expansion tank, air separator, and pressure relief valve.

In this experimental setup, power plant low-pressure steam supplies heat to the hot water in a steam-to-hot-water heat exchanger. This high enthalpy hot water exiting the heat exchanger is supplied as heating fluid to the evaporator of the ORC power unit. The low enthalpy hot water exiting the evaporator is returned to the heat exchanger to gain heat. Thus the hot water is looping between the steam-to-hot-water heat exchanger and the power unit evaporator. The outlet of the steam condensate is connected to the power plant condensate piping through a steam trap.

The hot water loop was designed to accommodate the performance test, where the ORC power unit was tested for different hot water flow rates and temperatures. As shown in Figure 2.1, on the hot water loop piping, a variable frequency drive (VFD) pump was used to control the frequency input to the pump motor, thereby controlling the pump speed and hot water flow rate in the loop.

For temperature control of the hot water, a steam flow control valve with electronic actuator was used, as shown in Figure 2.1, to obtain the desired temperature of hot water exiting the heat exchanger, which is supplied as heating fluid to the power unit's evaporator. By varying the steam flow rate through the heat exchanger, the desired hot water temperature was obtained. An electronic actuator was used to remotely control the steam valve opening through a National Instruments LabVIEW program. The LabView VI software program takes the desired hot water temperature as input and, based on the actual hot water temperature, a control signal is initiated by LabView, which controls the valve opening position. A normally closed (NC) valve was used for safety reasons.

2.3.2 Heat Sink Loop

Because the experimental setup was at the UAF power plant, the cooling source was water from a fire hydrant just outside the building.

Figure 2.1 shows the heat sink loop, an open cold water loop. The major components of the loop are manual flow control valve, check valve, pump, and two 3-way butterfly valves with a bypass line for temperature control. The temperature of water from the fire hydrant is always around $10^{o}C$ ($50^{o}F$). The working principle of the loop is that cold water from the fire hydrant flows through the power unit's condenser extracting excess heat from the refrigerant, thereby

cooling the refrigerant to condenser pressure. The warm water from the condenser is diverted to a heat sink. The bypass line is used to test the power unit for cold water temperatures other than 10°C during the performance testing. The 3-way butterfly valves were operated such that a portion of warm water from the condenser was recirculated through the bypass, mixed with the cold water from the fire hydrant, and supplied to the power unit. The warm water flow through the bypass line was achieved by operating the butterfly valves and turning on the pump. The 3-way butterfly valve positions were adjusted until the desired cold water temperature into the power unit was reached. The manual flow control valve mounted directly on the fire hydrant outlet was used to control the cold water flow rate to the power unit.

The water pressure from the fire hydrant was enough to move water along the loop. The pump, 3-way butterfly valves, and bypass were used only when the power unit was tested for cold water temperatures other than 10°C (i.e., only during the performance test), otherwise, they were shut off.

2.3.3 Electrical System

As the ORC power unit was in the UAF power plant, what power it generated was tied into the UAF motor control center (also located in the plant), where it was uploaded to the UAF power distribution system. Figure 2.2 shows a line diagram of electrical wiring from the power unit generator to the motor center and wiring for both hot and cold water pumps. Here the electrical wiring is done in such a way that when the ORC unit is generating power, it uploads power to the motor center as well as to the hot and cold water pumps. When the unit is not generating power, the hot and cold water pumps can still be operated from power drawn from the motor center. As shown in Figure 2.2, from the power unit circuit breaker (CB) box, a 3/0AWG (American wire gauge) metal clad (MC) 3-conductor with ground cable was connected to the UAF motor center CB box to upload power to the university power system. From the same power unit CB box, a #4AWG cable was used to connect a VFD CB box of the hot water pump and safety switch of the cold water pump, as shown in Figure 2.2. For powering the motor of the hot water pump from the VFD and the motor of the cold water pump from the safety switch, #8AWG and #10 AWG cables were used, respectively.

The 50 kW ORC power unit's generator power output had a line voltage of 480V, and full load current of 75A, 3-phase, and 60Hz.

The hot water pump, which is rated for VFD operation, had a 20hp (14.9kW) rated motor size with input of 460V/24A. The cold water pump had a 15hp (11.2kW) rated motor size with input of 460V/18A.

2.3.4 Parameters Measured, Instrumentation, and Data Collection

The main goal of this paper is to give the 50kW ORC power unit's performance test results, which include heat input, heat rejected, system operating power output (i.e., the power uploaded to grid), efficiencies, emissions, fuel savings, and payback period. Parameters measured are the direct measurements taken from installed measuring equipment (i.e., instrumentation that will be used in the data reduction process for further analysis of the system.

2.3.4.1 Parameters Measured

The parameters measured during testing of the 50kW ORC power unit were: (i) hot water flow rate, inlet and outlet temperatures to the power unit (V_{HW}, $T_{HW,in,P}$, $T_{HW,out,P}$), (ii) cold water flow rate, inlet and outlet temperatures to the power unit (V_{CW}, $T_{CW,in,P}$, $T_{CW,out,P}$), (iii) electrical power output of the power unit (P_{Net}), (iv) electrical power consumed by the power unit pump ($P_{Pump,P}$), (v) hot water pump power ($P_{Pump,HW}$), and (vi) cold water pump power ($P_{Pump,CW}$). Note that electrical power output of the power unit (P_{Net}) already makes allowance for the power unit pump electrical power consumption (Figure 2.2). Cold water pump power consumption was estimated based on hot water pump power (for the same flow rate) due to use of the fire hydrant as the cold water source.

2.3.4.2 Instrumentation and Data Collection

For flow rate, as shown in Figure 2.1, Kamstrap Ultraflow® ultrasonic flow meters were used to measure the hot water and cold water flow rates supplied to the power unit. A Kamstrap Multical-601® calculator, which has flow rate display, was used to manually note the flow rates. Omega® type-K thermocouples were used to measure the inlet and outlet temperatures of hot water and cold water. Temperature measurements were stored in Excel format using the LabView VI program (see next paragraph). As shown in Figure 2.2, for electrical power measurement, EKM-353EDM electrical meters were used to measure electrical power generated by the power unit, and power consumption of the power unit pump and hot water pump. The electrical meter manufacturer had custom software that was used for reading real-time electrical power measurement. This real-time data were stored in text format at every 30s interval, for future data reduction.

Data acquisition and control (DAQ) functions were performed using a LabView virtual instrument program (VI) operating on a National Instruments (NI) PCI-MIO-16E module. LabView VI software was used to read the real-time data and to store these data at one second intervals in Excel format for future data reduction. For temperature measurement, an NI SCXI-1120 analog input board was used. Steam valve position was controlled by a simple LabView VI software program and SCIX-1121 analog I/O board. The LabView VI software program takes the desired hot water temperature as input and, based on the actual hot water temperature, a control signal is initiated by LabView, which controls the valve opening position.

2.4 Experimental Procedure

For evaluating the power unit and its components at different hot water and cold water flow rates and temperatures, the performance test procedure is detailed in the following steps:

1. First, the cold water flow rate is set at the desired value by turning the manual flow rate valve near the fire hydrant. The temperature of the cold water from the fire hydrant is around 50^{o}F.
2. At this cold water flow rate, we then use the LabVIEW software to operate the steam flow control valve to set the desired temperature for the hot water supply to the ORC power unit.
3. By varying the hot water pump VFD frequency (e.g., VFD frequency of 24Hz corresponds to $27.2m^3$/hr (120gpm) and 55Hz to $68.1m^3$/hr (300gpm) of hot water flow), we set the desired hot water flow rate. The hot water flow rate can be read in the flow meter display in cubic-meter/hour.
4. After setting all four parameters (hot water and cold water flow rates and temperatures) at desired conditions, we wait approximately 30 minutes for steady-state conditions for data collection.
5. Steady-state data collection is done for 30 minutes at one set of hot water and cold water temperatures and flow rates. This completes the performance test for that one set.
6. Now we change the hot water flow rate to the next value (e.g., 120gpm to 160gpm) by varying the VFD frequency while keeping the other three parameters the same. Then Step-4 and Step-5 are repeated. In this manner we continue performing the tests at other hot water flow rates.
7. Now we change the hot water supply temperature using Step-2, and we repeat Step-3, Step-4, and Step-5 for different hot water flow rates.

8. Step-2, Step-3, Step-4 and Step-5 are repeated iteratively for the three cold water flow rates listed in Table 2.5.

During steady-state data collection (Step-5 above) for 30 minutes, the hot water and cold water temperatures are stored by LabVIEW in Excel format at a frequency of 1sec. The hot water and cold water flow rates are manually noted from the respective flow meter calculator displays. The values for electrical power generated by the power unit and the parasitic power consumption by the pumps are stored in text format at a frequency of 30sec. For each case of hot water and cold water flow rate and temperature, all steady-state measured parameters are averaged for the data reduction process.

2.5 Data Reduction

This section gives the mathematical expressions used in obtaining the derived parameters from measured parameters, which will be useful in further analysis of the power unit. This section also discusses the procedure and methodology adopted to estimate the reductions in emissions and CO_2 and the economic impact of installing an ORC power unit on a village diesel power plant.

Heat supplied ($Q_{HW,Su}$) by hot water to the evaporator of the power unit is obtained by,

$$Q_{HW,Su} = V_{HW} \times \rho_{HW} \times (h_{HW,in,P} - h_{HW,out,P}) \quad (2.1)$$

Here density of hot water (ρ_{HW}), inlet enthalpy ($h_{HW,in,P}$) and outlet enthalpy ($h_{HW,out,P}$) of hot water to the power unit were obtained based on evaporator hot water inlet and outlet temperatures and using the NIST REFPROP 8.0 [17] program. ρ_{HW} is the average density of hot water obtained at inlet and outlet evaporator hot water temperatures.

Heat rejected ($Q_{CW,Rej}$) to cold water by the condenser of the power unit is obtained by,

$$Q_{CW,Rej} = V_{CW} \times \rho_{CW} \times (h_{CW,out,P} - h_{CW,in,P}) \quad (2.2)$$

Here density of cold water (ρ_{CW}), inlet enthalpy ($h_{CW,in,P}$) and outlet enthalpy ($h_{CW,out,P}$) of cold water to the power unit were obtained based on condenser cold water inlet and outlet temperatures and using the NIST REFPROP 8.0 [17] program. ρ_{CW} is the average density of cold water obtained at inlet and outlet condenser cold water temperatures.

System operating power output (P_{OP}) is the power generated by the power unit that was uploaded to the university power system, given by Eq. (2.3), which considers the power unit pump and cold water pump powers. Here in calculating system operating power output (P_{OP}), the ORC power unit pump and cold water pump power consumptions were only considered because,

in general, a stationary diesel engine is equipped with a jacket water pump to dissipate heat to atmosphere using air coolers and as stated in "Introduction" section that most of the rural Alaska diesel gen-sets are equipped with jacket water heat recovery system which may have a pump already installed. Taking this into account, the electrical power consumed by the hot water pump is neglected assuming the already installed jacket water pump can be used to overcome the ORC power unit evaporator pressure drop. P_{OP} will be used in annual diesel fuel saved, emissions reductions and economic outcome calculations discussed in following paragraphs. Here both P_{Net} and $P_{Pump,P}$ are measured parameters explained in the "Parameters measured" section above. Eq. (2.4) gives the expression for system operating efficiency (η_{OP}) which is the ratio of P_{OP} and $Q_{HW,Su}$.

$$P_{OP} = P_{Net} - P_{Pump,CW} \tag{2.3}$$

$$\eta_{OP} = \frac{P_{OP}}{Q_{HW,Su}} \tag{2.4}$$

Liters (or gallons) of diesel fuel saved per year ($F_{S/Y}$) was calculated using Eq. (2.5), which was based on system operating power output (P_{OP}), 355 power unit working days per year with 10 days of maintenance, and stationary diesel engine-specific fuel consumption. A stationary diesel engine-specific fuel consumption of 3.7kWh/lit (14kWh/gal) [18, 19] is a reasonable value for rural Alaska village diesel gen-sets. The dollar amount saved on diesel fuel per year ($F_{\$/Y}$) was calculated based on diesel fuel saved per year ($F_{S/Y}$) and diesel fuel cost of $5.0/gal, which is a reasonable value for rural Alaska stationary diesel generator power plants.

$$F_{S/Y} = \frac{P_{OP} \times 355 \times 24}{3.7} \tag{2.5}$$

2.5.1 Economic Analysis

The economic impact of installing an ORC power unit on a rural Alaska village power plant was evaluated based on payback period calculations. The payback period is determined when enough money has accumulated at given simple interest rate to offset the total initial investment cost ($T_{ini.Cap}$) and annual maintenance cost based on annual cost savings. Here annual cost savings is the dollar amount saved on diesel fuel per year ($F_{\$/Y}$) by operating the ORC power unit on recovered waste heat from a rural Alaska diesel engine power plant. Note that dollar amount saved on diesel fuel per year ($F_{\$/Y}$) was calculated based on 355 power unit working days per year with 10 days of maintenance.

The total initial investment cost ($T_{ini.Cap}$) can be divided into component costs ($C_\$$) and installation costs ($I_\$$). Component costs ($C_\$$) are the material and instrumentation cost incurred building the whole heat recovery system and data acquisition system. For the present case, the component costs ($C_\$$) include cost of purchasing the ORC power unit, steam-to-hot water heat exchanger, steam valve, hot and cold water pumps, air separator, expansion tank, pressure relief valve, pipes for hot water and cold water, flow meters, thermocouples, Gruvlok fittings, supporting structural material (e.g., struts, pipe hangers), electrical cables, other miscellaneous parts (e.g., nuts, bolts, tees, pipe couplings), shipping charges. Table 2.3 lists these categorized component costs. The estimated total component cost is $191,000.

Installation costs ($I_\$$) may include such things as the number of days and personnel required for installation, cost of labor per hour per person, and travel cost (if any). Based on our experience with the experimental system it would require 5 people and 30 days to complete installation of the hot water loop, cold water loop, electrical system, and instrumentation to the ORC power unit (assuming all components are available for installation). At a labor cost of $70/person/hour and $5,000 for travel, the total cost of installing ($I_\$$) the whole system comes to $89,000. This value was used in the payback-period calculations. Therefore, the total initial investment cost ($T_{ini.Cap}$) was estimated at $280,000.

According to the power unit manufacturer and from our reliability test experience, the maintenance requirements for this ORC machine are similar to those for air-conditioning and refrigeration systems, and minimal in terms of economic concern. The anticipated maintenance requirement is mostly visual inspection and simple measurements, small changes (e.g., belts, lubricant, filters, batteries), and simple cleaning jobs. Lin [1] and Raghupatruni [3] determined that two days of maintenance per year was required for the exhaust heat recovery system. The effect of 10 maintenance days (considered in this paper for payback period estimation) on economics is estimated to supersede the effect of maintenance requirements in estimated real machine turnoff days plus labor and parts needed.

2.5.2 Reductions in Emissions and CO_2

As the ORC power unit was designed to operate on waste heat from a village diesel gen-set (i.e., free heating source); it would offset some of the power needs directly from the village diesel generator and in turn lead to emission reduction. Annual emission reductions were estimated based on the annual system operating power output by the power unit (355 power unit

working days per year with 10 days of maintenance) and stationary diesel engine emissions given in Table 2.4. Annual CO_2 reductions were based on liters (or gallons) of diesel fuel saved per year ($F_{S/Y}$). Table 2.4 gives the TIER-4 interim emission standards set by the EPA for non-road diesel engine gen-sets [20, 21].

2.6 Results

The purpose of this paper is to present the performance test results conducted on a 50kW ORC power unit. They will be used to estimate the economic effect of application of this unit on individual gen-sets. The 600-hour reliability test results are briefly discussed below. Then the performance test results are discussed in detail.

2.6.1 Reliability Test Results

The reliability test was done on the ORC power unit at full load (i.e., 50kW expander power output) for 600hrs to know the long-term endurance and performance of the unit. The average hot water supply temperature was 104.2°C and flow rate of 36.28m^3/h. Similarly, the average cold water temperature and flow rate were 9.7°C and 37.15m^3/h, conditions based on manufacturer specification for full load operation. The following observations were made from reliability test results:

1. During the reliability test, no major problems, such as drift in power output during long-term operation or power unit shutdown, were observed with the ORC power unit.
2. The average electrical power output (P_{Net}) by the power unit was 47.8kW (expander power less ORC pump power) with system operating efficiency (η_{OP}) of 7.5%.
3. The ORC power unit's achieved screw expander efficiency (ratio of expander output to heat input) of 8.4% at full-load operation was well within the manufacturer's claim of 8.5%.
4. Payback period of 2years and 2.3years was obtained with 0% and 10% interest rate on capital, respectively.

2.6.2 Performance Test Results

As listed in Table 2.2, the performance test on the 50kW ORC power unit was conducted varying four different input parameters namely hot water flow rate, hot water temperature, cold water flow rate and cold water temperature. Figures 2.3 to 2.5 give the performance test results for cold water supply temperature of 10°C and varying the three other parameters. Figures 2.3 to 2.5 were plotted based on the measured average values for hot water and cold water supply temperature and flow rate; also for the power unit electrical power output (P_{Net}), electrical power

consumption by power unit pump ($P_{Pump,P}$) and cold water pump ($P_{Pump,CW}$). The average values are the average obtained from 30min sampled data after the system reached steady-state condition, as discussed in Section 2.4 above. Temperatures were sampled at a frequency of 1sec; electrical power data were sampled at a frequency of 30sec; and flow rate data were noted manually from the flow meter display screen. Figure 2.3 gives the heat input to the evaporator of the power unit for 5 hot water flow rates, 5 hot water supply temperatures, 3 cold water flow rates, and cold water supply temperature of 10°C. Figure 2.4 and Figure 2.5 are the plots for heat rejected by the working fluid to cold water in the condenser and system operating power output, respectively, for 5 hot water flow rates, 5 hot water supply temperatures, 3 cold water flow rates, and cold water supply temperature of 10°C. Similar types of curves (similar to Figures 2.3 to 2.5) are obtained for cold water supply temperature of 20°C. They are not explicitly given here, but they are used in plotting performance curves. Figures 2.6 to 2.11 are the performance curves for the ORC power unit deduced from data obtained from the performance test for four different input parameters, as listed in Table 2.2 and discussed below.

2.6.2.1 Discussions

For a given hot water supply temperature and cold water flow rate, heat supplied by hot water ($Q_{HW,Su}$) to the power unit evaporator increased with the increase of hot water flow rate, as shown in Figure 2.3. For example, at a hot water supply temperature of 79.4°C (175°F) and cold water flow rate of 36.34m^3/hr (160gpm), heat supplied by hot water increased from 327.4kW at 27.17m^3/hr of hot water flow rate to 380.7kW at 68.43m^3/hr of hot water flow rate.

In some cases of hot water supply temperature and cold water flow rate, the irregular nature in increase of $Q_{HW,Su}$ is due to occasional disturbance in hot water supply temperature resulting from a surge in power plant steam supply condition. For example, at hot water supply temperature of 90.5°C (195°F) and cold water flow rate of 36.34m^3/hr (Figure 2.3), the actual hot water supply temperature was 91.03°C at 36.34m^3/hr to 90.38°C at 45.4m^3/hr. It could be observed from Figure 2.4 and Figure 2.5, that if there is any disturbance in hot water supply temperature, the same trends (of heat supplied in Figure 2.3) are followed for heat rejection to cold water and operating power output.

As the hot water flow rate increased for a given hot water supply temperature, the heat input to the power unit reached asymptotic condition (Figure 2.3) (i.e., for a given hot water supply temperature the heat absorption by working fluid in the evaporator reached a limiting value for

higher hot water flow rates). The same trends were observed for system operating power output as it reached asymptotic condition for higher hot water flow rates (Figure 2.5). The reason for this asymptotic condition is that the ORC power unit evaporator reached its design capacity. Another limitation from the ORC unit PLC software prevents the screw expander from generating more than the rated load of 50kW. The PLC software limitation, which limits the R-245fa flow entering the screw expander, is one of the many safety features protecting the screw expander from over-speeding.

From Figure 2.3 to Figure 2.5, one could observed that for a given hot water flow rate and hot water supply temperature, the effect of cold water flow rate on heat input to the power unit evaporator, heat rejected to cold water in the condenser, and system operating power output is minimal. For example, at a hot water flow rate of 45.4m^3/h (200gpm) and hot water supply temperature of 90.5°C (195°F),for cold water flow rates of 27.2m^3/h (120gpm), 36.34m^3/h (160gpm) and 45.4m^3/h (200gpm); the heat supplied by hot water was 467.75kW, 471.67kW, and 492.42kW, respectively. Heat rejected to cold water was 418.4kW, 422.37kW, and 446.29kW, respectively. System operating power output (P_{OP}) was 32.43kW, 32.93kW, and 33.23kW. Therefore, in plotting the performance curves in Figure 2.6 to Figure 2.11, for a given hot water flow rate and hot water supply temperature, it was determined to average the heat input, heat rejected, and P_{OP} over 3 cold water flow rates. That is, in the above example, at hot water flow rate of 45.4m^3/h (200gpm) and hot water supply temperature of 90.5°C (195°F) heat supplied by hot water was 477.28kW, heat rejected to cold water was 429.0kW, and system operating power output (P_{OP}) was 32.86kW.

Figures 2.6 to 2.11 plot the heat supplied by hot water, heat rejected to cold water, system operating power output, efficiency, payback period, and reductions in CO_2 emissions for different hot water supply temperatures, hot water flow rates, and cold water supply temperatures of 10°C and 20°C. On each of these plot (Figure 2.6 to Figure 2.11), the top plot is for 10°C cold water temperatures and the bottom plot is for 20°C cold water temperatures. All six plot are presented on the same hot water supply temperature scale with the same color coding for ease of reading (e.g. at hot water supply temperature of 101.6°C (215°F) and hot water flow rate of 45.4m^3/h, from Figure 2.6 the hot water heat input to the evaporator is 606.6kW and 588.8kW for 10°C and 20°C cold water temperature respectively; from Figure 2.7 heat rejection to cold water is 552.61kW and 468.9kW for 10°C and 20°C cold water temperature respectively; from

Figure 2.8 the system operating power output is 44.18kW and 41.8kW for 10°C and 20°C cold water temperature respectively; from Figure 2.9 the system operating efficiency is 7.3% and 7.1% for 10°C and 20°C cold water temperature respectively; from Figure 2.10 the payback period of 2.4years and 2.6years for 10% interest rate on capital could be achieved for 10°C and 20°C cold water temperature respectively; and from Figure 2.11 CO_2 reductions of 300short-tons/year and 282.3short-tons/year for 10°C and 20°C cold water temperature respectively could be achieved. Payback periods and CO_2 reductions were calculated based on equations and procedure discussed in above section "Data Reduction".

In Figures 2.6 to 2.11, for cold water temperature of 20°C, the results were presented only up to the maximum hot water supply temperature of 101.6°C (215°F). This is because low saturated steam pressure in the power plant prevented the hot water supply temperature reaching the expected maximum of 107.2°C (225°F) during the test.

2.6.3 Example Based on Above Performance Curves

From the Power Cost Equalization (PCE) program data [18] published by the Alaska Energy Authority for fiscal year 2011, and based on available diesel engine data at the location; Tok, Alaska, was selected as the field site for evaluating diesel engine waste heat recovery for power generation using the ORC system. According to PCE data, Tok annual electrical load is 10,902,597kWh, and all of this power is generated using an isolated Caterpillar 2MW diesel engine. Table 2.5 gives the engine specifications. Table 2.6 gives the values for diesel engine power output, specific fuel consumption, exhaust temperature, heat rejected by engine to jacket water, and exhaust at different loads of the engine. Note that the heat present in exhaust is based on a lower heating value of exhaust (i.e., cooling exhaust up to only 176.6°C or 350°F) to avoid acid formation in the exhaust manifold.

From the annual electrical load consumption, the average electrical load on the diesel engine is 1250kW (1676.2hp). Taking 1.3MW (1700hp) as the average load on a diesel engine, the average percent load on a diesel engine is 65.7%. By interpolation with between 50% and 75% engine data for 65.7%, Table 2.6 also gives the diesel engine data at this load.

To evaluate ORC performance for waste heat recovery from stationary diesel engines, two cases were simulated: jacket water heat recovery system alone and a combined jacket water and exhaust heat recovery system. For both of these simulation cases, it was assumed that a water cooling source as heat sink was readily available at 10°C, the approximate year-round

groundwater temperature in Tok, with flow rate ranging from 27.2m^3/h (120gpm) to 45.4m^3/h (200gpm).

Table 2.5 gives the engine jacket water temperature at 99°C (210.2°F). With the assumption that 45.4m^3/h (200gpm) jacket water is bypassed to be supplied as heat source for the ORC power unit, Table 2.7 gives the results for operating this ORC power system on waste heat from the jacket water of the 2MW diesel engine.

Observed from Table 2.6 is that the exhaust temperature at 65.7% engine load is 402°C, well above the 107.2°C (225°F) required for the ORC to generate maximum system operating power. For the simulated case of combined jacket water and exhaust heat recovery system, if the heat recovery system is designed such that the jacket water from the engine is first passed through the exhaust heat exchanger, it is possible to achieve a 107.2°C (225°F) hot water supply temperature for the ORC power unit evaporator. Table 2.7 also gives the ORC power unit performance for both jacket water and combined jacket water and exhaust heat recovery systems. In Table 2.7 the heat input to the power unit, system operating power output, efficiency, payback period, and CO_2 reductions can be obtained from Figures 2.6 to 2.11. For combined jacket water and exhaust heat recovery, a system operating power output of 45.7kW, with payback period of 2.3years could be achieved. Considerable reductions in emissions could be achieved, as listed in Table 2.7. These potential reductions were calculated based on the EPA TIER-4 interim reduction standards discussed earlier.

2.7 Conclusions

The testing system for heat source loop, heat sink loop, electrical system, and instrumentation was designed and installation went smoothly. The power unit was tested for performance according to the experimental procedure discussed. The following conclusions can be drawn from experimental test results:

1. Application of this 50kW ORC power unit for waste heat recovery application from stationary diesel gen-sets should be reliable and feasible in rural Alaska, as the level of expertise required to operate and maintain the power unit is expected to be minimal.
2. The effect of the cold water flow rate on heat input, heat rejection, and power output was minimal for a given cold water supply temperature, hot water flow rate, and hot water supply temperature.

3. For a given hot water supply temperature with the increase of hot water flow rate, the heat input to power unit and system operating power output reached asymptotic condition.
4. Performance curves were plotted for heat input to evaporator, heat rejected to cold water, system operating power output, efficiency, payback period, and CO_2 emission reductions with respect to hot water supply temperature of 10^oC and 20^oC cold water supply temperatures, respectively.
5. For all hot water supply temperatures above 68.3^oC (155^oF), a payback period of less than 6.5years and 8years could be achieved for 10^oC and 20^oC cold water temperatures, respectively.
6. An example to evaluate the present ORC system using the field diesel engine data is presented for both jacket water heat recovery and combined jacket water and exhaust heat recovery systems using the developed performance curves. The example shows that the performance data obtained from this experiment can be used to simulate and evaluate the application of this ORC system to Alaska village gen-sets for power output, efficiency, payback period, and emission reductions.
7. For a jacket water temperature of 99^oC (210.2^oF), a 41.7kW system operating power output was achievable, with 7.2% efficiency and 2.6years payback. From our observation of example results, if the waste heat is from both jacket water and exhaust heat exchanger, it is possible to generate 45.7kW system operating power output with 7.4% efficiency and 2.3years payback using this ORC power unit working on waste heat from stationary diesel engines.
8. Considerable annual emission and CO_2 (greenhouse gas/GHG) reduction could be obtained if the ORC power unit was operated year round on waste heat from diesel engines.
9. Taking into account the 370,000 MWh of electrical consumption of Alaska and the 38% fuel efficiency of a diesel engine, nearly 486,800 MWh of heat energy is present in jacket water and exhaust heat. Using this waste heat, at 7% ORC efficiency, about 34,080 MWh of electricity can possibly be generated, which would increase the diesel engine fuel efficiency to 41.5%, with CO_2 reductions of 27,000 short-tons/year, fuel savings of 9,214,800 lit/year (2,434,300 gal/year) and fuel cost savings of $12,171,500/year.

2.8 Acknowledgments

The authors gratefully acknowledge financial support provided by the Alaska Energy Authority, the Denali Commission, and the Alaska Department of Environmental Conservation. We would also like to thank Gwen Holdmann, Brent Sheets, and Ross Coen from the Alaska Center for Energy and Power for providing managerial assistance to complete this project on time. The authors acknowledge ACEP for providing tools and equipment for installation, the UAF power plant for providing lab space for performing the experiment and UAF Facilities Services for providing personnel during installation of unwieldy and heavy components.

2.9 References

[1] Lin, C.S., "Capture of heat energy from diesel engine exhaust," Final report prepared for National Energy Technology Laboratory, DOE Award # DE-FC26-01NT41248, November, 2008.

[2] Alaska Department of Environmental Conservation, "Ground Water in Alaska," March 2005.

[3] Raghupatruni, P., "Performance Analysis of Capture of Heat Energy from Diesel Engine Exhaust," Master's Thesis, University of Alaska Fairbanks, 2007.

[4] Raghupatruni, P., Lin, C.S., Witmer, D., Bargar, E., Schmid, J., Johnson, T., and Avadhanula, V.K., "An Experimental Feasibility Study of Using Diesel Exhaust for Space Heating in Alaskan Villages," Proceedings of the Tenth International Conference on Advanced Computational Methods and Experiments in Heat Transfer, Maribor, Slovenia, WIT Press, Vol.61, pp. 93-104, July 2008.

[5] Directions in Engine-Efficiency and Emissions Research (DEER) Conference Presentations, http://www1.eere.energy.gov/vehiclesandfuels/resources/proceedings/index.html. Accessed July 16th 2012.

[6] Holdmann, G., "The Chena Hot Springs 400 kW Geothermal Power Plant: Experience Gained During the First Year of Operation," Transactions of the Geothermal Resource Council, Vol.31, pp 509-514, Davis, CA, September 2007.

[7] Leslie, N.P., Zimron, O., Sweetser, R.S., and Stovall, T.K., "Recovered energy generation using an Organic Rankine Cycle system," ASHRAE Transactions # CH-09-024, Vol. 115, Part 1, ASHRAE Winter Conference, Chicago, 2009.

[8] Canada, S., Cohen, G., Cable, R., Brosseau, D., and Price, H., "Parabolic trough Organic Rankine Cycle solar power plant," Presented at the 2004 DOE Solar Energy Technologies Program Review Meeting, Denver, Colorado, October 25–28, 2004.

[9] Bini, R., Schwarz, D.A., Gaia, M., Bertuzzi, P., and Righini, W., "Operational results of the first biomass CHP plant in Italy based on an Organic Rankine Cycle turbogenerator and overview of a number of plants in operation in Europe since 1998," Proceedings of the 2nd World Conference on Biomass for Energy, Industry and Climate Protection, Rome, Italy, pp. 1716 – 1721, May10-14, 2004.

[10] Turboden ORC plants for Industrial Heat Recovery. Turboden press release URL: http://www.turboden.eu/it/public/downloads/11-COM.P-18-rev.4_HR_ENG.pdf. Accessed July 17th 2012.

[11] Leibowitz, H. and Mirolli, M., "First Kalina combined-cycle plant tested successfully," Power Engineering, Vol. 101(5), pp. 45-48, 1997.

[12] Valdimarsson, P., "The Kalina power plant in Husavik – Why Kalina and what has been learned," Workshop on Electricity Generation from Enhanced Geothermal Systems, Strasbourg, France, Sepetember 14-16, 2006.

[13] Knapek, E. and Kittl, G., "Unterhaching power plant and overall system," Proceedings of the European Geothermal Congress, Unterhaching, Germany, May 30 - June 1, 2007.

[14] Yamamoto, T., Furuhata, T., Arai, N., and Mori, K., "Design and Testing of the Organic Rankine Cycle," Journal of Energy, Vol.26, pp. 239-251, 2001.

[15] Quoilin, S., "Experimental study and modeling of a low temperature Rankine cycle for small scale cogeneration," Master's Thesis, University of Liege, May 2007.

[16] Reid, A.D., "Low temperature power generation using HFE-7000 in a Rankine cycle," Master's Thesis, San Diego State University, July 2010.

[17] Lemmon, E.W., Huber ML, and McLinden MO, "NIST Standard Reference Database 23: Reference Fluid Thermodynamic and Transport Properties-REFPROP," Version 8.0, National Institute of Standards and Technology, Standard Reference Data Program, Gaithersburg, 2007.

[18] Alaska Energy Authority, "Statistical report of the power cost equalization program for fiscal year 2011," 23rd Edition, April 2012.

[19] Lockard, D., Witmer, D., and Holdmann, G., "Ammonia fuel for use in rural Alaska," Ammonia Fuels Conference, Minneapolis, September 29, 2008.

[20] U.S. Environmental Protection Agency, "Control of emissions of air pollution from non-road diesel engines and fuel," Rules and Regulations, Vol.69 (124), pp. 38980, June 29, 2004.

[21] U.S. Environmental Protection Agency, "Emission facts: Average carbon dioxide emissions resulting from gasoline and diesel fuel," EPA420-F-05-001, February 2005.

Table 2.1 Review conducted for available heat-to-power conversion systems

Company	Unit	Price	$/kW	Status/Notes in Summer-2008
Organic Rankine cycle systems				
Global Energy	30kW	$60,000	$2,000	30kW unit sold, expected to be online by September 2008.
Global Energy	80kW	No price quote	N/A	As of July 14, 2008 being built in Toronto
Barber-Nicholes	Custom design	$200K -$1M	N/A	Would require a custom design. It is unclear how long it would take for a unit to be delivered
ElectraTherm	50kW to 65kW	$120,000	$2,400-$2,700	Unit available but must be proven before it becomes commercially viable
TransPacific Energy	115kW	$250,000	$2,174	No units installed, only designs.
Deluge Inc.	250kW	$400,000	$1,600	Not ORC but thermal hydraulic engine. Built first 250kW unit and is being installed in HI.
Ormat	> 200kW	No price quote	N/A	As of summer-2008 recovering heat from a diesel generator is not available.
Ammonia-water vapor absorption power systems				
Energy Concepts	400kW absorption cycle	No price quote	N/A	Not clear if a specific unit is available or if their product would be custom designed per application
Rexorce	250kW Thermal Engine	No price quote	$1,500	Modified Kalina Cycle. Expect to be completed in a few months
Sterling engine systems				
ReGen Power	500kW	No price quote	$1000 - $2000	3 months into 18-month development cycle. Hope to have 10kW prototype at end of 2008. Also hope to have 250kW and 1MW units in future.

Table 2.2 Various hot water and cold water flow rates at which power unit was tested

Hot water temperatures, °C (°F)	Hot water flow rate, m^3/hr (gpm)	Cold water temperatures, °C (°F)	Cold water flow rate, m^3/hr (gpm)
68.33 (155)	27.25 (120)	10 (50)	27.25 (120)
79.44 (175)	36.34 (160)	20 (68)	36.34 (160)
90.56 (195)	45.4 (200)		45.4 (200)
101.67 (215)	56.8 (250)		
107.22 (225)	68.1 (300)		

Table 2.3 Total component cost incurred building the experimental system

Component	Cost ($)
50kW ORC Power unit	119,388.00
Steam loop	8,997.22
Hot water loop	16,762.03
Cold water loop	14,613.57
Electrical system	3567.91
Instrumentation	21,246.25
Structural material	5,409.22
Miscellaneous parts and other costs	948.38
Total component cost	**190,932.58**

Table 2.4 TIER-4 interim EPA emissions standards for non-road diesel engines [20, 21]

NO_X g/kWh (lb/kWh)	Particulate matter (PM) g/kWh (lb/kWh)	CO g/kWh (lb/kWh)	HC g/kWh (lb/kWh)	CO_2 kg/lit (lb/gal)
3.5 (0.0077161)	0.10 (0.0002204)	3.5 (0.0077161)	0.40 (0.0008818)	2.66 (22.2)

Table 2.5 Diesel engine specifications

Diesel Engine	Caterpillar C175-16
Brake power	1.9MW (2588BHP)
Number of cylinders	16
Compression ratio	16.7
Speed	1200rpm
Jacket water temperature	99°C (210.2°F)
Jacket water flow rate	120m^3/h (528gpm)
Aspiration	Turbocharged (no EGR)

Table 2.6 Diesel engine specifications at various loads

Percent load	Brake power, hp (MW)	Diesel fuel consumption, lit/s (gpm)	Heat rejection to jacket water, kW	Exhaust temperature, °C	Heat present in exhaust at 176.6°C (350°F), kW
100	2588 (1.9)	0.131 (2.08)	1009.3	417.8	869.9
75	1941 (1.4)	0.101 (1.61)	753.9	404.1	686.7
50	1294 (1.0)	0.070 (1.12)	510.4	398.6	478.3
25	647 (0.5)	0.040 (0.63)	294.1	340.4	231.3
65.7	1700 (1.3)	0.090 (1.42)	663.2	402	609.1

Table 2.7 Estimated ORC performance for operating on waste heat recovery from diesel engine

Parameter	Jacket water heat only	Jacket water + Exhaust heat
Hot water supply temperature to ORC power unit	99°C (210.2°F)	107.2°C (225°F)
Hot water flow rate to ORC power unit	45.4m^3/h (200gpm)	45.4m^3/h (200gpm)
Heat input to evaporator of ORC power unit	576.5kW	617.7kW
System operating power output	41.7kW (355.7MWh/year)	45.7kW (390MWh/year)
System operating efficiency	7.2%	7.4%
Diesel fuel saved	96190.4lit/year (25410.8gal/year)	105382.5lit/year (27840gal/year)
Dollar amount saved on diesel fuel	$127060/year	$139200/year
Payback period @ 0% interest	2.2years	2years
Payback period @ 10% interest	2.6years	2.3years
Reductions in CO_2 emissions	282short-tons/year	309short-tons/year
Reductions in NO_X emissions	1245kg/year	1364kg/year
Reductions in HC emissions	142.3kg/year	156kg/year
Reductions in CO emissions	1245kg/year	1364kg/year
Reductions in PM emissions	35.5kg/year	39kg/year

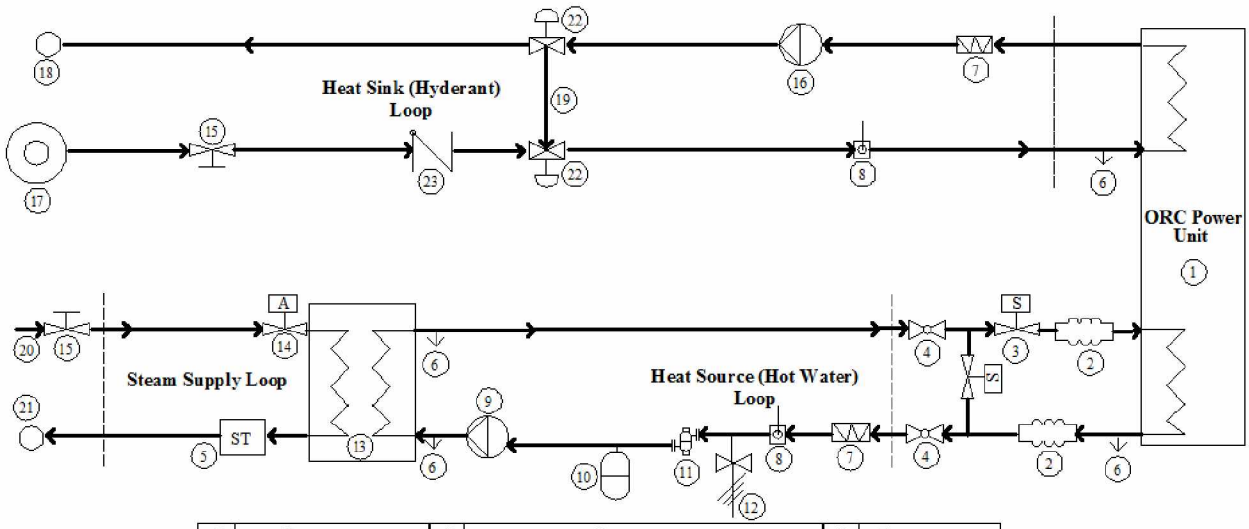

#	Component	#	Component	#	Component
1	ORC power unit	12	Pressure relief valve	23	Check valve
2	Expansions joints	13	Steam-to-hot water heat exchanger		
3	Solenoid valve	14	Steam control valve with actuator		
4	Ball valve	15	Manual control valve		
5	Steam trap	16	Pump (Constant flow rate)		
6	Drain	17	Hydrant source (Cooling water source)		
7	Temperature mixer	18	Cooling water from GM (Hydrant sink)		
8	Ultrasonic flow meter	19	By-pass for temperature control on coolant side		
9	VFD Pump	20	Steam inlet		
10	Expansion tank	21	Steam condensate outlet		
11	Rolairtrol air separator	22	3-way butterfly valve with actuator		

Figure 2.1 Experimental setup for testing 50kW ORC power unit

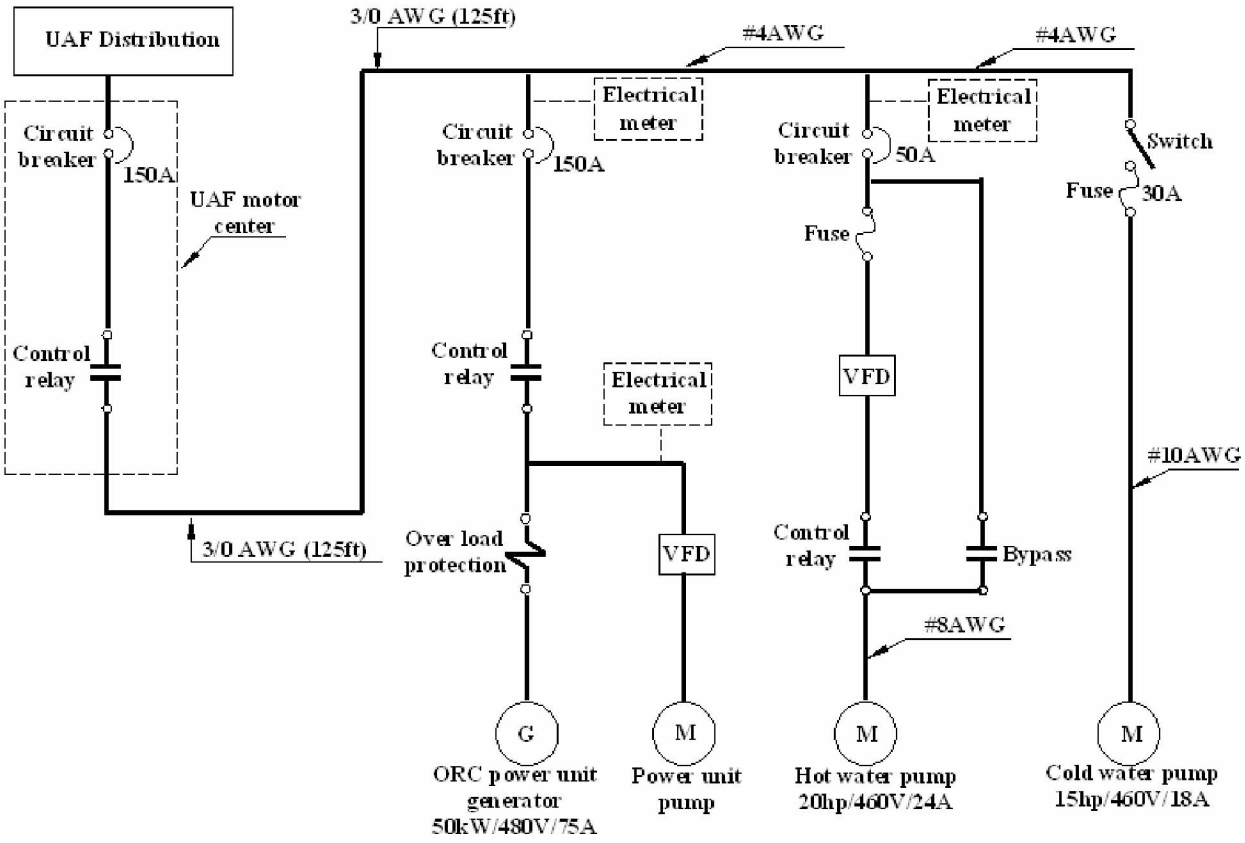

Figure 2.2 Line diagram for electrical wiring for uploading power to UAF system and for powering hot water and cold water pumps

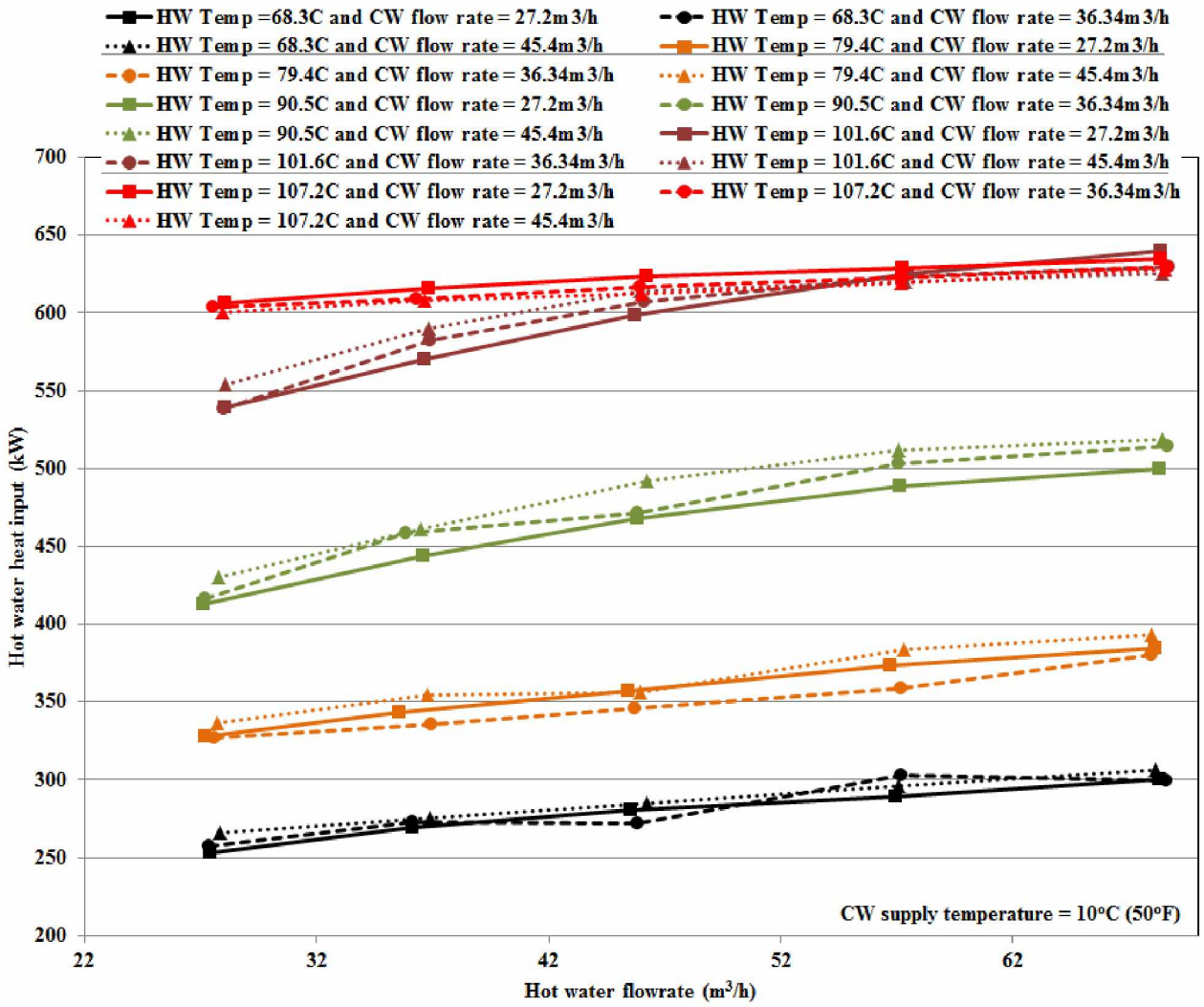

Figure 2.3 Heat input to power unit evaporator vs. hot water flow rates at different hot water supply temperatures and cold water flow rates

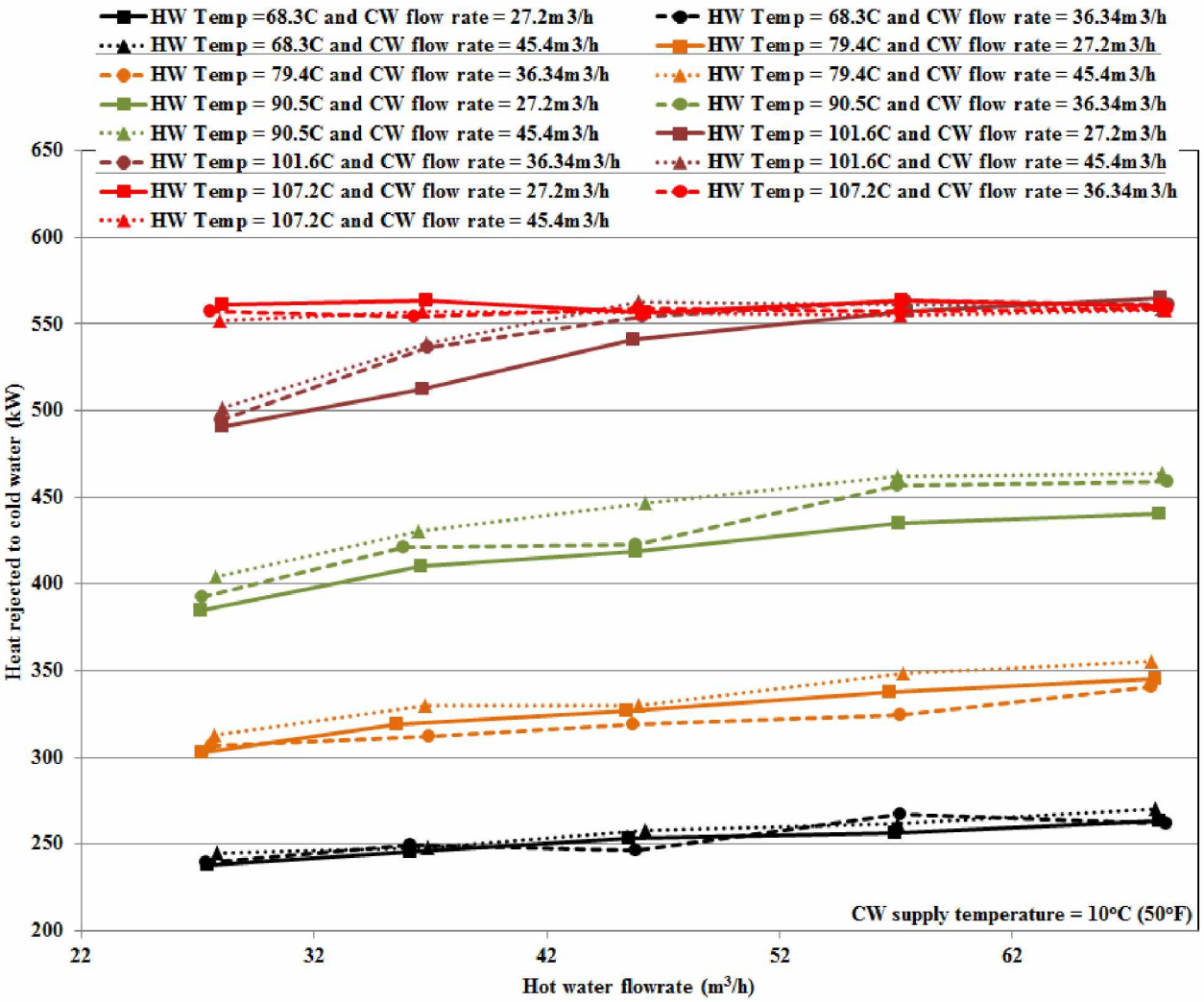

Figure 2.4 Heat rejected to cold water in power unit condenser vs. hot water flow rates at different hot water supply temperatures and cold water flow rates

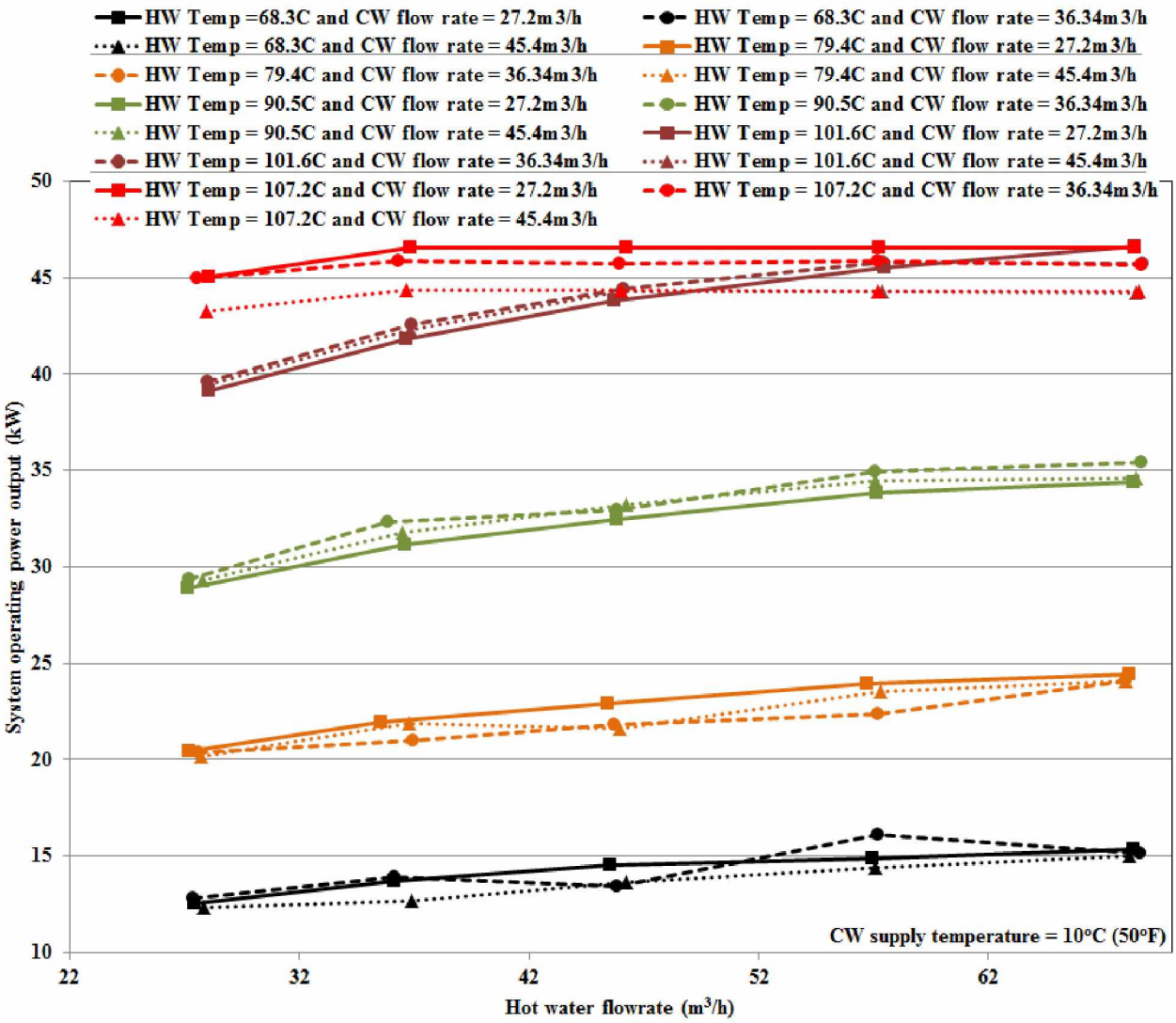

Figure 2.5 System operating power output vs. hot water flow rates at different hot water supply temperatures and cold water flow rates

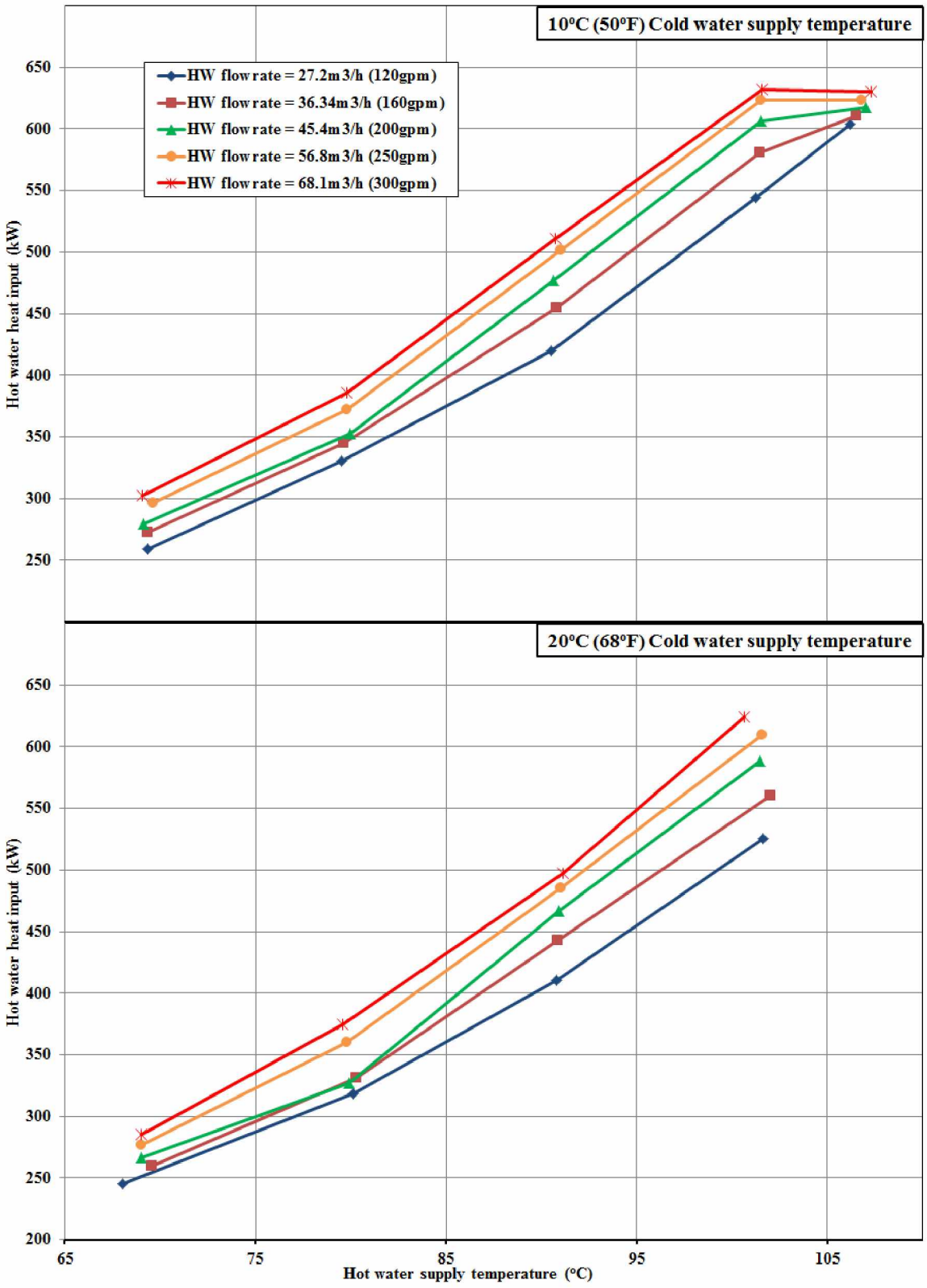

Figure 2.6 Heat input vs. hot water supply temperature

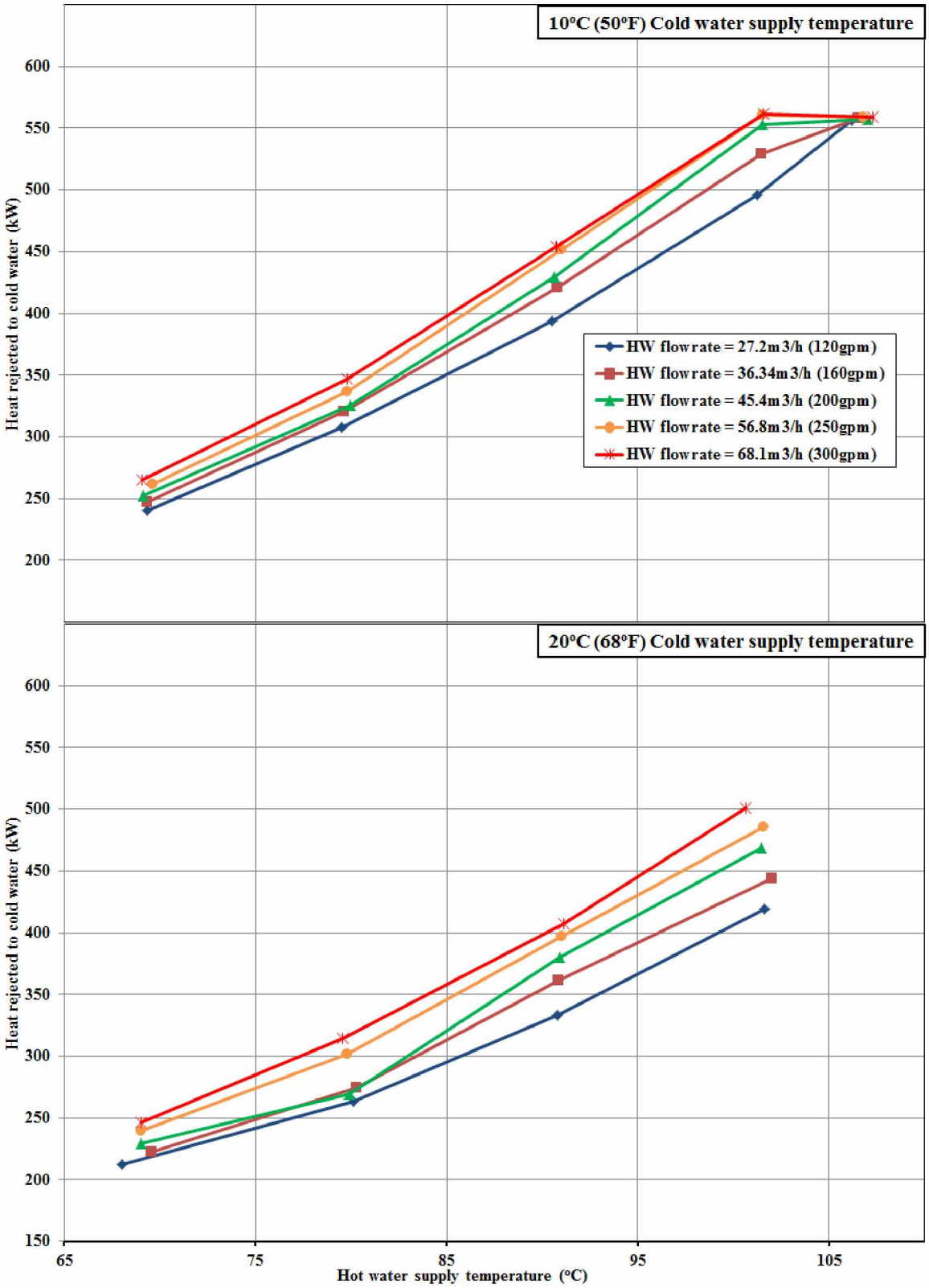

Figure 2.7 Heat rejected vs. hot water supply temperature

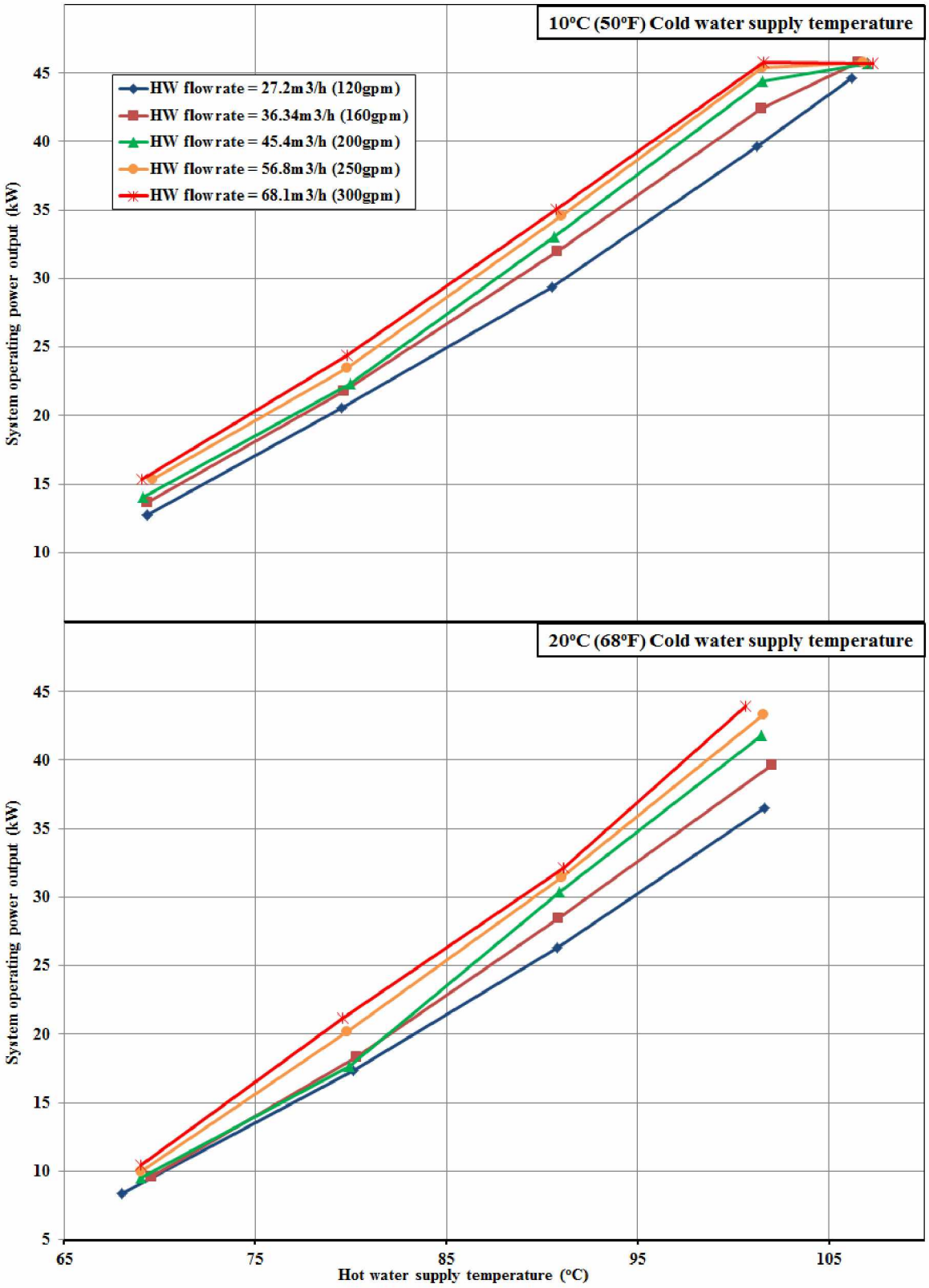

Figure 2.8 System operating power output vs. hot water supply temperature

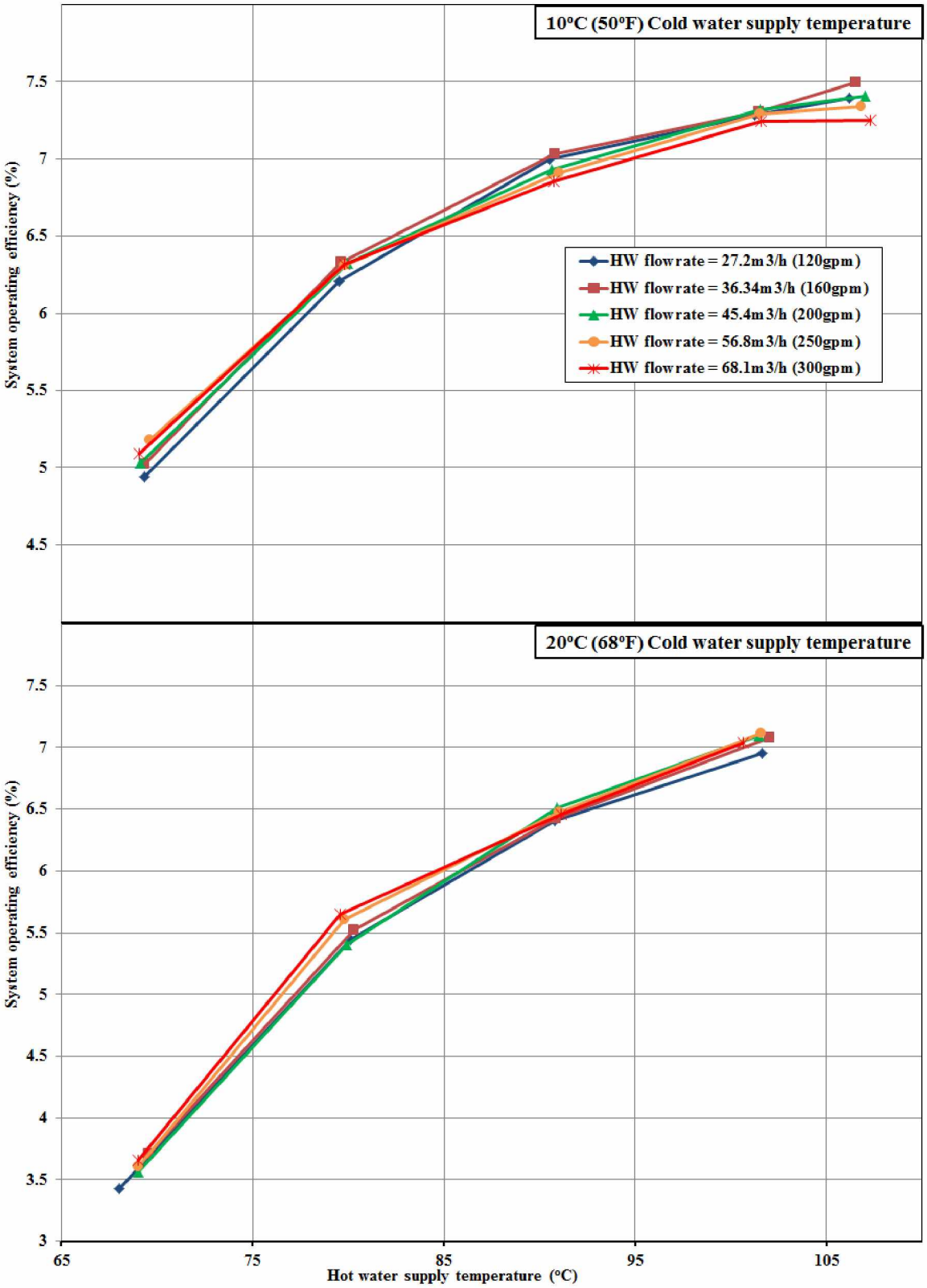

Figure 2.9 System operating efficiency vs. hot water supply temperature

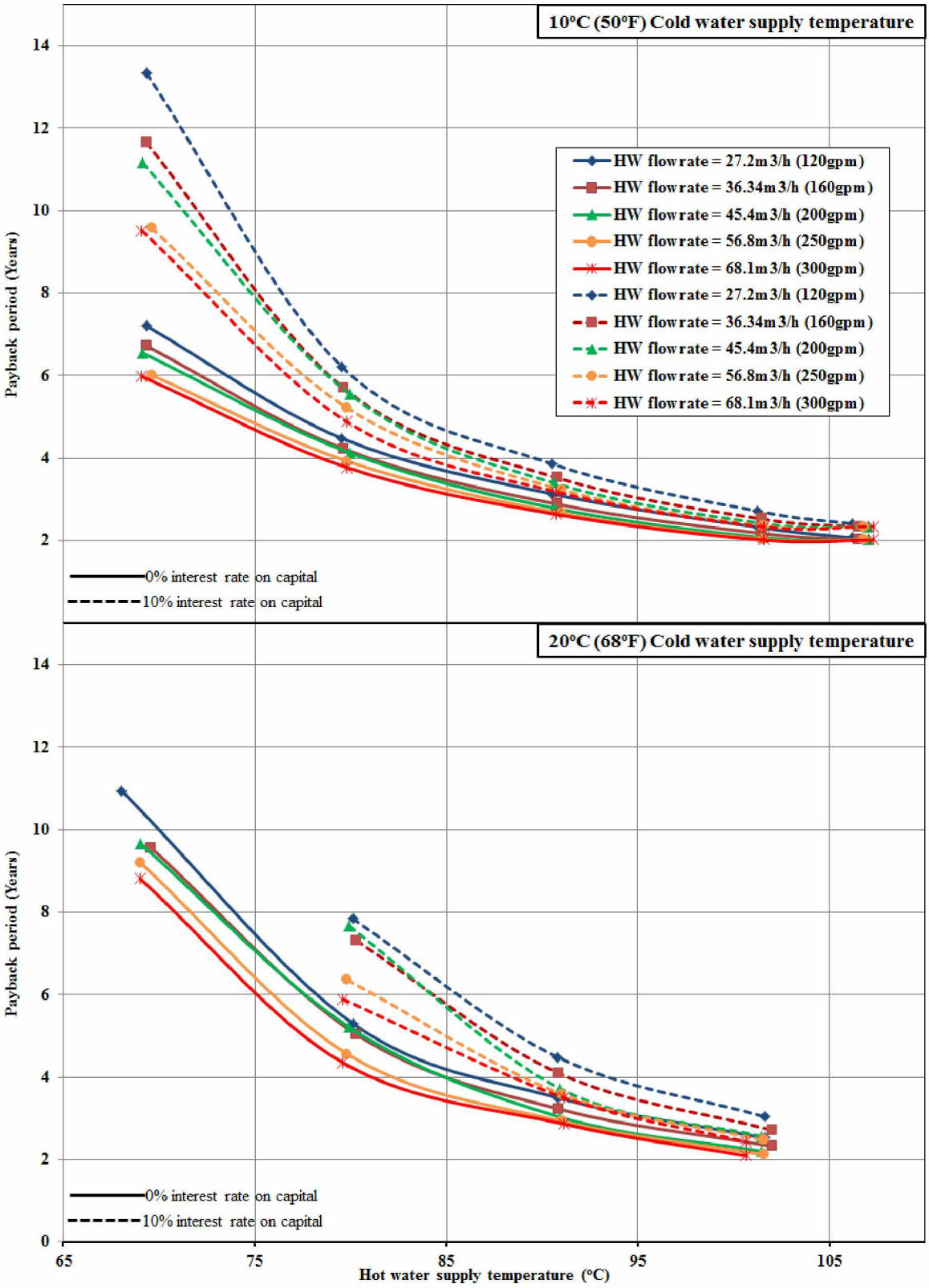

Figure 2.10 Payback period vs. hot water supply temperature

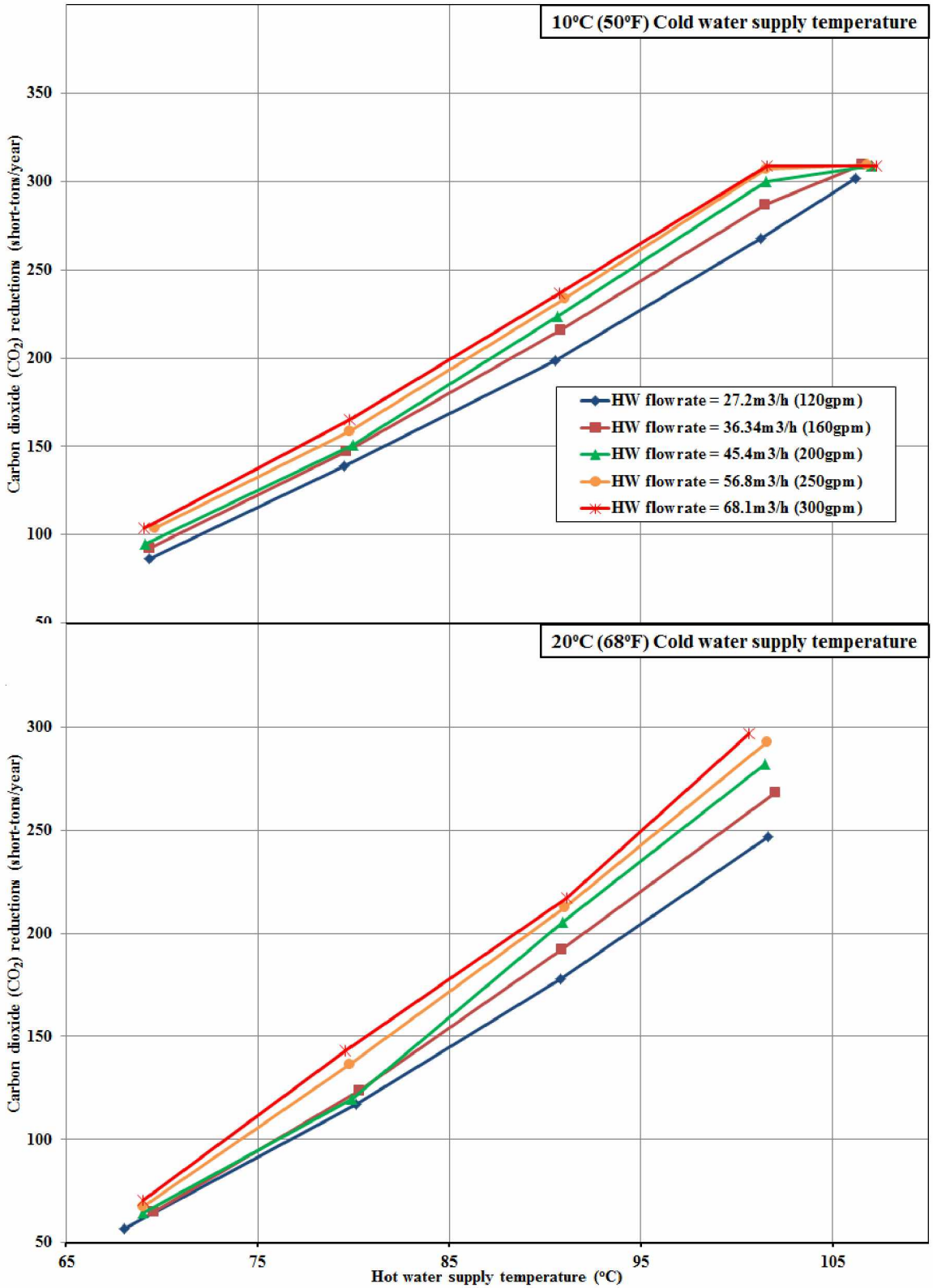

Figure 2.11 CO_2 reductions vs. hot water supply temperature

Chapter 3. Empirical Models for Screw Expander Based on Experimental Data from Organic Rankine Cycle System Testing*

3.1 Abstract

The screw expander discussed in this work was part of a 50kW organic Rankine cycle (ORC) system. The ORC was tested under different conditions of heat source and heat sink. In conjunction with collecting data for the ORC system, experimental data were also collected for the individual components of the ORC, vis-a-vis: evaporator, pre-heater, screw expander, working fluid pump, and condenser. Experimental data for the screw expander were used to develop the two empirical models discussed in this paper for estimating screw expander performance. As the physical parameters of the screw expander discussed in this article are not known, a "black-box" approach was followed to estimate screw expander power output based on expander inlet and outlet pressure and temperature data. Refrigerant R245fa was used as the working fluid in the ORC. The experimental data showed that the screw expander had ranges of pressure ratio (2.70 to 6.54), volume ratio (2.54 to 6.20) and power output (10kW to 51.5kW). Of the two empirical models, the first model is based on the polytropic expansion process, in which an expression for the polytropic exponent is found by applying regression curve-fitting analysis as a function of the expander pressure ratio and volume ratio. In the second model, an expression for screw expander work output is found by applying regression curve-fitting analysis as a function of the expander isentropic work output. The predicted screw expander power output using the polytropic exponent model was within ±10% of experimental values; the predicted screw expander power output using the isentropic work output model was within ±7.5% of experimental values.

3.2 Keywords

Screw expander; polytropic exponent; isentropic work; pressure ratio; volume ratio; regression analysis

3.3 Nomenclature

r_p = screw expander operating pressure ratio

r_v = screw expander volume ratio

w_p = polytropic work output in kJ/kg

---

* Avadhanula, V.K., and Lin, C.S., "Empirical models for screw expander based on experimental data from organic Rankine cycle system testing", ASME Journal of Engineering for Gas Turbines and Power, Vol.136, June 2014.

P_2 = R245fa pressure at pre-heater inlet (state-2) in kPa

P_4 = R245fa pressure at expander inlet (state-4) in kPa

P_5 = R245fa pressure at expander outlet (state-5) in kPa

v_4 = R245fa specific volume at expander inlet (state-4) in m^3/kg

v_5 = R245fa specific volume at expander outlet (state-5) in m^3/kg

n = polytropic exponent

n_c = polytropic exponent from curve-fitting

w_{SE} = screw expander work output in kJ/kg

w_s = isentropic work output in kJ/kg

$w_{SE,o}$ = dimensionless screw expander work output

$w_{S,o}$ = dimensionless isentropic work output

h_o = enthalpy of refrigerant R245fa in kJ/kg at standard temperature and pressure

W_{SE} = screw expander power output in kW

W_{net} = ORC power unit net power output in kW

W_{pump} = ORC pump power consumption in kW

$\dot{m}_R$ = refrigerant R245fa mass flow rate in kg/s

$\dot{V}_h$ = hot water flow rate in m^3/h

η_h = efficiency of heat transfer from hot water to refrigerant R245fa in evaporator and pre-heater

η_S = screw expander isentropic efficiency

h_6 = hot water supply enthalpy at state-6 in kJ/kg

h_8 = hot water return enthalpy at state-8 in kJ/kg

h_2 = R245fa enthalpy at pre-heater inlet (state-2) in kJ/kg

h_4 = R245fa enthalpy at evaporator outlet (state-4) in kJ/kg

ρ_h = average hot water density, in kg/m^3, obtained at hot water supply and return temperature

T_6 = hot water supply temperature in ^oC

T_8 = hot water return temperature in ^oC

T_2 = R245fa temperature at pre-heater inlet (state-2) in ^oC

T_4 = R245fa temperature at evaporator outlet or expander inlet (state-4) in ^oC

T_5 = R245fa temperature at expander outlet (state-5) in ^oC

3.4 Introduction and Literature Review

In recent years, due to environmental concerns and increasing fuel prices, the demand for use of low-grade heat sources (i.e., heat sources with low temperature and/or low heat value) has been steadily increasing. One such low-grade heat source is waste heat from stationary diesel engines used for electrical power generation. In stationary diesel engines, about one-third of the energy stored in the fossil fuel is converted into useful work; the remaining two-thirds of that fuel energy are lost, mainly in the form of jacket water heat and exhaust gases. If this waste heat were recovered for useful purposes, considerable improvements in diesel engine efficiency and the power plant as a whole could be attained. One of the many applications where diesel engine waste heat could be harvested is the thermal power cycle of the organic Rankine cycle (ORC), which is the focus of this work.

Stationary diesel engine waste heat recovery is a natural consideration as a low-grade heat source in Alaska, where approximately 180 rural villages use diesel generators to run independent electrical power systems. In 2007, the combined electrical consumption of these 180 villages was 370,000 MWh [1]. It should be noted that the size of the diesel gen-sets in operation in these villages varies from about 100kW to 1MW in electrical capacity. With waste heat availability of 1MW or less, an ORC system with less than 100kW (at 10% thermal efficiency) power output would be desirable.

The ORC is similar to the traditional steam Rankine cycle; the only difference is the working fluid. The working fluids generally used in an ORC are refrigerants, such as R11, R113, R123, R134a, R245fa, HFE-7000. As shown in Figure 3.1, a typical ORC consists of a pump, a preheater, an evaporator, the expansion machine (expander), and a condenser. The working fluid is pressurized through the pump and supplied to the preheater and evaporator, where it is heated by the heat source (heating fluid loop in Figure 3.1). The working fluid exiting the evaporator is in a vapor or liquid/vapor condition, which is expanded in the expander while power is generated. The low-pressure working fluid exiting the expansion machine is liquefied in the condenser by a cooling source (cooling fluid loop in Figure 3.1) and returned to the pump. In a diesel engine waste heat application of the ORC, the heat source may be engine jacket liquid, exhaust gases, or a combination of the two. The cooling source could be a lake, a river, an underground well, air-cooled radiators, or a cooling tower, based on the ORC installation location and the economic viability of the cooling source.

In the ORC process described above, the preheater, evaporator, and condenser are heat exchangers; primarily brazed plate heat exchangers are used in current small scale ORC applications (i.e., less than 100kW power units). The type of working fluid pump used in an ORC is usually a feed pump or a centrifugal pump with variable frequency drive (VFD). Because of low heat source temperatures and the high probability of two phase working fluid at the expander inlet, expanders which are resilient to two phase mixtures are preferred for small scale ORC applications. Examples of commonly used expansion machines in small scale ORC applications are twin screw expanders [2, 3, 4, 5, 6], scroll expanders [7, 8, 9, 10], and turbines [11, 12]. Of all available expansion machines, the screw expander is the most practical one used in commercial ORC applications. This paper focuses on screw expanders for which (i) experimental data were collected as part of ORC testing, and (ii) two empirical model equations were developed to predict the performance characteristics of screw expanders. The following paragraphs include a brief literature review of Rankine cycles with screw expander systems and a brief description of work presented in this paper.

3.4.1 Screw Expanders

Screw-type expanders (and also compressors) are positive displacement devices consisting of helical screw rotors with male and female rotors. Figure 3.2 [3] shows a cut-away sectional view of a screw expander; the major components are labeled. The male and female rotors are separated by narrow clearances (on the order of 50 microns [5]), obtained by bearing and timing gears. As the high pressure working fluid enters the expander at the inlet port, the volume of the working fluid expands between the rotors and the expander housing (to the discharge port pressure), and causes the rotors to rotate. As the fluid volume expands to the discharge port pressure, it exerts pressure on the rotors and causes them to rotate, thereby transferring power from the working fluid to the screw expander shaft, which is connected to the electric generator. It has been reported in literature that screw expanders can admit two-phase mixtures i.e., low enthalpy value working fluids, to generate electrical power, which makes them suitable for low-grade heat recovery applications.

Kaneko and Hirayama [2] in 1985 carried out a detailed experimental and theoretical study on the performance of helical screw expanders with air as the working fluid. The screw expander was tested for different rotor tip speeds and air flow rates. Output power ranged from 2kW to

12kW, with adiabatic efficiency ranging from 40% to 70% for varying rotor tip speeds. These observations were based on experimental data obtained from a prototype screw expander.

Ng et al. [3] in 1990 reported on the performance of a screw expander for a trilateral flash cycle, which used saturated steam as the working fluid at the expander inlet. The authors reported on the experimental results for screw expander for different pressure ratios (from 2 to 27) and volumetric expansion ratios (from 2 to 5.3). The screw expander brake power output ranged from 4kW to 185kW, and isentropic efficiency ranged from approximately 55% to 85%. The authors conducted a detailed analysis of screw expanders with experimental data and developed an empirical relation for screw expander output.

Smith et al. [4] in 1995 conducted experiments on a screw expander incorporated in a trilateral flash cycle (TFC) with R-113 as the working fluid. The expander isentropic efficiency ranged from 30% to 72%, and power output ranged from 5kW to 25kW. In 2005, Smith et al. [5] reported improved screw expander performance over the years by reducing loss; they tested a screw expander (with no specific cycle) with R-113 as the working fluid. The screw expander adiabatic efficiency ranged from approximately 50% to 85%, and power output ranged from 10kW to 25kW. In both the cases, the authors are reporting the results of experiments or analytical models.

In 2005, a 120kW ORC system using geothermal heat was commissioned in Birdsville, Australia [6], with a screw expander as the expansion device. The geothermal supply water was at 98^{o}C and the heat sink was at 25^{o}C. Isopentane was used as the working fluid. 80kW net cycle power output was obtained with a heat-to-power conversion efficiency of 6%. No information of screw expander efficiency or performance was provided.

3.4.2 Present Work

In the work presented herein, the authors at the University of Alaska Fairbanks (UAF) tested a 50kW ORC system, manufactured by ElectraTherm, Inc., with a twin screw expander as a power generating device [13]. As shown in the authors' previous publication [13], the ORC power unit was tested under different heat source and heat sink supply conditions by varying hot water and cold water supply flow rates and temperatures for performance mapping. As part of the testing, for the purpose of studying the performance of expander, the data acquisition for screw expander was carried out and observations of the same are reported in the present work.

The following sections discuss two curve-fitting models for performance prediction of a screw expander, experimental setup and procedure, data collection and reduction processes, and the results. To predict the performance of a screw expander, the first model is based on the polytropic exponent; the second model is based on the isentropic work output. For both models, a data fit coefficient of determination (R^2) of 0.97 was obtained. For all experimental data in this work, the working fluid at the screw expander inlet (state-4 in Figure 3.1) was in a superheated vapor condition. Throughout this paper, we will continue to refer to Figure 3.1, which is a schematic of the ORC discussed, for clarification and to reference state points in the ORC process.

3.5 Empirical Correlations for Predicting Screw Expander Performance

A screw expander is a positive-displacement rotary work-producing device. The physical construction of a screw expander is quite complicated [14]. Physical parameters, such as rotor configuration (number of male and female lobes), rotor diameter, wrap angle, rotor profile, clearances, and built-in volume ratio affect the performance and output of a screw expander [3, 15]. For proprietary reasons, the physical parameters of the screw expander under study cannot be disclosed. Therefore, in the work presented, the screw expander was analyzed using a "black-box" approach i.e., based on the measured parameters of inlet and outlet pressures and temperatures, two models are proposed and analyzed for estimating expander power output. The first model is based on the polytropic process; the second model is based on the isentropic work output process. In each case, regression curve-fitting analysis was used; for the first model, a polytropic index of "n" with respect to operating pressure ratio (r_p) and volume ratio (r_v) was fitted; for the second model, the screw expander work output with respect to isentropic work output was fitted. In finding the curve-fitting coefficients of model-I and model-II, discussed below, regression analysis was conducted using the DataFit program [16], which uses the widely applied Levenberg-Marquardt method.

For dimensionless expressions of the derived empirical equation, two dimensionless relationships useful in this screw expander study are the operating pressure ratio (r_p) and volume ratio (r_v), given by Eq. (3.1) and Eq. (3.2),

$$r_p = \frac{P_4}{P_5} \tag{3.1}$$

$$r_v = \frac{v_5}{v_4} \tag{3.2}$$

where, P_4 and P_5 are the screw expander inlet and outlet pressures in kPa, and v_4 and v_5 are the inlet and outlet specific volumes in m^3/kg; these correspond to state-4 and state-5 respectively in Figure 3.1. The specific volume for refrigerant R245fa at the respective state points was obtained with the NIST REFPROP 8.0 [17] program using measured temperature and pressure data from the experiment.

3.5.1 Model-I

Figure 3.3, below, is a P-V diagram that shows the ideal polytropic expansion process (process 4-a-b-5) for a screw expander. In an ideal polytropic case, a screw expander consists of constant pressure admission (process 4-to-a), polytropic expansion along the index "n" (process a-to-b), and constant pressure discharge (process b-to-5). The work output for the process a-b is usually represented by the area under the polytropic expansion curve P-V. Considering the "black-box" approach, a screw expander can be treated as a steady-flow, work-producing device. The work output of a steady-flow device undergoing the polytropic expansion process from "a" to "b" is given by [18],

$$w_p = -\int_a^b v dp \tag{3.3}$$

Using the polytropic relation of $Pv^n = C$, Eq. (3.3) can be reduced to,

$$w_p = \frac{nP_a v_a}{n-1}\left[1 - \frac{P_b v_b}{P_a v_a}\right] \tag{3.4}$$

In Eq. (3.4), w_p is the polytropic work output of a screw expander in kJ/kg, where P is pressure in kPa, v is specific volume in m^3/kg, and n is the polytropic index. For the expansion process of 4-a-b-5,

$$\frac{P_a}{P_b} = \frac{P_4}{P_5} = r_p \tag{3.5}$$

$$\frac{v_b}{v_a} = \frac{v_5}{v_4} = r_v \tag{3.6}$$

Therefore, Eq. (3.4) reduces to,

$$w_p = \frac{nP_4 v_4}{n-1}\left[1 - \frac{r_v}{r_p}\right] \tag{3.7}$$

However, in practical screw expander operation, there are numerous losses associated with ill-matching of pressures, leakage losses, and mechanical losses. which reduce the actual work output of the expander [3, 15]. Some of the losses are depicted in Figure 3.3 and include: (i) admission losses (4-to-a'), (ii) irreversibility losses (a'-to-b' or a'-to-b''), (iii) losses due to ill-matched expander exit pressure and condenser pressure, causing either a blowdown effect (b' to

c') or a blowback effect (b'' to c''), (iv) and discharge losses (c'-to-5 or c''-to-5). Because clearances are necessary between the moving rotors and the rotors and expander casing, there are inherent leakage losses, and these reduce the actual work output of the screw expander [3, 15]. In addition to the losses described above, there are mechanical losses from friction in the screw expander and generator bearings.

With all the losses described above, it is important to know the physical parameters of the expander so that the work output of the screw expander can be estimated. The physical parameters of the present screw expander are not known, so an expression similar to Eq. (3.7) is assumed for estimating the work output (w_{SE}) of the screw expander; this is given by Eq. (3.8) below. In Eq. (3.8), r_p and r_v are given by Eq. (3.1) and Eq. (3.2); n_c is the fitted polytropic exponent given by Eq. (3.9), and is obtained as a function of r_p and r_v.

$$w_{SE} = \frac{n_c P_4 v_4}{n_c - 1}\left[1 - \frac{r_v}{r_p}\right] \tag{3.8}$$

$$n_c = A\left(\frac{\ln(r_p)}{\ln(r_v)}\right) + B\left(\frac{\ln(r_p)}{\ln(r_v)}\right)^2 + C\left(\frac{\ln(r_p)}{\ln(r_v)}\right)^3 \tag{3.9}$$

From our calculations, we observed that the addition of more terms in Eq. (3.9) (4^{th} order or higher) was negligible for the outcome. Using Eq. (3.8) n_c, values were calculated using the experimental data vis-a-vis the screw expander work output, r_p, r_v, P_4, and v_4. Specific volume for refrigerant R245fa at respective state points was obtained using measured temperature and pressure data. These n_c values and respective r_p and r_v values were used to find the curve-fitting coefficients A, B, and C in Eq. (3.9) by regression analysis of experimental data using DataFit software [16].

For n_c, logarithmic expression of the form Eq. (3.9) is considered because of two reasons: (i) polytropic exponent takes the form $\left(\frac{\ln(r_p)}{\ln(r_v)}\right)$ when obtained from $Pv^n = C$ (ii) for r_p=1, the work output of screw expander by Eq. (3.8) should be zero.

3.5.2 Model-II

In the second model, the screw expander work output (w_{SE}) was estimated using the expander isentropic work output (w_s). For a screw expander (or any expansion machine), the isentropic work output (w_s) is given by Eq. (3.10) below,

$$w_s = (h_4 - h_{5s}) \tag{3.10}$$

where w_s is the isentropic work output in kJ/kg, h_4 is the enthalpy of the working fluid (R245fa) at the expander inlet (state-4 in Figure 3.1) in kJ/kg, and h_{5s} is the expander exit enthalpy of R245fa at state-5, if the expansion process is isentropic to the condenser pressure.

To estimate the work output (w_{SE}) of the screw expander, a dimensionless polynomial equation, as in Eq. (3.11), was fitted using regression analysis. Eq. (3.12) and Eq. (3.13) were used for the dimensionless form of Eq. (3.11),. h_o is the enthalpy of refrigerant (working fluid) in kJ/kg at standard temperature and pressure (i.e., 25°C and 101.325kPa). L, M, N, O, and P are the curve-fitting coefficients obtained by regression analysis using DataFit software [16]

$$w_{SE,o} = L * w_{s,o}^4 + M * w_{s,o}^3 + N * w_{s,o}^2 + O * w_{s,o} + P \tag{3.11}$$

where,

$$w_{SE,o} = \frac{w_{SE}}{h_o} \tag{3.12}$$

$$w_{s,o} = \frac{w_s}{h_o} \tag{3.13}$$

3.6 Experimental Setup and Procedure

The schematic of the experimental setup for testing the 50kW ORC power unit was presented in the authors' previous publication [13], where the power unit was tested by varying the heat source and heat sink supply conditions (i.e., temperature and flow rate) to estimate the performance characteristics. The heat source for the ORC power unit was hot water from a temperature- and flow rate-controlled heat source; the heat sink was cold water from a nearby fire hydrant, with a modification loop added for supply temperature and flow rate control as shown in Figure 3.1, the heating fluid loop is the hot water loop and the cooling fluid loop is the cold water in this study. The power generated from the ORC power unit was uploaded to the UAF grid.

Figure 3.1 is a schematic line diagram of the present ORC machine, with all instrumentation components labeled for data collection. Refrigerant R245fa, which is non-flammable and has zero ozone depletion potential, was the working fluid for the ORC. It should be noted that in the experiment described here, the experimental setup was designed to test the ORC power unit as a whole, not specifically the screw expander performance. Concurrent with the test of the ORC power unit under various hot and cold water supply conditions, steady-state data collection was carried out for various components of the ORC power unit (i.e., screw expander, evaporator, pre-

heater, condenser, pump). These experimental data were used to model the performance of the screw expander.

As a reference for our readers, Table 3.1 shows the hot water and cold water flow rate and temperature conditions under which the ORC power unit was tested. From Table 3.1 it can be inferred that the ORC power unit was tested under 150 different hot water and cold water supply conditions. However, only the experimental data from 100 cases is used in this work due to large fluctuations in saturated steam supply pressure from the UAF power plant, which was the heat source for hot water. In some cases, these conditions did not allow for steady-state operation of the ORC and data collection. After setting all four parameters of hot water and cold water flow rates and temperatures for each case, we waited approximately 30 minutes to attain a steady-state condition before collecting data. We collected data for 30 minutes at one set of hot water and cold water temperature and flow rate; this completed the test for one set of hot water and cold water flow rate and temperature. Using this procedure, we tested the ORC power unit under each hot water and cold water condition listed in Table 3.1. For each case of hot water and cold water flow rate and temperature, all steady-state measured parameters were averaged for the data reduction process, which is discussed in detail in the following sections.

3.7 Parameters Measured, Instrumentation, and Data Collection

Table 3.2 gives the measured parameters used in this analysis. In Table 3.2, hot water temperatures (state-6 and state-8 in Figure 3.1) and flow rate are used to estimate the refrigerant (R245fa) flow rate; this will be discussed shortly. The pressures and temperatures of the expander inlet (state-4) and outlet (state-5), and electrical meter data were used to model the screw expander, using model-I and model-II above.

Temperatures and pressures at various state points (listed in Table 3.2) were measured using Omega type-K (Chromel-Alumel) thermocouples and Stellar Technology's ST1500 pressure transducers. Temperature and pressure measurements were stored in a Microsoft Excel format using the LabView VI program (see below). A Kamstrup ULTRAFLOW ultrasonic flow meter was used to measure the hot water flow rate. The Kamstrup MULTICAL-601 calculator, which has a digital display screen, was used to manually notate the flow rates. EKM-353EDM-N electrical meters, manufactured by EKM Metering, were used to collect data on the power unit net power and pump power consumption. The electrical meter manufacturer had custom software

which was used to measure real-time electrical power; these data were stored in text format at 30 second intervals for future data reduction.

Data acquisition and control (DAQ) functions for temperature and pressure measurement were done using the LabView virtual instrument program (VI), operating on a National Instruments (NI) PCI-MIO-16E module. LabView VI software was used to read the real-time data and store it at one second intervals in a Microsoft Excel format for future data reduction. For temperature measurement, an NI SCXI-1120 analog input board was used. For pressure measurement, an NI SCXI-1121 analog input board and a SCXI-1320 accessory were used.

3.8 Computational Method

This section presents the mathematical expressions and methodology used to obtain the derived parameters from measured parameters; this will be useful for modeling a screw expander. For the data reduction process, all measured parameters are averaged over a 30 minute data sampling period after the system has reached a steady-state condition for the hot water flow rate and temperature and the cold water flow rate and temperature, as discussed in Section 3.6 above. Temperatures and pressures were sampled at one second frequencies; electrical power data were sampled at 30 second intervals; flow rate data were notated manually from the flow meter display screen.

The ORC power unit net power output (W_{net}) and the ORC pump power consumption (W_{pump}) are measured parameters (see Figure 3.1 and Table 3.2). Therefore, the screw expander power output (W_{SE}), in kW, is estimated as,

$$W_{SE} = W_{net} + W_{pump} \tag{3.14}$$

$$w_{SE} = \frac{W_{SE}}{\dot{m}_R} \tag{3.15}$$

In Eq. (3.15), the screw expander work output (w_{SE}) in kJ/kg is used in model-I and model-II, discussed above, and $\dot{m}_R$ is the refrigerant mass flow rate in kg/s. Screw expander isentropic efficiency (η_S) is expressed as the ratio of the screw expander work output (w_{SE}) and the isentropic work output (w_S).

3.8.1 Refrigerant Mass Flow Rate ($\dot{m}_R$)

From the schematic of the ORC cycle (Figure 3.1), it can be inferred that there is no flow meter installed to measure the R245fa flow rate. The refrigerant mass flow rate was estimated

using the energy balance on the hot water side (heating fluid side) of the ORC system, which is given by Eq. (3.16) as,

$$\dot{m}_R = \frac{\eta_h \times [(\dot{V}_h/3600) \times \rho_h \times (h_6 - h_8)]}{(h_4 - h_2)} \tag{3.16}$$

Here, η_h is the efficiency of heat transfer from hot water to refrigerant R245fa in the evaporator and pre-heater, which is assumed as 95%, with a 5% heat loss to the environment. This is a reasonable assumption for brazed plate heat exchangers [19]. In Eq. (3.16), $\dot{m}_R$ is the refrigerant mass flow rate in kg/s, $\dot{V}_h$ is the hot water flow rate in m^3/h, h_6 and h_8 are hot water enthalpy at state-6 (supply) and state-8 (return) in kJ/kg, h_2 and h_4 are R245fa enthalpy at state-2 (pre-heater inlet) and state-4 (evaporator outlet) in kJ/kg. ρ_h is the average hot water density in kg/m^3, obtained at the hot water supply and return temperature. The NIST REFPROP 8.0 [17] program was used to read the thermodynamic properties of the respective fluids. Uncertainty in calculated $\dot{m}_R$ is discussed in the following section.

3.9 Uncertainty of Experimental Data for Reduced Parameters ($\dot{m}_R$, w_{SE}, and n_c)

To estimate the experimental uncertainty in refrigerant mass flow rate ($\dot{m}_R$), Eq. (3.16) is rewritten as Eq. (3.17), below, to avoid finding an expression for enthalpy in terms of temperature and pressure. $C_{p,h}$ is the average hot water specific heat in kJ/kg-K, obtained at the hot water supply and return temperature. $C_{p,R}$ is the average R245fa specific heat, in kJ/kg-K, obtained at state-2 (pre-heater inlet) and state-4 (evaporator outlet).

$$\dot{m}_R = \frac{\eta_h \times [(\dot{V}_h/3600) \times \rho_h \times C_{p,h}(T_6 - T_8)]}{C_{p,R}(T_4 - T_2)} \tag{3.17}$$

The experimental uncertainty in refrigerant mass flow rate can be determined from the standard approach presented by Coleman and Steele [20], which is given in Eq. (3.18). The parameters which we measured were the hot water volume flow rate ($\dot{V}_h$), hot water supply (T_6) and return (T_8) temperatures, and refrigerant pressures and temperatures at state-2 and state-4.

$$\frac{\delta \dot{m}_R}{\dot{m}_R} = \left[\left(\frac{\delta \dot{V}_h}{\dot{V}_h}\right)^2 + \left(\frac{\delta T_6}{T_6}\right)^2 + \left(\frac{\delta T_8}{T_8}\right)^2 + \left(\frac{\delta T_4}{T_4}\right)^2 + \left(\frac{\delta T_2}{T_2}\right)^2 \right]^{1/2} \tag{3.18}$$

The uncertainty in measurements of temperature for the type-k thermocouple used in this experiment was ±1.1°C (obtained from manufacturer data) between -200°C and 1250°C. This equates to a mean temperature of 86.5°C within the range of measurements for this experiment, $(\delta T/T)$ = 1.3%. The ultrasonic flow meter had an uncertainty in measurement $\left(\delta \dot{V}_h/\dot{V}_h\right)$ of 0.5% (Table 3.2). In Eq. (3.17), values for ρ_h, $C_{p,h}$ and $C_{p,R}$ were obtained with the NIST

REFPROP 8.0 [17] program for the respective fluids. Since these parameters were not measured in our experiment, they were not considered in this uncertainty analysis. Finally, combining all the uncertainties in Eq. (3.18), the uncertainty in estimating the refrigerant mass flow rate is $\left(\frac{\delta \dot{m}_R}{\dot{m}_R}\right) = 2.6\%$.

From Eq. (3.14) and Eq. (3.15), the uncertainty in screw expander work output (w_{SE}) is $\frac{\delta w_{SE}}{w_{SE}} = \left[\left(\frac{\delta W_{net}}{W_{net}}\right)^2 + \left(\frac{\delta W_{pump}}{W_{pump}}\right)^2 + \left(\frac{\delta \dot{m}_R}{\dot{m}_R}\right)^2\right]^{1/2}$. Combining the uncertainties in electrical meters (Table 3.2) and refrigerant mass flow rate, the uncertainty in screw expander work output $\left(\frac{\delta w_{SE}}{w_{SE}}\right)$ = 2.7%.

To estimate the uncertainty of the polytropic exponent (n_c), Eq. (3.8) is re-written and is given by Eq. (3.19) below. The uncertainty of the polytropic exponent $\left(\frac{\delta n_c}{n_c}\right)$ is given by Eq. (3.20).

$$n_c = \frac{w_{SE}}{w_{SE} - P_4 v_4 + P_5 v_5} \tag{3.19}$$

$$\frac{\delta n_c}{n_c} = \left[2\left(\frac{\delta w_{SE}}{w_{SE}}\right)^2 + \left(\frac{\delta P_4}{P_4}\right)^2 + \left(\frac{\delta v_4}{v_4}\right)^2 + \left(\frac{\delta P_5}{P_5}\right)^2 + \left(\frac{\delta v_5}{v_5}\right)^2\right]^{1/2} \tag{3.20}$$

As the relation of the specific volume of refrigerant R245fa is not known with respect to pressure and temperature, the uncertainty in refrigerant specific volume $\left(\frac{\delta v}{v}\right)$ is taken as 1%, which is the uncertainty in prediction of specific volume by the NIST REFPROP 8.0 [17], obtained from the fluid information section of the program for R245fa. Uncertainty in pressure measurement is given in Table 3.2. Combining all the uncertainties in Eq. (3.20), the uncertainty in the polytropic exponent $\left(\frac{\delta n_c}{n_c}\right)$ = 4%.

3.10 Results and Discussion

Figure 3.4, Figure 3.5 and Figure 3.6 show the experimental data with respect to pressure ratio (r_p), for volume ratio (r_v), refrigerant mass flow rate ($\dot{m}_R$), screw expander supply pressure (P_4), screw expander power output (W_{SE}) and isentropic efficiency of the screw expander (η_S). Extensive experimental data are given in Figure 3.4 to Figure 3.6 as comparison for future researchers working on screw expanders. In finding the curve-fitting coefficients of model-I and model-II, discussed above, the DataFit program [16] was used for regression analysis. One important thing to note in the presented analysis is that only 50 experimental data points (from a

total of 100 data points as stated in Section 3.6 above) were used to curve-fit both models; all 100 data points were used to check for goodness of fit. For example, in curve-fitting of Eq. (3.9) for the polytropic exponent in the proposed model-I, the experimental data of 50 cases covering the whole r_p range was selected and used to find the curve-fitting coefficients A, B, and C; all 100 experimental data points were used to check the percentage of error in the predicted polytropic exponent values, compared to the polytropic exponent calculated from experimental data. A similar type of analysis was done for the model-II, that is 50 experimental data points were used for curve-fitting and all 100 data points were used to check for goodness of fit.

For the proposed model-I, screw expander performance based on the polytropic exponent, the curve-fitting coefficients for Eq. (3.9) were evaluated using regression analysis as A = 6.0364, B = –10.2929, and C = 5.2598, with a coefficient of determination (R^2) of 0.97; Eq. (3.9) becomes,

$$n_c = 6.0364\left(\frac{\ln(r_p)}{\ln(r_v)}\right) - 10.2929\left(\frac{\ln(r_p)}{\ln(r_v)}\right)^2 + 5.2598\left(\frac{\ln(r_p)}{\ln(r_v)}\right)^3 \quad (3.21)$$

Eq. (3.21) is valid for refrigerant R245fa with $2.70 \leq r_p \leq 6.54$ and $2.54 \leq r_v \leq 6.20$, and with the refrigerant inlet to the screw expander is saturated/superheated vapor condition. It should be noted that in all cases of experimental data, the expander inlet (state-4) and expander outlet (state-5) refrigerant condition was superheated vapor. Figure 3.7 and Figure 3.8 show the results of screw expander modeling based on the polytropic exponent (model-I). From Figure 3.7, the predicted polytropic exponent values using Eq. (3.21) were within ±1% of the polytropic exponent, based on experimental data. Figure 3.8 shows that the predicted screw expander power output using Eq. (3.8) and Eq. (3.21) were within ±10% of the experimental power output values.

For the proposed model-II, screw expander performance based on isentropic work output, the curve-fitting coefficients for Eq. (3.11) were evaluated using regression analysis as L = 10176.6515, M = –2877.4007, N = 291.0713, O = –11.7825 and P = 0.1874, with coefficient of determination (R^2) of 0.97; Eq. (3.11) becomes,

$$w_{SE,o} = 10176.6515 * w_{s,o}^4 - 2877.4007 * w_{s,o}^3 + 291.0713 * w_{s,o}^2 - 11.7825 * w_{s,o} + 0.1874 \quad (3.22)$$

Eq. (3.22) is valid for refrigerant R245fa with $424.4\text{kPa} \leq P_4 \leq 1027.3\text{kPa}$ and $10\text{kW} \leq W_{SE} \leq 51.5\text{kW}$, and with refrigerant inlet to screw expander is saturated/superheated vapor condition. Figure 3.9 shows that the predicted screw expander power output using Eq. (3.22) is within ±7.5% of the experimental power output value.

From the above results it can be inferred that model-II gives a better prediction for screw expander power output than model-I. In predicting screw expander power output, model-I uses four measurement parameters vis-a-vis screw expander inlet and outlet temperatures and pressures (in Eq. (3.21) and Eq. (3.8)), whereas model-II uses three measurement parameters vis-a-vis screw expander inlet temperature and pressure (for determining enthalpy of state-4) and outlet pressure (for determining the isentropic enthalpy to state-5). In general, the fewer the parameters used, the smaller the equipment uncertainty introduced in the prediction. Moreover, model-I involves two computation steps to find the n_c , using Eq. (3.21) and the screw expander work output using Eq. (3.8); in model-II, work output is directly derived from isentropic work using Eq. (3.22).

In general, in a practical application if we have to choose a model for screw expander in developing a theoretical model for whole ORC system, model-II is a better choice over model-I for the following reason. When modeling an ORC system, the available parameters would generally be heat source and cooling source temperatures and flow rates. From the heat source temperature and heat availability, the expander inlet condition can be estimated, based on the evaporator and pre-heater model (i.e., state-4 can be determined in Figure 3.1). From the cooling source temperature, the saturation temperature of refrigerant can be determined based on heat exchanger pinch point analysis, the pressure of refrigerant at that saturation temperature can be determined, and this will be the expander outlet pressure (state-5 in Figure 3.1). For model-II, as explained in Section 3.5.2 above, the isentropic work output requires obtaining the enthalpy of refrigerant at the expander inlet and the isentropic enthalpy at the expander exit pressure. In model-I, volume ratio (r_v) requires determining the expander exit specific volume (v_5 in Eq. (3.2)) which, for single phase fluids, is determined by the measureable refrigerant properties of pressure and temperature. Therefore in model-I apart from knowing the expander exit pressure we also need to know the expander exit temperature to predict the screw expander performance.

3.11 Conclusions

In the work presented, experimental data were collected for a screw expander that was part of a 50kW ORC system test. Experimental setup, instrumentation, data collection, and data processing procedures are also briefly discussed. Experimental data from the screw expander were used to develop two empirical models for estimating screw expander performance. The first empirical model was based on the polytropic process, in which the regression curve-fitting

expression for the polytropic exponent with respect to the expander pressure ratio (r_p) and volume ratio (r_v) was fitted; this was used for power output estimation. In the second empirical model, the non-dimensional form of the screw expander work output was fitted with respect to the non-dimensional form of the isentropic work output. Brief conclusions for this work are listed below.

1. In the first curve-fitting model (model-I) for a screw expander based on the polytropic process, the predicted polytropic exponent values using a curve-fitting equation were within ±1% and screw expander power output values were within ±10% when compared to the experimental data.
2. In the second curve-fitting model (model-II) for screw expander-based isentropic work output, the predicted screw expander power output values were within ±7.5% when compared to experimental data.
3. The curve-fitting model based on the isentropic work output better predicted screw expander performance over the model based on the polytropic process.
4. As explained in Section 3.10, the screw expander model based on isentropic work has a more general application, such as in the theoretical modeling of the whole ORC system, than the polytropic exponent model. In the isentropic model (model-II), the parameters used are the screw expander inlet enthalpy (state-4) and exit pressure (usually the condenser pressure determined from cooling source temperature). In the polytropic exponent model, we need to know the pressure and temperature, which is possible only when the expander exit is in single phase condition, in order to determine the expander exit (state-5) specific volume.

3.12 Acknowledgments

The authors gratefully acknowledge the financial support provided by the Alaska Energy Authority, the Denali Commission, and the Alaska Department of Environmental Conservation. The authors would also like to thank Gwen Holdmann, Brent Sheets and Ross Coen from the Alaska Center for Energy and Power (ACEP) for providing the managerial support necessary for this project to be completed on time. The authors further acknowledge ACEP for providing the tools and equipment to install the experimental unit, the UAF Power Plant for providing lab space to conduct the experiment, and UAF Facilities Services for providing personnel to install tough and heavy components.

3.13 References

[1] Lin, C.S., "Capture of heat energy from diesel engine exhaust," Final report prepared for National Energy Technology Laboratory, DOE Award # DE-FC26-01NT41248, November, 2008.

[2] Kaneko, T. and Hirayama, N., "Study of fundamental performance of helical screw expanders," The Japan Society of Mechanical Engineers, Vol.28 (243), pp.1970-1976, 1985.

[3] Ng, K.C., Bong, T.Y., and Lim, T.B., "A thermodynamic model for the analysis of screw expander performance", Journal of Heat Recovery Systems & CHP, Vol.10 (2), pp.119-133, 1990.

[4] Smith, I.K, Stosic, N., and Aldis, C., "Trilateral flash cycle system – A high efficiency power plant for liquid resources," Proceedings of World Geothermal Congress, 1995.

[5] Smith, I.K., Stosic, N., and Kovacevic, A., "Screw expanders increase output and decrease the cost of geothermal binary power plant systems," Transactions of Geothermal Resource Council, 2005.

[6] Birdsville organic Rankine cycle geothermal power station. http://www.ergon.com.au/__data/assets/pdf_file/0008/4967/EGE0425-birdsville-geothermal-brochure-r3.pdf. Accessed June 28th 2012.

[7] Quoilin, S., "Experimental study and modeling of a low temperature Rankine cycle for small scale cogeneration," Master's Thesis, University of Liege, May 2007.

[8] Reid, A.D., "Low temperature power generation using HFE-7000 in a Rankine cycle," Master's Thesis, San Diego State University, July 2010.

[9] Johnston, J.R., "Evaluation of expanders for use in a solar-powered Rankine cycle heat engine," Master's Thesis, The Ohio State University, 2001.

[10] Aoun, B. and Clodic, D.F., "Theoretical and experimental study of an oil-free scroll vapor expander," International Compressor Engineering Conference, Purdue, July 14-17, 2008.

[11] Yamamoto, T., Furuhata, T., Arai, N., and Mori, K., "Design and Testing of the Organic Rankine Cycle," Journal of Energy, Vol.26, pp. 239-251, 2001.

[12] Kang, S.H., "Design and experimental study of ORC (organic Rankine cycle) and radial turbine using R245fa working fluid," Journal of Energy, Vol.41, pp.514-524, 2012.

[13] Avadhanula, V. K., Lin, C. S., and Johnson, T., "Testing a 50kW ORC at Different Heating and Cooling Source Conditions to Map the Performance Characteristics," SAE Technical Paper # 2013-01-1649, April 2013.

[14] Margolis, D.L., "Analytical modeling of helical screw turbines for performance prediction," ASME Journal of Engineering for Power, Vol.100, pp.482-487, July 1978.

[15] Taniguchi, H., Kudo, K., Giedt, W.H., Park, I., and Kumazawa, S., "Analytical and experimental investigation of two-phase flow screw expanders for power generation," Journal of Engineering for Gas Turbines and Power, Vol.110, pp.628-635, October 1988.

[16] DataFit: Data curve-fitting (nonlinear regression) and data plotting software, Version 9.0.59, Oakdale Engineering, Oakdale, PA, 2011. Available from http://www.curvefitting.com.

[17] Lemmon, E.W., Huber, M.L., and McLinden, M.O., "NIST Standard Reference Database 23: Reference Fluid Thermodynamic and Transport Properties-REFPROP," Version 8.0, National Institute of Standards and Technology, Standard Reference Data Program, Gaithersburg, 2007.

[18] Cengel, Y.A. and Boles, M.A., "Thermodynamics: An engineering approach," Fifth edition, The McGraw-Hill Publishing Companies, Inc., New York, 2006.

[19] Muley, A. and Manglik, R.M., "Experimental study of turbulent flow heat transfer and pressure drop in a plate heat exchanger with chevron plates," Transactions of ASME Journal of Heat Transfer, Vol.121, pp.110-117, February 1999.

[20] Coleman, H.W. and Steele, W.G., "Experimentation and Uncertainty Analysis for Engineers," Second edition, John Wiley & Sons, Inc., New York, 1999.

Table 3.1 Various hot water and cold water flow rates and temperatures at which the power unit was tested

Hot water temperatures, °C (°F)	Hot water flow rate, m^3/h (gpm)	Cold water temperatures, °C (°F)	Cold water flow rate, m^3/h (gpm)
68.3 (155)	27.2 (120)	10 (50)	27.2 (120)
79.4 (175)	36.3 (160)	20 (68)	36.3 (160)
90.5 (195)	45.4 (200)		45.4 (200)
101.7 (215)	56.8 (250)		
107.2 (225)	68.1 (300)		

Table 3.2 Parameters measured, instrumentation and uncertainty in measurement

Parameter	State point on Figure 3.1	Instrumentation	Units	Uncertainty in measurement
Hot water supply temperature	T_6	Omega type-K thermocouple	°C	±1.1°C
Hot water return temperature	T_8	Omega type-K thermocouple	°C	±1.1°C
Hot water flow rate	$\dot{V}_6 = \dot{V}_8 = \dot{V}_h$	Kamstrup Ultraflow ultrasonic flow meter	m^3/h	0.5%
Refrigerant R245fa temperature – inlet to pre-heater	T_2	Omega type-K thermocouple	°C	±1.1°C
Refrigerant R245fa pressure – inlet to pre-heater	P_2	ST1500 Pressure transducer	kPa	0.2%
Refrigerant R245fa temperature – outlet of evaporator or inlet to expander	T_4	Omega type-K thermocouple	°C	±1.1°C
Refrigerant R245fa pressure – outlet of evaporator or inlet to expander	P_4	ST1500 Pressure transducer	kPa	0.2%
Refrigerant R245fa temperature – outlet of expander	T_5	Omega type-K thermocouple	°C	±1.1°C
Refrigerant R245fa pressure – outlet of expander	P_5	ST1500 Pressure transducer	kPa	0.2%
ORC power unit net power	$W_{net} = W_{11}$	EKM-353EDM-N	kW	0.5%
ORC pump power	$W_{pump} = W_{12}$	EKM-353EDM-N	kW	0.5%

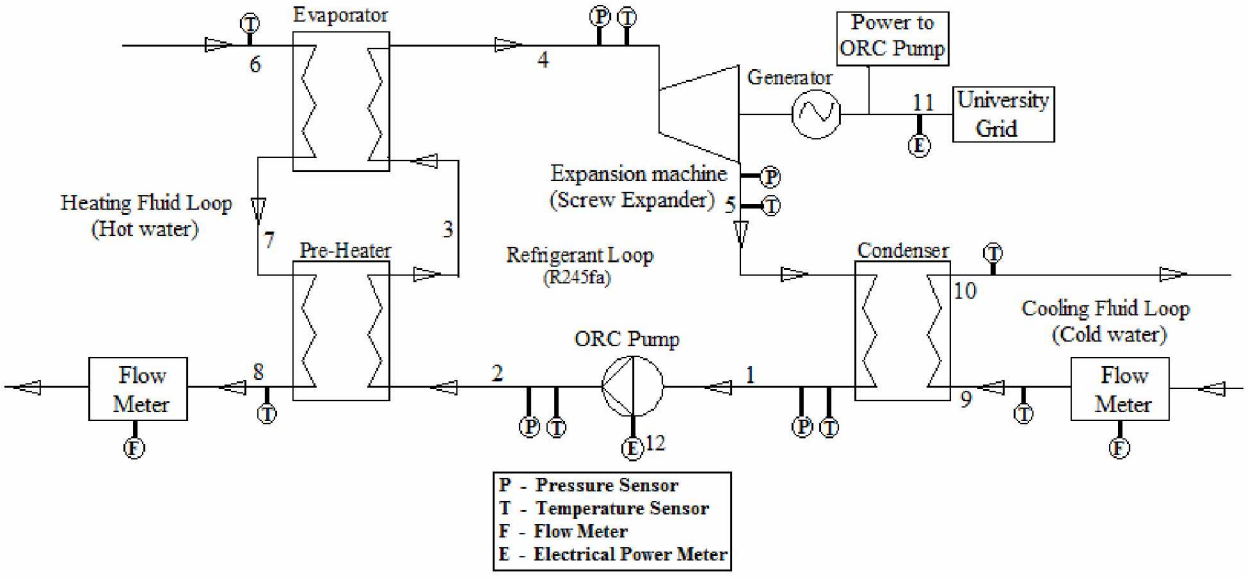

Figure 3.1 Schematic of organic Rankine cycle

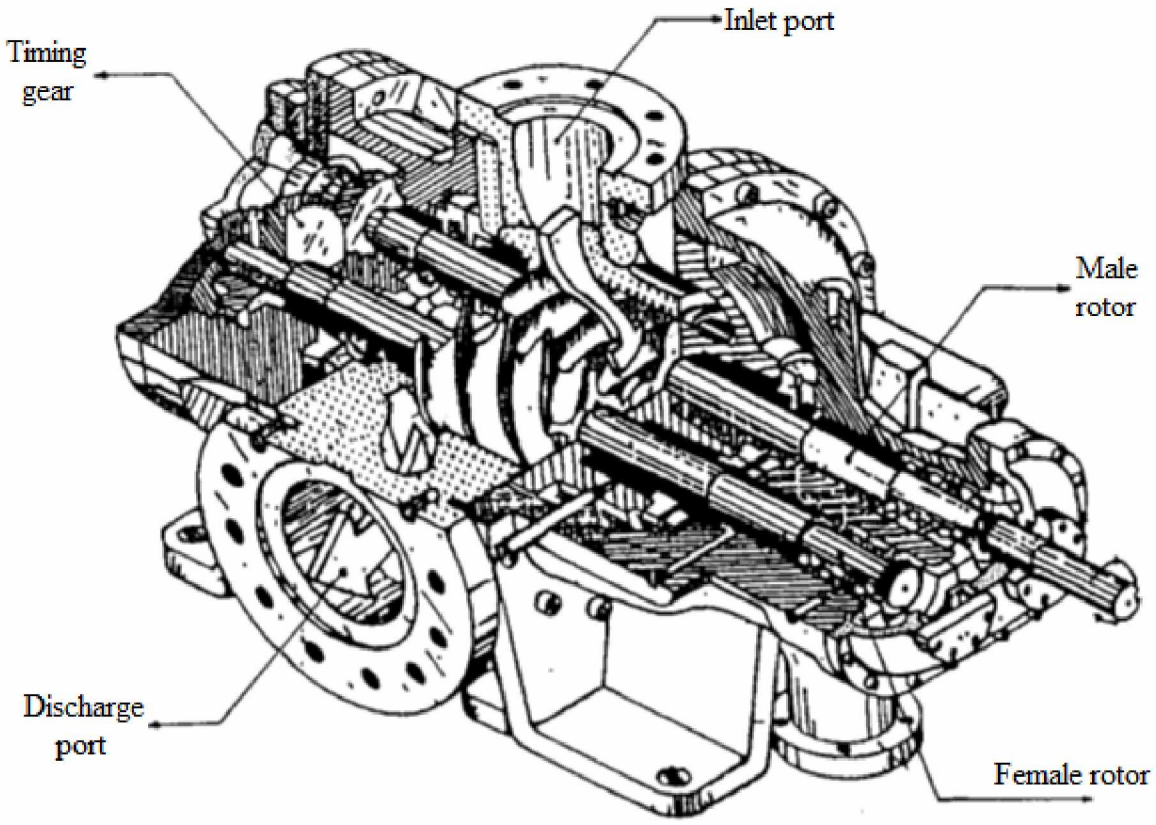

Figure 3.2 Schematic of screw expander with main components labeled [3]

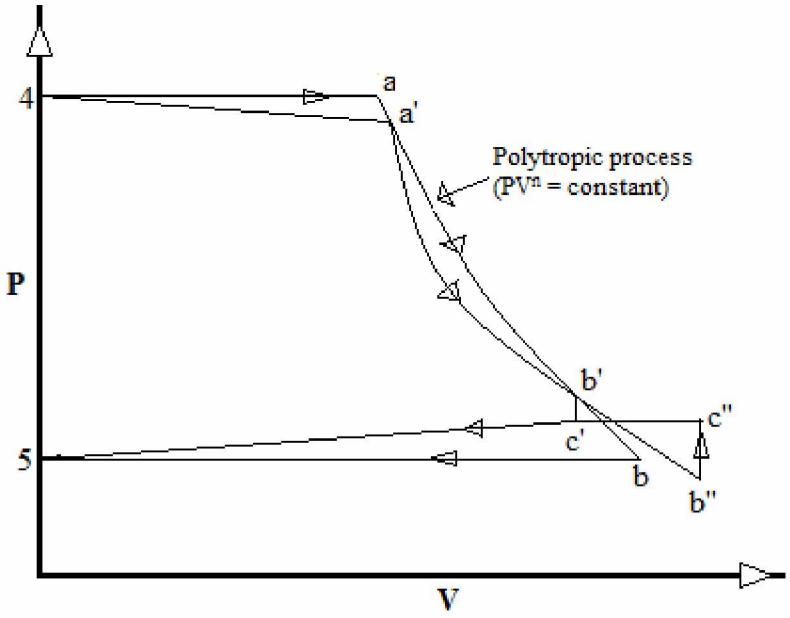

Figure 3.3 Expansion path for ideal polytropic expansion process (4-a-b-5), expansion path with blowdown (4-a'-b'-c'-5), and expansion path with blowback (4-a'-b"-c"-5)

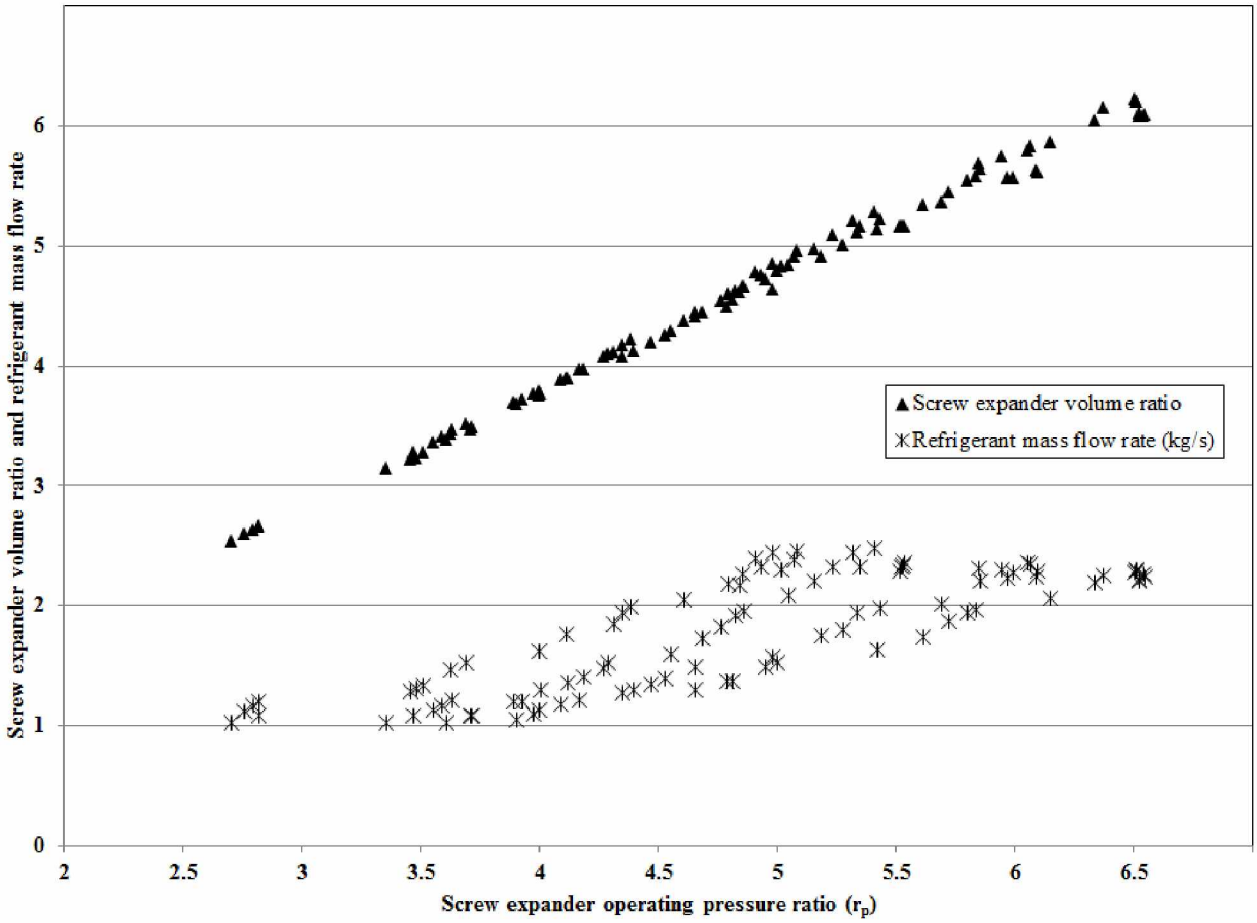

Figure 3.4 Screw expander volume ratio (r_v) and refrigerant mass flow rate with respect to screw expander pressure ratio (r_p)

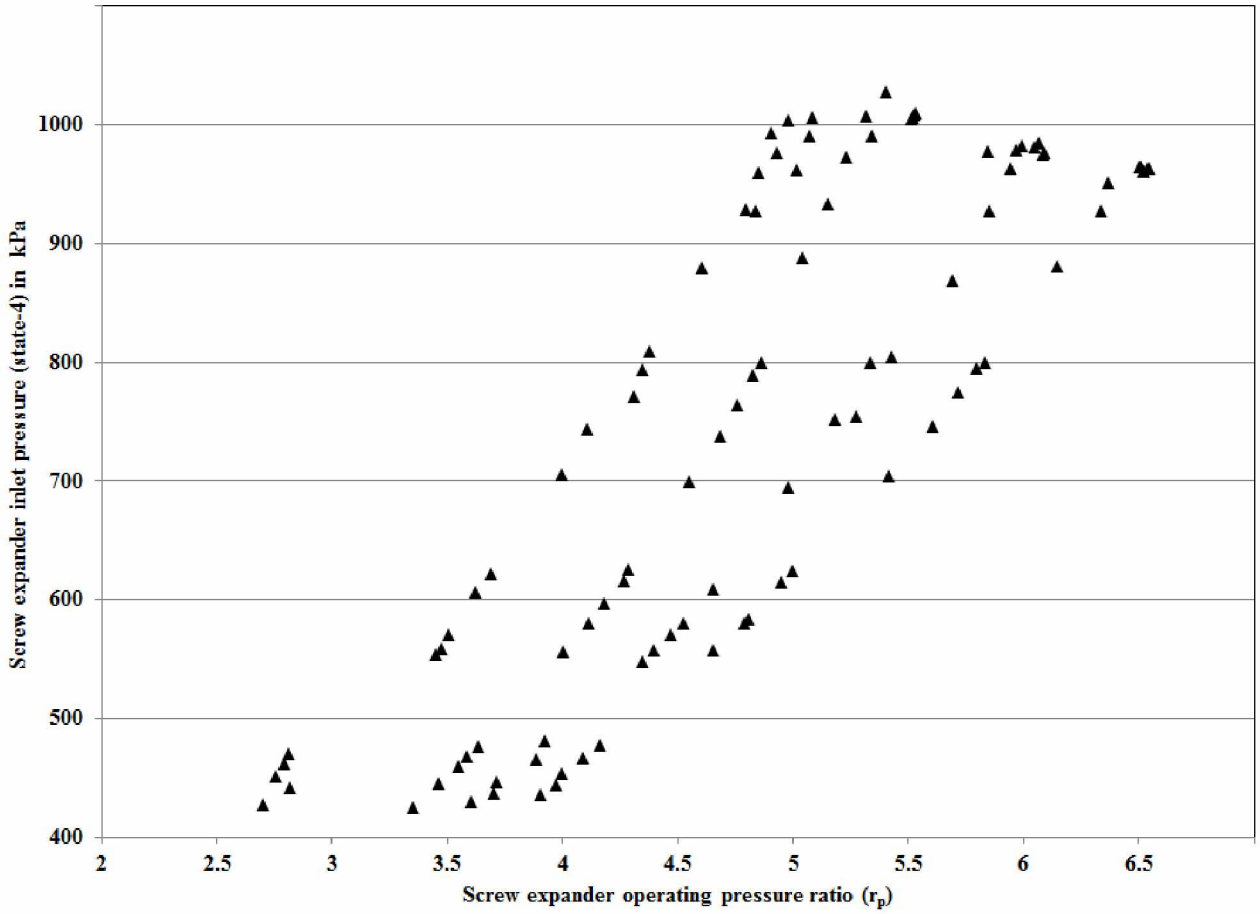

Figure 3.5 Screw expander inlet pressure (state-4) with respect to screw expander pressure ratio (r_p)

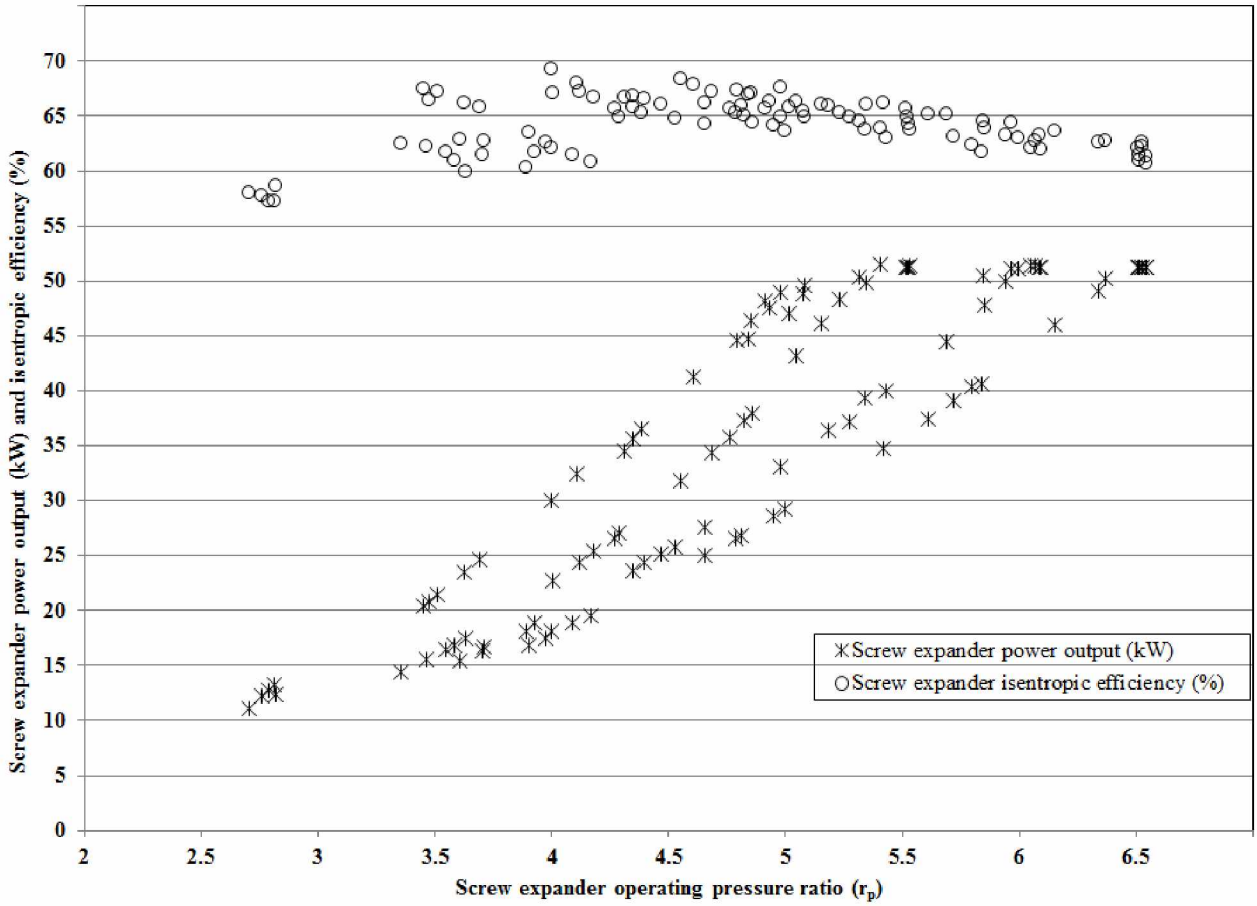

Figure 3.6 Screw expander power output ($\boldsymbol{W_{SE}}$) and isentropic efficiency ($\boldsymbol{\eta_S}$) with respect to screw expander pressure ratio (r_p)

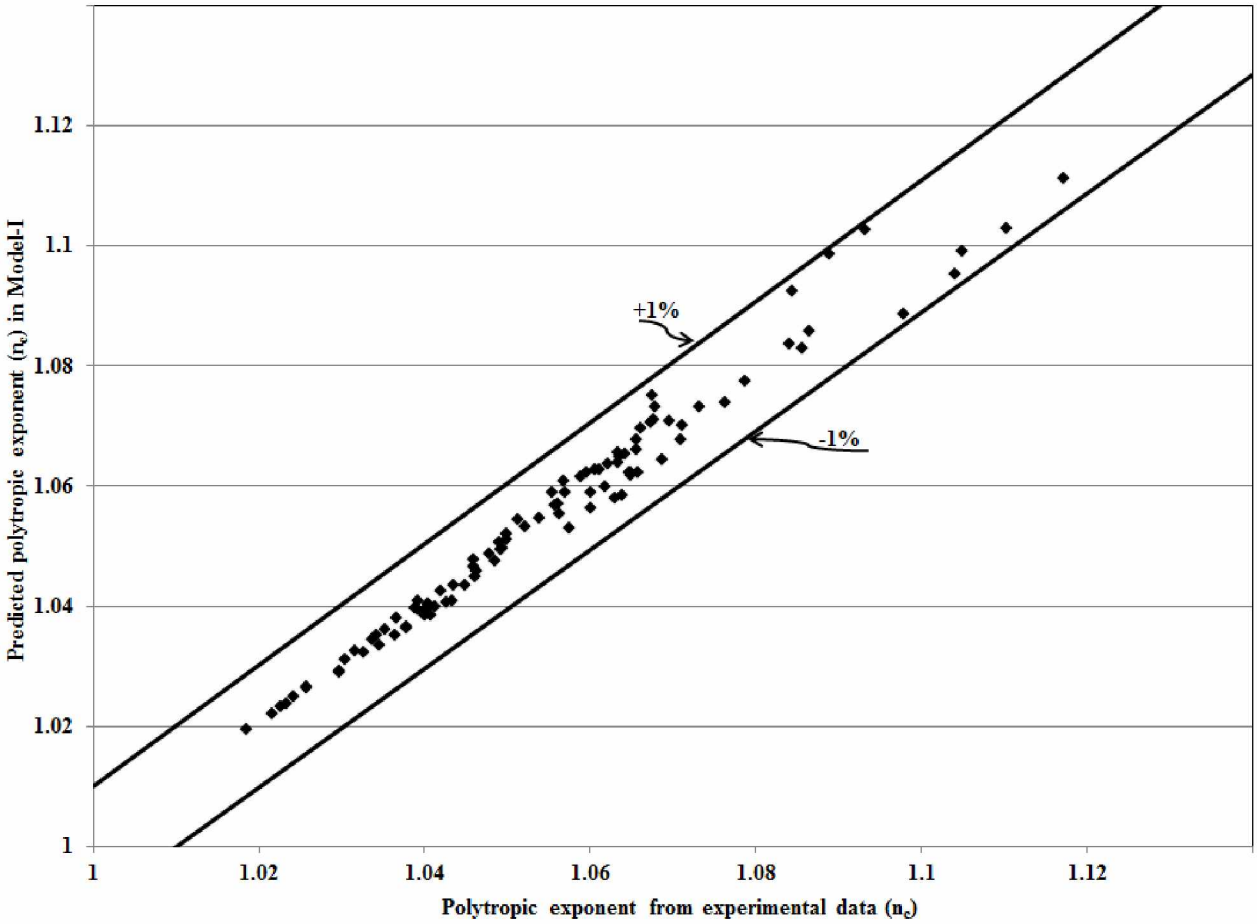

Figure 3.7 Comparison of predicted data with experimental data for polytropic exponent (n_c) in Model-I

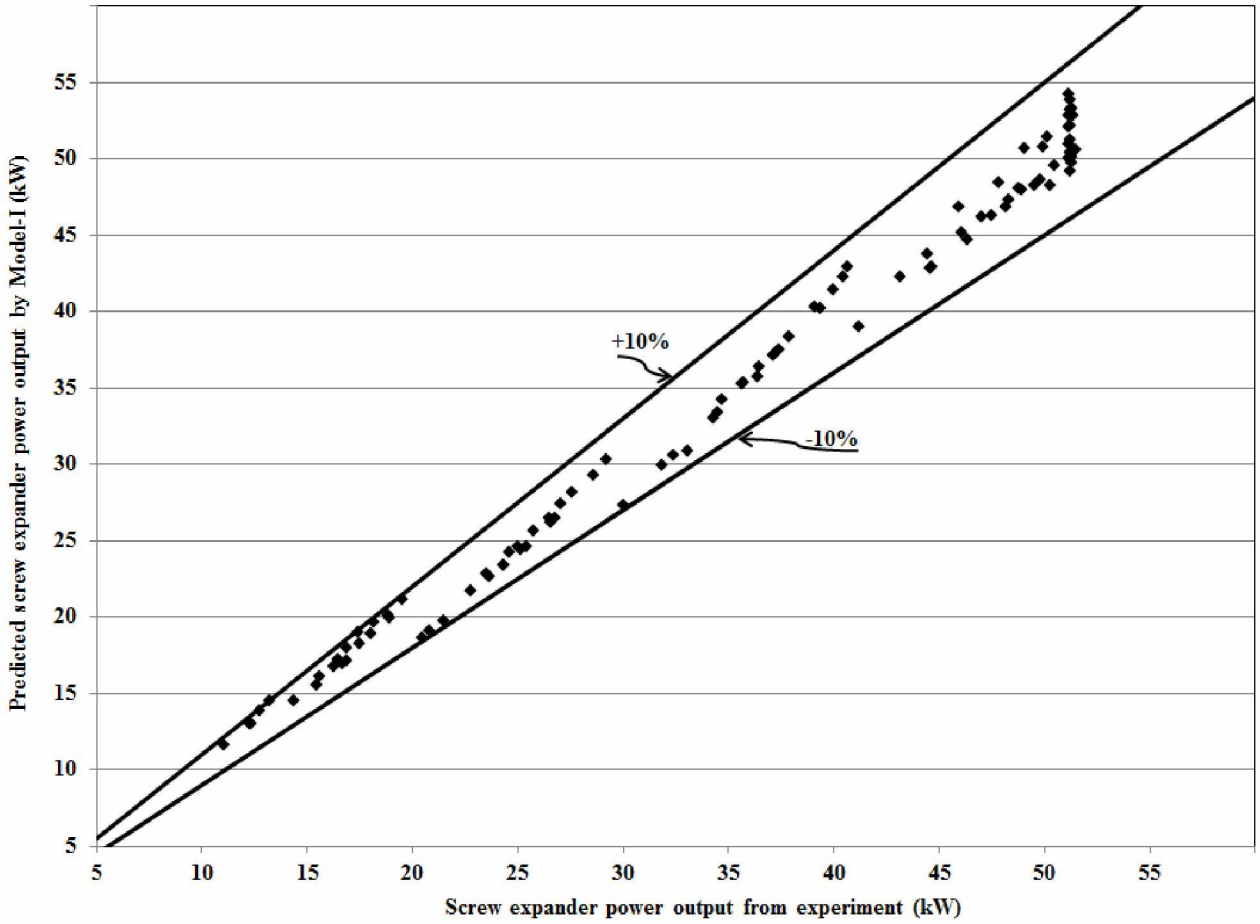

Figure 3.8 Comparison of predicted data with experimental data for screw expander power output ($\boldsymbol{W_{SE}}$) in Model-I

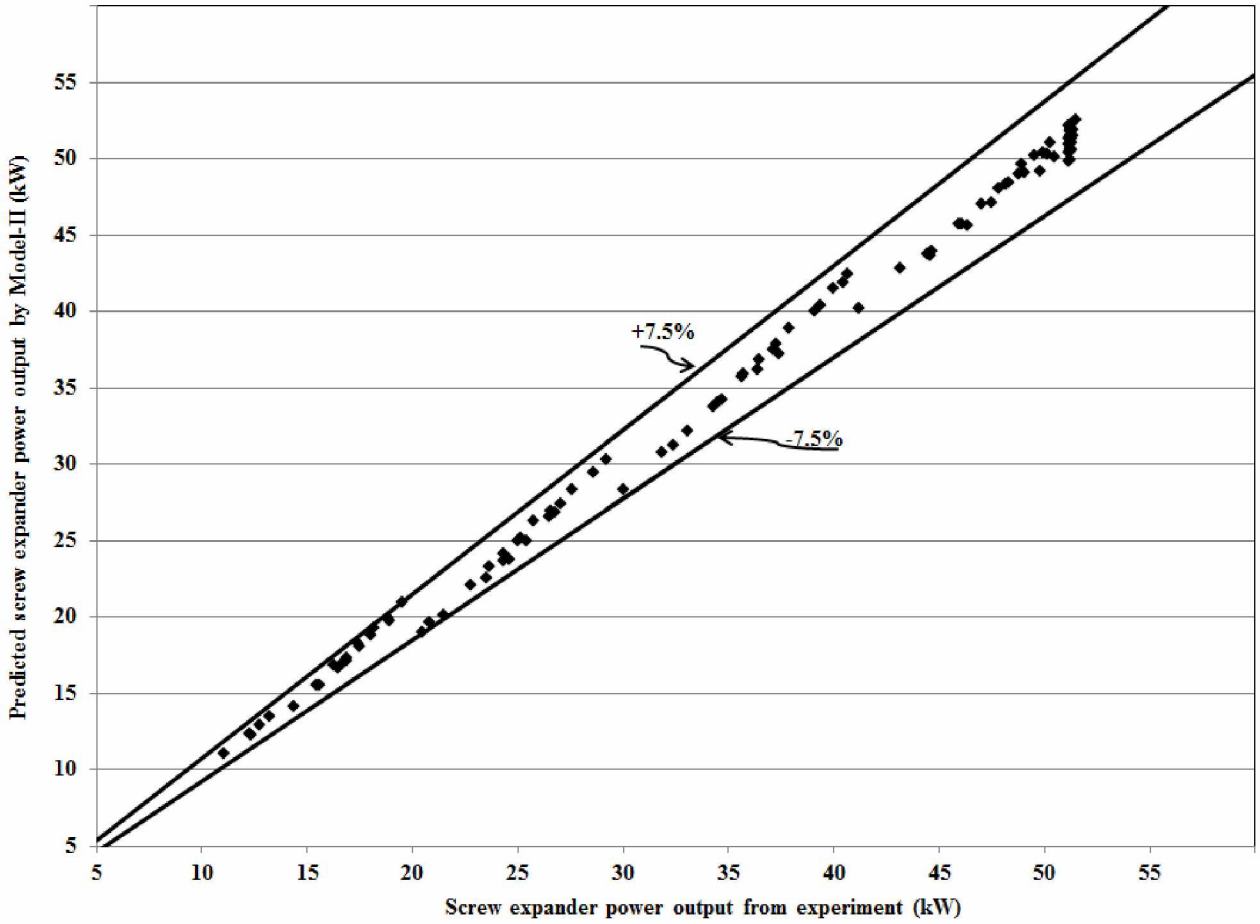

Figure 3.9 Comparison of predicted data with experimental data for screw expander power output ($\boldsymbol{W_{SE}}$) in Model-II

Chapter 4. Heat Transfer Correlations for R245fa in Preheater, Evaporator, and Condenser using Experimental Data from 50 kW Organic Rankine Cycle (ORC) System Testing*

4.1 Abstract

This paper presents the experimental results pertaining to single-phase, evaporation, and condensation heat transfer of R245fa in the preheater, evaporator, and condenser of a 50 kW ORC system testing. The experimental data used in this study were part of testing a 50 kW ORC system for different hot water and cold water conditions. The preheater, evaporator, and condenser are brazed plate heat exchangers (BPHEs) in this study. For single-phase heat transfer in the preheater, a Dittus-Boelter type of correlation was developed for R245fa and hot water. The correlation for hot water from the preheater analysis was used to obtain hot water and cold water heat transfer coefficient values in the evaporator and condenser from respective experimental data. For R245fa evaporation in BPHEs, two correlations were developed based on two-phase equation formats given by NIST [1] and Jokar et al. [2]. Predicted R245fa evaporation heat transfer data based on NIST [1] is within an error of –12.3% and +16.5% and on Jokar et al. [2] within an error of ±13.7% when compared with experimental data. Nucleate boiling was found to be the dominant heat transfer regime in the evaporator. The proposed correlation for condensation of R245fa in the condenser was based on the correlation format given by Jokar et al. [2] and Hayes et al. [3], and 95% of predicted heat transfer values were within an error range of ±25% when compared with experimental data.

4.2 Keywords

Brazed plate heat exchanger, single-phase, evaporation, condensation, R245fa, heat transfer correlation, organic Rankine cycle

4.3 Nomenclature

t = thickness of the plate (m)

P = pressure (MPa)

P_c = R245fa critical pressure (MPa)

T = temperature (^{o}C)

---

* Avadhanula, V.K., Lin, C.S., and Das, D.K., "Heat Transfer Correlations for R245fa in Preheater, Evaporator and Condenser using Experimental Data from 50 kW Organic Rankine Cycle (ORC) System Testing", Currently Under Review in Heat Transfer Engineering, May 2015.

x = quality (kg/kg)

W_1 and W_2 = plate width (m)

L_1 and L_2 = plate length (m)

b = mean channel spacing (m)

μ = dynamic viscosity (kg/m s)

Re = Reynolds number

Re_{eq} = equivalent Reynolds number

Pr = Prandtl number

A = heat transfer area of a heat exchanger (m^2)

A_f = Flow area in heat exchanger (m^2)

D_h = hydraulic diameter (=2b in m)

N_{ch} = number of channels on one fluid side in a BPHE

N_{th} = number of thermal plates in a BPHE

Nu = Nusselt number

G = mass flux (kg/m^2 s)

G_{eq} = equivalent mass flux (kg/m^2 s)

$\dot{m}$ = mass flow rate (kg/s)

h = enthalpy (kJ/kg)

C_p = specific heat (kJ/kg K)

U = overall heat transfer coefficient (W/m^2 K)

ΔT_{lm} = log-mean temperature deference (^oC)

ΔT = temperature difference (^oC)

Q = heat transfer rate (kW)

α = heat transfer coefficient (W/m^2 K)

k = thermal conductivity (W/m K)

Bo = boiling number

q'' = heat flux (kW/m^2)

ω = acentric factor

σ = surface tension (N/m)

ρ = density (kg/m^3)

$\dot{V}$ = volume flow rate (m^3/h)

X_{tt} = Martinelli parameter

Subscripts

f = saturated liquid condition

g = saturated vapor condition

ref = refrigerant R245fa

hw = hot water

cw = cold water

p = preheater

e = evaporator

c = condenser

exp = experimental

cal = calculated

sup = superheated

sub = sub-cooled

$boil$ = two-phase boiling

$cond$ = two-phase condensation

ij = property average of $state - i$ and $state - j$ (e.g., $C_{p,68} = (C_{p,6} + C_{p,8})/2$)

pm = plate material

avg = average

s = plate surface

4.4 Introduction

The use of BPHEs has increased greatly in recent years due to their smaller footprint in space-limited applications, their capacity to withstand higher pressure (30 bar to 45 bar), and developments in manufacturing techniques. Nowadays BPHEs find applications in almost all process industries where heat transfer fluids on either side are relatively clean. Due to proprietary concerns, physical parameters (such as plate width, plate thickness, chevron angle, and mean channel spacing) of BPHEs which provide major considerations in heat transfer correlations for these heat exchangers are not readily available from manufacturers or their catalogs. Wang, Sunden and Manglik [4] have done an extensive literature search and in their textbook have separate chapters for single-phase and two-phase (evaporative and condensation) thermal-

hydraulic analysis done by various authors on plate heat exchangers. The following paragraphs give a general literature review on plate heat exchanger application in single-phase, evaporative, and condensation heat transfer.

The application of gasket plate heat exchangers for single-phase flow has been widely used since the 1930s in pulp and paper, pharmaceutical, personal care and hygiene industries. Zahid Ayub [5] compiled, along with a brief historical background, an extensive literature review for thermal-hydraulic performance of plate heat exchangers in single-phase flow. Of the many researchers who have reported thermal-hydraulic performance of plate heat exchangers in single-phase flow, some of the noted ones are [6–16]. Almost all the researchers have reported a Dittus-Boelter [17] type of correlation for single-phase heat transfer and have classified the correlations based on plate chevron angle. Shah and Focke [18] tried to standardize gasket plate heat exchanger design and developed a step-by-step procedure for rating and sizing problems.

In the late 1970s, BPHEs were developed, and because of their capability to withstand high pressure, their use as two-phase heat transfer components steadily increased in refrigeration, air-conditioning, heat and power, and heat recovery industries, mainly as evaporators and condensers. Several heat transfer correlations for single-phase can be found in the open literature, but limited information is available regarding two-phase heat transfer. Of the studies available for two-phase heat transfer, many are for evaporative heat transfer; very few studies have been done on condensation. With little literature available for R245fa (the working fluid in the present study), most of the experimental work for evaporation and condensation in PHEs was done using R134a and R410a because of their ability to replace ozone depletion refrigerants.

Djordjevic and Kabelac [19] reported experimental results from testing R134a and ammonia in PHEs (with two different chevron angles) for flow boiling conditions. No heat transfer and pressure drop correlations were given, but the experimental results obtained were compared with heat transfer correlations available in the literature.

Wang et al. [20] did extensive experimental study on seven different plate heat exchangers for steam condensation. From the experimental results obtained, they suggested an iterative calculation procedure for steam condensation in PHEs, and finally heat transfer and pressure drop empirical correlations were presented with an agreement of ±20% with experimental data.

Jokar et al. [2] experimentally investigated the evaporation and condensation of R134a in three plate heat exchangers used in automotive refrigeration systems and compared the results

with the literature. They suggested heat transfer and pressure drop correlations for evaporation and condensation based on dimensional analysis done on experimental data. They also concluded that the conventionally used macro-channel correlations for mini-channel PHEs may not be valid. The proposed correlations were within an agreement of ±25% with experimental data. The same research team, Hayes et al. [3], studied the CO_2 condensation in three PHEs and proposed a heat transfer correlation similar to that of Jokar at al.[2], with an agreement of ±10% with experimental data.

Kuo et al. [21] experimentally investigated the condensation heat transfer and pressure drop of R410a in plate heat exchangers. They compared the experimental results with condensation correlations in the literature and finally proposed a correlation for condensation heat transfer and pressure drop with an agreement with experimental data of ±25%.

NIST [1] reported experimental results of testing R22, R290, R290/R600a mixture and R32/R152a mixture in BPHEs for evaporation and condensation. They compared their results with correlations available in the literature and proposed the only heat transfer correlation for evaporation and condensation with one equation for R22, R290 and R290/R600a mixture and another equation for R21/R152a mixture. The proposed correlations were within an agreement of ±25% with experimental data. In their report, they proposed many evaporator and condenser heat transfer correlation formats, which can be used by future researchers in developing two-phase heat transfer correlations for BPHEs.

Longo and Gasparella [22] reported experimental results of thermal-hydraulic testing of R134a, R410a, and R236fa in BPHEs for evaporation. No heat transfer and pressure drop correlations were given, but the results obtained were compared with heat transfer correlations available in the literature with an agreement of ±20%.

Kaiyong Hu et al. [23] reported experimental results of thermal-hydraulic performance of R245fa in a BPHE as an evaporator as part of ORC system testing. No heat transfer and pressure drop correlations were given; only the experimental results were presented.

From the above literature study, it can be observed that many heat transfer correlations for single-phase, evaporative, and condensation of fluids in BPHEs are from individual testing of heat exchangers and not from system-testing data (such as ORC, refrigeration system). Also, for refrigerant R245fa, limited data is available in the open literature for evaporation and condensation in BPHEs. In addition, many correlations available for two-phase heat transfer in

the open literature are based on a number of plates below 10 (with very few refrigerant channels), which does not represent industrial-scale units, where the number of plates is usually much greater than 20. In this study on the preheater, evaporator, and condenser with R245fa as heat transfer fluid, the authors tried to illuminate these areas of research. The methodology presented in this study may be used as a procedure to determine heat transfer correlations for BPHEs when physical parameters of the heat exchangers are unknown.

4.4.1 Present Work

In the work presented, the authors tested a 50kW ORC system, manufactured by ElectraTherm, Inc., with a twin screw expander as a power generating device. The ORC power unit was performance tested in a lab environment at the University of Alaska Fairbanks (UAF) for different heat source and heat sink conditions. For this testing, the heat source was hot water and the heat sink was cold water (see Section 4.6 below). During the lab experiment, in conjunction with collecting data for the ORC system (i.e., temperatures and flow rates on hot water and cold water loops, screw expander power output, and parasitic pump power consumptions), experimental data were also collected for the individual components of the ORC on the refrigerant loop (mainly the refrigerant pressures and temperatures at inlet and outlet of respective components), namely the preheater, evaporator, screw expander, working fluid pump, and condenser (Figure 4.1). In the present work, using the lab experimental data, correlations for convective heat transfer coefficients were developed for refrigerant R245fa in the preheater, evaporator, and condenser. In this ORC system, the preheater, evaporator and condenser are brazed plate heat exchangers. Throughout this paper, we will continue to refer to Figure 4.1(schematic of the ORC discussed) and Figure 4.2 (temperature versus flow path diagrams for preheater, evaporator and condenser) for clarification and to reference state points in the ORC process.

4.5 Methodology

This section mainly explains the methodology used to obtain heat transfer correlations for R245fa in the preheater, evaporator and condenser. Due to proprietary concerns, no information on geometric specification of the BPHEs used was available to the research group. In this section we also discuss the method to obtain physical parameters for heat exchangers used in this study.

From the schematic of the ORC cycle (Figure 4.1) it can be inferred that there is no flow meter installed on the refrigerant loop to measure R245fa flow rate. The refrigerant mass flow

rates were estimated using an energy balance on the hot water side (heating fluid side) of the ORC system. These were published in the authors' previous study on the screw expander [24] based on the same experimental data. For the reader's convenience, the refrigerant mass flow rate estimation procedure is given in Section 4.8.5. The same R245fa flow rates from the authors' previous study [24] will be taken for this heat exchanger analysis.

Below are the assumptions used in this BPHE study:

1. Heat loss of 5% in transferring heat from hot water to refrigerant in preheater and evaporator.
2. Refrigerant is in saturated liquid condition (x_3=0) at preheater exit.
3. No heat loss in condenser.
4. Major heat transfer in evaporator and condenser is due to latent heat of vaporization and condensation of R245fa in respective heat exchangers.
5. Pressure drop in the heat exchangers was considered negligible as no differential pressure measuring instrumentation was installed.

Applying energy balance for preheater experimental data, the quality of refrigerant at state-3 (preheater exit) ranged from 0.06 to 0.33. For simplicity in this analysis, saturated liquid condition is considered at preheater exit (second assumption above) with boiling and superheating taking place in evaporator. By using an energy balance for the preheater (or evaporator) with saturated liquid condition at preheater exit (i.e., x_3=0), the corresponding temperature of hot water at preheater inlet (T_{7f} in Figure 4.2) was calculated and will be explained in Section 4.8.2. Therefore, in the preheater, liquid refrigerant from the pump exit (state-2) is heated to saturated liquid condition (state-3f) using hot water exiting the evaporator (state-7f). In the preheater it is single-phase liquid-to-liquid heat transfer between hot water and refrigerant. Using the experimental data and simple computer code, a Dittus-Boelter [17] type of heat transfer correlation for hot water and refrigerant is found in the preheater analysis. The convective heat transfer correlation for hot water developed from the preheater analysis will be used in calculating hot water and cold water heat transfer coefficient values in the evaporator and condenser using the respective experimental data.

In the ORC system under consideration, for all the test-run cases, the evaporator exit condition (screw expander inlet condition) of R245fa is superheated vapor; no two-phase vapor/liquid mixture condition at state-4 was observed. In the evaporator, the saturated liquid from the preheater exit first goes through boiling (i.e., latent heat of vaporization) and then is

superheated to state-4. From the experimental data it was observed that on average more than 93% of heat transfer in the evaporator is due to latent heat of vaporization of R245fa with very little superheating region. Therefore, in the evaporator analysis a single expression for the evaporative heat transfer coefficient for refrigerant was found. This expression is valid for the whole evaporator and will be explained in Section 4.8.3.

In all test-run cases of the ORC system under consideration, the low-pressure refrigerant exiting the screw expander (state-5) is superheated vapor, and refrigerant exiting the condenser (state-1) is sub-cooled liquid: no two-phase vapor/liquid mixture conditions were observed at state-5 or state-1. Therefore, the condenser has three heat transfer zones: single-phase superheated, two-phase condensing, and single-phase sub-cooling zones. But from the experimental data it was observed that, on average more than 91% of heat transfer was due to latent heat of condensation of R245fa with little superheating and sub-cooling regions. Therefore in the condenser analysis a single correlation for condensation heat transfer coefficient for refrigerant was found also. This expression is valid for the whole condenser and will be explained in Section 4.8.4 below.

The necessary BPHE geometric parameters in the present analysis are mean channel spacing (b), plate thickness (t), number of plates, port-to-port width (W_2) and length (L_2) (see Figure 4.3). The BPHEs for the preheater, evaporator, and condenser in the ORC system studied were manufactured by Kaori Heat Treatment Co. By measuring the outer dimensions (W_1 and L_1 in Figure 4.3) and looking for a model that matches the measured dimensions in the manufacturer's catalog [25], the heat exchanger model for the preheater, evaporator, and condenser were determined as listed in Table 4.2. From the catalog, W_2 and L_2 (Figure 4.3) dimensions for each heat exchanger were noted (Table 4.2), which will be used in further analysis of the heat exchangers. The number of plates in each heat exchanger was manually counted and listed in Table 4.2.

BPHE mean channel spacing (b) of 0.002 m and plate thickness (t) of 0.0004 m was taken, which are widely used dimensional values in the literature [1, 2, 14, 21].

In the present study, the NIST REFPROP 9.1 [26] program was used to read thermodynamic and transport properties of water and refrigerant R245fa.

Wherever applicable, fluid properties are taken as average of respective state points i.e., for example, in single-phase R245fa heat transfer correlation in preheater (Eq. (4.13)), μ_{23f} in Re_{23f} is the R245fa dynamic viscosity which is the average of μ_2 at state-2 and μ_{3f} at state-3f.

4.6 Experimental Setup and Procedure

The purpose of this lab testing of the ORC power unit is to collect data which matches possible waste heat conditions from diesel engine generator sets. The ORC power unit was tested under controlled heating and cooling conditions at the UAF power plant, and data were collected as different diesel engine waste heat conditions were simulated. The schematic of the experimental setup for testing the 50 kW ORC power unit was presented in the authors' previous publication [27], where the power unit was tested by varying the heat source and heat sink supply conditions (i.e., temperature and flow rate) to estimate the performance characteristics.

Low-pressure saturated steam readily available from the UAF power plant was used as the heat source in the lab experiment. A secondary hot water loop, which exchanges heat with steam in a steam-to-hot water heat exchanger, was used to supply heat to the ORC power unit. Therefore the heat source for the ORC power unit was temperature- and flow rate-controlled hot water; the heat sink was cold water from a nearby fire hydrant, with a modification loop added for supply temperature and flow rate control as shown in in Figure 4.1; the heating fluid loop is the hot water loop and the cooling fluid loop is the cold water in the lab experiment. The power generated from the ORC power unit was uploaded to the UAF grid.

Figure 4.1 is a schematic line diagram of the present ORC machine, with all instrumentation components labeled for data collection. Refrigerant R245fa, which is non-flammable and has zero ozone depletion potential, was the working fluid for the ORC. It should be noted that in the experiment described here, the experimental setup was designed to test the ORC power unit as a whole, not specifically its components performance (screw expander, evaporator, preheater). Concurrent with the test of the ORC power unit under various hot and cold water supply conditions, steady-state data collection was carried out for various components of the ORC power unit (i.e., screw expander, evaporator, pre-heater, condenser, and pump). These experimental data were used to find overall heat transfer coefficient for the preheater, evaporator and condenser and there by develop heat transfer correlations for R245fa in respective heat exchangers.

Table 4.1 shows the hot water and cold water flow rate and temperature conditions under which the ORC power unit was tested. From Table 4.1, it can be inferred that the ORC power unit was tested under 150 different hot water and cold water supply conditions, 75 cases for cooling water at 10°C (50°F) and 75 cases for 20°C (68°F). During the actual testing, for a cold water inlet temperature of 20°C, only one stable cold water flow rate was obtainable for each specific hot water temperature and flow rate. This stability problem was not fully investigated, but may have resulted from the performance characteristics of the two manual control valves of the cooling water loop. Therefore, the ORC power unit was tested for a total of 100 cases instead of 150 cases (75 cases for cooling water at 10°C and 25 cases for 20°C). The reduced number of test cases for 20°C cooling water temperature may not critically affect the importance and applicability of the experiment results to achieve the goals of this project, because the effect of cooling water flow rate on system performance is relatively less than that of other input parameters (i.e., hot water temperature and flow rate and cold water temperature), described in [27] and [28].

After setting all four parameters (i.e., hot water and cold water flow rates and temperatures for one case), we waited approximately 30 minutes to attain a steady-state condition before collecting data. We collected data for 30 minutes at one set of hot water and cold water temperature and flow rates; this completed the test for one set of hot water and cold water flow rate and temperature. Using this procedure, we tested the ORC power unit under each hot water and cold water condition listed in Table 4.1. For each case of hot water and cold water flow rate and temperature, all steady-state measured parameters were averaged for the data reduction process, discussed in detail in the following sections.

4.7 Parameters Measured, Instrumentation and Data Collection

Table 4.3 gives the measured parameters used in this analysis. Temperatures and pressures at various state points (listed in Table 4.3) were measured using Omega type-K (Cr-Al) thermocouples and Stellar Technology's ST1500 pressure transducers. Temperature and pressure measurements were stored in an Excel spreadsheet format using the LabView VI program (see below). Kamstrup ULTRAFLOW ultrasonic flow meters were used to measure the hot water and cold water flow rates. The Kamstrup MULTICAL-601 calculator, which has a digital display screen, was used to manually notate the flow rates. Apart from above-listed parameters, electrical

data were also noted for the ORC net power output and pump power consumption using electrical meters [24].

In Table 4.3, hot water temperatures (state-6 and state-8 in Figure 4.1) and flow rate are used to estimate the refrigerant (R245fa) flow rate in the ORC system. Measured parameters in this section will be used in determining R245fa heat transfer coefficient correlations for the preheater, evaporator and condenser and will be discussed in Section 4.8 below.

Data acquisition and control (DAQ) functions for temperature and pressure measurement were done using the LabView virtual instrument program (VI), operating on a National Instruments (NI) PCI-MIO-16E module. LabView VI software was used to read the real-time data and store it at one second frequencies in a Microsoft Excel format for future data reduction. For temperature measurement, an NI SCXI-1120 analog input board was used. For pressure measurement, an NI SCXI-1121 analog input board and an SCXI-1320 accessory were used.

4.8 Computational Method

In this section we will quantitatively discuss the computation procedure used for preheater, evaporator and condenser analysis as discussed in Section 4.5 above and also expressions for general brazed plate heat exchanger parameters such as the heat transfer area, flow area, hydraulic diameter, Reynolds number will be presented.

4.8.1 General Formulas for Brazed Plate Heat Exchangers

Heat transfer area (A) for a heat exchanger is given by,

$$A = N_{th} \times (W_2 \times L_2) \tag{4.1}$$

The term $(W_2 \times L_2)$ is the projected area for one single plate. Hydraulic diameter, an important parameter in heat exchanger analysis, is calculated by,

$$D_h = 2b \tag{4.2}$$

Flow area (A_f) for a BPHE is given by,

$$A_f = N_{ch} \times (W_2 \times b) \tag{4.3}$$

Here, N_{ch} is the number of channels on one fluid side. Mass flux (G) and Reynolds number (Re) for a flowing fluid in the BPHE is given by,

$$G = \frac{\dot{m}}{A_f} \tag{4.4}$$

$$Re = \frac{GD_h}{\mu} \tag{4.5}$$

Combining Eq. (4.2), Eq. (4.3) and Eq. (4.4) into Eq. (4.5), Re reduces to the form,

$$Re = \frac{2\dot{m}}{\mu N_{ch} W_2} \tag{4.6}$$

In Eq. (4.1) to Eq. (4.6), wherever applicable, we will use suffix hw, cw, and ref for respective fluids of hot water, cold water and refrigerant R245fa followed by suffix p, e, and c to represent respective heat exchangers for preheater, evaporator and condenser.

4.8.2 Preheater Analysis

As shown in Figure 4.1 and Figure 4.2, in the preheater, the high pressure liquid refrigerant from pump exit (state-2) is heated to liquid/vapor condition (state-3) while extracting heat from hot water from state-7 to state-8. As discussed in Section 4.5, refrigerant quality at state-3 ranged from 0.06 to 0.33. For the purpose of simplicity in the present analysis, (single-phase heat transfer in the preheater), saturated liquid condition is considered at the preheater exit with boiling and superheating of R245fa taking place in the evaporator. Therefore in the preheater, the liquid refrigerant from pump exit (state-2) is heated to saturated liquid condition (state-3f in Figure 4.2). Using an energy balance on the preheater, the hot water temperature at state-7f in Figure 4.2 can be calculated by:

$$T_{7f} = T_8 + \frac{Q_{ref,p}}{0.95\dot{m}_{hw} C_{p,68}} \tag{4.7}$$

$Q_{ref,p}$ ($=\dot{m}_{ref}(h_{3f} - h_2)$) is the heat absorbed by R245fa in the preheater, and $Q_{hw,p}$ ($=\dot{m}_{hw} C_{p,68}(T_{7f} - T_8)$) is the heat supplied by hot water in the preheater. 0.95 in Eq. (4.7) and Eq. (4.8) represents 5% heat loss in the preheater from hot water to refrigerant (first assumption). Here T_8, h_{3f} ($f(P_3, x_3 = 0)$) and h_2 ($f(P_2, T_2)$) are from experimental data.

$$0.95\dot{m}_{hw} C_{p,68}(T_{7f} - T_8) = \dot{m}_{ref}(h_{3f} - h_2) \tag{4.8}$$

Average heat transferred between hot water and R245fa in the preheater, Q_p, is the average of $Q_{hw,p}$ and $Q_{ref,p}$. Q_p will be used in the heat transfer equation and is given by:

$$Q_p = U_{exp,p} A_p \Delta T_{lm,p} \tag{4.9}$$

$$\Delta T_{lm,p} = \frac{(T_{7f} - T_{3f}) - (T_8 - T_2)}{ln\left(\frac{T_{7f} - T_{3f}}{T_8 - T_2}\right)} \tag{4.10}$$

In Eq. (4.9), A_p is calculated by Eq. (4.1) and the log-mean temperature difference ($\Delta T_{lm,p}$) by Eq. (4.10). The experimental overall heat transfer coefficient ($U_{exp,p}$) values for the preheater were obtained using experimental data and Eq. (4.9). Using the plate heat exchanger analogy, the preheater overall heat transfer coefficient ($U_{cal,p}$) takes the form,

$$\frac{1}{U_{cal,p}} = \frac{1}{\alpha_{hw,p}} + \frac{t}{k_{pm}} + \frac{1}{\alpha_{ref,p}} \tag{4.11}$$

In the preheater, as discussed above in Section 4.5, it is single-phase liquid-to-liquid heat transfer and in Eq. (4.11) for hot water and refrigerant heat transfer coefficients ($\alpha_{hw,p}$, $\alpha_{ref,p}$), a Dittus-Boelter [17] type of correlation is considered which is given by,

$$Nu_{hw,p} = c_1\left(Re_{7f8}^{c_2}\right)\left(Pr_{7f8}^{c_3}\right) \tag{4.12}$$

$$Nu_{ref,p} = c_4\left(Re_{23f}^{c_5}\right)\left(Pr_{23f}^{c_6}\right) \tag{4.13}$$

In Eq. (4.12) and Eq. (4.13), the effect of temperature-dependent viscosity is neglected. c_1, c_2, c_3, c_4, c_5 and c_6 are correlation constants and D_h is the hydraulic diameter which is twice the channel spacing (b). Further discussion on developed correlations is presented in section 4.9.1 below.

4.8.3 Evaporator Analysis

As discussed in the Section 4.5, the saturated liquid refrigerant at state-3f from the preheater first goes through boiling resulting in latent heat of vaporization and then is superheated to state-4 while extracting heat from the hot water from state-6 to state-7f in the evaporator. For all the test run cases, the refrigerant evaporator exit condition was superheated vapor; no 2-phase liquid/vapor mixtures were observed at state-4.

In the evaporator, heat is absorbed by R245fa ($Q_{ref,e} = \dot{m}_{ref}(h_4 - h_{3f})$) while heat is supplied by hot water ($Q_{hw,e} = \dot{m}_{hw}C_{p,68}(T_6 - T_{7f})$), and their relation is given by Eq. (4.14). In Eq. (4.14), 0.95 represents 5% heat loss in the evaporator from hot water to refrigerant (first assumption). Here T_6, h_{3f} ($f(P_3, x_3 = 0)$) and h_4 ($f(P_4, T_4)$) are from experimental data.

$$0.95\dot{m}_{hw}C_{p,68}\left(T_6 - T_{7f}\right) = \dot{m}_{ref}(h_4 - h_{3f}) \tag{4.14}$$

Average heat transferred between hot water and R245fa in evaporator, Q_e, is the average of $Q_{hw,e}$ and $Q_{ref,e}$. Q_e will be used in the heat transfer equation and is given by,

$$Q_e = U_{exp,e}A_e\Delta T_{lm,e} \tag{4.15}$$

$$\Delta T_{lm,e} = \frac{Q_e}{\left(\frac{Q_{boil,e}}{\Delta T_{lm,boil,e}}\right)+\left(\frac{Q_{sup,e}}{\Delta T_{lm,sup,e}}\right)} \tag{4.16}$$

$$Q_{boil,e} = \dot{m}_{ref}(h_{3g} - h_{3f}) \tag{4.17}$$

$$\Delta T_{lm,boil,e} = \frac{(T_{6g} - T_{3g}) - (T_{7f} - T_{3f})}{ln\left(\frac{T_{6g} - T_{3g}}{T_{7f} - T_{3f}}\right)} \tag{4.18}$$

$$T_{6g} = T_{7f} + \frac{Q_{boil,e}}{0.95\dot{m}_{hw}C_{p,68}} \tag{4.19}$$

$$Q_{sup,e} = \dot{m}_{ref}(h_4 - h_{3g}) \tag{4.20}$$

$$\Delta T_{lm,sup,e} = \frac{(T_6 - T_4) - (T_{6g} - T_{3g})}{ln\left(\frac{T_6 - T_4}{T_{6g} - T_{3g}}\right)} \tag{4.21}$$

In Eq. (4.15), A_e is calculated by Eq. (4.1). Log-mean temperature difference ($\Delta T_{lm,e}$) is given by Eq. (4.16) for the entire evaporator and is determined from a weighted average of LMTDs for each zone of the evaporator vis-a-vis two-phase boiling and superheat. The LMTDs for two-phase boiling and superheat zones are calculated using Eq. (4.17) through Eq. (4.21) above.

Therefore, by using Eq. (4.15), experimental overall heat transfer coefficient ($U_{exp,e}$) values for the evaporator can be obtained from experimental data. The hot water correlation developed in the preheater analysis is considered here in determining hot water heat transfer coefficients, that is, Eq. (4.12) is used to obtain $\alpha_{hw,e}$ values from evaporator hot water data. Therefore, by using Eq. (4.22) for the evaporator, the experimental R245fa heat transfer coefficient ($\alpha_{ref,exp,e}$) values were obtained.

$$\frac{1}{\alpha_{ref,exp,e}} = \frac{1}{U_{exp,e}} - \frac{t}{k_{pm}} - \frac{1}{\alpha_{hw,e}} \tag{4.22}$$

The authors tried to fit the experimental data to different formats of two-phase evaporation heat transfer correlations available in the literature, mainly the correlation given by Jokar et al. [2] and various correlation formats given in an NIST [1] document. Two types of correlations, one given by NIST [1] and another by Joker et al. [2] fit the present R245fa evaporator experimental data well. The NIST [1] correlation form is given by Eq. (4.23) and Jokar et al. [2] by Eq. (4.24). Both Eq. (4.23) and Eq. (4.24) are in dimensionless form. In Eq. (4.24) and Eq. (4.26), $G_{ref,e}$ is obtained by Eq. (4.4) above. Further discussion on these correlations is given in Section 4.9.2 below.

$$Nu_{ref,cal,e} = a_1 Re_{eq,ref,e}^{a_2} \times Pr_{3f}^{a_3} \times \left[a_4\left(Bo_{ref,e} \times 10^4\right)^{a_5} + a_6\right] \times \omega^{a_7} \tag{4.23}$$

$$Nu_{ref,cal,e} = b_1 Re_{eq,ref,e}^{b_2} \times Pr_{3f}^{b_3} \times \left(\frac{G_{ref,e}^2}{\rho_{3f}^2 C_{p,3f} \Delta T_{s,ref,e}}\right)^{b_4} \left(\frac{\rho_{3f}^2 (h_{3g} - h_{3f})}{G_{ref,e}^2}\right)^{b_5} \left(\frac{\rho_{3f}\sigma_{3f}}{\mu_{3f} G_{ref,e}}\right)^{b_6} \left(\frac{\rho_{3f}}{\rho_{3f} - \rho_{3g}}\right)^{b_7} \tag{4.24}$$

$$Re_{eq,ref,e} = \frac{G_{eq,ref,e} D_h}{\mu_{3f}} \tag{4.25}$$

$$G_{eq,ref,e} = G_{ref,e}\left[0.5 + 0.5\left(\frac{\rho_{3f}}{\rho_{3g}}\right)^{0.5}\right] \tag{4.26}$$

$$Bo_{ref,e} = \frac{q''_{ref,e}}{G_{ref,e}(h_{3g} - h_{3f})} \tag{4.27}$$

$$q''_{ref,e} = \frac{Q_{ref,e}}{A_e} \tag{4.28}$$

$$\omega = -log_{10}\left(\frac{P_4}{P_c}\right) \tag{4.29}$$

$$\Delta T_{s,ref,e} = T_{s,e} - T_{avg,ref,e} \tag{4.30}$$

$$T_{s,e} = \frac{T_{avg,hw,e} + T_{avg,ref,e}}{2} \tag{4.31}$$

$$T_{avg,hw,e} = \frac{T_6 + T_{7f}}{2} \tag{4.32}$$

$$T_{avg,ref,e} = \frac{T_4 + T_{3f}}{2} \tag{4.33}$$

4.8.4 Condenser Analysis

As mentioned in Section 4.5, the condenser in the present ORC system has three zones vis-a-vis superheated, two-phase condensing and sub-cooled zones with more than 91% of heat transfer in the two-phase zone on average for all the experimental run cases. A similar evaporator type of analysis is done for the condenser in determining the heat transfer correlation; differences being: (i) presence of a sub-cooled region in the condenser which accounts for an extra term in the denominator of Eq. (4.35) for the sub-cooled region, (ii) the 5% heat loss is not considered in condenser analysis. The reason for not considering 5% heat loss in the condenser is due to its large (volume wise) capacity and also during a personal communication with the ORC commissioning engineer during initial setup stating that all of the refrigerant present in the ORC system can be filled in the condenser. Equations for the condenser analysis are similar to the evaporator and, for the reader's convenience, some are listed below.

Average heat transferred between cold water and R245fa in the condenser, Q_c, is the average of $Q_{cw,c}$ and $Q_{ref,c}$. Q_c will be used in the heat transfer equation and is given by,

$$Q_c = U_{exp,c} A_c \Delta T_{lm,c} \tag{4.34}$$

$$\Delta T_{lm,c} = \frac{Q_c}{\left(\frac{Q_{sup,c}}{\Delta T_{lm,sup,c}}\right) + \left(\frac{Q_{cond,c}}{\Delta T_{lm,cond,c}}\right) + \left(\frac{Q_{sub,c}}{\Delta T_{lm,sub,c}}\right)} \tag{4.35}$$

$$Q_{sub,c} = \dot{m}_{ref}(h_{5f} - h_1) \tag{4.36}$$

$$\Delta T_{lm,sub,c} = \frac{(T_{5f}-T_{9f})-(T_1-T_9)}{ln\left(\frac{T_{5f}-T_{9f}}{T_1-T_9}\right)} \tag{4.37}$$

$$T_{9f} = T_9 + \frac{Q_{sub,c}}{\dot{m}_{cw}C_{p,910}} \tag{4.38}$$

Using equations like Eq. (4.36) to Eq. (4.38), other terms in the denominator of Eq. (4.35) can be determined and, finally, $\Delta T_{lm,c}$ for all the experimental runs. Therefore, using Eq. (4.34), experimental overall heat transfer coefficient ($U_{exp,c}$) values for the condenser can be obtained from the experimental data. The same heat transfer correlation, developed for hot water in the preheater analysis, is considered here in determining cold water heat transfer coefficients. That is, Eq. (4.12) is used to obtain $\alpha_{cw,c}$ values from condenser cold water data. By using an equation similar to Eq. (4.22) for the condenser, the experimental R245fa condensation heat transfer coefficient ($\alpha_{ref,exp,c}$) values were obtained.

Similar to the evaporator, different correlation formats were fitted to the experimental R245fa condensation data. The correlation formats given by Yan and Lin [29], Kuo et al. [21], Jokar et al [2] and various formats given in the NIST [1] document were tried. For the condenser, the correlation format given by Jokar et al. [2] fit very well to the present R245fa condenser experimental data and is given by Eq. (4.39). Similar equations to Eq. (4.25) to Eq. (4.33) can be used for the condenser data to obtain the parameters in Eq. (4.39). Further discussion on this correlation is given in Section 4.9.3 below.

$$Nu_{ref,cal,c} = d_1 Re_{eq,ref,c}^{d_2} \times Pr_{5f}^{d_3} \times \left(\frac{G_{ref,c}^2}{\rho_{5f}^2 C_{p,5f}\Delta T_{s,ref,c}}\right)^{d_4} \left(\frac{\rho_{5f}^2(h_{5g}-h_{5f})}{G_{ref,c}^2}\right)^{b_5} \left(\frac{\rho_{5f}\sigma_{5f}}{\mu_{5f}G_{ref,c}}\right)^{b_6} \left(\frac{\rho_{5f}}{\rho_{5f}-\rho_{5g}}\right)^{b_7} \tag{4.39}$$

4.8.5 Refrigerant Mass Flow Rate

From the schematic of the ORC cycle (Figure 4.1), it can be inferred that there is no flow meter installed to measure the R245fa flow rate. For the reader's convenience, the refrigerant mass flow rate calculation procedure is given in this section from [24]. The refrigerant mass flow rate was estimated using the energy balance on the hot water side of the ORC system, which is given by Eq. (4.40) as,

$$\dot{m}_{ref} = \frac{0.95\times[(\dot{V}_{hw}/3600)\times\rho_{68}\times C_{p,68}(T_6-T_8)]}{(h_4-h_2)} \tag{4.40}$$

Here, 0.95 is the efficiency of heat transfer from hot water to refrigerant R245fa in the evaporator and preheater, which is assumed as 95%, with a 5% heat loss to the environment (first assumption in present study). This is a reasonable assumption for brazed plate heat exchangers [13].

4.9 Results and Discussions

A 50 kW ORC power unit was tested in a lab environment at different hot water and cold water supply conditions for performance mapping. The data pertaining to the preheater, evaporator and condenser was used in the present study to develop R245fa heat transfer correlations for single-phase, two-phase evaporation, and two-phase condensation in the respective heat exchangers. In this section the heat transfer correlation results developed are presented for the three heat exchangers as discussed in Section 4.5 above.

4.9.1 Preheater Heat Transfer Correlation Results

Typical ranges for values of the single-phase correlation constants c_1 to c_6 in Eq. (4.12) and Eq. (4.13) can be found in the literature [1, 2, 14, 16, 21, 22, 30, 31] and are summarized below:

$$0.023 \leq c_1, c_4 \leq 1.98,$$

$$0.326 \leq c_2, c_5 \leq 0.89,$$

$$0.333 \leq c_3, c_6 \leq 0.5,$$

By using simple computer code in Microsoft® Excel® VBA, all possible combinations for the constants c_1 to c_6 were used to compute $U_{cal,p}$ using Eq. (4.11), Eq. (4.41), and Eq. (4.42). These are the proposed single-phase heat transfer correlations for hot water and refrigerant in the preheater, respectively. Figure 4.4 shows the comparison results for calculated $U_{cal,p}$ using Eq. (4.11), Eq. (4.41), and Eq. (4.42) against experimental $U_{exp,p}$ from Eq. (4.9). 91% of the predicted overall heat transfer coefficients for the preheater were within ±20% with respect to experimental values. Eq. (4.41) will be used for obtaining hot water and cold water heat transfer coefficients from evaporator and condenser experimental data, respectively.

$$Nu_{hw,p} = 0.01\left(Re_{7f8}^{1.05}\right)\left(Pr_{7f8}^{0.9}\right) \tag{4.41}$$

$$Nu_{ref,p} = 0.01\left(Re_{23f}^{1.05}\right)\left(Pr_{23f}^{0.47}\right) \tag{4.42}$$

The hot water mass flux ranged from 467.2 kg/m^2•s to 1192.8 kg/m^2•s and Eq. (4.41) for hot water heat transfer correlation is generally valid for $4204.8 \leq Re_{7f8} \leq 16769.5$ and $1.7 \leq Pr_{7f8} \leq 2.9$. The refrigerant R245fa mass flux ranged from 65.1 kg/m^2•s to 158.4 kg/m^2•s. Single-phase

heat transfer correlation for refrigerant R245fa (Eq. (4.42)) is generally valid for $720 \leq Re_{23f} \leq 2226.7$ and $4.9 \leq Pr_{23f} \leq 5.7$.

4.9.2 R245fa Evaporator Heat Transfer Correlation Results

In the evaporator, the refrigerant mass flux ($G_{ref,e}$) ranged from 38.6 kg/m^2•s to 94 kg/m^2•s while the Reynolds number ($Re_{ref,e}$) ranged between 583.5 and 2163.7. Similarly, in the evaporator, the R245fa equivalent mass flux ($G_{eq,ref,e}$) ranged from 159.6 kg/m^2•s to 254.3 kg/m^2•s while the equivalent Reynolds number ($Re_{eq,ref,e}$) ranged between 2412.3 and 5855.

Eq. (4.43) and Eq. (4.44) below gives the proposed R245fa evaporation heat transfer correlations for NIST [1] and Jokar et al. [2] correlation forms (Eq. (4.23) and Eq. (4.24) above), respectively. The correlation constants (a_1 to a_7 for Eq. (4.23) and b_1 to b_7 for Eq. (4.24)) were obtained using the present evaporator experimental data for R245fa. Figure 4.5 shows the comparison of calculated versus experimental evaporator heat transfer coefficients for R245fa. The predicted R245fa evaporator heat transfer coefficients using Eq. (4.43) were within –12.3% and +16.5% compared to experimental values with root mean square (RMS) error of 8.3. The predicted R245fa evaporator heat transfer coefficients using Eq. (4.44) were within ±13.7% compared to the experimental values with RMS error of 8.7.

$$Nu_{ref,cal,e} = 0.0017 Re_{eq,ref,e}^{2.38} \times Pr_{3f}^{1.35} \times [0.25(Bo \times 10^4)^{-0.000716} - 0.249] \times \omega^{1.84} \quad (4.43)$$

$$Nu_{ref,cal,e} = 0.847 Re_{eq,ref,e}^{1} \times Pr_{3f}^{0.9} \times \left(\frac{G_{ref,e}^2}{\rho_{3f}^2 C_{p,3f} \Delta T_{s,ref,e}}\right)^{0.6} \left(\frac{\rho_{3f}^2 (h_{3g} - h_{3f})}{G_{ref,e}^2}\right)^{-0.3} \left(\frac{\rho_{3f} \sigma_{3f}}{\mu_{3f} G_{ref,e}}\right)^{1.4} \left(\frac{\rho_{3f}}{\rho_{3f} - \rho_{3g}}\right)^{1} \quad (4.44)$$

In an evaporator, two types of heat transfer regime exist: two-phase convective boiling and nucleate boiling [4]. Thonon [32] gave a quantitative criterion to determine the dominant heat transfer regime in the evaporative process based on the boiling number (Bo) and the Martinelli parameter (X_{tt}) that is given by Eq. (4.45). In the Martinelli parameter of Eq. (4.46), average vapor quality is taken as 0.5. Figure 4.6 clearly shows the domination of the nucleate boiling regime for R245fa evaporation for all the experimental data in the present study.

$$\begin{matrix} Bo X_{tt} > 0.00015 \; for \; Nucleate \; Boliling \\ Bo X_{tt} < 0.00015 \; for \; Two \; phase \; Convective \; Boliling \end{matrix} \quad (4.45)$$

$$X_{tt} = \left(\frac{1-0.5}{0.5}\right)^{0.9} \left(\frac{\rho_{3f}}{\rho_{3g}}\right)^{0.5} \left(\frac{\mu_{3f}}{\mu_{3g}}\right)^{0.1} \quad (4.46)$$

4.9.3 R245fa Condenser Heat Transfer Correlation Results

In the condenser, the refrigerant mass flux ($G_{ref,c}$) ranged from 11.6 kg/m^2•s to 28.2 kg/m^2•s while the Reynolds number ($Re_{ref,c}$) ranged between 107.4 and 310.5. Similarly, in the condenser, the R245fa equivalent mass flux ($G_{eq,ref,c}$) ranged from 76.5 kg/m^2•s to 177 kg/m^2•s while the equivalent Reynolds number ($Re_{eq,ref,c}$) ranged between 782.3 and 1857.7.

Eq. (4.47) gives the proposed R245fa condensation heat transfer correlations for the Jokar et al. [2] correlation form (Eq. (4.39) above). The correlation constants (d_1 to d_7 for Eq. (4.39)) were obtained using the present condenser experimental data for R245fa. Figure 4.7 shows the comparison of calculated versus experimental condenser heat transfer coefficients for R245fa. Of the predicted R245fa condenser heat transfer coefficient values using Eq. (4.47), 95% were within ±25% error compared to experimental values with root mean square (RMS) error of 8.7. 83% of the predicted values were within an error of ±20% with respect to experimental values.

$$Nu_{ref,cal,c} = 0.1 Re_{eq,ref,c}^{1} \times Pr_{5f}^{0.2} \times \left(\frac{G_{ref,c}^2}{\rho_{5f}^2 C_{p,5f} \Delta T_{s,ref,c}}\right)^{1.3} \left(\frac{\rho_{5f}^2 (h_{5g} - h_{5f})}{G_{ref,c}^2}\right)^{1} \left(\frac{\rho_{5f} \sigma_{5f}}{\mu_{5f} G_{ref,c}}\right)^{0.05} \left(\frac{\rho_{5f}}{\rho_{5f} - \rho_{5g}}\right)^{2} \quad (4.47)$$

4.10 Uncertainty Analysis for Calculated Parameters

The uncertainty for the measured parameters is given in Table 4.3. The uncertainty analysis for the calculated parameters was determined by the standard approach presented by Coleman and Steele [33]. Table 4.4 presents the uncertainty in calculated values for refrigerant mass flow rate, preheater overall heat transfer coefficient, and two-phase heat transfer correlations for the evaporator and condenser. The uncertainty in calculated values was observed to be smaller than the predicted values using respective correlations.

4.11 Conclusions

In the work presented, the authors at UAF tested a 50 kW ORC power unit for various hot water and cold water conditions. Experimental data pertaining to the preheater, evaporator and condenser was used to develop R245fa heat transfer correlations in respective heat exchangers in accordance with available correlation in the literature. The pressure drop in the heat exchangers was considered negligible, as no differential pressure measuring instruments were installed. The

proposed correlations in the present study can be used to develop a theoretical model for an ORC using models for scroll-expander [34] and screw-expander [24].

The developed single-phase heat transfer correlations for hot water and R245fa in the preheater had an agreement of within ±20% with respect to experimental values. The correlation for hot water from the preheater analysis was used to obtain hot water and cold water heat transfer coefficient values in the evaporator and condenser from respective experimental data.

Two heat transfer correlations were proposed for evaporation of R245fa in a BPHE. The first was based on NIST [1] correlation form that is within an error of –12.3% and +16.5% with respect to experimental data. The second proposed heat transfer correlation was based on Jokar et al. [2] with an error range of ±13.7% when compared with experimental data. Based on a criterion from Thonon et al. [32], the dominant heat transfer regime in the evaporator was observed to be nucleate boiling.

The proposed correlation for condensation of R245fa in the condenser was based on Jokar et al. [2], and 95% of the predicted heat transfer values were within an error range of ±25% when compared with experimental data.

4.12 References

[1] Palmer, S.C., Payne, W.V., and Domanski, P.A., "Evaporation and condensation heat transfer performance of flammable refrigerants in a brazed plate heat exchanger," NIST Internal Report # 6541, July 2000.

[2] Jokar, A., Hosni, M.H., and Eckels, S.J., "Dimensional analysis on the evaporation and condensation of refrigerant R134a in minichannel plate heat exchangers," Applied Thermal Engineering, Vol.26, pp. 2287-2300, 2006.

[3] Hayes, N., Jokar, A., and Ayub, Z.H., "Study of carbon dioxide condensation in chevron plate exchangers; heat transfer analysis," Vol.54, pp. 1121-1131, 2011.

[4] Wang, L., Sunden, B., and Manglik, R.M., "Plate heat exchangers: Design, applications and performance," WIT Press, MA, 2007.

[5] Ayub, Z.H., "Plate heat exchanger literature survey and new heat transfer and pressure drop correlations for refrigerant evaporators," Heat Transfer Engineering, Vol.24(5), pp. 3-16, 2003.

[6] Savostin, A.F., and Tikhonov, A.M., "Investigation of the characteristics of plate-type heat surfaces," Thermal Engineering, Vol.17(9), pp. 113-117, 1970.

[7] Okada, K., Ono, M., Tominura, T., Okuma, T., Konno, H., and Ohtani, S., "Design and heat transfer characteristics of new plate heat exchanger," Heat Transfer – Japanese Research, Vol.1(1), pp. 90-95, 1972.

[8] Tovazhnyanski, L.L., Kapustenko, P.A., and Tsibulnik, V.A., " Heat transfer and hydraulic resistance in channels of plate heat exchangers," Energetika, Vol.9, pp. 123-125, 1980.

[9] Focke, W.W., Zachariades, J., and Olivier, I., "The effect of the corrugation inclination angle on the thermohydraulic performance of plate heat exchangers," International Journal of Heat and Mass Transfer, Vol.28(8), pp. 1469-1479, 1985.

[10] Chisholm, D. and Wanniarachchi, A.S., "Maldistribution in single-pass mixed-channel plate heat exchangers," Compact Heat Exchangers for Power and Process Industries, HTD-ASME, Vol.201, pp. 262-267, New York, 1992.

[11] Heavner, R.L., Kumar, H., and Wanniarachchi, A.S., "Performance of an industrial plate heat exchangers: Effect of chevron angle," AIChe Symposium Series, Vol.89(295), pp. 262-267, New York, 1993.

[12] Muley, A. and Manglik, R.M., "Enhanced heat transfer characteristics of single-phase flows in a plate heat exchanger with mixed chevron plates," Journal of Enhanced Heat Transfer, Vol.4(3), pp. 187-201, 1997.

[13] Muley, A. and Manglik, R.M., "Experimental study of turbulent flow heat transfer and pressure drop in a plate heat exchanger with chevron plates," Transactions of ASME Journal of Heat Transfer, Vol.121, pp.110-117, February 1999.

[14] Ray, D., Das, D.K., and Vajjha, R.S., "Experimental and numerical investigations of nanofluids performance in compact minichannel plate heat exchanger," International Journal of Heat and Mass Transfer, Vol.71, pp. 732-746, 2014.

[15] Thonon, B., "Design method for plate evaporators and condensers," 1st International Conference on Process Intensification for the Chemical Industry, BHR Group Conference Series Publication # 18, pp. 37-47, 1995.

[16] Warnakulasuriya, F.S.K. and Worek, W.M., "Heat transfer and pressure drop properties of high viscous solutions in plate heat exchangers," International Journal of Heat and Mass Transfer, Vol.51, pp. 52-67, 2008.

[17] Bejan, A., "Heat transfer," John Wiley & Sons, Inc., New York, 1993.

[18] Shah, R.K. and Focke, W.W., "Plate heat exchangers and their design theory," in: Shah, R.K., Subbarao, E.C., and Mashelkar, R.A., Heat Transfer Equipment Design, Hemisphere, pp. 227-254, Washington, DC, 1988.

[19] Djordjevic, E. and Kabelac, S., "Flow boiling of R134a and ammonia in a plate heat exchanger," International Journal of Heat and Mass Transfer, Vol.51, pp.6235-6242, 2008.

[20] Wang, L., Christensen, R., and Sunden, B., "An experimental investigation of steam condensation in plate heat exchangers," International Journal of Heat Exchangers, Vol.1(2), pp. 125-149, 2000.

[21] Kuo, W.S., Lie, Y.M., Hsieh, Y.Y., and Lin, T.F., "Condensation heat transfer and pressure drop of refrigerant R410A flow in vertical plate heat exchanger," International Journal of Heat and Mass Transfer, Vol.48, pp. 5205-5220, 2005.

[22] Longo, G.A. and Gasparella, A., "Heat transfer and pressure drop during HFC refrigerant vaporization inside a brazed plate heat exchanger," International Journal of Heat and Mass Transfer, Vol.50, pp. 5194-5203, 2007.

[23] Hu, K., Zhu, J., Li, T., and Zhang, W., "R245fa evaporation heat transfer and pressure drop in a brazed plate heat exchanger for organic Rankine cycle (ORC)," Proceedings World Geothermal Congress, Melbourne, Australia, April 2015.

[24] Avadhanula, V.K. and Lin, C.S., "Empirical models for screw expander based on experimental data from organic Rankine cycle system testing," ASME Journal of Engineering for Gas Turbines and Power, Vol.136, June 2014.

[25] Kaori Brazed Plate Heat Exchanger Catalogue. http://www.kaori-taiwan.com/pdf/brazed-plate/BPHE-20101013.pdf. Accessed August 31st, 2013.

[26] Lemmon, E.W., Huber, M.L., and McLinden, M.O., "NIST Standard Reference Database 23: Reference Fluid Thermodynamic and Transport Properties-REFPROP," Version 9.1, National Institute of Standards and Technology, Standard Reference Data Program, Gaithersburg, 2013.

[27] Avadhanula, V.K., Lin, C.S., and Johnson, T., "Testing a 50kW ORC at Different Heating and Cooling Source Conditions to Map the Performance Characteristics," SAE Technical Paper # 2013-01-1649, April 2013.

[28] Lin, C.S., Avadhanula, V.K., Mokkapati, V., Huang, D., and Sheets, B., "Guidelines for Effectively Applying an ORC System to Rural Alaska Diesel Power Industry Based on Experimental Data," SAE Technical Paper # 2015-01-1607, April 2015.

[29] Yan, Y.Y. and Lin, T.F., "Condensation heat transfer and pressure drop of refrigerant R134a in a small pipe," International Journal of Heat and Mass Transfer, Vol.42, pp. 697-708, 1999.

[30] Longo, G.A., Gasparella, A., and Sartori, R., "Experimental heat transfer coefficients during refrigerant vaporization and condensation inside herringbone-type plate heat exchangers with enhanced surfaces," International Journal of Heat and Mass Transfer, Vol.47, pp. 4125-4136, 2004.

[31] Palm, B. and Claesson, J., "Plate heat exchangers: Calculation methods for single- and two-phase flow," Heat Transfer Engineering, Vol.27(4), pp. 88-98, 2006.

[32] Thonon, B., and Vidil, R., and Marvillet, C., "Recent research and developments in plate heat exchangers," Journal of enhanced heat transfer, Vol.2, pp.149-155, 1995.

[33] Coleman, H.W. and Steele, W.G., "Experimentation and Uncertainty Analysis for Engineers," Second edition, John Wiley & Sons, Inc., New York, 1999.

[34] Quoilin, S., "Experimental study and modeling of a low temperature Rankine cycle for small scale cogeneration," Master's Thesis, University of Liege, May 2007.

Table 4.1 Various hot water and cold water flow rates and temperatures at which the power unit was tested

Hot water temperature, °C (°F)	Hot water flow rate, m^3/h (gpm)	Cold water temperature, °C (°F)	Cold water flow rate, m^3/h (gpm)
68.3 (155)	27.2 (120)	10 (50)	27.2 (120)
79.4 (175)	36.3 (160)	20 (68)	36.3 (160)
90.5 (195)	45.4 (200)		45.4 (200)
101.7 (215)	56.8 (250)		
107.2 (225)	68.1 (300)		

Table 4.2 BPHE physical parameters used in present study

Parameter	Preheater	Evaporator	Condenser
W_2 (m)	0.174	0.22	0.22
L_2 (m)	0.456	0.65	0.65
Mean channel spacing, b, (m)	0.002	0.002	0.002
Plate thickness, t, (m)	0.0004	0.0004	0.0004
Number of plates including end plates	91	121	401
Number of thermal plates (N_{th})	89	119	399
Total number of fluid channels	90	120	400
Number of channels on one fluid side (N_{ch})	45	60	200
Model number from manufacturers catalog	K205	K400	K400
Heat transfer area, A, (m^2)	7.06	17.017	57.057
Flow area, A_f, (m^2)	0.0156	0.0264	0.088

Table 4.3 Parameters measured, instrumentation and uncertainty in measurement

Parameter	State point on Figure 4.1 and Figure 4.2	Instrumentation	Range	Uncertainty in measurement
Hot water supply temperature to evaporator	T_6	Omega type-K thermocouple	68°C – 108.1°C	±1.1°C
Hot water temperature return from evaporator or supply to preheater	T_7	Omega type-K thermocouple	63°C – 104.3°C	±1.1°C
Hot water return temperature from preheater	T_8	Omega type-K thermocouple	60.3°C – 100°C	±1.1°C
Hot water flow rate	$\dot{V}_6 = \dot{V}_7 = \dot{V}_8 = \dot{V}_{hw}$	Kamstrup Ultraflow ultrasonic flow meter	27.1 m^3/h – 68.7 m^3/h	0.5%
Refrigerant R245fa temperature – inlet to preheater	T_2	Omega type-K thermocouple	12.1°C – 29°C	±1.1°C
Refrigerant R245fa pressure – inlet to preheater	P_2	ST1500 Pressure transducer	465.7 kPa – 1109.5 kPa	0.2%
Refrigerant R245fa temperature – outlet of preheater or inlet to evaporator	T_3	Omega type-K thermocouple	59°C – 93.2°C	±1.1°C
Refrigerant R245fa pressure – outlet of preheater or inlet to evaporator	P_3	ST1500 Pressure transducer	436 kPa – 1065.4 kPa	0.2%
Refrigerant R245fa temperature – outlet of evaporator or inlet to expander	T_4	Omega type-K thermocouple	65.9°C – 107.1°C	±1.1°C
Refrigerant R245fa pressure – outlet of evaporator or inlet to expander	P_4	ST1500 Pressure transducer	424.4 kPa – 1027.3 kPa	0.2%
Cold water supply temperature	T_9	Omega type-K thermocouple	11.2°C – 21.9°C	±1.1°C
Cold water return temperature	T_{10}	Omega type-K thermocouple	15.5°C – 29.8°C	±1.1°C
Cold water flow rate	$\dot{V}_9 = \dot{V}_{10} = \dot{V}_{cw}$	Kamstrup Ultraflow ultrasonic flow meter	24.4 m^3/h – 70 m^3/h	0.5%
Refrigerant R245fa temperature – outlet of expander or inlet of condenser	T_5	Omega type-K thermocouple	26.7°C – 43.2°C	±1.1°C
Refrigerant R245fa pressure – outlet of expander or inlet of condenser	P_5	ST1500 Pressure transducer	111.4 kPa – 202.1 kPa	0.2%
Refrigerant R245fa temperature – outlet of condenser	T_1	Omega type-K thermocouple	11.7°C – 28.4°C	±1.1°C
Refrigerant R245fa pressure – outlet of condenser	P_1	ST1500 Pressure transducer	107.0 kPa – 188.3 kPa	0.2%

Table 4.4 Uncertainty in calculated parameters

Parameter	Range	Uncertainty
Refrigerant mass flow rate ($\dot{m}_{ref}$)	1.02 kg/s – 2.4 kg/s	2.6%
Preheater overall heat transfer coefficient ($U_{cal,p}$)	414.8 W/m^2 K – 1308.9 W/m^2 K	8.6%
Evaporator two-phase heat transfer coefficient ($\alpha_{ref,exp,e}$)	1416.3 W/m^2 K – 3500.6 W/m^2 K	10.9%
Condenser two-phase heat transfer coefficient ($\alpha_{ref,exp,e}$)	1188.9 W/m^2 K – 1591.8 W/m^2 K	12.4%

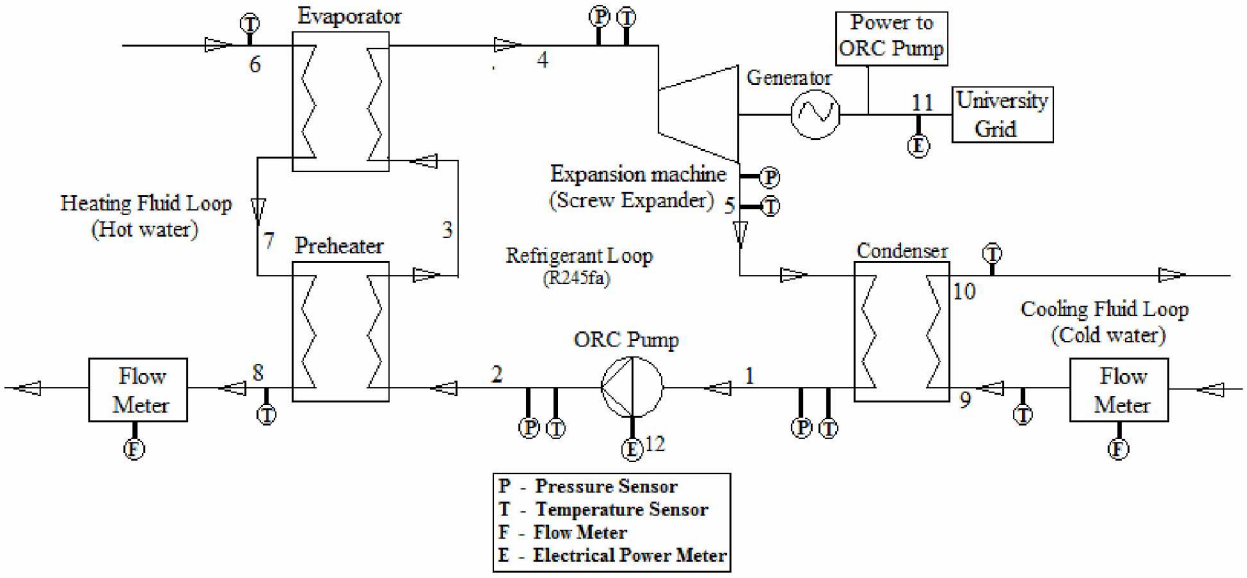

Figure 4.1 Schematic of organic Rankine cycle system under consideration

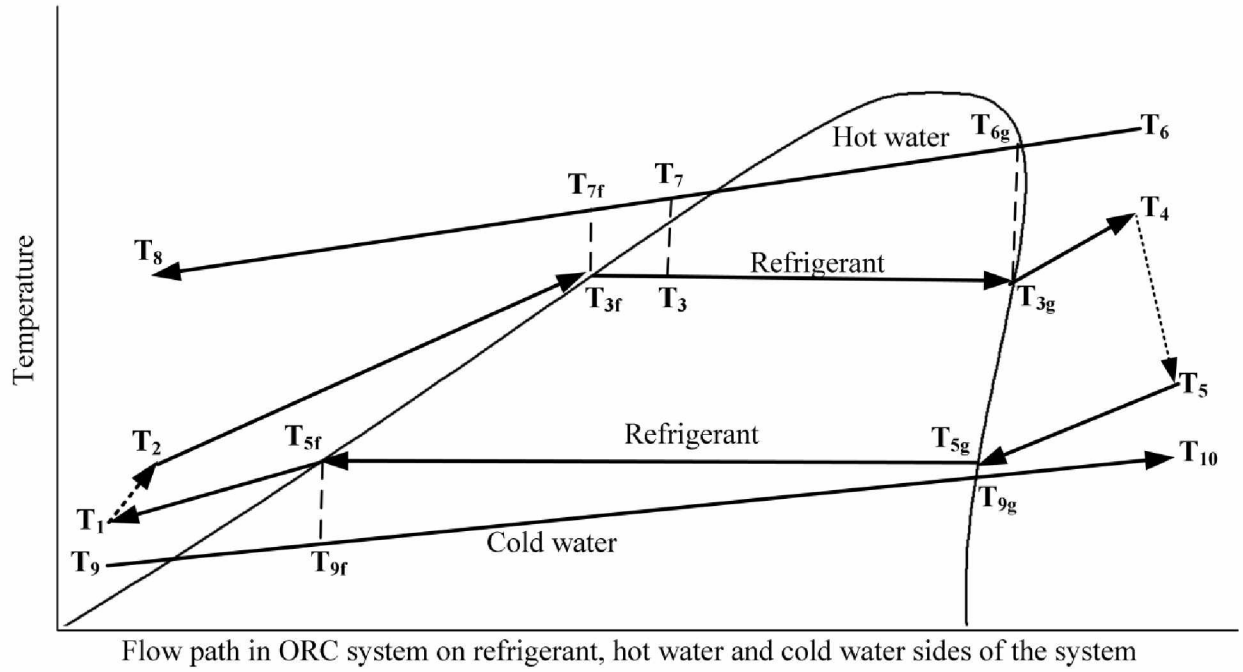

Figure 4.2 Temperature diagrams for the BPHEs used as preheater, evaporator, and condenser in this study

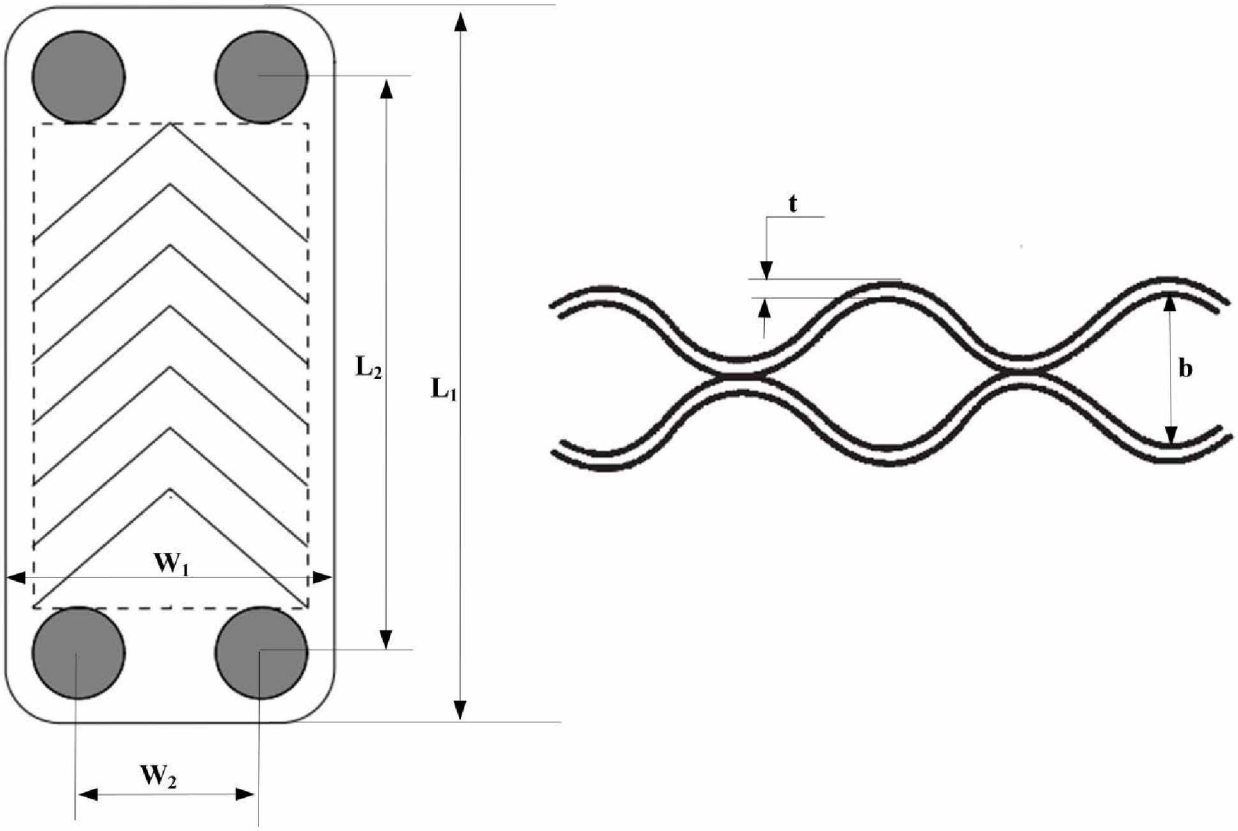

Figure 4.3 BPHE physical parameters used in present work

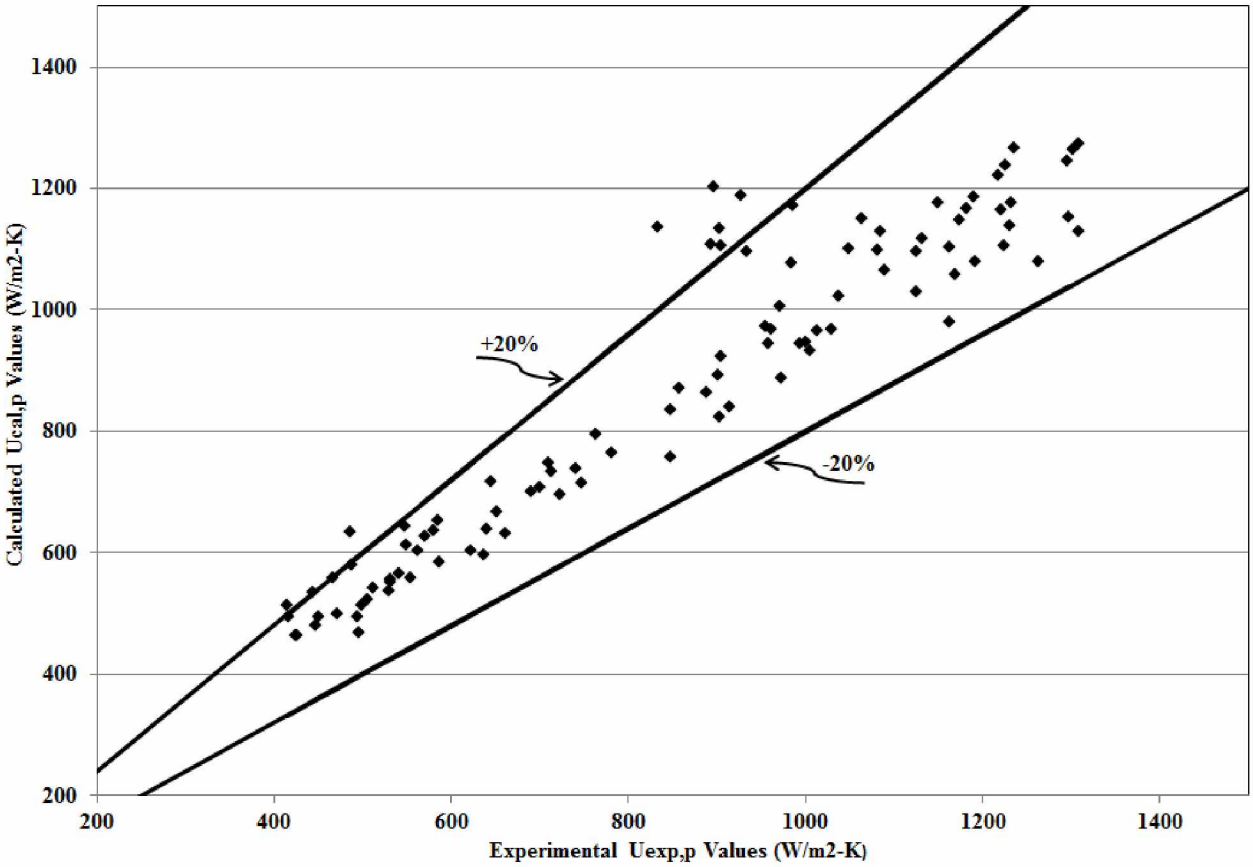

Figure 4.4 Comparison of calculated data with experimental data for preheater overall heat transfer coefficient

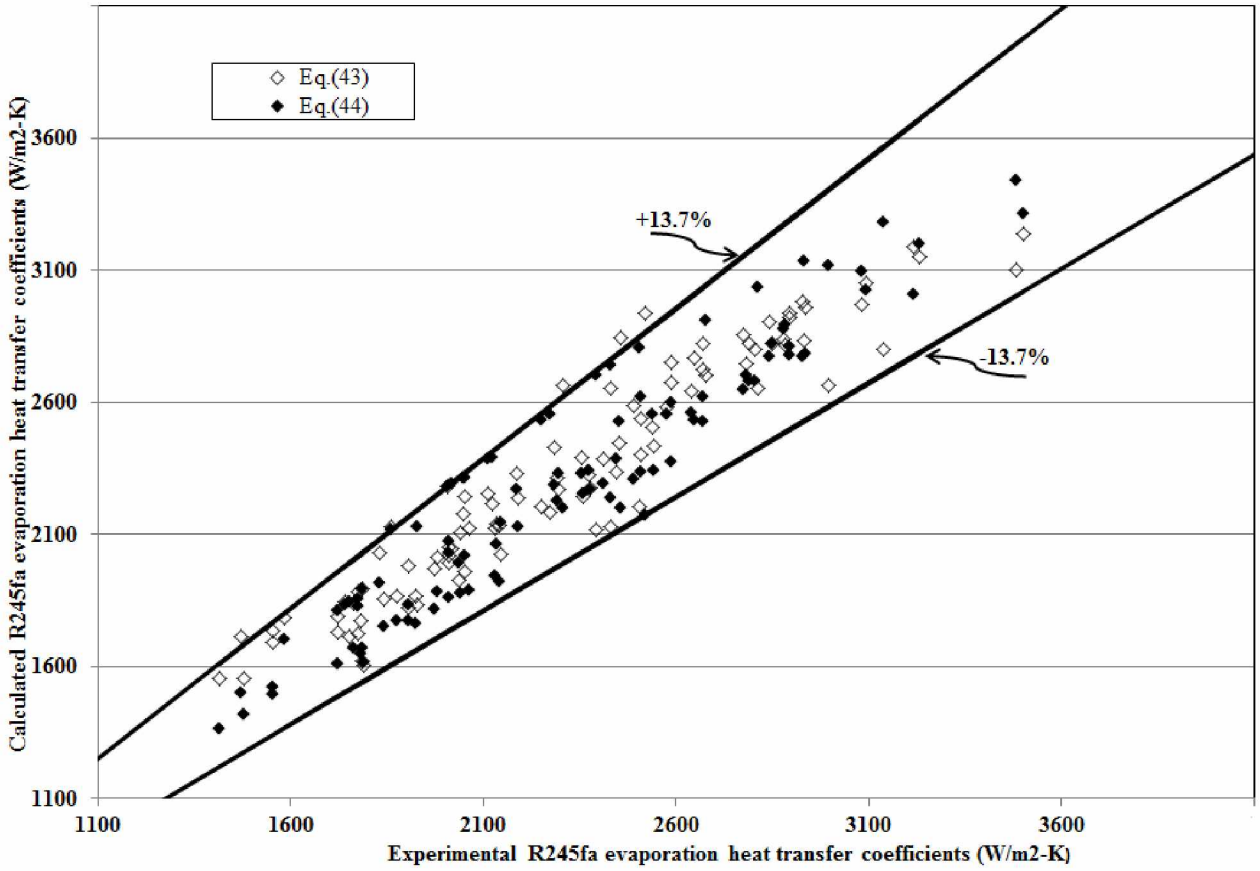

Figure 4.5 Comparison of calculated data with experimental data for R245fa evaporation heat transfer coefficient

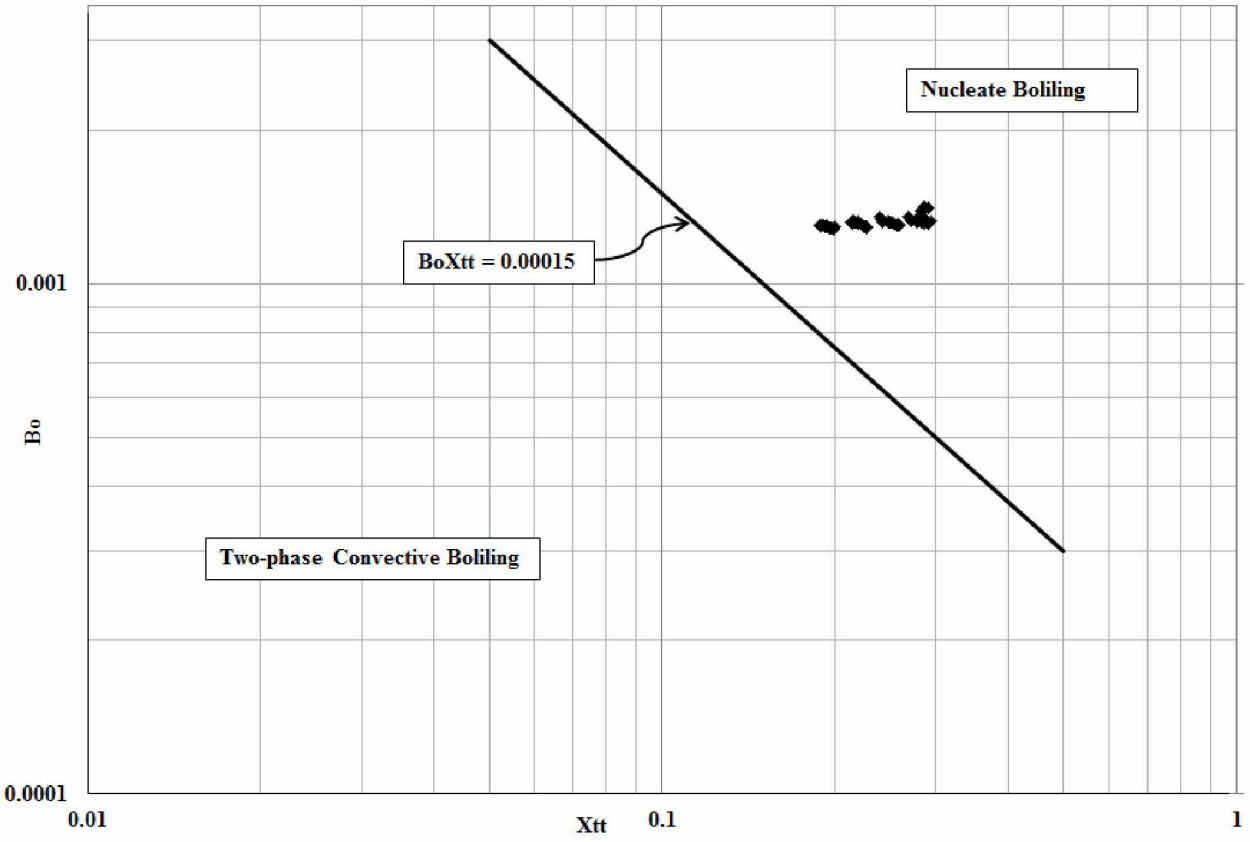

Figure 4.6 Thonon et al. [32] criterion showing the dominant nucleate boiling regime in evaporator

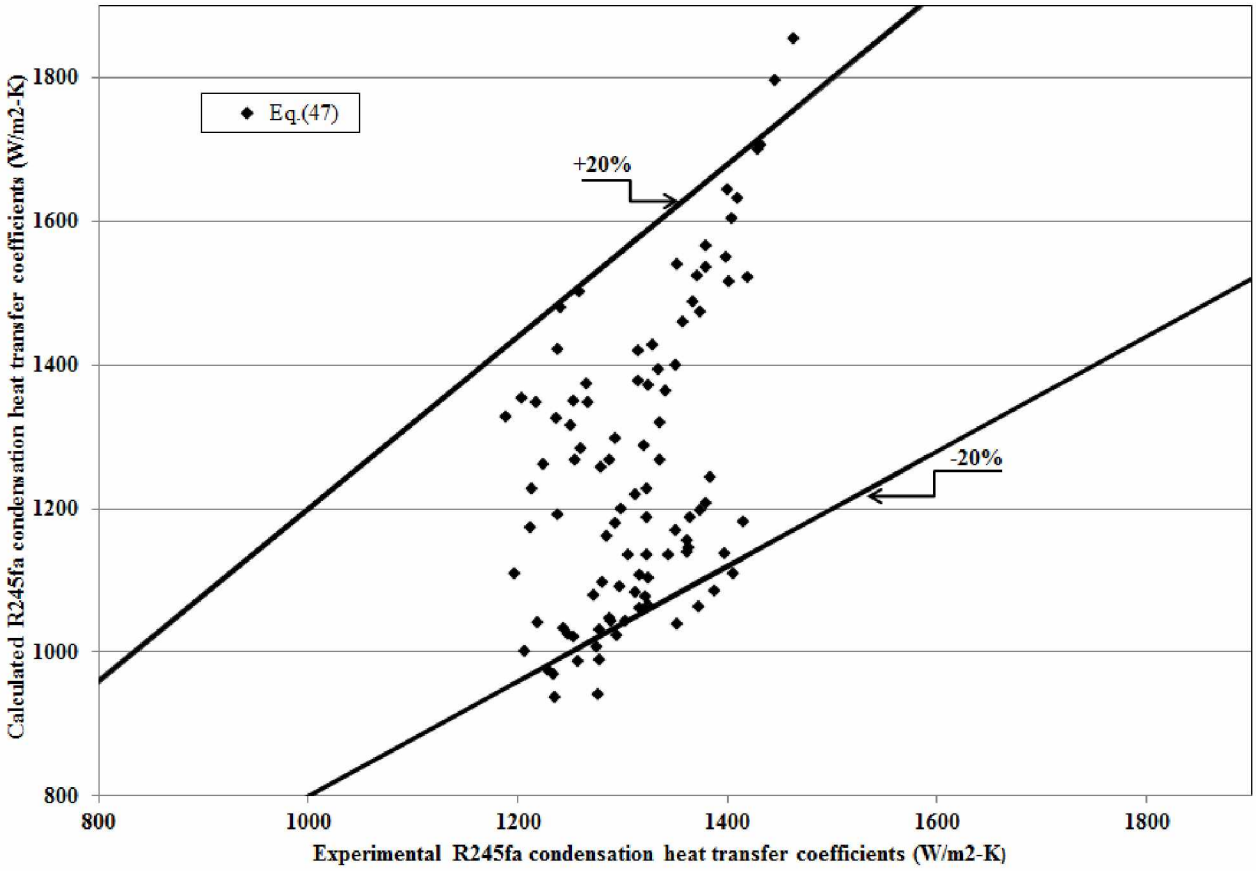

Figure 4.7 Comparison of calculated data with experimental data for R245fa condensation heat transfer coefficient

Chapter 5. Parametric Modeling of 50 kW Organic Rankine Cycle using Experimental Data*

5.1 Abstract

The intention of this work is to develop a parametric model of an organic Rankine cycle (ORC) system, which can be applied to predict the performance of the system under different input conditions possibly obtainable from waste heat from a variety of diesel gen-sets. The lab experimental data were collected under controlled input conditions (temperatures and flow rates of heating and cooling fluids) and the developed model was validated by field data with the ORC system installed on a 2 MW Caterpillar field gen-set. Using lab experimental data, the authors proposed in previous publications an empirical model for screw expanders and heat transfer correlations for heat exchangers. In the study described here, a calculation procedure was developed with those proposed correlations to model a 50 kW ORC system to estimate performance parameters such as heat input, power output, heat rejection, and working fluid pump power consumption. The developed model was validated using both lab experimental data and field installation data. The model-predicted values for expander power were within -9.8% and +12.5% for lab experimental data and -1.6% and 5.8% for field data. Model-predicted values for heat supplied by heating fluid in the evaporator and preheater values were within -6.5% and +12.1% for lab experimental data and -3% and 6.4% for field data.

5.2 Keywords

Organic Rankine cycle, brazed plate heat exchanger, screw-expander, two-phase heat transfer, empirical model, evaporation, condensation, diesel engine, waste heat recovery

5.3 Nomenclature

t = thickness of the plate (m)

P = pressure (MPa)

P_c = R245fa critical pressure (MPa)

T = temperature (^{o}C)

x = quality (kg/kg)

W_1 and W_2 = plate width (m)

L_1 and L_2 = plate length (m)

---

* Avadhanula, V.K., and Lin, C.S., "Parametric Modeling of 50 kW Organic Rankine Cycle using Experimental Data", Prepared for Submission in Journal of Applied Thermal Engineering, May 2015.

b = mean channel spacing (m)

μ = dynamic viscosity (kg/m s)

Re = Reynolds number

Re_{eq} = equivalent Reynolds number

Pr = Prandtl number

A = heat transfer area of a heat exchanger (m^2)

A_f = Flow area in heat exchanger (m^2)

D_h = hydraulic diameter (=2b in m)

N_{ch} = number of channels on one fluid side in a BPHE

N_{th} = number of thermal plates in a BPHE

G = mass flux (kg/m^2 s)

G_{eq} = equivalent mass flux (kg/m^2 s)

$\dot{m}$ = mass flow rate (kg/s)

h = enthalpy (kJ/kg)

C_p = specific heat (kJ/kg K)

U = overall heat transfer coefficient (W/m^2 K)

ΔT_{lm} = log-mean temperature deference (^oC)

ΔT = temperature difference (^oC)

Q = heat transfer rate (kW)

α = heat transfer coefficient (W/m^2 K)

k = thermal conductivity (W/m K)

σ = surface tension (N/m)

ρ = density (kg/m^3)

W_{SE} = screw expander power output (kW)

W_{pu} = R245fa pump power (kW)

$h_o = f(25^oC, 0.101325\ MPa)$ for R245fa

RMS error = root mean square error

60:40 PG/W = 60% propylene glycol and 40% water by mass

Subscripts

f = saturated liquid condition

g = saturated vapor condition

ref = refrigerant R245fa

hf = heating fluid

cf = cooling fluid

p = preheater

e = evaporator

c = condenser

pu = pump

SE = screw expander

exp = experimental

sup = superheated

sub = sub-cooled

$boil$ = two-phase boiling

$cond$ = two-phase condensation

ij = property average of $state - i$ and $state - j$ (e.g., $k_{910} = (k_9 + k_{10})/2$)

pm = plate material

avg = average

s = plate surface

o = dimensionless form

5.4 Introduction

In recent years, due to environmental concerns and high fuel prices, the demand for use of low-grade heat sources (i.e., heat sources with low temperature and/or low heat value) has been steadily increasing. One such low-grade heat source is waste heat from stationary diesel engines used for electrical power generation. In stationary diesel engines, about one-third of the energy stored in the fossil fuel is converted into useful work; the remaining two-thirds of that fuel energy is lost, mainly in the form of jacket water heat and exhaust gases. If this waste heat were recovered for useful purposes, considerable improvements in diesel engine efficiency and in efficiency of the power plant as a whole could be made. One of the many applications where diesel engine waste heat could be recovered is the thermal power cycle of the organic Rankine cycle (ORC), which is the focus of this work.

Stationary diesel engine waste heat recovery is an obvious choice as a low-grade heat source in Alaska, where approximately 180 rural villages use diesel generators to run independent electrical power systems. In 2007, the combined electrical consumption of these 180 villages was 370,000 MWh [1]. It should be noted that the size of the diesel gen-sets in operation in these villages varies from about 50 kW to 1 MW in electrical usage. With waste heat availability of 1MW or less, an ORC system with less than 100kW (at 10% thermal efficiency) power output would be desirable.

The ORC is similar to the traditional steam Rankine cycle; the only difference is the working fluid. The working fluids generally used in an ORC are refrigerants, such as R11, R113, R123, R134a, R245fa, and HFE-7000. As shown in Figure 5.1, a typical ORC consists of a pump, preheater, evaporator, expansion machine (expander), and condenser. The working fluid is pressurized through the pump and supplied to the preheater and evaporator, where it is heated by the heat source (heating fluid loop in Figure 5.1). The working fluid exiting the evaporator is in a vapor or liquid/vapor condition, which is expanded in the expander while power is generated. The low-pressure working fluid exiting the expansion machine is liquefied in the condenser by a cooling source (cooling fluid loop in Figure 5.1) and returned to the pump. In a diesel engine waste heat application of the ORC, the heat source may be engine jacket water, exhaust gases, or a combination of the two. The cooling source could be a lake, a river, an underground well, air-cooled radiators, or a cooling tower, based on the ORC installation's location and the economic viability of the cooling source.

In the open literature, few studies are available that present detailed ORC models developed using experimental data and accounting for individual component characteristics of the cycle. Even those models available are based on lab ORC setups for temporary experimental studies, not on commercial units. Sylvain Quoilin [2, 3] developed an ORC model using experimental data by interconnecting component models (i.e., heat exchangers, pump, and scroll expander). Again, their ORC system was for temporary lab setup with a scroll expander as the power generating unit and power output ranging from 0.67 kW to 1.03 kW. In a lab environment, Kang [4] tested a 30 kW ORC system with R245fa as the working fluid and a radial turbine as the power generating unit.

In the literature, it is possible to find information on small, lab-setup ORC systems with power ranging from watts (20 W to 1 kW) [2, 5, 6] and large scale ORC units with power

ranging from a few hundred kilowatts to megawatts [7–14]. The ORC theoretical models available in literature [15–22] are based on thermodynamic, energy balance, and heat transfer equations, and not on an experimental basis. In this study, a 50 kW commercial ORC system which can be used for waste heat recovery from rural Alaska diesel gen-sets, was tested by the authors in a lab environment to develop an ORC model. The developed model was validated with the field installation data presented in the following sections.

5.4.1 Present Work

At the University of Alaska Fairbanks (UAF), the authors tested a 50kW ORC system manufactured by ElectraTherm, Inc., in lab environment for reliability and performance analysis [23, 24]. Refrigerant R245fa, which is non-flammable and has zero ozone depletion potential, was the working fluid for the ORC. During the lab experiment, data was collected for the ORC system (i.e., temperatures and flow rates on hot water and cold water loops, screw expander power output, parasitic pump power consumptions). Experimental data were also collected for the individual components of the ORC on the refrigerant loop (mainly the refrigerant pressures and temperatures at inlet and outlet of respective components), vis-a-vis the preheater, evaporator, screw expander, working fluid pump, and condenser (Figure 5.1). Using the lab experimental data, various heat transfer correlations for heat exchangers and empirical correlations for the screw expander were studied in the author's previous publications [25, 26].

After lab testing at UAF, the ORC unit was permanently located in Tok, Alaska, installed on a 2 MW Caterpillar diesel engine for jacket water heat recovery. Due to the remote location of field installation, the instrumentation on the ORC system was limited to temperatures and flow rates on heat source and heat sink loops, screw expander power output, and parasitic pump power consumptions; and no measurements were made on the refrigerant side of the system.

Usually the information readily available for a village diesel engine would be heat source conditions (e.g., jacket water temperatures and flow rates) and heat sink conditions. Using this information, for performing the feasibility analysis (e.g., payback period analysis) of installing the present ORC system on village diesel engines, we need to know the net power generated by the ORC system for the given conditions. In the work presented here, using the lab experimental data and empirical models for ORC system components, a calculation procedure was developed to predict this ORC's screw expander power output. The developed calculation procedure was validated using field data. Throughout this paper, we will continue to refer to Figure

5.1(schematic of the ORC discussed) and Figure 5.2 (temperature versus ORC flow path diagram) for clarification and to reference state points in the ORC process.

5.5 Lab Experimental Setup

For more than a brief discussion of the lab experimental setup, the authors recommend previous publications [23–26]. The schematic of the experimental setup for testing the 50 kW ORC power unit was presented in the authors' previous publication [23], where the power unit was tested by varying the heat source and heat sink supply conditions (i.e., temperature and flow rate) to estimate performance characteristics. The heat source for the ORC power unit was hot water from a temperature- and flow rate-controlled heat source; the heat sink was cold water from a nearby fire hydrant, with a modification loop added for supply temperature and flow rate control (i.e., in Figure 5.1, the heating fluid loop is the hot water loop and the cooling fluid loop is the cold water loop in this experimental study). The power generated from the ORC power unit was uploaded to the UAF grid.

Figure 5.1 is a schematic line diagram of the present ORC machine, with all instrumentation components labeled for data collection during the experimental run at UAF. As a reference for our readers, Table 5.1 gives the hot water and cold water flow rate and temperature conditions under which the ORC power unit was tested at UAF. Note that in the experiment described here, the experimental setup was designed to test the ORC power unit as a whole, not specifically ORC component performances. Concurrent with the test of the ORC power unit under various hot and cold water supply conditions, steady-state data collection was carried out for various components of the power unit (i.e., screw expander, evaporator, pre-heater, condenser, and pump). Using this experimental data, the authors in previous studies, proposed empirical models for screw expander [25] and heat transfer correlations for R245fa in heat exchangers [26] namely preheater, evaporator and condenser, which will be used in this analysis to develop a calculation procedure to predict ORC power output.

5.6 Field Installation of ORC Unit

After performance testing in a lab environment, the 50 kW ORC power unit under consideration was part of a field installation, for jacket water recovery, in the Tok, Alaska, diesel power plant. In this section, we will discuss the installation setup, parameters measured and instrumentation for data collection in installing the ORC system on the 2 MW Caterpillar diesel engine which was the permanent installation location. Based on the Power Cost Equalization

(PCE) program [27] data for fiscal year 2011, the Tok annual electrical load is 10,902,597 kWh, virtually all this power was generated using an isolated Caterpillar 2 MW diesel engine.

In field testing of the ORC power unit, diesel engine jacket water was the heat source and underground well water was the heat sink. The heat source was provided with a 60:40 propylene glycol/water (60:40 PG/W) mixture loop. The 60:40 PG/W mixture flows between the engine jacket and the power unit evaporator and preheater, where the 60:40 PG/W mixture supplies heat to refrigerant in the evaporator and preheater. The underground well water was pumped to extract excess heat from refrigerant in the condenser of the power unit, and the return water was discharged into a nearby drain field. Therefore, in Figure 5.1 for the field installation, heating fluid is 60:40 PG/W and cooling fluid is cold water.

Due to the remoteness of the field installation site, only a few parameters related to overall ORC performance were measured. Table 5.2 lists the parameters measured during field testing of the ORC unit. No data collection was carried out on the refrigerant loop. The data were collected only for a brief period of time from October 2013 to November 2013. These data were used to validate the results obtained using the system model derived from thermal/hydraulic principle and lab experimental data.

As shown in Table 5.2, a Multical-601 energy meter, of which a Kamstrup Ultraflow ultrasonic flow meter and a Kamstrup Pt500 temperature sensor are part, was used to measure flow rate and temperatures for both 60:40 PG/W and cold water loops. The hourly average data for flow rate and temperatures were stored in a Multical-601 energy meter calculator. Custom software (LogView) provided by the energy meter manufacturer was used to download this hourly average flow rate and temperature data to a computer in the Excel spreadsheet format.

As shown in Figure 5.1 and Table 5.2, for electrical power measurement, EKM-353EDM-N electrical meters were used to measure net electrical power generated by the ORC power unit and power consumption by the power unit pump. The electrical meter manufacturer had custom software (EKM Metering) that was used for reading real-time electrical power measurement to the computer, and these real-time data were stored in text format at every 30-second interval for further data reduction. To match the 30-second interval electrical data to hourly energy meter data, electrical data were averaged over the hour for data reduction purposes.

During the field testing no variation in 60:40 PG/W flow rate ($\dot{m}_{hf}$), cold water flow rate ($\dot{m}_{cf}$), and cold water supply temperature (T_9) was observed throughout the data collection

period, as PG/W and cold water had constant flow rate pumps and underground well water temperature did not change. Therefore, the observed values for 60:40 PG/W flow rate ($\dot{m}_{hf}$) was 7.9 kg/s (28.4 m^3/h), cold water flow rate ($\dot{m}_{cf}$) was 4 kg/s (14.5 m^3/h) and cold water supply temperature was 1.5°C. Due to diesel gen-set load fluctuations from day to night and atmospheric temperature, the PG/W supply temperature (T_6) varied from 76.8°C to 86.5°C during the field data collection period.

5.7 Methodology

Before discussing methodology related to the present study, this paragraph gives some observations from the lab experimental run. In the ORC system under consideration, for all lab experiment test-run cases, the evaporator exit condition (screw expander inlet condition) for R245fa is superheated vapor; no two-phase vapor/liquid mixture condition at state-4 was observed. Also, the low-pressure refrigerant exiting the screw expander (state-5) is in superheated vapor condition, and refrigerant exiting the condenser (state-1) is in sub-cooled liquid condition. No two-phase vapor/liquid mixture conditions were observed at state-5 or at state-1.

In this section, the calculation procedure developed using lab experimental data is explained in detail. In the ORC process described in the above, the preheater, evaporator, and condenser are heat exchangers; primarily brazed plate heat exchangers (BPHE) are used in the current 50 kW ORC power unit. The working fluid pump is a Grundfos feed-pump with variable frequency drive (VFD). A proprietary twin screw expander is the power block used which converts high enthalpy working fluid exiting the evaporator (Figure 5.1) into mechanical work. The twin screw expander is connected to the generator for electrical power generation.

In the present study, ORC modeling procedure consists of solving system of equations related to the component models of present ORC to estimate ORC power output. Below are few assumptions considered in the present study, most of them taken from previous heat exchangers publication [26].

1. Heat loss of 5% in transferring heat from hot water to refrigerant in preheater and evaporator.
2. Refrigerant is in saturated liquid condition ($x_{3f} = 0$) at preheater exit.
3. No heat loss in condenser.
4. Major heat transfer in evaporator and condenser is due to latent heat of vaporization and condensation of R245fa, respectively.

5. Pressure drop in the heat exchangers is considered negligible (i.e., in Figure 5.1 and Figure 5.2 $P_2 = P_{3f} = P_4$ and $P_1 = P_5$).
6. The single-phase heat transfer correlation (Eq. (5.12c)) for water proposed by the authors in a previous study of a BPHE [26] is also valid for 60:40 PG/W mixture in the field installation data.
7. Regression curve-fitting relations for P_4 (Eq. (5.7)), $\dot{m}_{ref}$ (Eq. (5.8)), P_5 (Eq. (5.9)) and T_5 (Eq. (5.10)) developed using lab experimental data are valid for field installation data.

In the present study, the NIST REFPROP 9.1 [28] program was used to read thermodynamic and transport properties of water and refrigerant R245fa wherever applicable. Thermophysical properties for 60:40 PG/W were taken from the ASHRAE handbook [29].

For all statistical nonlinear regression analysis purposes and to find curve-fitting coefficients, in the present study, DataFit program [30] was used, which uses the widely applied Levenberg-Marquardt method.

Wherever applicable, fluid properties are taken as average of respective state points. For example, in single-phase heating fluid heat transfer correlation in the evaporator (Eq. (5.12c)), μ_{67f} in Re_{67f} is the heating fluid dynamic viscosity which is the average of μ_6 at state-6 and μ_{7f} at state-7f.

For performing the economic feasibility analysis of installing the present ORC system on village diesel engines, we need to know the net power generated by the ORC system. Usually the information readily available for a village diesel engine would be heat source conditions and heat sink conditions. Table 5.3 lists all the parameters (20 parameters) at each state point along the ORC process on heating fluid, cooling fluid and refrigerant sides shown in Figure 5.1. For estimating ORC power output, usually only four parameters listed in Table 5.3 are known, they are heating fluid flow rate ($\dot{m}_{hf}$) and supply temperature (T_6), cooling fluid flow rate ($\dot{m}_{cf}$) and supply temperature (T_9), which reduced the number of unknowns to 16. Considering the above assumption of negligible pressure drop in the heat exchangers, the number of unknowns reduces to 13. The assumption of saturated liquid condition at preheater exit or evaporator inlet (state-3f) (i.e., $x_{3f} = 0$), reduces the number of unknowns to 12. Generally, we have two mathematical relations for solving heat exchanger problems, namely energy balance and heat transfer relation. For the components of the ORC shown in Figure 5.1, we have two equations for the condenser, two equations for the evaporator, one each for the preheater, screw expander and pump. All

seven equations (Eq. (5.11) to Eq. (5.17)) are listed in following sections with explanations. From actual pump work (estimated using Eq. (5.16)), we can evaluate pump outlet condition of state-2 in Figure 5.1 (using Eq.(5.18)). Therefore, we have twelve unknowns with eight equations. Here, for the preheater, only energy balance relation (Eq. (5.17)) is considered due to the second assumption above of $x_{3f} = 0$.

Using the lab experimental data and nonlinear regression analysis, four additional curve-fitting relations were developed for estimating screw expander inlet pressure (P_4), refrigerant mass flow rate in the system ($\dot{m}_{ref}$), screw expander outlet pressure (P_5) and screw expander outlet temperature (T_5). Addition of these four curve-fitting relations increases the number of equations to twelve with the number of unknowns remaining unchanged at twelve. These twelve equations are solved to determine twelve unknowns to model the ORC power unit. The calculation procedure described here will be validated with field data.

Section 4.7.1 gives the general heat exchanger parameter equations that will be used in evaporator and condenser heat transfer analysis. Sections 4.7.2 to 4.7.7 give all the correlations derived from lab experimental data that will be used in the step-by-step calculation procedure described in Section 4.7.8. Sections 4.7.2 to 4.7.7 are almost in the same order as they appear in the calculation procedure of Section 4.7.8.

5.7.1 General Formulas for Brazed Plate Heat Exchangers

For the reader's convenience, heat exchanger parameters from the author's previous publication [26] are provided below. Table 5.4 and Figure 5.3 list the physical parameters for the heat exchangers used in this analysis. Heat transfer area (A) for a heat exchanger is given by,

$$A = N_{th} \times (W_2 \times L_2) \tag{5.1}$$

The term $(W_2 \times L_2)$ is the projected area for a single plate. Hydraulic diameter, an important parameter in heat exchanger analysis, is calculated by,

$$D_h = 2b \tag{5.2}$$

Flow area (A_f) for a BPHE is given by,

$$A_f = N_{ch} \times (W_2 \times b) \tag{5.3}$$

Here, N_{ch} is the number of channels on one fluid side. Mass flux (G) and Reynolds number (Re) for a flowing fluid in a BPHE are given by,

$$G = \frac{\dot{m}}{A_f} \tag{5.4}$$

$$Re = \frac{GD_h}{\mu} \tag{5.5}$$

Combining Eq. (5.2), Eq. (5.3) and Eq. (5.4) into Eq. (5.5), Re reduces to the form,

$$Re = \frac{2\dot{m}}{\mu N_{ch} W_2} \tag{5.6}$$

In Eq. (5.1) to Eq. (5.6), we will use suffix hf, cf, and ref for respective fluids of heating fluid, cooling fluid and refrigerant R245fa followed by suffix p, e, and c to represent respective heat exchangers for preheater, evaporator and condenser.

5.7.2 Regression Curve-fitting Relations for P_4, $\dot{m}_{ref}$, P_5 and T_5 using Lab Experimental Data

As discussed in the earlier paragraphs of this section, in order to solve for the eleven unknowns we have seven equations (Eq. (5.7) to Eq. (5.10) below) and four relations in the dimensionless form for P_4, $\dot{m}_{ref}$, P_5 and T_5 are developed in the present subsection. Note that only lab experimental data were used in proposed correlations of Eq. (5.7) to Eq. (5.10), and no field testing data were used.

Table 5.5 lists the curve-fitting coefficients for Eq. (5.7) to Eq. (5.10) obtained by DataFit [30] nonlinear regression analysis program. Note that Equations (5.7) to (5.10) are given in dimensionless form and their definition for dimensionless form is given in Table 5.3. Table 5.5 also lists the ranges of validity of Eq. (5.7) to Eq. (5.10).

To maintain a superheated vapor condition at screw expander inlet (state-4), the working fluid pump's VFD is controlled using proprietary Program Logic Controller (PLC) program. The PLC determines the expander inlet pressure (P_4) based on feedback from heating fluid flow conditions ($\dot{m}_{hf}$, T_6), cooling fluid temperature (T_9) and R245fa saturated pressure at T_6 (P_{sat6}), and controls the pump VFD accordingly. Based on the VFD signal the pump supplies refrigerant mass flow rate into the system ($\dot{m}_{ref}$) to maintain P_4. Therefore, a curve-fitting correlation for P_4 (Eq. (5.7)) in terms of $\dot{m}_{hf}$, T_6, T_9 and P_{sat6}; and $\dot{m}_{ref}$ (Eq. (5.8)) in terms of P_4 is presented with coefficient of determination (R^2) of 0.99. Figure 5.4 and Figure 5.5 give the comparison of experimental data with predicted data using Eq. (5.7) and Eq. (5.8) for P_4 and $\dot{m}_{ref}$, respectively. Ninety-seven percent of predicted P_4 values using Eq. (5.7) were within ±4.9% with root mean square (RMS) error of 0.018.

From Figure 5.5, we can observe that $\dot{m}_{ref}$ values were predicted using experimental P_4 values and P_4 values from Eq. (5.7). 99% of predicted $\dot{m}_{ref}$ values using Eq. (5.8) and

experimental P_4 values were within ±4.8% with RMS error of 0.04. 97% of predicted $\dot{m}_{ref}$ values using Eq. (5.8) and P_4 values from Eq. (5.7) were within ±6% with RMS error of 0.06.

$$P_{4,o} = \left(\mathrm{a} * \dot{m}_{hf,o}^{\mathrm{b}}\right) + \left(\mathrm{c} * T_{6,o}^{\mathrm{d}}\right) + \left(\mathrm{e} * T_{9,o}^{\mathrm{f}}\right) + \left(\mathrm{g} * P_{sat6,o}^{h}\right) \tag{5.7}$$

$$\dot{m}_{ref,o} = \left(\mathrm{a} * P_{4,o}^{5}\right) + \left(b * P_{4,o}^{4}\right) + \left(\mathrm{c} * P_{4,o}^{3}\right) + \left(\mathrm{d} * P_{4,o}^{2}\right) + \left(\mathrm{e} * P_{4,o}\right) \tag{5.8}$$

Generally, in a heat exchanger study, the inlet fluid condition (temperatures and flow rates) on both sides is known and the outlet condition (usually outlet temperatures) is determined by solving energy balance and heat transfer equations. Similarly, in the present study the condenser inlet condition on the cooling fluid side (inlet flow rate and temperature) is known, but it is not known on the refrigerant side. Two curve-fit relations for refrigerant pressure (P_5) and temperature (T_5) at condenser inlet are developed in dimensionless form, as given by Eq. (5.16) and Eq. (5.17). The reason for selecting condenser inlet condition (state-5) instead of preheater inlet (state-2) is because of the dependence of state-2 on condenser performance. P_5 and T_5 depend on screw expander output and cooling fluid conditions, and are interdependent. Different types of curve-fit correlations in dimensionless forms were tried using the DataFit [30] statistical analysis program before arriving at Eq. (5.9) and Eq. (5.10) with R^2 of 0.99.

From Figure 5.6, which is a comparison of experimental P_5 data with predicted data using Eq. (5.9), we can observe that P_5 values were predicted using experimental $\dot{m}_{ref}$ values and $\dot{m}_{ref}$ values from Eq. (5.8). 97% of predicted P_5 values using Eq. (5.9) and experimental $\dot{m}_{ref}$ values were within ±2.7% with RMS error of 0.0017. 98% of predicted P_5 values using Eq. (5.9) and $\dot{m}_{ref}$ values from Eq. (5.8) were within ±4.4% with RMS error of 0.003.

Similarly from Figure 5.7, which is a comparison of experimental T_5 data with predicted data using Eq. (5.10), we can observe that T_5 values were predicted using experimental P_5 values and P_5 values from Eq. (5.9). 99% of predicted T_5 values using Eq. (5.10) and experimental P_5 values were within ±3.5% with RMS error of 0.49. 99% of predicted T_5 values using Eq. (5.10) and P_5 values from Eq. (5.9) were within ±4.9% with RMS error of 0.64.

$$P_{5,o} = \left(\mathrm{a} * \dot{m}_{cf,o}^{\mathrm{b}} * \dot{m}_{ref,o}^{\mathrm{c}} * T_{6,o}^{\mathrm{d}}\right) + \left(\mathrm{e} * T_{9,o}^{\mathrm{f}}\right) \tag{5.9}$$

$$T_{5,o} = \left(\mathrm{a} * \dot{m}_{cf,o}\right) + \left(\mathrm{b} * T_{9,o}\right) + \left(\mathrm{c} * P_{5,o}\right) + \left(d * w_{SE,o}\right) + e \tag{5.10}$$

5.7.3 Evaporator (state-3f, state-4, state-6 and state-7f in Figure 5.1)

In the evaporator, saturated liquid refrigerant from state-3f is first heated to saturated vapor (state-3g in Figure 5.2) condition and then to superheated vapor to state-4 while extracting heat

from heating fluid (state-6 to state7f). Energy balance and heat transfer relations for evaporator are given by,

$$\dot{m}_{ref}(h_4 - h_{3f}) = 0.95\dot{m}_{hf}C_{p,hf}(T_6 - T_{7f}) \tag{5.11}$$

$$Q_e = U_e A_e \Delta T_{lm,e} \tag{5.12}$$

In Eq. (5.11), 0.95 represents 5% heat loss in the preheater from heating fluid to refrigerant (first assumption). In Eq. (5.12), Q_e is the average heat transfer between hot fluid and R245fa in the evaporator. Q_e is the average of $(Q_{hf,e} = \dot{m}_{hf}C_{p,hf}(T_6 - T_{7f}))$ and $(Q_{ref,e} = \dot{m}_{ref}(h_4 - h_{3f}))$. Definitions for terms in Eq. (5.12), that is, U_e and $\Delta T_{lm,e}$, are given by Eq. (5.12a) and Eq. (5.12d).

Expressions for $\alpha_{ref,e}$ (Eq. (5.12b)) and $\alpha_{hf,e}$ (Eq. (5.12c)) are from the previous study on heat exchangers [26]. Note that only lab experimental data were used in proposed correlations for $\alpha_{ref,e}$ and $\alpha_{hf,e}$ and no field testing data were used. Log-mean temperature difference ($\Delta T_{lm,e}$), given by Eq. (5.12d), is for the entire evaporator and is determined from a weighted average of LMTDs for each zone of evaporator vis-a-vis two-phase boiling and superheat. The LMTDs for two-phase boiling and superheat zones are calculated using Eq. (5.12e) through Eq. (5.12h) below. Here wherever applicable, $h_{3f} = f(P_4, x_{3f} = 0)$; $h_{3g} = f(P_4, x_{3g} = 1)$; $T_{3f} = T_{3g} = f(P_4, x_{3f} = 0 \; or \; 1)$. Other terms in Eq. (5.12b) are evaluated using Eq. (5.12i) through Eq. (5.12n).

$$\frac{1}{U_e} = \frac{1}{\alpha_{hf,e}} + \frac{t}{k_{pm}} + \frac{1}{\alpha_{ref,e}} \tag{5.12a}$$

$$\alpha_{ref,e} = 0.847 Re_{eq,ref,e}^{1.0} * Pr_{3f}^{0.9} * \left(\frac{G_{ref,e}^2}{\rho_{3f}^2 C_{p,3f} \Delta T_{s,ref,e}}\right)^{0.6} \left(\frac{\rho_{3f}^2 (h_{3g} - h_{3f})}{G_{ref,e}^2}\right)^{-0.3} \left(\frac{\rho_{3f}\sigma_{3f}}{\mu_{3f} G_{ref,e}}\right)^{1.4} \left(\frac{\rho_{3f}}{\rho_{3f} - \rho_{3g}}\right)^{1.0} \left(\frac{k_{3f}}{D_h}\right) \tag{5.12b}$$

$$\alpha_{hf,e} = 0.01\left(Re_{67f}^{1.05}\right)\left(Pr_{67f}^{0.9}\right)\left(\frac{k_{67f}}{D_h}\right) \tag{5.12c}$$

$$\Delta T_{lm,e} = \frac{Q_e}{\left(\frac{Q_{2p,e}}{\Delta T_{lm,2p,e}}\right) + \left(\frac{Q_{sup,e}}{\Delta T_{lm,sup,e}}\right)} \tag{5.12d}$$

$$Q_{2p,e} = \dot{m}_{ref}(h_{3g} - h_{3f}) \tag{5.12e}$$

$$\Delta T_{lm,2p,e} = \frac{(T_{6g} - T_{3g}) - (T_{7f} - T_{3f})}{ln\left(\frac{T_{6g} - T_{3g}}{T_{7f} - T_{3f}}\right)} \tag{5.12f}$$

$$Q_{sup,e} = \dot{m}_{ref}(h_4 - h_{3g}) \tag{5.12g}$$

$$\Delta T_{lm,sup,e} = \frac{(T_6 - T_4) - (T_{6g} - T_{3g})}{ln\left(\frac{T_6 - T_4}{T_{6g} - T_{3g}}\right)} \tag{5.12h}$$

$$Re_{eq,ref,e} = \frac{G_{eq,ref,e}\, D_h}{\mu_{3f}} \tag{5.12i}$$

$$G_{eq,ref,e} = G_{ref,e}\left[0.5 + 0.5\left(\frac{\rho_{3f}}{\rho_{3g}}\right)^{0.5}\right] \tag{5.12j}$$

$$\Delta T_{s,ref,e} = T_{s,e} - T_{avg,ref,e} \tag{5.12k}$$

$$T_{s,e} = \frac{T_{avg,hf,e} + T_{avg,ref,e}}{2} \tag{5.12l}$$

$$T_{avg,hf,e} = \frac{T_6 + T_{7f}}{2} \tag{5.12m}$$

$$T_{avg,ref,e} = \frac{T_{3f} + T_4}{2} \tag{5.12n}$$

5.7.4 Screw Expander (state-4 and state-5 in Figure 5.1)

Screw-type expanders are positive displacement devices consisting of helical screw rotors with male and female rotors. The male and female rotors are separated by narrow clearances, on the order of 50 microns, obtained by bearing and timing gears. As the high pressure working fluid enters the expander at the inlet port (state-4), the volume of the working fluid increases between the rotors and the expander housing (to the discharge port pressure), and causes the rotors to rotate. As the fluid volume increases to the discharge port pressure (state-5), it exerts pressure on the rotors and causes them to rotate, thereby transferring power from the working fluid to the screw expander shaft, which is connected to the electric generator. It has been reported in the literature that screw expanders can admit two-phase mixtures (i.e., low enthalpy value working fluids) to generate electrical power, making them suitable for low-grade heat recovery applications.

For proprietary reasons, the physical parameters of the screw expander under study cannot be disclosed. Therefore, for the work presented in [25], the screw expander was analyzed using a "black-box" approach based on the measured lab experimental parameters of inlet (state-4) and outlet (state-5) pressures and temperatures, the authors proposed a screw expander model (Eq. (5.13)) in previous publication [25] based on isentropic work and it will be used in this study. To estimate the expander power output using Eq. (5.13) the parameters needed are $\dot{m}_{ref}$, T_4 and P_4

(for h_4), and P_5 (for h_{5s}). Note that only lab experimental data were used in the proposed screw expander correlation of $w_{SE,o}$ and no field testing data were used.

$$w_{SE,o} = 10176.6515 * w_{s,o}^4 - 2877.4007 * w_{s,o}^3 + 291.0713 * w_{s,o}^2 - 11.7825 * w_{s,o} + 0.1874 \quad (5.13)$$

$$w_{SE,o} = \frac{W_{SE}}{\dot{m}_{ref} h_o} \quad (5.13a)$$

$$w_{s,o} = \frac{(h_4 - h_{5s})}{h_o} \quad (5.13b)$$

Eq. (5.13) is valid for refrigerant R245fa with 424.4kPa ≤ P_4 ≤ 1027.3kPa and 10kW ≤ W_{SE} ≤ 51.5kW, and with refrigerant inlet to screw expander in saturated/superheated vapor condition. The predicted screw expander power output using Eq. (5.13) was within ±7.5% of the experimental measured power output values.

5.7.5 Condenser (state-5, state-1, state-9 and state-10 in Figure 5.1)

In the condenser, the low-pressure refrigerant exiting the screw expander (state-5 in Figure 5.1) is cooled to sub-cooled liquid using the cooling fluid. For all the lab experiment cases, in the present ORC system under consideration, the low-pressure refrigerant exiting the screw expander (state-5) is in superheated vapor condition and refrigerant exiting the condenser (state-1) is in sub-cooled liquid condition (i.e., no two-phase vapor/liquid mixture conditions were observed at state-5 and state-1 respectively). Eq. (5.14) and Eq. (5.15) below are the energy balance and heat transfer expressions related to the condenser respectively, which is a brazed plate heat exchanger.

$$Q_c = \dot{m}_{cf} C_{p,cf} (T_{10} - T_9) = \dot{m}_{ref} (h_5 - h_1) \quad (5.14)$$

$$Q_c = U_c A_c \Delta T_{lm,c} \quad (5.15)$$

$$\frac{1}{U_c} = \frac{1}{\alpha_{cf,c}} + \frac{t}{k_{pm}} + \frac{1}{\alpha_{ref,c}} \quad (5.15a)$$

$$\alpha_{ref,c} = 0.1 Re_{eq,ref,c}^{1.0} * Pr_{5f}^{0.2} * \left(\frac{G_{ref,c}^2}{\rho_{5f}^2 C_{p,5f} \Delta T_{s,ref,c}}\right)^{1.3} \left(\frac{\rho_{5f}^2 (h_{5g} - h_{5f})}{G_{ref,c}^2}\right)^{1.0} \left(\frac{\rho_{5f} \sigma_{5f}}{\mu_{5f} G_{ref,c}}\right)^{0.05} \left(\frac{\rho_{5f}}{\rho_{5f} - \rho_{5g}}\right)^{2.0} \left(\frac{k_{5f}}{D_h}\right) \quad (5.15b)$$

$$\alpha_{cf,c} = 0.01 (Re_{910}^{1.05})(Pr_{910}^{0.9}) \left(\frac{k_{910}}{D_h}\right) \quad (5.15c)$$

Expressions for $\alpha_{ref,c}$ and $\alpha_{cf,c}$ are from the previous study on heat exchangers [26]. Note that only lab experimental data were used in proposed correlations for $\alpha_{ref,c}$ and $\alpha_{cf,c}$, no field testing data were used. Log-mean temperature difference ($\Delta T_{lm,c}$) is given by Eq. (5.15d) for the entire condenser and is determined from a weighted average of LMTDs for each zone of condenser vis-a-vis superheat, two-phase condensing and sub-cooled. The LMTDs for superheat, two-phase condensing and sub-cooled zones are calculated using Eq. (5.15e) through Eq. (5.15l) below. Here wherever applicable, $h_{5f} = f(P_5, x_{5f} = 0)$; $h_{5g} = f(P_5, x_{5g} = 1)$; $T_{5f} = T_{5g} = f(P_5, x_{5f} = 0 \; or \; 1)$. Similar equations to Eq. (5.12i) through Eq. (5.12n) can be used to determine other terms in Eq. (5.15b).

$$\Delta T_{lm,c} = \frac{Q_c}{\left(\frac{Q_{sup,c}}{\Delta T_{lm,sup,c}}\right)+\left(\frac{Q_{2p,c}}{\Delta T_{lm,2p,c}}\right)+\left(\frac{Q_{sub,c}}{\Delta T_{lm,sub,c}}\right)} \tag{5.15d}$$

$$Q_{sup,c} = \dot{m}_{ref}(h_5 - h_{5g}) \tag{5.15e}$$

$$\Delta T_{lm,sup,c} = \frac{(T_5 - T_{10}) - (T_{5g} - T_{9g})}{ln\left(\frac{T_5 - T_{10}}{T_{5g} - T_{9g}}\right)} \tag{5.15f}$$

$$T_{9g} = T_{10} - \frac{Q_{sup,c}}{\dot{m}_{cf} C_{p,cf}} \tag{5.15g}$$

$$Q_{2p,c} = \dot{m}_{ref}(h_{5g} - h_{5f}) \tag{5.15h}$$

$$\Delta T_{lm,2p,c} = \frac{(T_{5g} - T_{9g}) - (T_{5f} - T_{9f})}{ln\left(\frac{T_{5g} - T_{9g}}{T_{5f} - T_{9f}}\right)} \tag{5.15i}$$

$$T_{9f} = T_{9g} - \frac{Q_{2p,c}}{\dot{m}_{cf} C_{p,cf}} \tag{5.15j}$$

$$Q_{sub,c} = \dot{m}_{ref}(h_{5f} - h_1) \tag{5.15k}$$

$$\Delta T_{lm,sub,c} = \frac{(T_{5f} - T_{9f}) - (T_1 - T_9)}{ln\left(\frac{T_{5f} - T_{9f}}{T_1 - T_9}\right)} \tag{5.15l}$$

5.7.6 Working Fluid Pump (state-1 and state-2 in Figure 5.1)

The working fluid pump is a Grundfos feed-pump with a variable frequency drive (VFD). The pump VFD is controlled by the ORC manufacturer proprietary PLC which is based on many factors such as heating fluid and cooling fluid inlet conditions, feedback from R245fa evaporator exit pressure sensor (P_4). Based on the pump VFD, refrigerant flow rate is determined by which evaporator exit conditions (state-4) are determined.

For working fluid pump power estimation, a linear curve-fit in terms of volumetric pump power consumption was developed using lab experimental data and is given by Eq. (5.16) below. The developed correlation had a coefficient of determination (R^2) of 0.991 and predicted pump power, using Eq. (5.16), is within ±6.5% with respect to lab experimental data (Figure 5.8). In Eq. (5.16) and Eq. (5.16a), h_o is the enthalpy of R245fa at 25°C and 0.101325MPa, and is used to get dimensionless terms; $\vartheta_1 = f(P_5, T_1)$ is the specific volume of R245fa at state-1. Note that only lab experimental data were used in proposed Eq. (5.16) and no field testing data were used.

$$w_{pu,o} = 1.86685\left(\frac{\vartheta_1(P_4 - P_5)}{h_o}\right) + 0.0010072 \tag{5.16}$$

$$w_{pu,o} = \frac{w_{pu}}{\dot{m}_{ref} h_o} \tag{5.16a}$$

5.7.7 Preheater (state-2, state-3f, state-7f and state-8 in Figure 5.1)

The high pressure liquid refrigerant exiting the working fluid pump (state-2) is heated to saturated liquid condition (state-3f) in the preheater using the heating fluid exiting the evaporator (state-7f). Therefore in the preheater it is liquid-to-liquid heat transfer from heating fluid to refrigerant. From working fluid pump analysis refrigerant state-2 (preheater inlet) condition is determined. State-3f (preheater exit) is in saturated liquid condition. From the evaporator analysis, heating fluid condition at state-7f is determined. Therefore, by using an energy balance relation for the preheater, the heating fluid condition at state-8 can be determined by Eq. (5.17) where 0.95 represents 5% heat loss in preheater from heating fluid to refrigerant (first assumption).

$$0.95\dot{m}_{hf} C_{p,hf}(T_{7f} - T_8) = \dot{m}_{ref}(h_{3f} - h_2) \tag{5.17}$$

5.7.8 Calculation Procedure

Figure 5.9 is the flowchart for the calculation procedure adopted in the present study. As discussed in the earlier part of this section, the information readily available for a village diesel engine would be heat source supply conditions ($\dot{m}_{hf}$, T_6) and heat sink supply conditions ($\dot{m}_{cf}$, T_9). Below gives the step-by-step description of the calculation procedure used in this study to model the present ORC system.

1. Read inputs $\dot{m}_{hf}$, T_6, $\dot{m}_{cf}$, and T_9.
2. From inputs evaluate P_4, $\dot{m}_{ref}$, and P_5 using Eq. (5.7), Eq. (5.8) and Eq. (5.9).

3. Evaporator: Using the conditions at state-6 (T_6) and state-3f (P_4, and $x_{3f} = 0$), evaluate state-4 (T_4) and state-7f (T_{7f}) using an evaporator energy balance and heat transfer equations of Eq. (5.11) and Eq. (5.12), respectively.
4. Screw expander: Using the conditions at state-4 (T_4, P_4) and state-5 (P_5), calculate screw expander power output (W_{SE}) using Eq. (5.13).
5. Evaluate T_5 using Eq. (5.10).
6. Condenser: Using the conditions at state-9 (T_9) and state-5 (T_5, P_5), evaluate state-1 (T_1) and state-10 (T_{10}) using a condenser energy balance and heat transfer equations of Eq. (5.14) and Eq. (5.15), respectively.
7. Working fluid pump: Using conditions at state-1 (T_1, P_5) and state-2 (P_4), evaluate pump power (W_{pu}) using Eq. (5.16).
8. Estimate T_2: Using the Eq. (5.18) for the working fluid pump, calculate h_2 and then evaluate $T_2 = f(P_4, h_2)$.

$$h_2 = h_1 + \left(\frac{W_{pu}}{\dot{m}_{ref}}\right) \tag{5.18}$$

9. Preheater: Using conditions at state-2 (T_2, P_4), state-3f (P_4, and $x_{3f} = 0$) and state-7f (T_{7f}), evaluate T_8 using preheater energy balance equation of Eq. (5.17).

5.8 Results and Discussion

A 50 kW ORC power unit was tested in the lab environment for different hot water and cold water conditions for performance mapping at UAF. The purpose of lab testing was to simulate different diesel engine waste heat conditions to the power unit and study its reliability and performance as a whole and its component performance in particular. Literature on these studies by the authors can be found in [23], [24], [25],and [26]. After the lab experiment, the power unit was installed on a 2 MW Caterpillar diesel engine generator for jacket water heat recovery. In the field installation, 60:40 PG/W and cold water were supplied as heating and cooling fluid to the power unit, as explained in Section 5.6.

As explained in Section 5.5, during the lab experiment, data collection was carried out not only for the ORC power unit as a whole (i.e., hot water and cold water supply and return temperatures, flow rates , power output, pump power consumption) but also on refrigerant loop for ORC components (i.e., screw expander, evaporator, preheater, condenser, pump). Using this component performance data, the authors proposed empirical models for screw expander [25]

and heat transfer correlations for R245fa in heat exchangers [26]. Note that in development of these empirical models only lab experimental data were used. No field data were used, as during the field installation no data collection was carried out on the refrigerant side of the system; and the only data collected was for 60:40 PG/W and cold water supply and return temperatures, respective flow rates, ORC power output, and R245fa pump power consumption.

In this study, with use of the previously proposed empirical models for screw expander [25] and heat transfer correlations for R245fa in heat exchangers [26], a step-by-step calculation procedure to predict ORC performance was developed in Section 5.7.8. The developed procedure was validated for both lab experimental data and field data. Assumed here is that as the heating fluid in the lab experiment (hot water) and the field installation (60:40 PG/W) are different, the single-phase heat transfer correlation for heating fluid (Eq. (5.12c)) developed using lab experimental data is also valid for 60:40 PG/W.

Figures 5.10 to 5.21 give the plots for predicted versus measured parameters for heat supplied by heating fluid in the evaporator and preheater (Q_{hf}, Figures 5.10 and 5.11), heat rejected to cooling fluid in the condenser (Q_{cf}, Figures 5.12 and 5.13), screw expander power output (W_{SE}, Figures 5.14 and 5.15), R245fa pump power consumption (W_{pu}, Figures 5. 16 and 5.17), heating fluid exit temperature for the preheater (T_8, Figures 5.18 and 5.19), and cooling fluid exit temperature for the condenser (T_{10}, Figures 5.20 and 5.21) for both lab experimental data and field data. Table 5.6 gives the range of error in predicted values for the above parameters when compared with measured parameters.

From Figure 5.10 to Figure 5.21 and Table 5.6, it can be inferred that the developed calculation procedure to model the present ORC system predicts the parameter values reasonably well when compared with measured values. The parameters useful from the ORC modeling output may be Q_{hf}, W_{SE}, W_{pu} and T_8. Heat supplied by heating fluid in the evaporator and preheater (Q_{hf}) is used in determining the amount of heat available from diesel gen set to the ORC system, thermal cycle efficiency of the ORC system and to estimate the improvement in fuel efficiency of the diesel power plant as a whole and emissions reduction.

For performing the economic feasibility analysis of installing the ORC power unit for diesel gen-set heat recovery, the net power generated by the power unit is needed, which is estimated as the difference between the screw expander power output (W_{SE}) and R245fa pump power consumption (W_{pu}). From Figure 5.18, we can note that the heating fluid temperature at the

preheater exit (T_8) ranges from 60°C to 100°C; the heating fluid exiting the power unit has a considerable amount of waste heat. Based on T_8 values we can estimate the additional amount of heat recovery possible from the heating fluid for other useful purposes, mainly for heating needs considering the geographical location of Alaska rural villages.

5.8.1 Adaptability of Developed Procedure for Other ORC Machines

A similar step-by-step calculation procedure, developed in the present study to predict 50 kW ORC performance, can be developed for other ORC heat engines for performance prediction if we have the experimental data pertaining to each component of the ORC. For example, consider another hypothetical ORC system which has a power range of 100 kW to 200 kW and uses different a working fluid (not R245fa), a radial turbine as the power block and shell-tube exchangers as heat transfer components for the preheater, evaporator and condenser. We can develop similar relations as Eq. (5.7) to Eq. (5.18) using the experimental data obtained by testing that ORC machine, and the only difference would be the correlation coefficient values in respective relations. The step-by-step calculation procedure explained in Section 5.7.8 would remain the same for predicting the performance of the ORC system.

5.9 Conclusions

In this study, the authors developed a calculation procedure to model a 50 kW ORC power unit using empirical relations for screw expander and heat transfer correlations for R245fa in heat exchangers. The proposed calculation procedure takes heating fluid and cooling fluid supply flow rate and temperature as input, usually the only information available in a village gen-set application. Performance parameters such as screw expander power output, working fluid pump power consumption, heat input to the ORC system in evaporator and preheater, and heat rejected by the ORC system in condenser were evaluated using the model; then they made comparisons with both experimental data and field installation data. The developed model was validated with both lab experimental data and field installation data.

As the ORC model is based on heat transfer and energy balance principles for heat exchangers, it can be used in modeling for any heating fluid and cooling fluid in the evaporator and condenser (heating and cooling fluids can be pure water or glycol/water mixtures). Using the model, we can predict the heating fluid temperature exiting the ORC power unit (i.e., heating fluid temperature at the preheater exit), and based on this we can design the waste heat recovery

system for other useful purposes, such as for space heating or municipal water heating applications.

5.10 References

[1] Lin, C.S., "Capture of heat energy from diesel engine exhaust," Final report prepared for National Energy Technology Laboratory, DOE Award # DE-FC26-01NT41248, November, 2008.

[2] Quoilin, S., "Experimental study and modeling of a low temperature Rankine cycle for small scale cogeneration," Master's Thesis, University of Liege, May 2007.

[3] Quoilin, S., Lemort, V., and Lebrun, J., "Experimental study and modeling of an organic Rankine cycle using scroll expander," Applied Energy, Vol.87, pp. 1260-1268, 2010.

[4] Kang, S.H., "Design and experimental study of ORC (organic Rankine cycle) and radial turbine using R245fa working fluid," Energy, Vol.41, pp.514-524, 2012.

[5] Yamamoto, T., Furuhata, T., Arai, N., and Mori, K., "Design and Testing of the Organic Rankine Cycle", Journal of Energy, Vol.26, pp. 239-251, 2001.

[6] Reid, A.D., "Low temperature power generation using HFE-7000 in a Rankine cycle," Master's Thesis, San Diego State University, July 2010.

[7] Holdmann, G., "The Chena Hot Springs 400 kW Geothermal Power Plant: Experience Gained During the First Year of Operation," Transactions of the Geothermal Resource Council, Vol.31, pp. 509-514, Davis, CA, September 2007.

[8] Leslie, N.P., Zimron, O., Sweetser, R.S., and Stovall, T.K., "Recovered energy generation using an Organic Rankine Cycle system," ASHRAE Transactions # CH-09-024, Vol. 115, Part 1, ASHRAE Winter Conference, Chicago, 2009.

[9] Pernecker, G. and Uhlig, S., "Low-enthalpy power generation with ORC-Turbogenerator: The Altheim project, Upper Austria," GHC bulletin, March 2002.

[10] Canada, S., Cohen, G., Cable, R., Brosseau, D., and Price, H., "Parabolic trough Organic Rankine Cycle solar power plant," Presented at the 2004 DOE Solar Energy Technologies Program Review Meeting, Denver, Colorado, October 25–28, 2004.

[11] Nasir, P., Jones, S., Schochet, D., and Posner, D., "Utilization of turbine waste heat to generate electric power at Neptune plant," Proceedings of 83rd Gas Processors Association Annual Convention, New Orleans, LA, March 2004.

[12] Bini, R., Schwarz, D.A., Gaia, M., Bertuzzi, P., and Righini, W., "Operational results of the first biomass CHP plant in Italy based on an Organic Rankine Cycle turbogenerator and overview of a number of plants in operation in Europe since 1998," Proceedings of the 2nd World Conference on Biomass for Energy, Industry and Climate Protection, Rome, Italy, pp. 1716 – 1721, May10-14, 2004.

[13] Obernberger, I., Thonhofer, P., and Reisenhofer, E., "Description and evaluation of the new 1,000kWe Organic Rankine Cycle process integrated in the biomass CHP plant in Lienz, Austria," Euroheat & Power, Vol.10, pp. 18-25, 2002.

[14] Turboden ORC plants for Industrial Heat Recovery. Turboden press release URL: http://www.turboden.eu/it/public/downloads/11-COM.P-18-rev.4_HR_ENG.pdf. Accessed July 17th 2012.

[15] Kuo, C.R., Hsu, S.W., Chang, K.H., and Wang, C.C., "Analysis of a 50 kW organic Rankine cycle system," Energy, Vol.36, pp.5877-5885, 2011.

[16] Sun, F., Ikegami, Y., Jia, B., and Arima, H., "Optimization design and exergy analysis of organic Rankine cycle in ocean thermal energy conversion," Applied Ocean Research, Vol.35, pp.38-46, 2012.

[17] Aly, S.E., "Diesel Engine Waste-Heat Power Cycle," Journal of Applied Energy, Vol.29 (3), pp. 179-189, 1988.

[18] Paolo, C., "Exergoeconomic Analysis and Optimization of Organic Rankine Cycles," Master's Thesis, University of Ontario Institute of Technology, 2012.

[19] Teng, H., Regner, G., and Cowland, C., "Waste heat recovery of heavy-duty diesel engines by Organic Rankine Cycle Part I: Hybrid energy system of diesel and rankine engines," SAE technical paper # 2007-01-0537, World congress, Detroit, Michigan, April 16-19, 2007.

[20] Grabinski, P., "Optimization of the performance of an Organic Rankine Cycle used as waste heat recovery system in a bio-liquid diesel engine power plant," Master's Thesis, University of Iceland, February 2011.

[21] Madhawa, H.H.D., Golubovic, M., Worek, W.M., and Ikegami, Y., "Optimum design criteria for an Organic Rankine Cycle using low-temperature geothermal heat source," Journal of Energy, Vol.32, pp. 1698-1706, 2007.

[22] Bombarda, P., Invernizzi, C.M., and Pietra, C., "Heat recovery from diesel engines: A thermodynamic comparison between Kalina and ORC cycles," Journal of Applied Thermal Engineering, Vol.30, pp. 212-219, 2010.

[23] Avadhanula, V.K., Lin, C.S., and Johnson, T., "Testing a 50kW ORC at Different Heating and Cooling Source Conditions to Map the Performance Characteristics," SAE Technical Paper # 2013-01-1649, April 2013.

[24] Lin, C.S., Avadhanula, V.K., Mokkapati, V., Huang, D., and Sheets, B., "Guidelines for Effectively Applying an ORC System to Rural Alaska Diesel Power Industry Based on Experimental Data," SAE Technical Paper # 2015-01-1607, April 2015.

[25] Avadhanula, V.K., and Lin, C.S., "Empirical models for screw expander based on experimental data from organic Rankine cycle system testing," ASME Journal of Engineering for Gas Turbines and Power, Vol.136, June 2014.

[26] Avadhanula, V.K., Lin, C.S., and Das, D.K., "Heat Transfer Correlations for R245fa in Preheater, Evaporator and Condenser using Experimental Data from 50 kW Organic Rankine Cycle (ORC) System Testing," Under Review in Heat Transfer Engineering, May 2015.

[27] Alaska Energy Authority, "Statistical report of the power cost equalization program for fiscal year 2011," 23rd Edition, April 2012.

[28] Lemmon, E.W., Huber, M.L., and McLinden, M.O., "NIST Standard Reference Database 23: Reference Fluid Thermodynamic and Transport Properties-REFPROP," Version 9.1, National Institute of Standards and Technology, Standard Reference Data Program, Gaithersburg, 2013.

[29] American Society of Heating, Refrigeration, and Air-Conditioning Engineers, ASHRAE Handbook of Fundamentals, ASHRAE, Atlanta, United States, 2009.

[30] DataFit: Data curve-fitting (nonlinear regression) and data plotting software, Version 9.0.59, Oakdale Engineering, Oakdale, PA, 2011. Available from http://www.curvefitting.com.

Table 5.1 Various hot water and cold water flow rates and temperatures at which the power unit was tested

Hot water temperature, °C (°F)	Hot water flow rate, m^3/h (gpm)	Cold water temperature, °C (°F)	Cold water flow rate, m^3/h (gpm)
68.3 (155)	27.2 (120)	10 (50)	27.2 (120)
79.4 (175)	36.3 (160)	20 (68)	36.3 (160)
90.5 (195)	45.4 (200)		45.4 (200)
101.7 (215)	56.8 (250)		
107.2 (225)	68.1 (300)		

Table 5.2 Parameters measured, instrumentation, and uncertainty in measurement during field testing of ORC power unit

Parameter	State point on Figure 5.1	Instrumentation	Units	Uncertainty in measurement	Frequency of data collection
60:40 PG/W supply temperature	T_6	Kamstrup Pt500 temperature sensor	°C	±1.1°C	1 hour (hourly average)
60:40 PG/W return temperature	T_8	Kamstrup Pt500 temperature sensor	°C	±1.1°C	1 hour (hourly average)
60:40 PG/W flow rate	$\dot{V}_6 = \dot{V}_8 = \dot{V}_h$	Kamstrup Ultraflow ultrasonic flow meter	m^3/h	0.5%	1 hour (hourly average)
Cold water supply temperature	T_9	Kamstrup Pt500 temperature sensor	°C	±1.1°C	1 hour (hourly average)
Cold water return temperature	T_{10}	Kamstrup Pt500 temperature sensor	°C	±1.1°C	1 hour (hourly average)
Cold water flow rate	$\dot{V}_9 = \dot{V}_{10} = \dot{V}_{cw}$	Kamstrup Ultraflow ultrasonic flow meter	m^3/h	0.5%	1 hour (hourly average)
ORC power unit net power	$W_{net} = W_{11}$	EKM-353EDM-N	kW	0.5%	30 seconds
ORC pump power	$W_{pump} = W_{12}$	EKM-353EDM-N	kW	0.5%	30 seconds

Table 5.3 Parameters for the ORC process shown in Figure 5.1

#	State point on Figure 5.1	Description	Units	Dimensionless form	Remarks
1	T_1	R245fa condenser outlet or pump inlet temperature	°C	$T_{1,o} = \frac{T_1 + 273.15}{273.15}$	
2	P_1	R245fa condenser outlet or pump inlet pressure	MPa	$P_{1,o} = \frac{P_1}{0.101325}$	$P_1 = P_5$
3	T_2	R245fa pump outlet or preheater inlet temperature	°C	$T_{2,o} = \frac{T_2 + 273.15}{273.15}$	
4	P_2	R245fa pump outlet or preheater inlet pressure	MPa	$P_{2,o} = \frac{P_2}{0.101325}$	$P_2 = P_{3f} = P_4$
5	T_{3f}	R245fa preheater outlet or evaporator inlet temperature	°C	$T_{3f,o} = \frac{T_{3f} + 273.15}{273.15}$	
6	P_{3f}	R245fa preheater outlet or evaporator inlet pressure	MPa	$P_{3f,o} = \frac{P_{3f}}{0.101325}$	$P_2 = P_{3f} = P_4$
7	T_4	R245fa evaporator outlet or expander inlet temperature	°C	$T_{4,o} = \frac{T_4 + 273.15}{273.15}$	
8	P_4	R245fa evaporator outlet or expander inlet pressure	MPa	$P_{4,o} = \frac{P_4}{0.101325}$	$P_2 = P_{3f} = P_4$
9	T_5	R245fa expander outlet or condenser inlet temperature	°C	$T_{5,o} = \frac{T_5 + 273.15}{273.15}$	
10	P_5	R245fa expander outlet or condenser inlet pressure	MPa	$P_{5,o} = \frac{P_5}{0.101325}$	$P_1 = P_5$
11	$\dot{m}_{ref}$	R245fa mass flow rate in the system	kg/s	$\dot{m}_{ref,o} = \frac{\dot{m}_{ref}}{2.2324}$	2.2324 kg/s is the R245fa mass flow rate at ORC rated power output of 50 kW
12	$\dot{m}_{hf}$	Heating fluid mass flow rate	kg/s	$\dot{m}_{hf,o} = \frac{\dot{m}_{hf}}{10}$	10 kg/s is the manufacturer recommended heating fluid mass flow rate for the ORC system
13	T_6	Heating fluid supply temperature to evaporator	°C	$T_{6,o} = \frac{T_6 + 273.15}{273.15}$	
14	T_{7f}	Heating fluid evaporator outlet or preheater inlet temperature	°C	$T_{7f,o} = \frac{T_{7f} + 273.15}{273.15}$	
15	T_8	Heating fluid return temperature from preheater	°C	$T_{8,o} = \frac{T_8 + 273.15}{273.15}$	

Table 5.3 continued…

16	$\dot{m}_{cf}$	Cooling fluid mass flow rate	kg/s	$\dot{m}_{cf,o} = \frac{\dot{m}_{cf}}{10}$	10 kg/s is the manufacturer recommended cooling fluid mass flow rate for the ORC system
17	T_9	Cooling fluid supply temperature to condenser	°C	$T_{9,o} = \frac{T_9 + 273.15}{273.15}$	
18	T_{10}	Cooling fluid return temperature from condenser	°C	$T_{10,o} = \frac{T_{7f} + 273.15}{273.15}$	
19	W_{SE}	Screw expander power output	kW	$w_{SE,o} = \frac{W_{SE}}{\dot{m}_{ref} h_o}$	
20	$W_p = W_{12}$	Working fluid pump power consumption	kW	$w_{p,o} = \frac{W_p}{\dot{m}_{ref} h_o}$	

Table 5.4 BPHE physical parameters used in present study [26]

Parameter	Preheater	Evaporator	Condenser
W_2 (m)	0.174	0.22	0.22
L_2 (m)	0.456	0.65	0.65
Mean channel spacing, b, (m)	0.002	0.002	0.002
Plate thickness, t, (m)	0.0004	0.0004	0.0004
Number of plates including end plates	91	121	401
Number of thermal plates (N_{th})	89	119	399
Total number of fluid channels	90	120	400
Number of channels on one fluid side (N_{ch})	45	60	200
Model number from manufacturer's catalog	K205	K400	K400
Heat transfer area, A, (m^2)	7.06	17.017	57.057
Flow area, A_f, (m^2)	0.0156	0.0264	0.088

Table 5.5 Curve-fitting coefficients for Eq. (5.7), Eq. (5.8), Eq. (5.9), and Eq. (5.10)

Curve-fitting coefficients	**Eq. (5.7) (P_4)**	**Eq. (5.8) ($\dot{m}_{ref}$)**	**Eq. (5.9) (P_5)**	**Eq. (5.10) (T_5)**
a	3.279675	7.343168E–05	0.873219	–4.56797E–03
b	0.25317	–2.2401E–03	–0.475401	0.25838
c	–6.55426E–06	2.51805E–02	0.643493	4.66865E–02
d	41.62771	–0.123778	0.51245	1.22736
e	–0.414341	0.332953	0.220987	0.7353
f	–0.020569	–	20.6878	–
g	0.022947	–	–	–
h	2.365646	–	–	–
Coefficient of determination (R^2)	0.992	0.994	0.994	0.99
RMS error	0.01877	0.063	0.003	0.647
Figure #	Figure 5.4	Figure 5.5	Figure 5.6	Figure 5.7
Ranges of Validity	7.3 kg/s ≤ $\dot{m}_{hf}$ ≤ 18.7 kg/s 68°C ≤ T_6 ≤ 108.1°C 11°C ≤ T_9 ≤ 22°C		7.3 kg/s ≤ $\dot{m}_{hf}$ ≤ 18.7 kg/s 68°C ≤ T_6 ≤ 108.1°C 6.7 kg/s ≤ $\dot{m}_{cf}$ ≤ 19.4 kg/s 11°C ≤ T_9 ≤ 22°C	7.3 kg/s ≤ $\dot{m}_{hf}$ ≤ 18.7 kg/s 68°C ≤ T_6 ≤ 108.1°C 6.7 kg/s ≤ $\dot{m}_{cf}$ ≤ 19.4 kg/s 11°C ≤ T_9 ≤ 22°C 10 kW ≤ W_{SE} ≤ 51.5 kW

Table 5.6 Results for predicted vs. measured values for various parameters along ORC process

	Heat supplied by heating fluid in evaporator and preheater (Q_{hf})	**Heat rejected to cooling fluid in condenser (Q_{cf})**	**Screw expander power output (W_{SE})**	**Working fluid pump power (W_{pu})**	**T_8**	**T_{10}**
	Lab experimental data					
Min. error	-6.5%	-7.7%	-9.8%	-11.2%	-2.4%	-2.7%
Max. error	12.1%	10.7%	12.5%	13.1%	0.83%	5.7%
Figure #	Figure 5.10	Figure 5.12	Figure 5.14	Figure 5.16	Figure 5.18	Figure 5.20
	Field installation Data					
Min. error	-3%	-3.2%	-1.6%	-3.3%	-0.98%	-3.2%
Max. error	6.4%	6.8%	5.8%	6.5%	0.7%	5.9%
Figure #	Figure 5.11	Figure 5.13	Figure 5.15	Figure 5.17	Figure 5.19	Figure 5.21

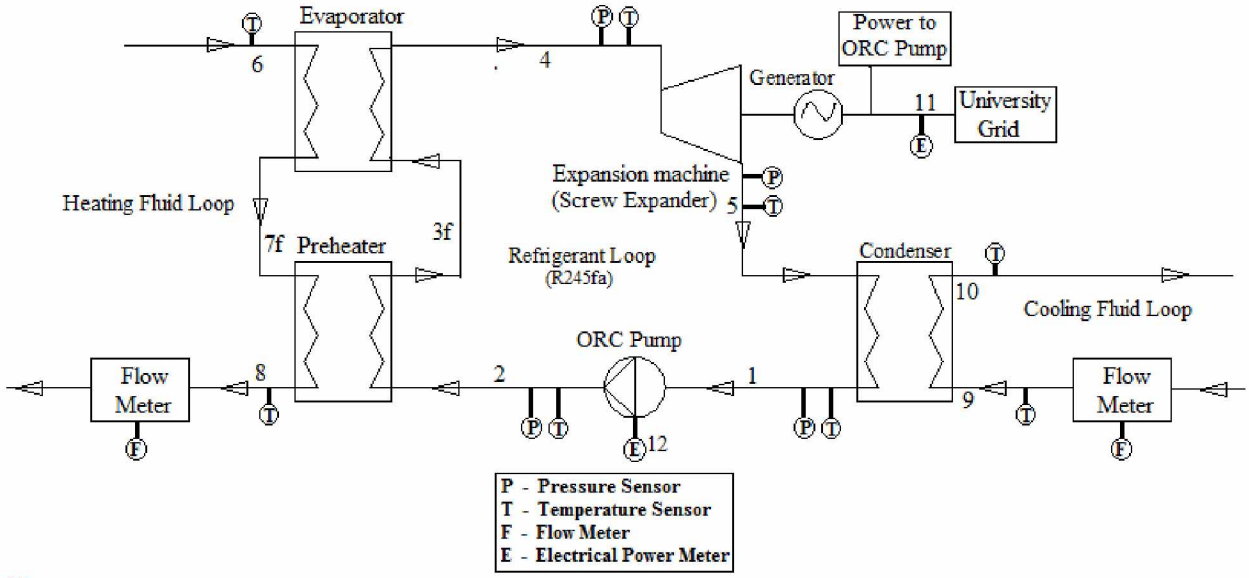

Note:
1. Heating fluid was hot water in experimental setup at UAF and 60/40 propylene glycol/water mixture in field installation.
2. Cooling fluid was cold water in both the installations.

Figure 5.1 Schematic of organic Rankine cycle system under consideration

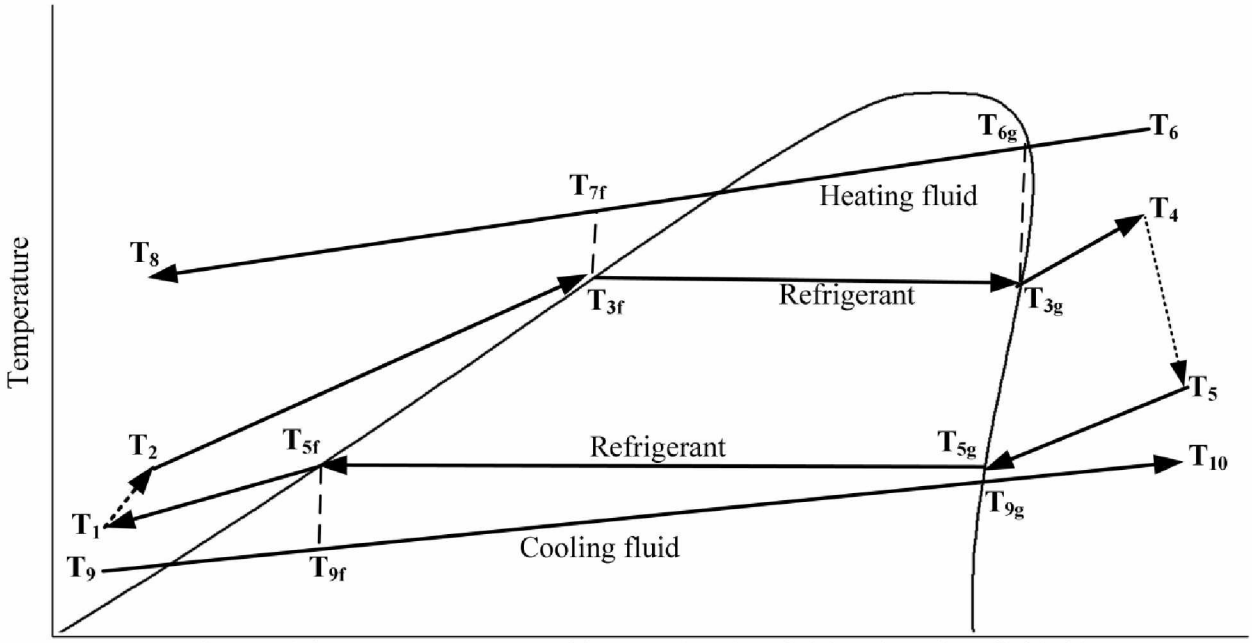

Figure 5.2 Depiction of flow path for refrigerant, heating fluid, and cooling fluid in an ORC system superimposed on R245fa T-s curve

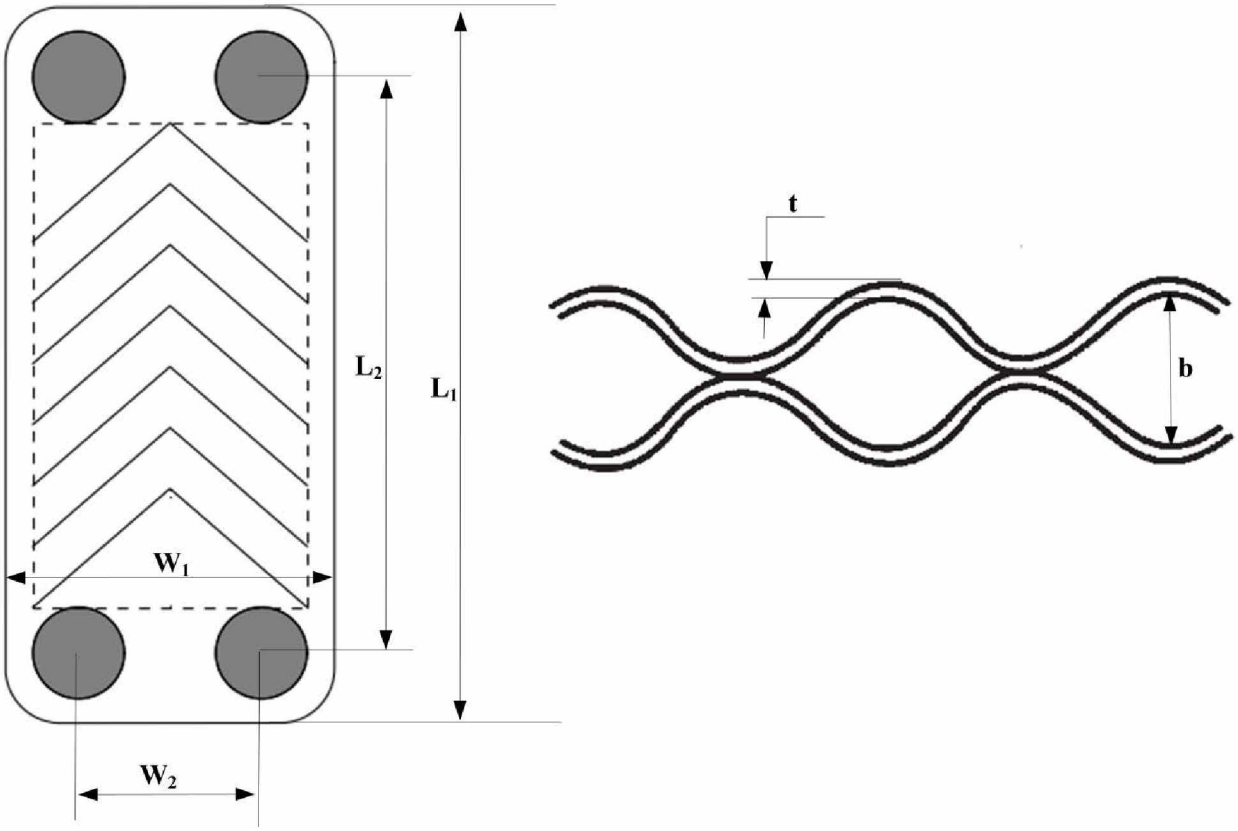

Figure 5.3 BPHE parameters used in present study

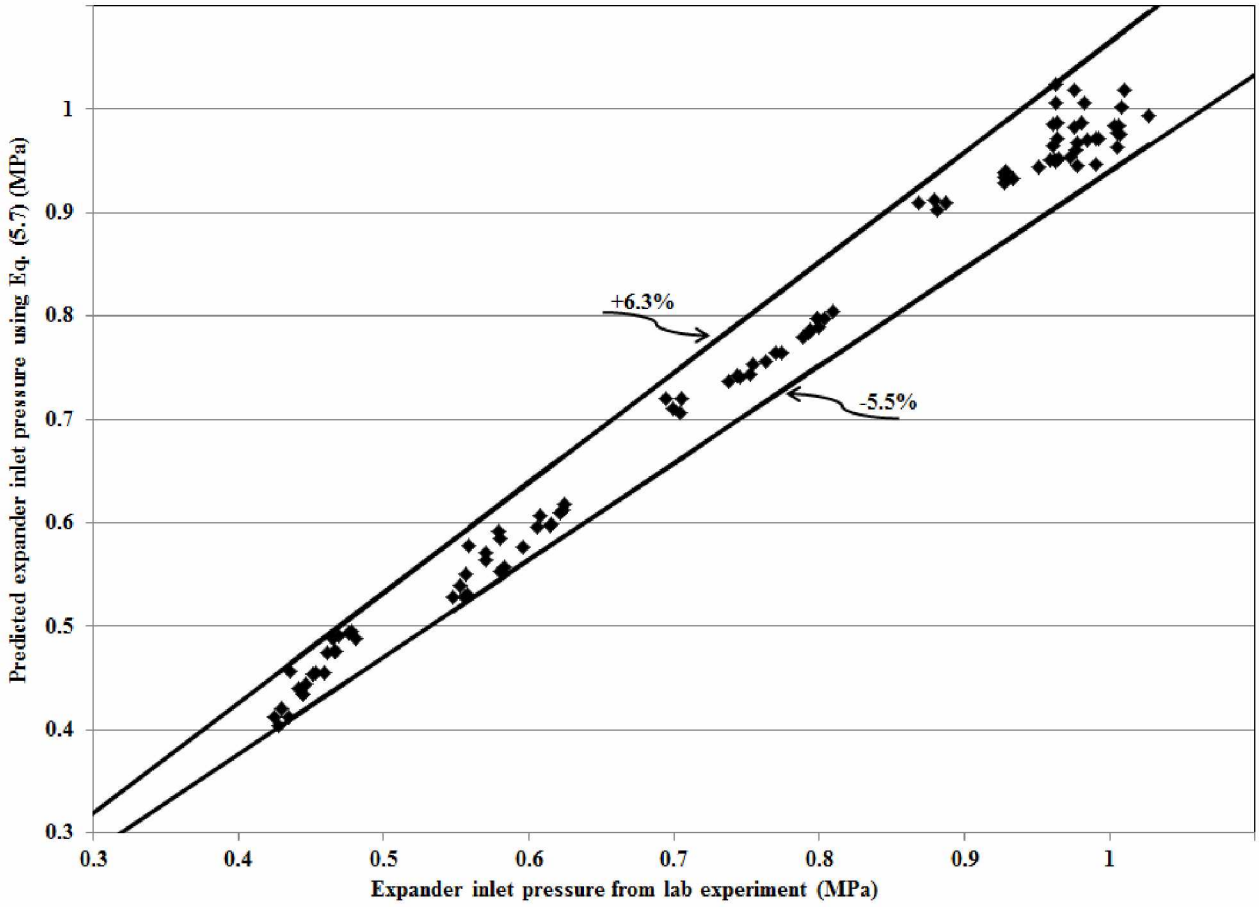

Figure 5.4 Comparison of predicted data with experimental data for expander inlet pressure (P_4) using model Eq. (5.7)

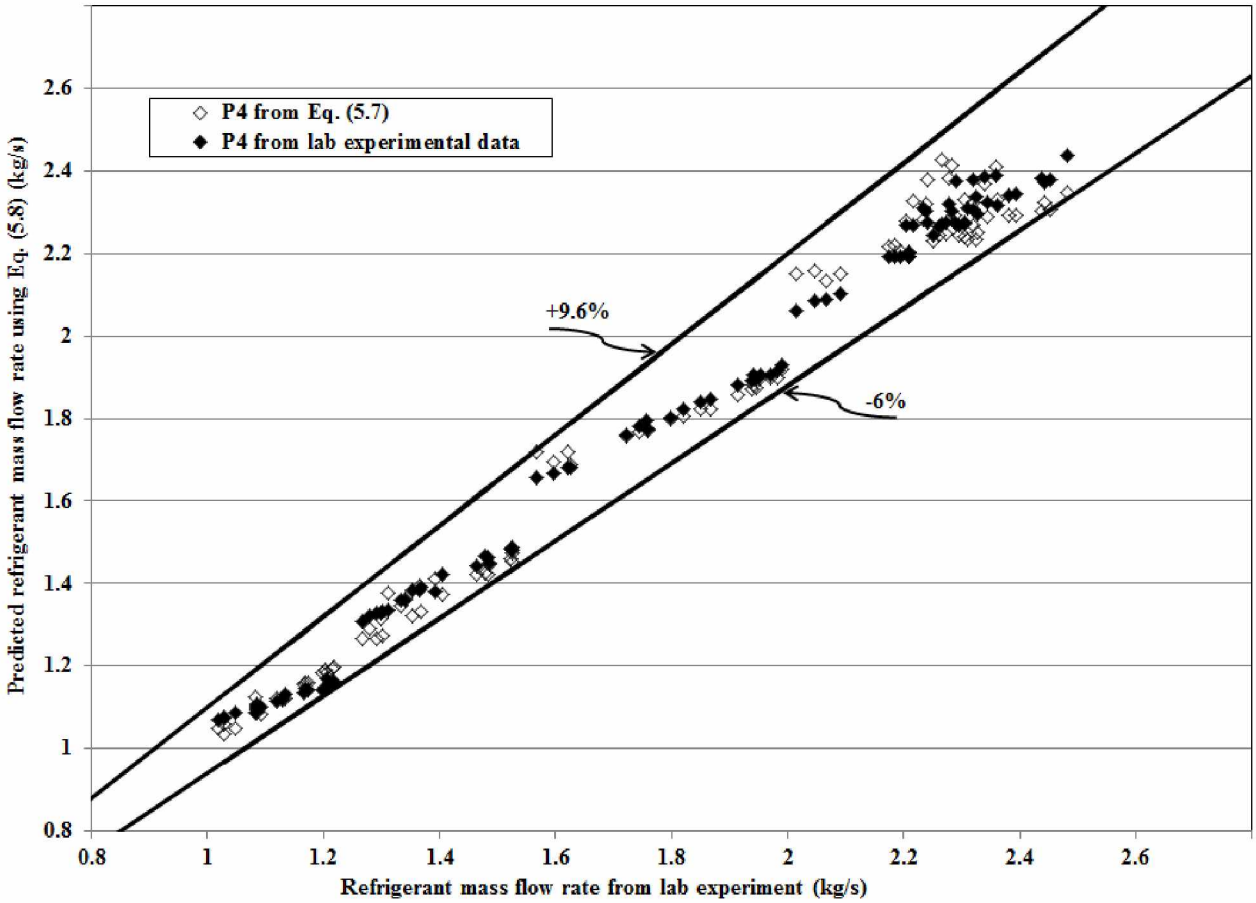

Figure 5.5 Comparison of predicted data with experimental data for refrigerant mass flow rate ($\dot{m}_{ref}$) using model Eq. (5.8)

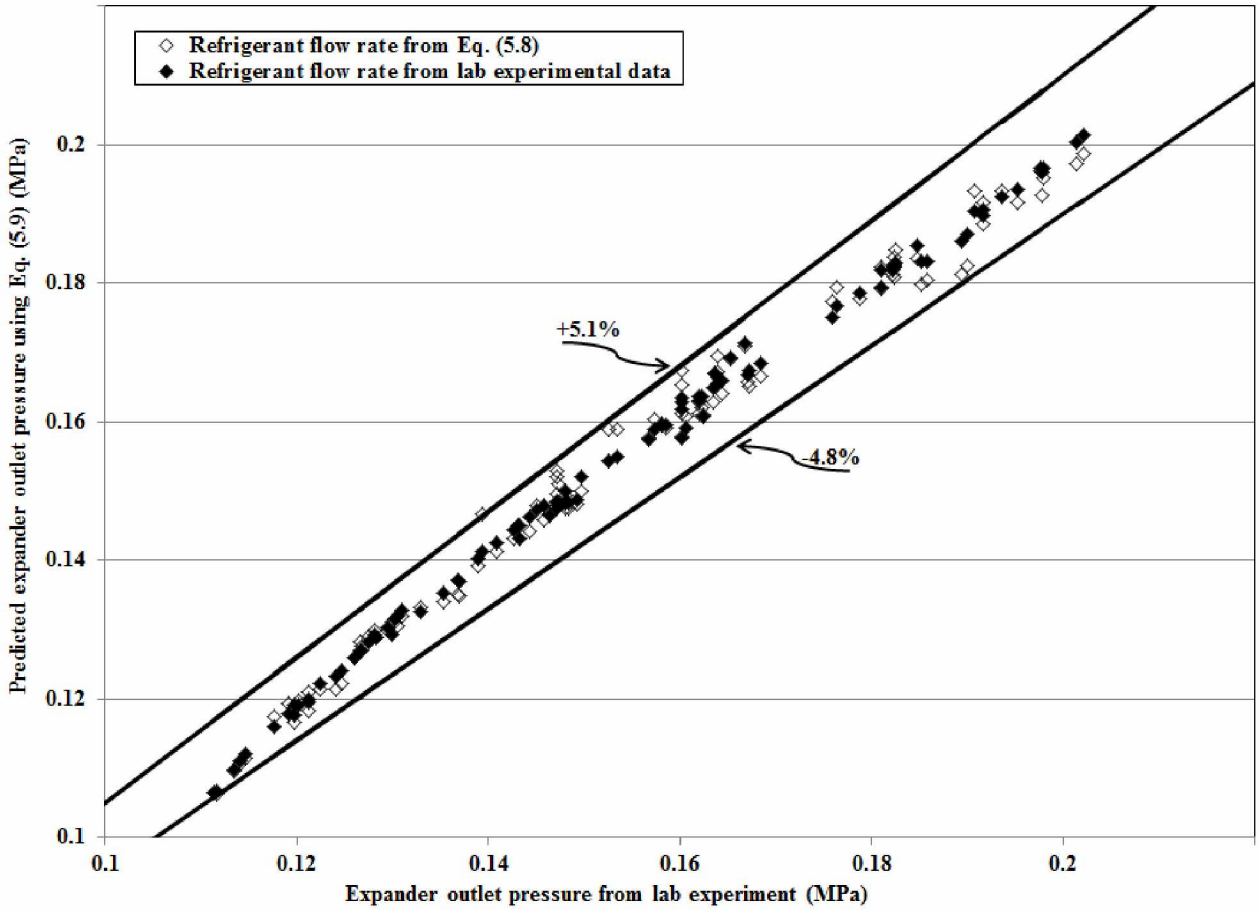

Figure 5.6 Comparison of predicted data with experimental data for expander outlet pressure ($\boldsymbol{P}_5$) using model Eq. (5.9)

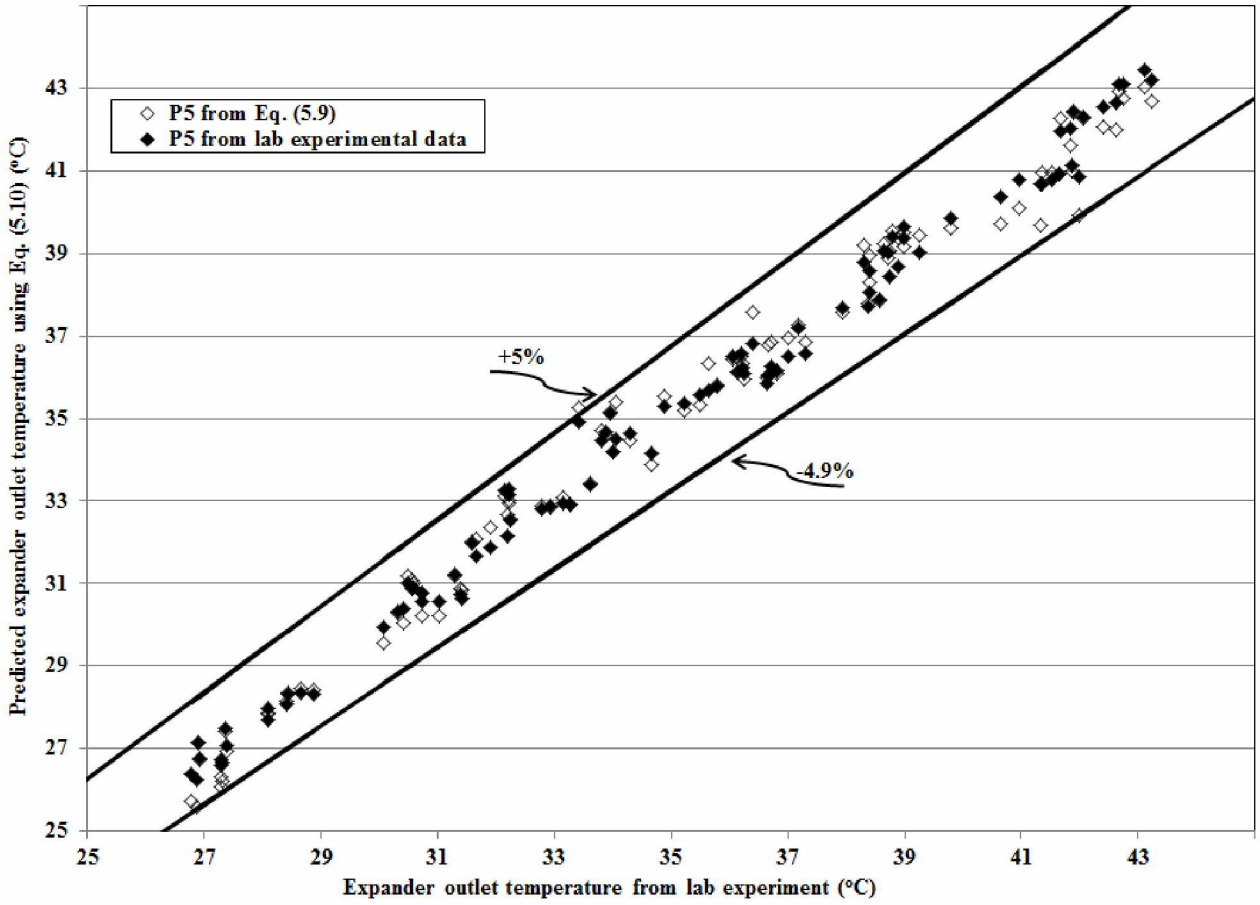

Figure 5.7 Comparison of predicted data with experimental data for expander outlet temperature (T_5) using model Eq. (6.10)

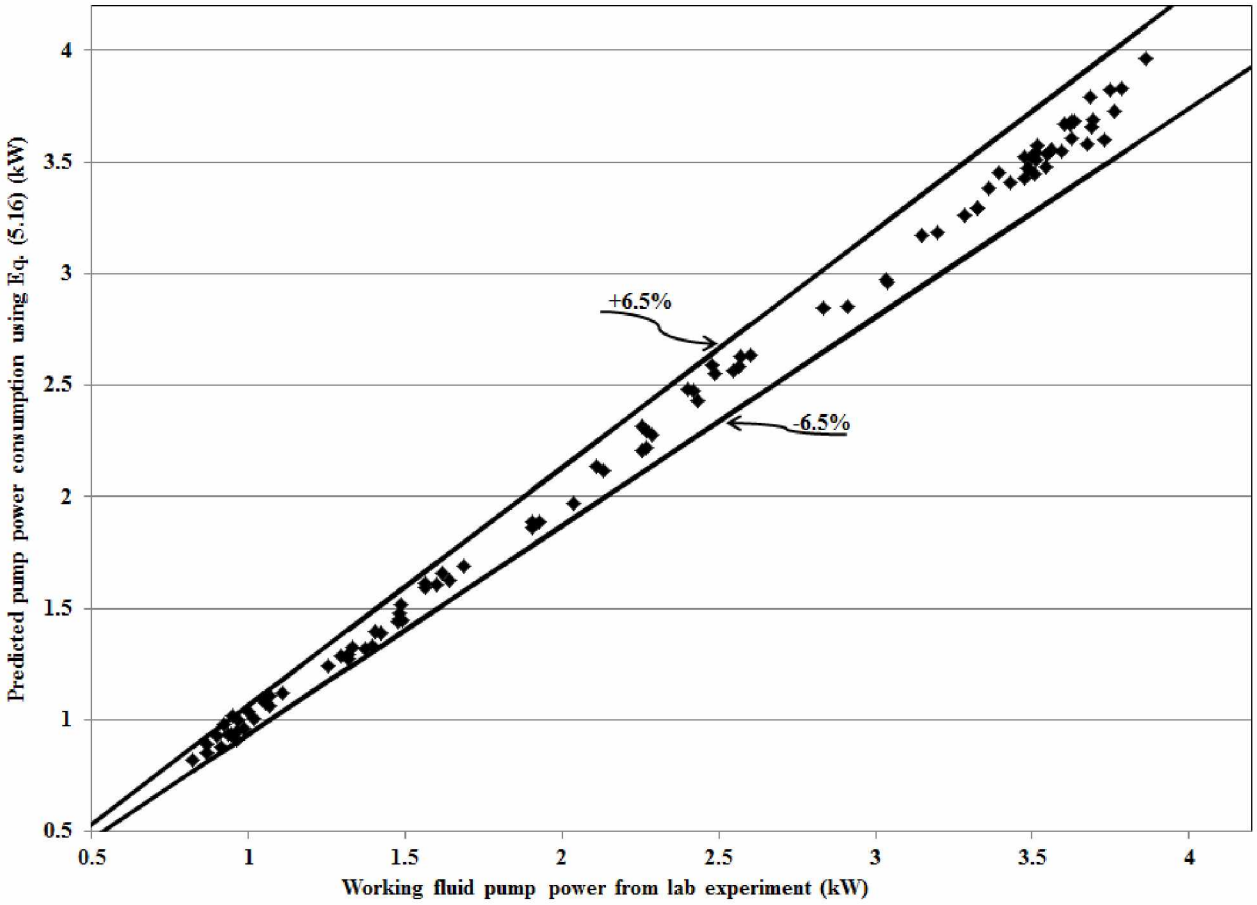

Figure 5.8 Comparison of predicted data with experimental data for pump power consumption ($\boldsymbol{W_{pu}}$) using model Eq. (5.16)

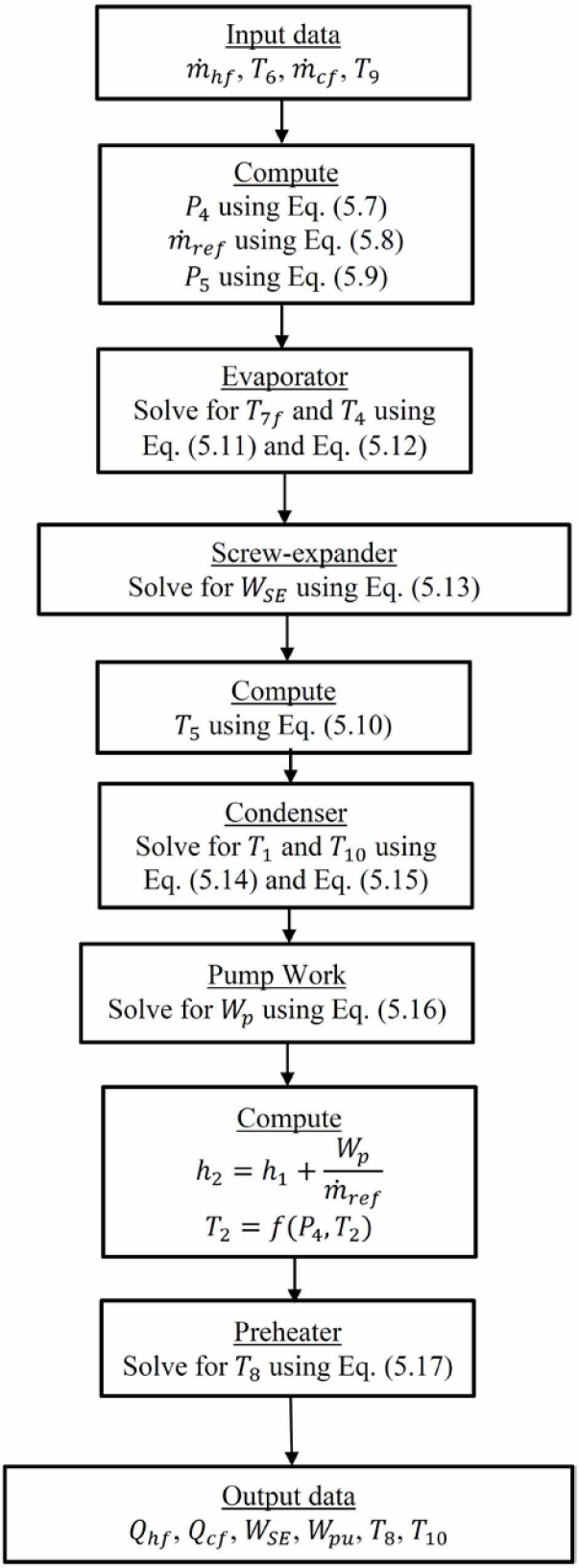

Figure 5.9 Flowchart for ORC model calculation procedure described in Section 5.7.8

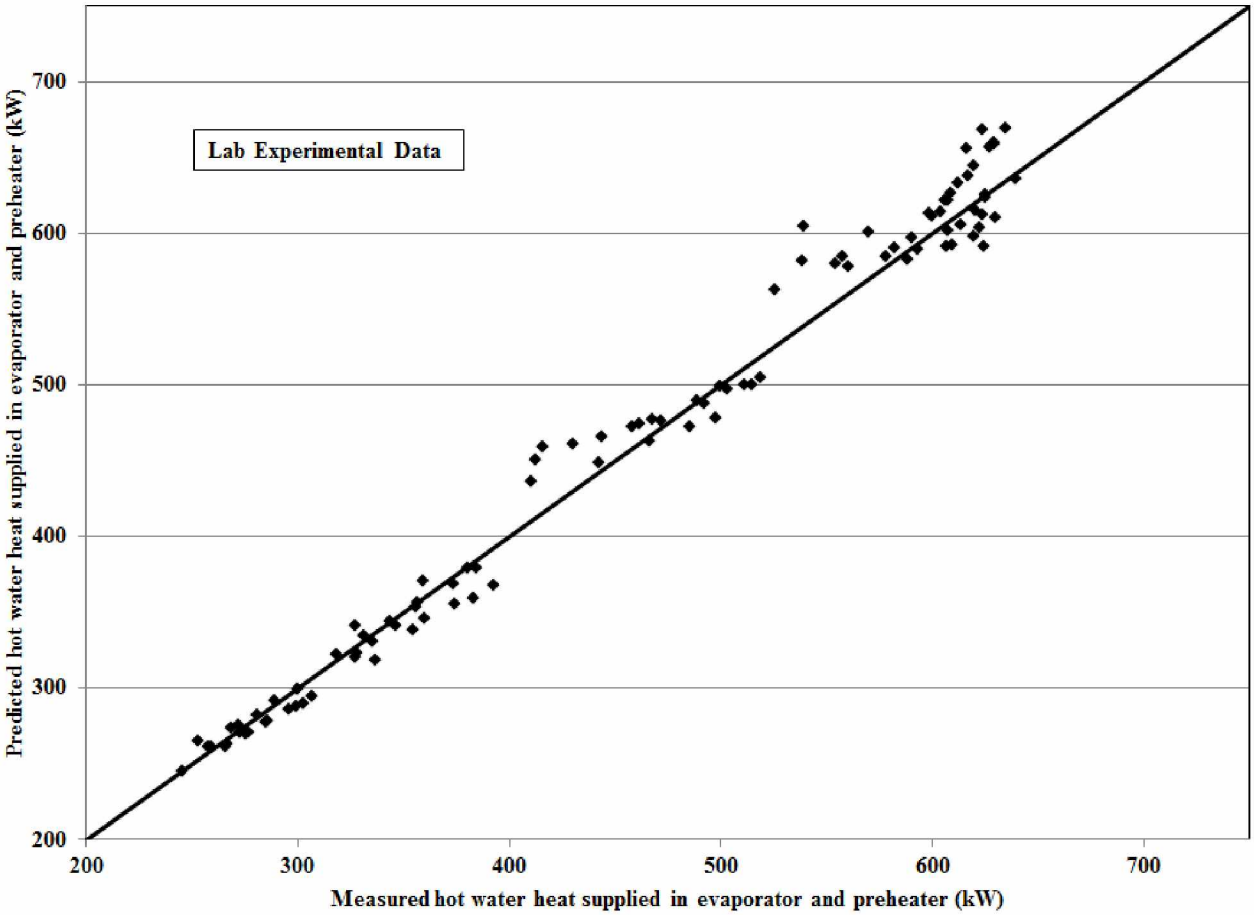

Figure 5.10 Predicted vs. measured values of Q_{hf} in evaporator and preheater for lab experimental data

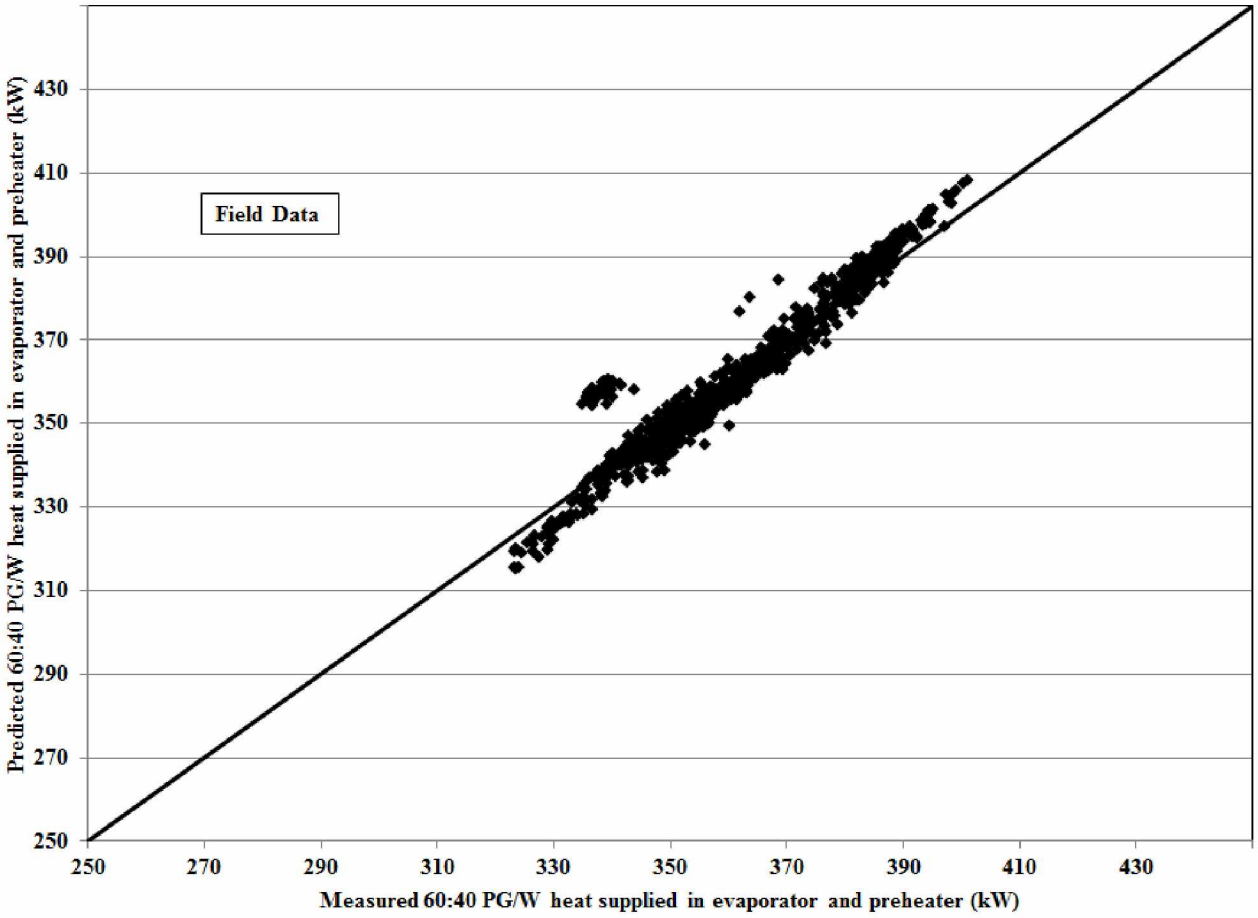

Figure 5.11 Predicted vs. measured values of $\boldsymbol{Q_{hf}}$ in evaporator and preheater for field installation data

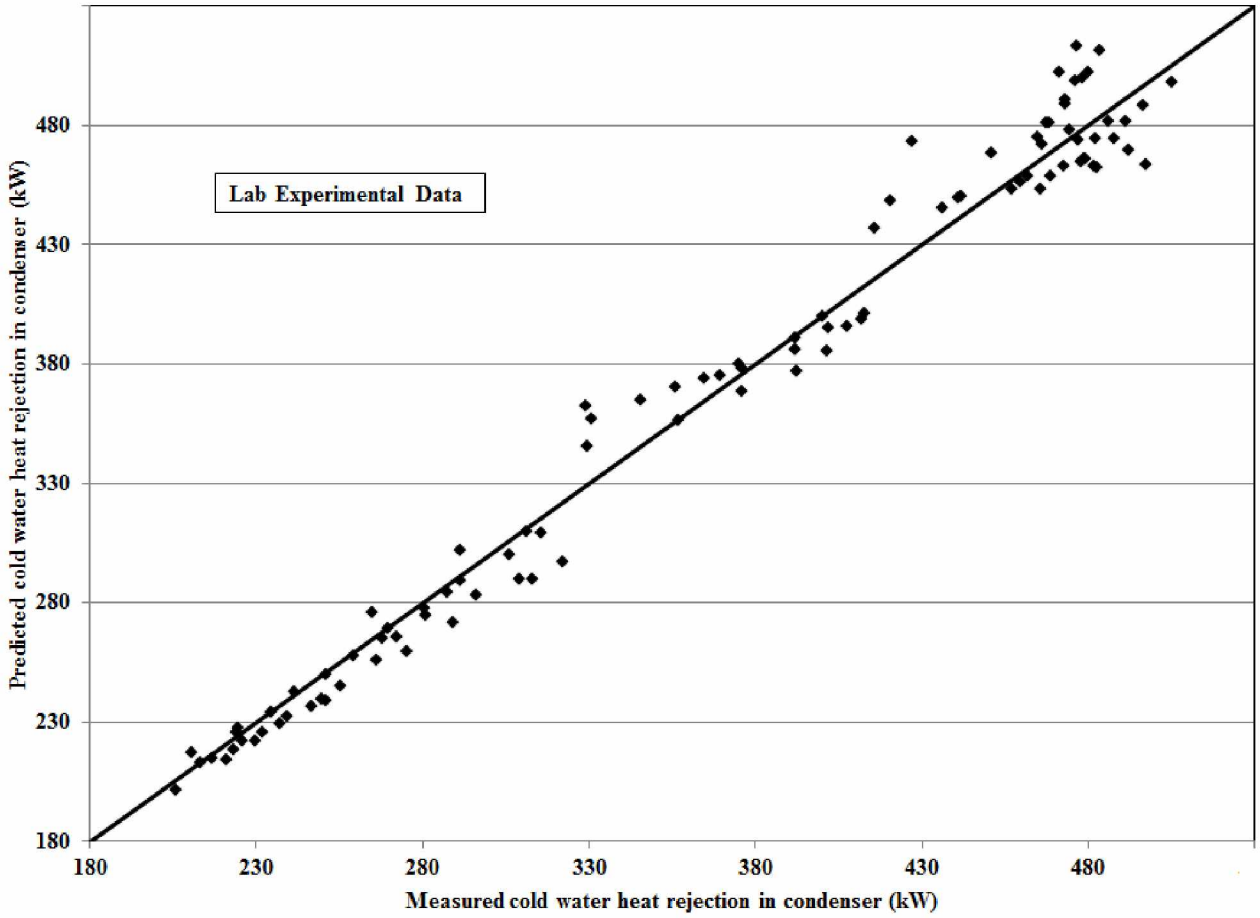

Figure 5.12 Predicted vs. measured values of $\boldsymbol{Q_{cf}}$ in condenser for lab experimental data

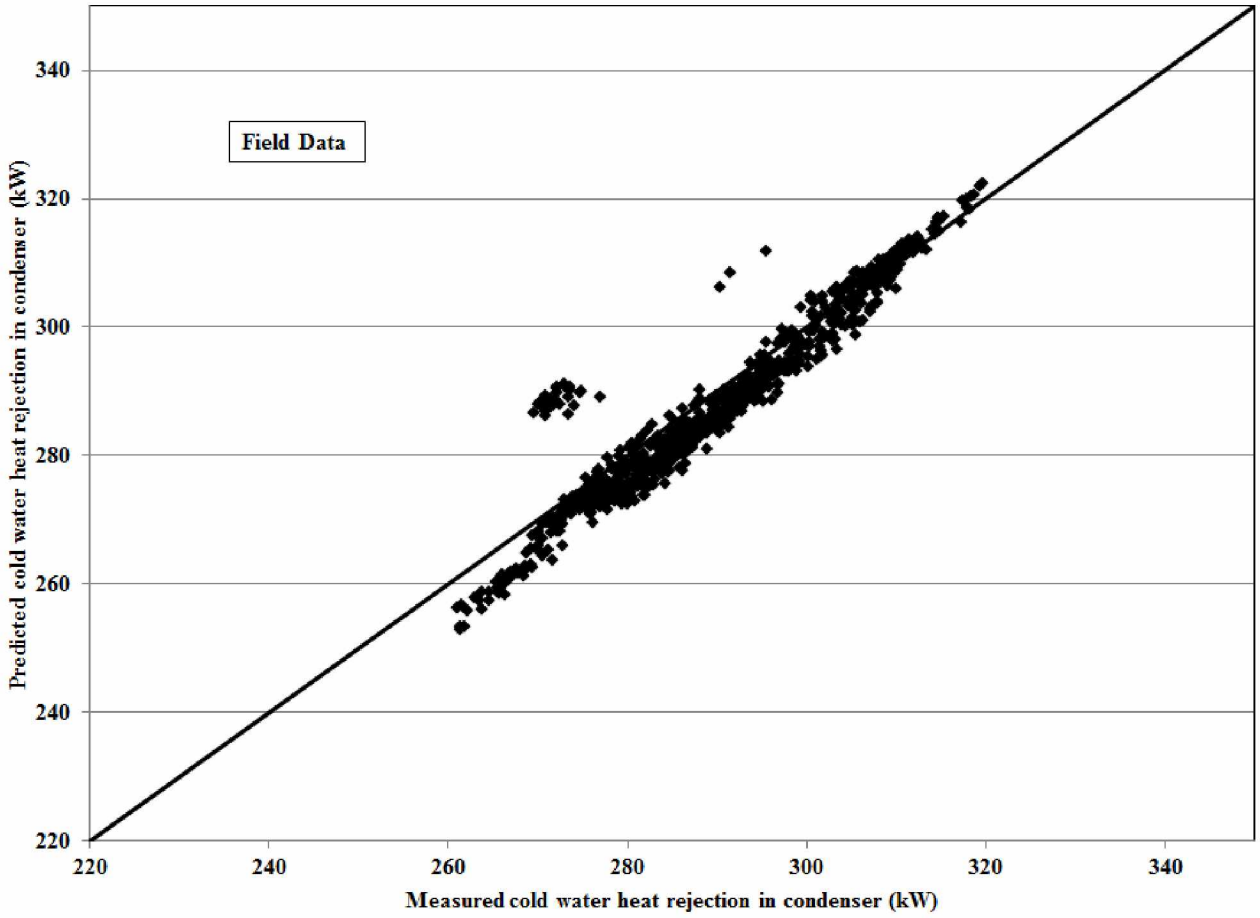

Figure 5.13 Predicted vs. measured values of $\boldsymbol{Q_{cf}}$ in condenser for field installation data

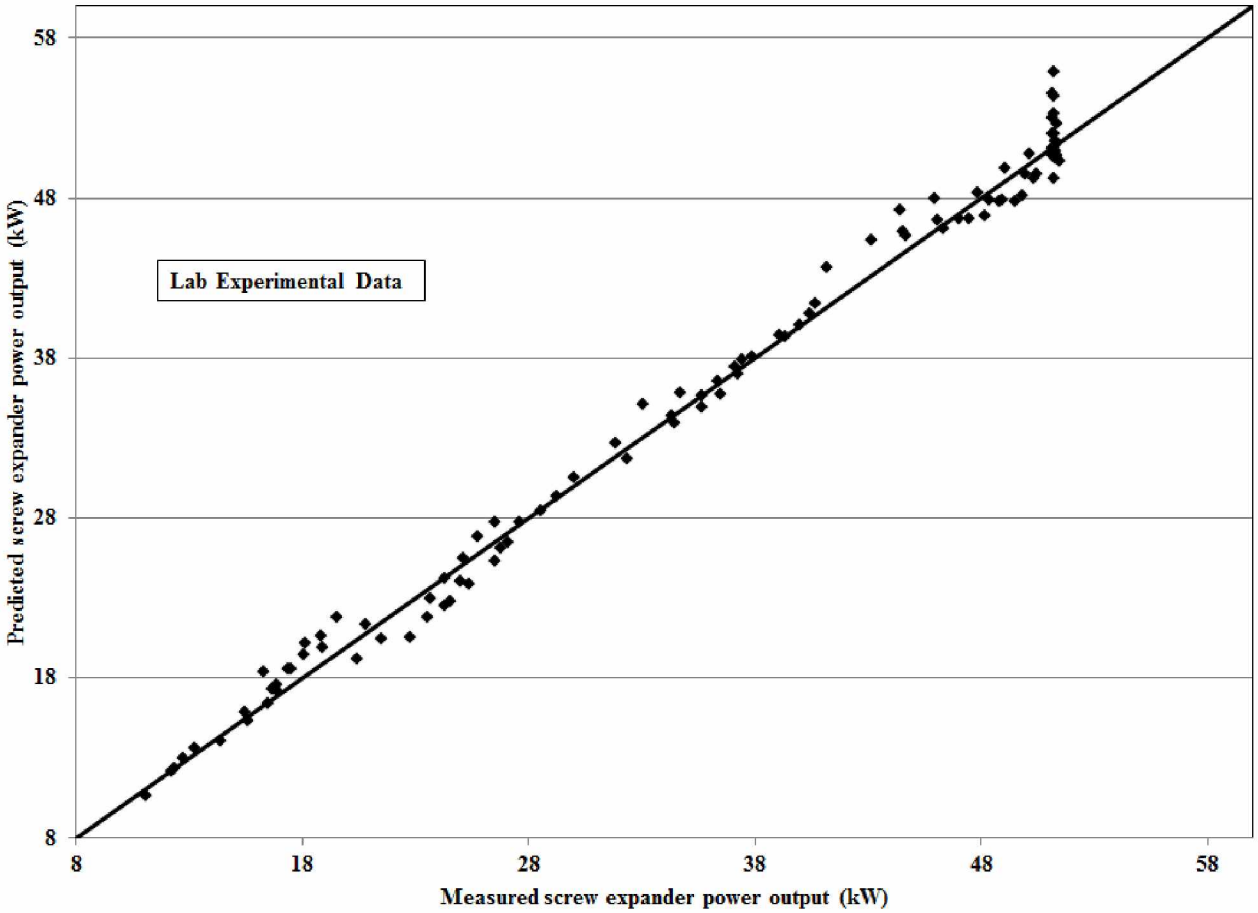

Figure 5.14 Predicted vs. measured values of W_{SE} for lab experimental data

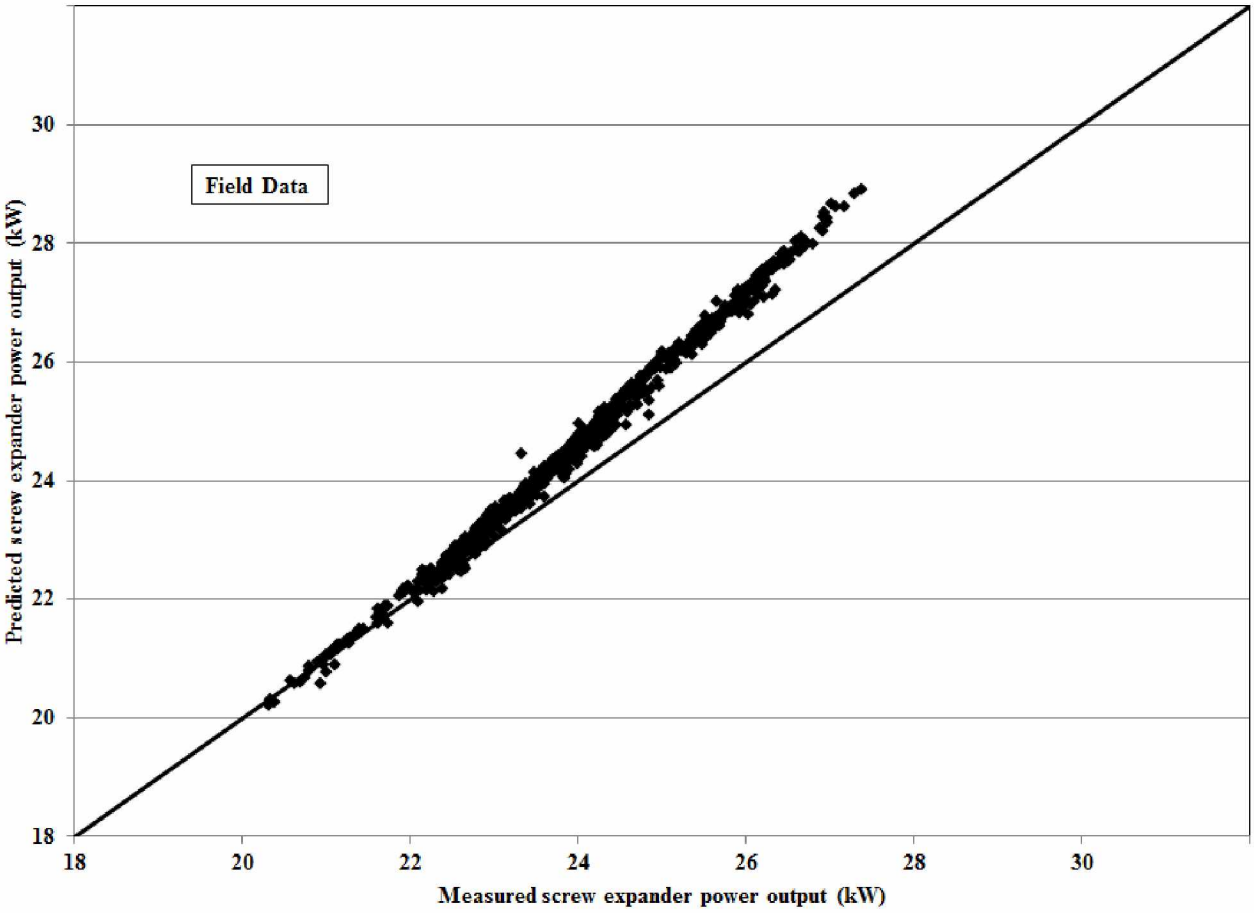

Figure 5.15 Predicted vs. measured values of W_{SE} for field installation data

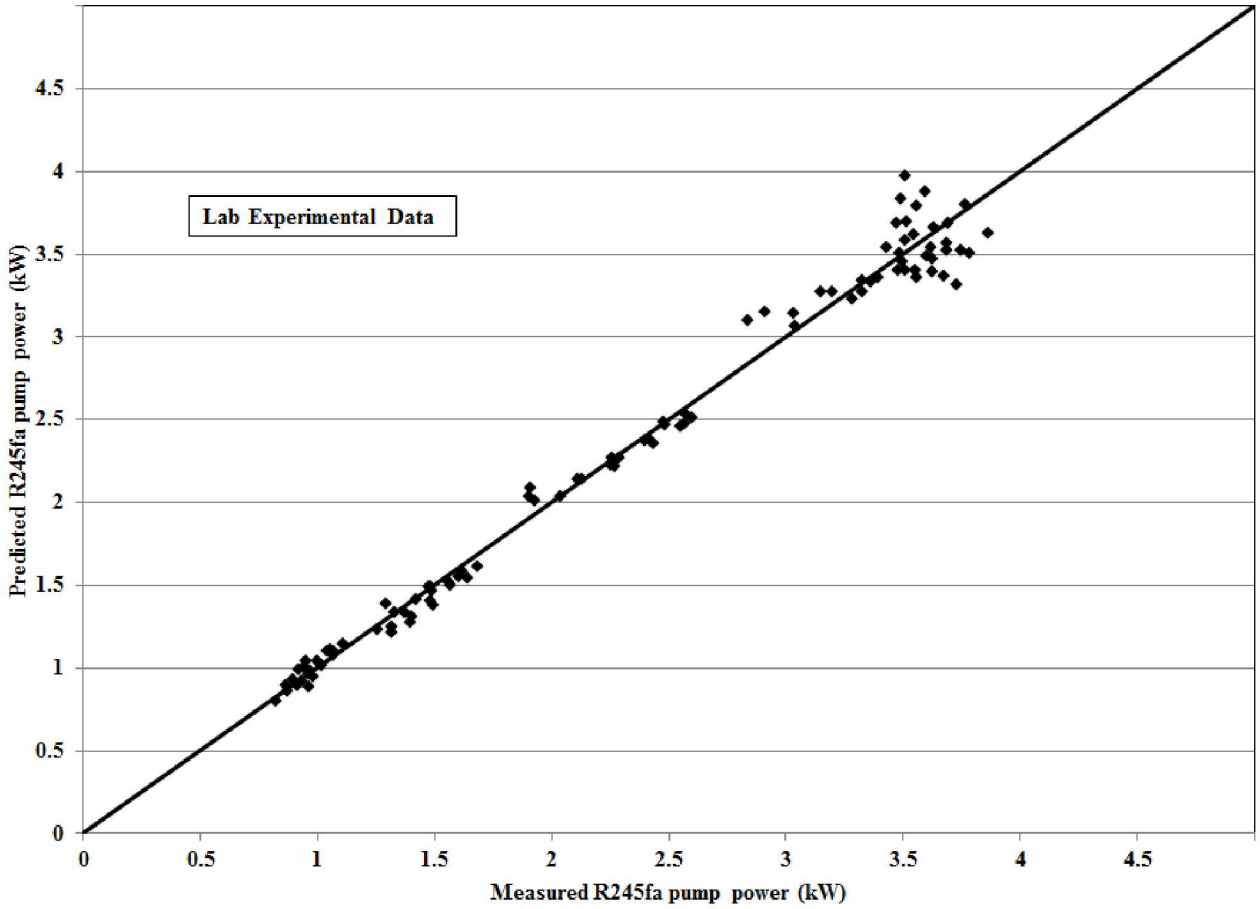

Figure 5.16 Predicted vs. measured values of $\boldsymbol{W_{pu}}$ for lab experimental data

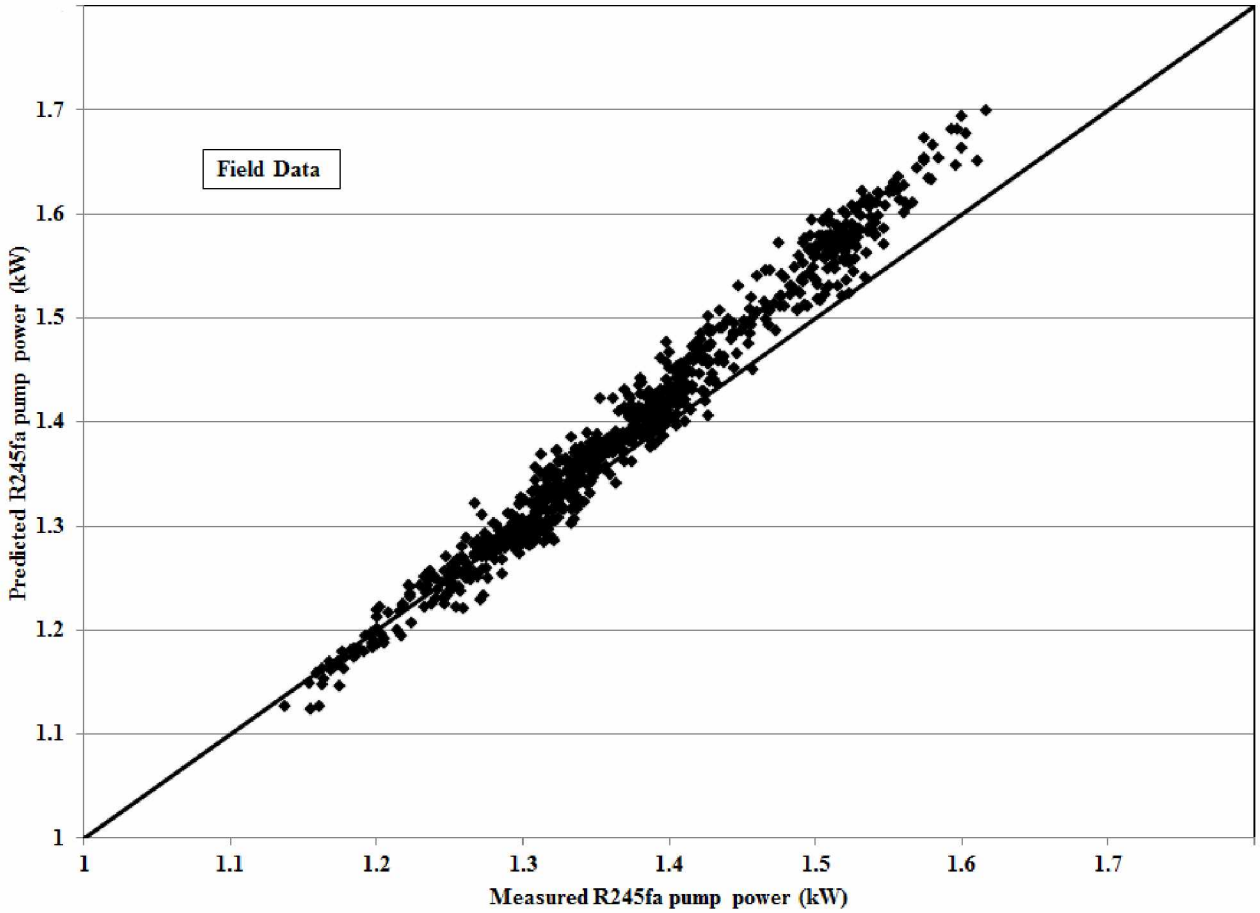

Figure 5.17 Predicted vs. measured values of W_{pu} for field installation data

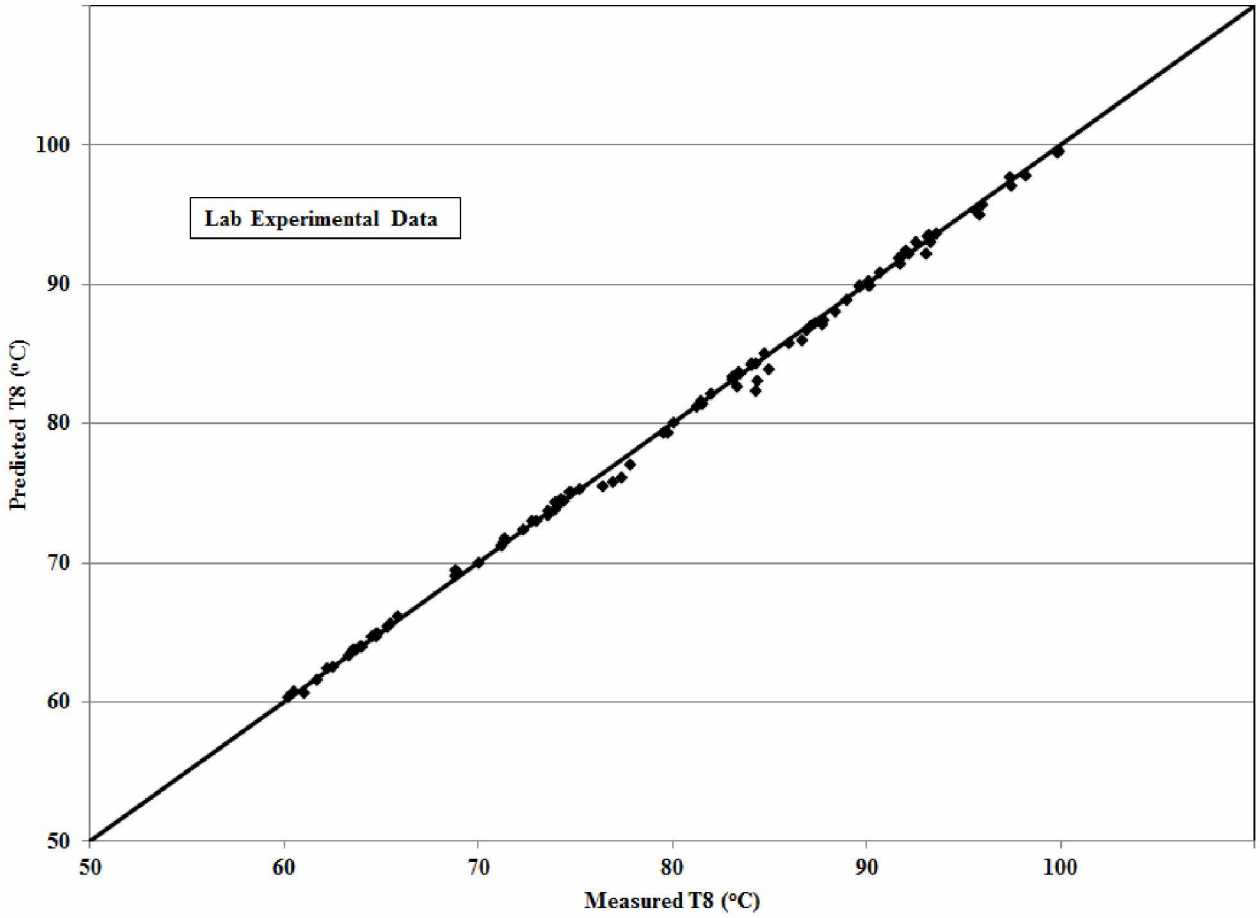

Figure 5.18 Predicted vs. measured values of T_8 for lab experimental data

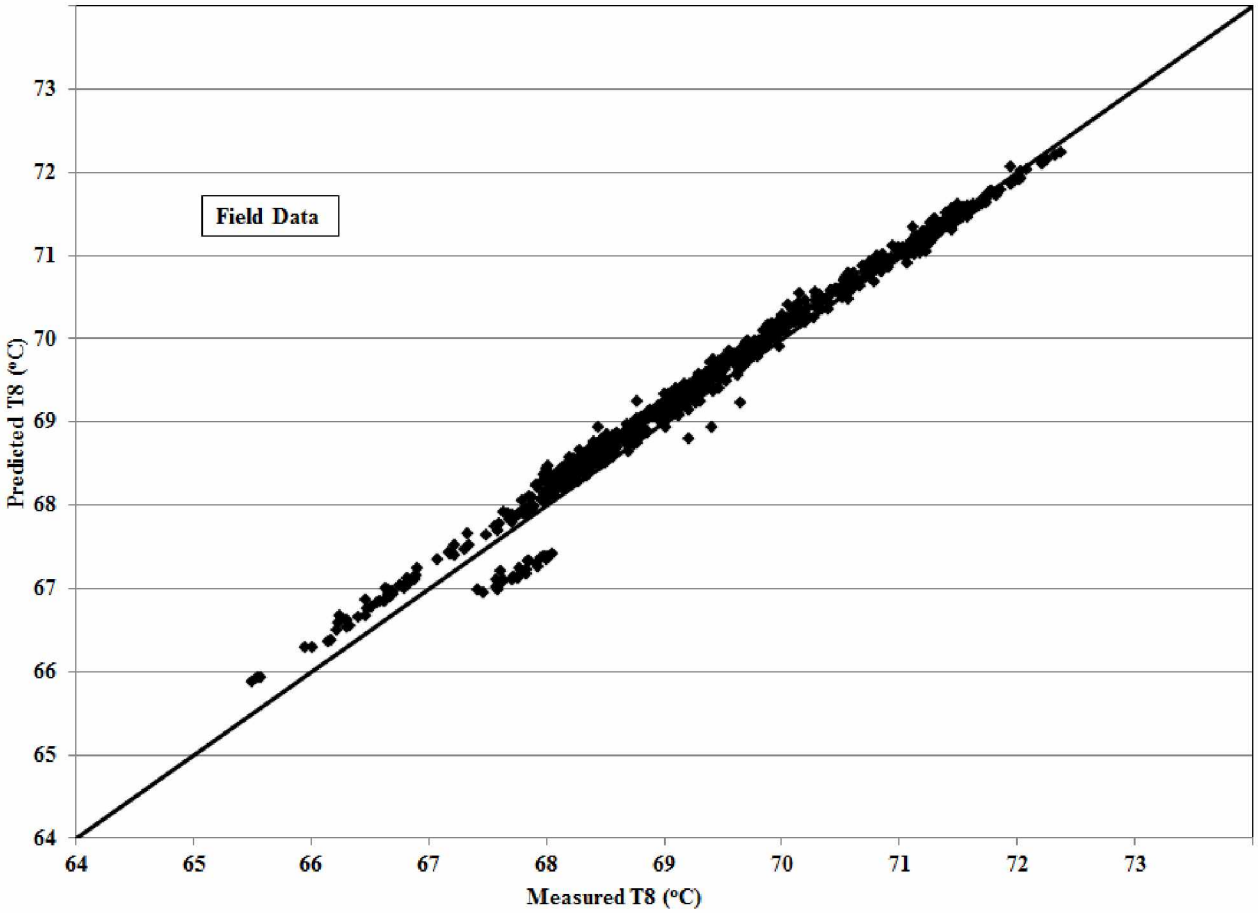

Figure 5.19 Predicted vs. measured values of T_8 for field installation data

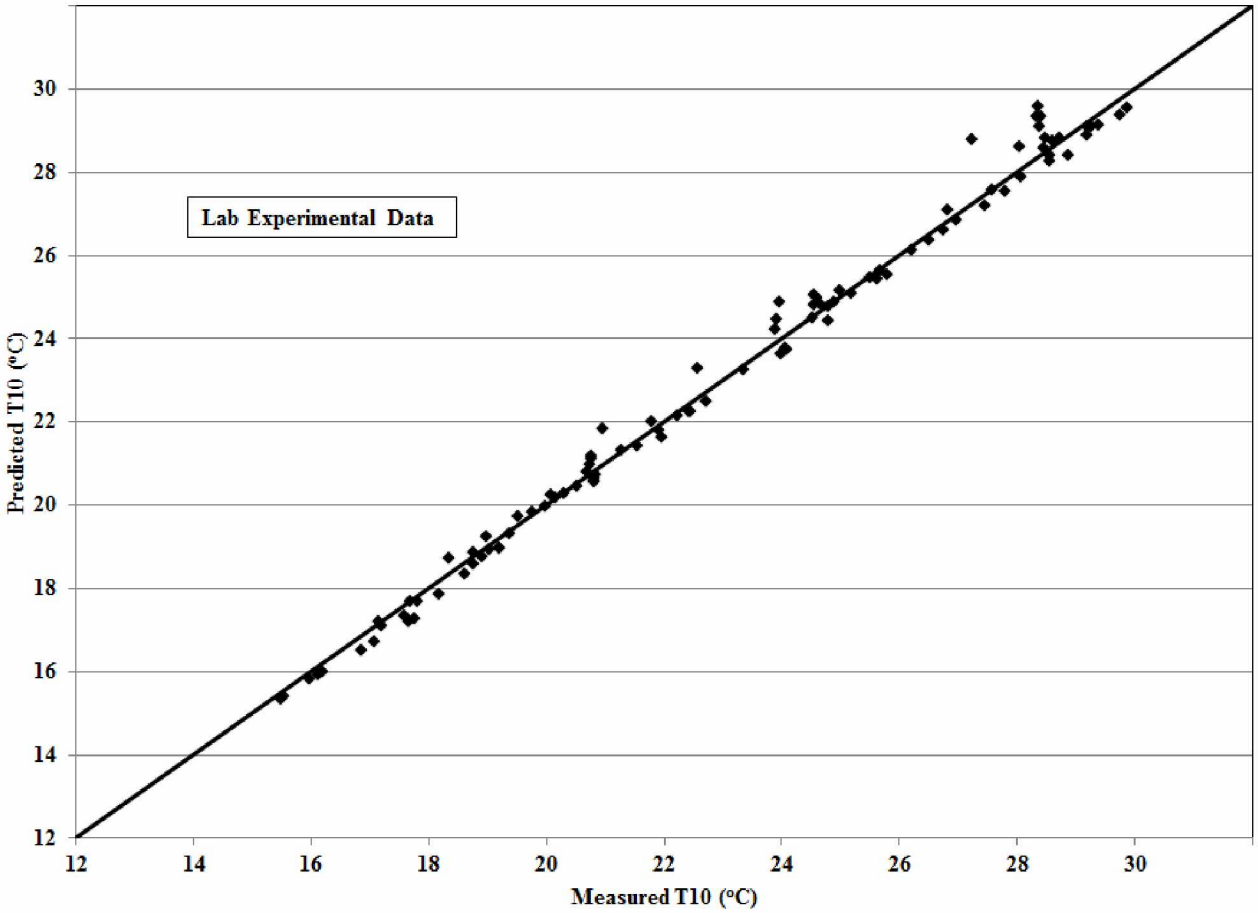

Figure 5.20 Predicted vs. measured values of T_{10} for lab experimental data

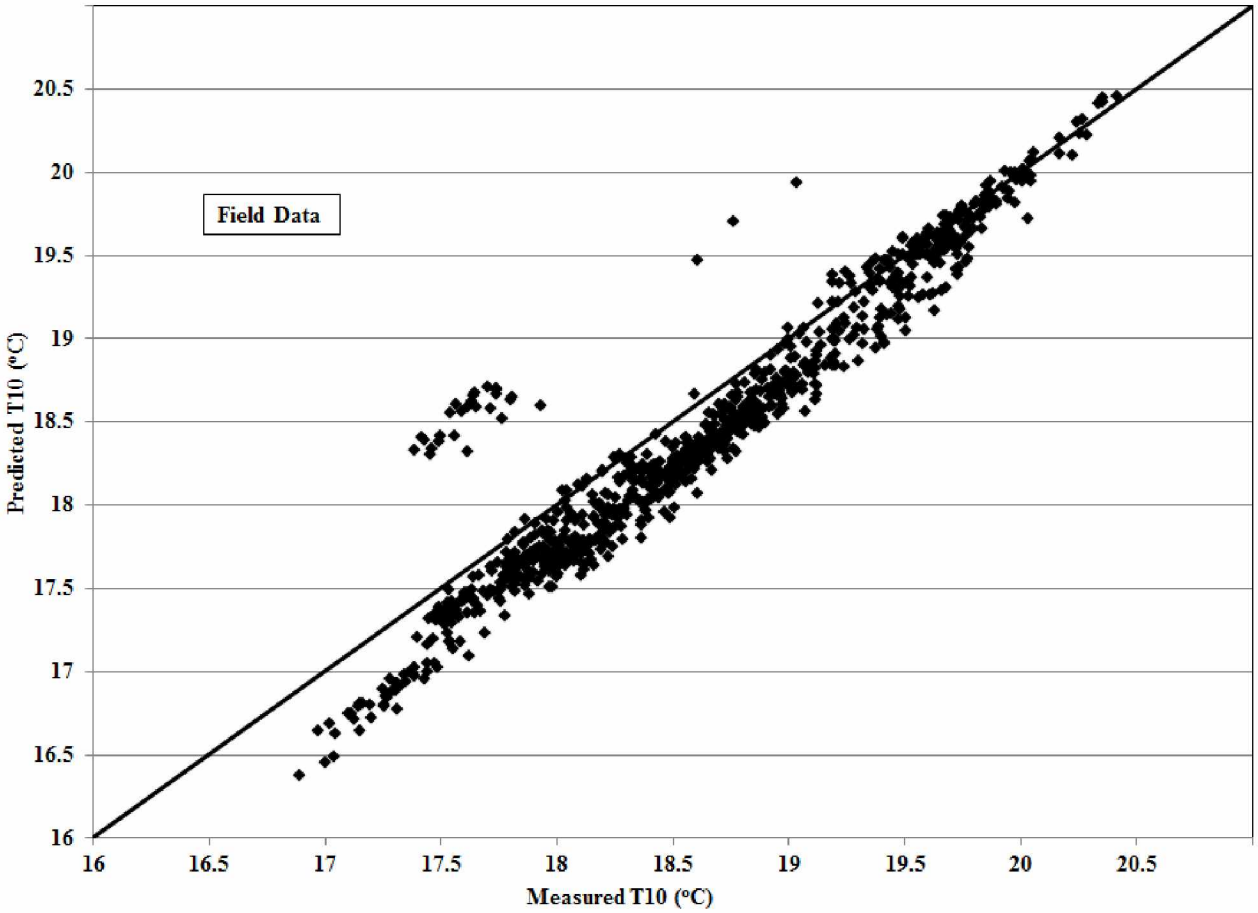

Figure 5.21 Predicted vs. measured values of T_{10} for field installation data

Chapter 6. Conclusions

6.1 Project Summary

A 50 kW organic Rankine cycle heat engine was selected for diesel engine waste heat recovery application. In a lab environment at UAF's combined heat-and-power (CHP) plant, the selected ORC power unit was tested for reliability and performance at different heat source and heat sink conditions while different diesel engine waste heat conditions were simulated. Hot water was the heat source and cold water was the heat sink. During 600-hours of reliability testing, the power unit was operated at the rated load of 50 kW. Then the power unit was performance tested at different hot water and cold water conditions. Extensive data collection was carried out during performance testing, not only for the ORC power unit as a whole, but also on the refrigerant side of the system for each ORC component.

After this testing, the power unit was installed on a 2 MW Caterpillar diesel engine for jacket water heat recovery in Tok, Alaska, and further tested. In field installation, 60/40 PG/W was the heat source and underground well water was the heat sink. Due to the remoteness of the field installation site, data were collected only for the ORC power unit as a whole (i.e., heat source, heat sink loops, power output, and pump power consumptions). No data were collected on the refrigerant side of the system.

Using the lab performance data, ORC performance maps were given for heat input, heat rejected, operating power output, payback period, and operating efficiency. Guidelines for applying this ORC on rural Alaska diesel generators were also presented with examples. The lab data pertaining to ORC components on the refrigerant side were used to develop empirical correlations for screw expanders and working fluid pumps, and heat transfer correlations for R245fa in preheaters, evaporators, and condensers. A single-phase heat transfer correlation was proposed for R245fa in the preheater and two-phase heat transfer correlations were proposed for the evaporator and condenser.

A parametric model, a step-by-step calculation procedure based on these empirical and heat transfer correlations, was developed to predict performance of the ORC system. The developed parametric model was validated using both lab experimental data and field installation data.

6.2 Conclusions for Testing a 50kW ORC at Different Heating and Cooling Source Conditions to Map Performance Characteristics

- Application of this 50 kW ORC power unit for waste heat recovery from stationary diesel gen-sets is expected to be reliable and feasible in rural Alaska, as maintenance requirements and level of expertise needed to operate the unit are expected to be minimal.
- The effect of cold water flow rate on heat input to the power unit's evaporator and preheater, heat rejection by the power unit in the condenser, and power output was observed to be minimal for a given cold water supply temperature, hot water flow rate, and hot water supply temperature.
- For a given hot water supply temperature, with the increase of hot water flow rate, the heat input to the power unit and system operating power output reached asymptotic conditions.
- Performance curves were plotted for heat input to the evaporator, heat rejected to cold water, system operating power output, efficiency, payback period, and CO_2 emission reductions with respect to hot water supply temperature of $10^{o}C$ and cold water supply temperature of $20^{o}C$, respectively.
- For all hot water supply temperatures except those $68.3^{o}C$ ($155^{o}F$) or lower, a payback period of less than 6.5 years and 8 years could be achieved for $10^{o}C$ and $20^{o}C$ cold water temperatures, respectively.
- An example to evaluate the present ORC system using the field diesel engine data is presented for jacket water heat recovery, and combined jacket water and exhaust heat recovery systems using the developed performance curves. The example shows that the performance data obtained from this experiment can be used to simulate and evaluate the application of this ORC system to Alaska village gen-sets for power output, efficiency, payback period, and emissions reduction.
- For jacket water temperature at $99^{o}C$ ($210.2^{o}F$), a system operating power output of 41.7kW was achievable with 7.2% efficiency and 2.6 years payback. If that waste heat is from both jacket water and exhaust heat exchanger, it is possible to generate 45.7kW system operating power output with 7.4% efficiency and 2.3 years payback.
- Considerable reductions in annual emissions and CO_2 (GHG) could be obtained if the ORC power unit were operated year round on waste heat from diesel engines.

- Taking into account the 370,000 MWh electrical consumption of Alaska and the 38% fuel efficiency of a diesel engine, nearly 486,800 MWh of heat energy is present in jacket water and exhaust heat. With use of this waste heat, at 7% ORC efficiency, about 34,080 MWh of electricity could be generated, which would increase the diesel engine fuel efficiency to 41.5%, with CO_2 reductions of 27,000 short-tons/year, fuel savings of 9,214,800 lit/year (2,434,300 gal/year), and fuel cost savings of $12,171,500/year.

6.3 Conclusions for Guidelines for Effectively Applying an ORC System to Rural Alaska Diesel Power Industry Based on Experimental Data

- Guidelines have been developed for effectively applying the 50kW ORC system to rural diesel generator sets. The guidelines are discussed as general principles, since each village has unique conditions related to ORC system application (i.e., fuel cost, infrastructure, cooling source). All guidelines are related to an outcome of economic benefit, and the decision of whether to adopt this ORC system is most likely determined by economic impact.
- The guidelines were divided into two categories: one based on village conditions, and the other based on ORC performance characteristics.
- Village condition-based guidelines took into account village preferences, the existence (or nonexistence) of waste heat for heating systems in the villages, the amount of heat availability, and other related infrastructure and requirements.
- ORC performance-based guidelines took into account general performance of the ORC system (e.g., reliability, potential economic benefit), heat-source properties (e.g., jacket and/or exhaust, maximum heat-source temperature, minimum power output requirements, quality and quantity of heat for multistage application, multi-ORC-unit applications, potential for using a different ORC system), cooling source properties (e.g., maximum cooling fluid temperature, cooling capacity), and the combined effect of heat source and cooling source (e.g., the importance of cooling temperature when heating temperature is low).
- Based on Power Cost Equalization report data, among 280 rural villages, only 26 villages can generate, on average, 10 kW or more of electrical power by applying the ORC system using only jacket water as a heat source.
- In cases where the heat source includes both jacket water and exhaust, 51 villages will be able to generate 10 kW or more of electrical power.

6.4 Conclusions for Empirical Models for Screw Expander Based on Experimental Data from Organic Rankine Cycle System Testing

- Lab experimental data from the screw expander were used to develop two empirical models for estimating screw expander performance. The first empirical model was based on the polytropic process, in which the regression curve-fitting expression for the polytropic exponent with respect to the expander pressure ratio (r_p) and volume ratio (r_v) was fitted. In the second empirical model, the non-dimensional form of the screw expander work output was fitted with respect to the non-dimensional form of the isentropic work output.
- In the first curve-fitting model (model-I) for a screw expander based on the polytropic process, the predicted polytropic exponent values using a curve-fitting equation were within ±1% and screw expander power output values were within ±10% when compared to the experimental data.
- In the second curve-fitting model (model-II) for a screw expander based on isentropic work output, the predicted screw expander power output values were within ±7.5% when compared to experimental data.
- The curve-fitting model based on isentropic work output better predicted screw expander performance than the model based on the polytropic process.

6.5 Conclusions for Heat Transfer Correlations for R245fa in Preheater, Evaporator, and Condenser using Experimental Data from 50 kW Organic Rankine Cycle (ORC) System Testing

- The lab experimental data pertaining to the preheater, evaporator and condenser were used to develop R245fa heat transfer correlations for single-phase, two-phase evaporation, and two-phase condensation in respective heat exchangers in accordance with available correlations in the literature.
- The proposed Dittus-Boelter type of single-phase heat transfer correlations for hot water and R245fa in the preheater had an agreement within ±20% with respect to experimental values.
- Two heat transfer correlations were proposed for evaporation of R245fa in the evaporator. The first was based on NIST correlation form and was within an error of –12.3% and +16.5% with respect to experimental data. The second proposed heat transfer correlation was based on Jokar et al., with an error range of ±13.7% when compared with experimental data.

- The second proposed correlation for R245fa evaporation better predicted evaporative heat transfer coefficient values when compared with experimental data.
- The dominant heat transfer regime in the evaporator was observed to be nucleate boiling.
- The proposed correlation for condensation of R245fa in the condenser was based on Jokar et al., and 95% of the predicted heat transfer values were within an error range of ±25% when compared with experimental data.

6.6 Conclusions for Parametric Modeling of 50 kW Organic Rankine Cycle using Experimental Data

- Using the correlations for the screw expander and heat transfer correlations for R245fa proposed in earlier chapters, a calculation procedure was developed to model ORC performance. Parameters, such as screw expander power output, working fluid pump power consumption, heat input to the ORC system in evaporator and preheater, and heat rejected by ORC system in condenser were evaluated using the model and were compared with both experimental and field installation data.
- The developed model was validated with both lab experimental data and field installation data.
- The predicted expander power use model was within -9.8% and +12.5% for lab experimental data and -1.6% and 5.8% for field data.
- Model-predicted heat supplied by heating fluid in the evaporator values were within -6.5% and +12.1% for lab experimental data and -3% and 6.4% for field data.
- Model-predicted heat rejected to cooling fluid in the condenser values were within -7.7% and +10.7% for lab experimental data and -3.2% and 6.8% for field data.
- Model-predicted working fluid pump power consumption was within -11.2% and +13.1% for lab experimental data and -3.3% and 6.5% for field data.
- As the ORC model was based on heat transfer and energy balance principles for heat exchangers, it can be used in modeling for any heating fluid and cooling fluid in the evaporator and condenser (e.g., heating fluid and cooling fluid can be pure water or glycol/water mixtures).
- Using the model, we can predict the heating fluid temperature exiting the ORC power unit (i.e., at preheater exit). Based on this we can design a waste heat recovery system for other useful purposes as well, such as heating applications (space heating or municipal water

heating).

6.7 Contributions of This Study

- Using the given performance maps of this ORC unit, rural Alaska diesel power plant personnel can quickly assess the power output they can expect by installing this ORC power unit on their diesel engine for waste heat recovery.
- The brazed plate heat exchangers studied in this ORC system are industrial-scale units (i.e., more than 20 plates). In the open literature, information about these heat exchangers is limited.
- In the open literature little to no information is available to the research community on screw-expander performance characteristics.
- Using the parametric model presented, a detailed performance outcome of ORC power unit installation on a diesel engine can be assessed.
- The parametric model described in this dissertation is a useful tool for power plant engineers designing efficient heat recovery systems such as a combination of waste heat for heating and waste heat to power.

Appendix A. Guidelines for Effectively Applying an ORC System to Rural Alaska Diesel Power Industry Based on Experimental Data*

A.1 Abstract

This paper presents test results of a 50 kW Organic Rankine Cycle (ORC) system and proposed guidelines for how to effectively apply this system to the rural Alaska power industry. In rural Alaska, approximately 180 villages rely on off-grid diesel generators for power. Most of the generators have capacities of about 1 MW or less. In general, the average operation efficiencies are noticeably less than 40%, with the rest of the fuel energy becoming heat. If the heat is not applied for useful application, it is called waste heat. Most of the wasted heat is contained in engine exhaust and jacket fluid and eventually dissipates into the environment. For rural Alaska, waste heat for heating is most effective; in many cases, waste heat for power may be needed for a variety of reasons. Many rural Alaskan villages are reluctant to apply exhaust heat recovery due to concerns about corrosion and soot accumulation in the exhaust system and their effect on emissions. Therefore, this work focuses on applying engine jacket fluid heat recovery for power generation; the potential for applying exhaust heat recovery is discussed only briefly.

For this project, heating and cooling systems serving as heat source and cooling sink, along with measurement instruments, have been installed in the ORC system. Measured data were analyzed to give system performance characteristics, which were then used to: generate a procedure to evaluate whether or not applying the ORC system can benefit individual rural villages; develop guidelines for how to effectively apply the ORC system to individual diesel generator sets; and estimate potential fuel savings from applying this system to the rural Alaska power industry. Along with these discussions, examples illustrate how to use the experimental results to match a generator to the ORC system based on expected payback period, and how to estimate the payback period for a selected village applying this ORC system.

A.2 Keywords

Heat recovery, organic Rankine cycle (ORC), performance characteristics, residual heat, payback period, off grid, diesel generator, jacket fluid, exhaust, rural Alaska villages.

---

* Lin, C.S., Avadhanula, V.K., Mokkapati, V., Huang, D., and Sheets, B., "Guidelines for Effectively Applying an ORC System to Rural Alaska Diesel Power Industry Based on Experimental Data", SAE Technical Paper # 2015-01-1607, April 2015.

A.3 Introduction and Literature Review

This paper presents test results of a 50kW ORC system and proposes guidelines for applying this system to the rural Alaska power industry. In rural Alaska, approximately 180 villages consume about 370,000 MWh [1] of electrical energy annually, using off-grid diesel generator sets. Most of the generators have capacities of about 1 MW or less. In general, these diesel generators operate in partial load conditions most of the time. The operation capacity of individual generators could range from about 50% of rated load to full load [1]. This makes the electrical power to fuel energy ratio much lower than the ratio at rated load; the rest of the fuel energy becomes heat, dissipating into the environment through engine jacket coolant, exhaust, and direct radiation. Using part of this waste heat would result in significant fuel savings.

There are different types of heat recovery applications available, such as applications for heating [1], power generation [2-14], refrigeration [15], and desalination [16]. In order to select the most suitable application, availability, feasibility, reliability, and potential benefit for individual villages must be considered. In general, Alaska villages have good quality of water, and heat recovery for desalination may not be needed [17]. In rural Alaska, waste heat for heating is widely considered the most efficient application; even though heating is crucial only for the cold season. In many cases, though, heating may not be the only application for waste heat, due to village infrastructure, costs resulting from long distances between power plants and locations that need heat, and the production of more waste heat than is needed for heating alone. A detailed report about waste heat for heating in rural Alaskan villages has been discussed in detail in [18–21]. Waste heat for power through heat engines is also considered, due to its acceptable efficiency (about 10%) for many generators used in rural Alaska, flexibility in electrical power utilization, and expected low maintenance (e.g., similar to steam engines or refrigeration systems). In addition, unlike heating, power is needed year-round.

Popular industrial heat engines converting heat-to-power include the organic Rankine cycle (ORC), which is a Rankine cycle that uses organic fluids instead of water, [2–11] and the Kalina cycle, an absorption cycle using an ammonia-water mixture as a working fluid [12–14]. ORC has been implemented at an industrial level with 8% to 18% waste heat recovery, which is a considerable amount. The thermodynamic efficiency of the Kalina cycle for waste heat recovery was reported to be 11% to 26%. A detailed literature review can be found in [22] for the organic

Rankine cycle and the ammonia-water vapor absorption power cycle for systems with an output of less than 500kW.

Most of the aforementioned applications are at an industrial scale (i.e., ORC output more than 100kW). Increasing fuel costs have led to more development of small-scale heat engines for waste heat recovery for power generation. Since many rural Alaskan villages are reluctant to apply exhaust for heat recovery due to concerns about possible corrosion and soot accumulation in the exhaust system, this work focuses on jacket fluid heat recovery only. In their research, the authors have not found commercial Kalina cycle engines for low-grade (i.e., low temperature) and low flux heat sources [3]. Therefore, this study focuses on ORC alone for a jacket liquid fluid heat source that has a temperature lower than 100^{o}C and heat source of about 1 MW or less.

The tasks of testing a 50kW ORC system (the only semi-commercial unit available at the beginning of this project) included: design of an experimental environment of heating source to simulate diesel jacket fluid conditions; measurement and analysis of performance data; development of system performance characteristics; development of guidelines for effective application of this system to rural Alaska; and evaluation of the impacts of applying this system to rural Alaska power plants. The guidelines derived are based on system performance characteristics. It is believed that the derived strategy may also be applicable to other ORC systems with similar performance characteristics.

A.4 Experimental Setup

Figure A.1 shows line diagrams of the ORC system, while Figure A.2 shows its heating and cooling loops. The experiment was conducted in the power plant at the University of Alaska Fairbanks (UAF), which can provide amounts of low-pressure saturated steam sufficient for heating (205.7kPa). Figures A.1 and Figure A.2 also show the components used for heating flow and cooling flow control (i.e., flow rate and temperature). Power plant steam was used to heat water for the ORC system. Details can be found in the final project report [3].

The major components of the 50kW ORC system are a pump, evaporator, expander, and condenser (Figure A.1). High pressure and high temperature R245fa vapor enters into the screw expander and exits as low-pressure vapor or a vapor/liquid mixture. This process converts thermal energy into work via a screw expander that is connected to the generator. The low-pressure refrigerant from the expander is cooled to a saturated or sub-cooled liquid in the condenser and then pumped from low pressure to high pressure and sent to the preheater and

evaporator. In the preheater and evaporator, the high-pressure liquid refrigerant is heated to the required saturated or superheated vapor. The high-pressure steam is then sent to the screw expander and the cycle continues.

In diesel generator waste heat recovery, the heating fluid used to heat ORC working fluid in the evaporator may be engine jacket fluid (water or a glycol/water mixture), heated liquid exiting the exhaust heat exchanger (if exhaust is used as a heat source), or both combined (in series or parallel); this is called the heat source loop. In the condenser, the ORC working fluid (R245fa) dissipates heat to cooling fluid (usually water), which may be from a cooling tower, radiator, large water body, or underground well; this is called the heat sink loop.

The pump is controlled by a variable frequency drive (VFD) for working fluid flow rate control. In the studied ORC system, the working fluid was R245fa, a non-flammable fluid with an ozone depletion potential of zero and no listed phase-out year. R245fa was used due to the match of refrigerant properties, range of operation temperatures, and temperature range of available heat sources (Table A.1).

Figure A.2 shows the experimental setup for testing the 50kW ORC power unit. The experimental setup for heat to power conversion consists of three major components: (i) heat source loop, (ii) heat sink loop, and (iii) ORC system. There are also systems for instrumentation and electrical power uploading (to the UAF grid), which are not shown in the figure. Details of instrumentation and electrical uploading systems can be found in the final report [3]. In this experiment, the heat source loop contains two sub loops: the steam supply loop and the hot water loop. The steam loop transfers heat from steam to water via a heat exchanger, and the hot water transfers heat to the working fluid of the ORC system via another heat exchanger (preheater and evaporator). In this paper, from here on, the word "evaporate" will be used to represent the combination of preheater and evaporator. In Figure A.2, the Steam Control Valve and the VFD pump are used to control the temperature and flow rate of hot water. Cold water from a fire hydrant was used in the cooling loop, in which the cooling condenser heat exchanger (Figure A.1) of the ORC system transfers leftover heat from the exit of the screw expander to the cooling water and releases the heat to the surroundings. The bypass line controlled by the double valves controls the flow rate and temperature of the cooling water entering the ORC condenser.

A.5 Parameters Measured and Instrumentations

This section mainly discusses the parameters measured, instruments installed for measurement, and data collection. The measurement results will then be used for data reduction and analyzed for system performance. Brief descriptions are given below and detailed descriptions can be found in the final report of this project [3].

A.5.1 Parameters Measured

The various parameters measured during the test of the 50kW ORC power unit were: (i) hot water flow rate and inlet and outlet temperatures to the power unit (V_{HW}, $T_{HW,in,P}$, $T_{HW,out,P}$), (ii) cold water flow rate and inlet and outlet temperatures to the power unit (V_{CW}, $T_{CW,in,P}$, $T_{CW,out,P}$), (iii) electrical power output of the power unit (P_{Net}), (iv) electrical power consumed by the working fluid pump of the power unit ($P_{Pump,P}$), (v) hot water pump power ($P_{Pump,HW}$), and (vi) cold water pump power ($P_{Pump,CW}$). Here it should be noted that the electrical power output of the power unit (P_{Net}) is the difference between the screw expander power output (P_{SE}) and the working fluid pump power consumption, which were measured separately.

A.5.2 Instrumentation

As shown in Figure A.2, Kamstrap Ultraflow ultrasonic flow meters were used to measure hot and cold water flow rates. The Kamstrap Multical-601 calculator, which has a flow rate display, was used to manually measure the flow rates. Omega type-K thermocouples were used to measure the inlet and outlet temperatures of the hot and cold water. Temperature measurements were stored in Excel spreadsheets using the LabView VI program. EKM-353EDM electrical meters were used to measure the electrical power generated by the power unit and the power consumption of the power unit pump and hot water pump. The cold water pump power consumption was not measured, as it was assumed to be the same as that of the hot water pump. The electrical meter manufacturer's custom software was used to record and store real-time data in text format at 30-second intervals for future data reduction.

Data acquisition and control (DAQ) functions were performed using a LabView virtual instrument program (VI) operating on a National Instruments (NI) PCI-MIO-16E module. LabView VI software was used to read the real-time data and to store the data at one-second intervals in Excel format for future data reduction. For temperature measurement, an NI SCXI-1120 analog input board was used. Steam valve position was controlled by the simple LabView VI software program and an SCXI-1121 analog I/O board. The LabView VI software program

uses desired hot water temperature as input and, based on the actual hot water temperature, a signal that controls the valve opening position is initiated by LabView.

A.6 Data Reduction Methodology

As mentioned before, the measured parameters include hot water flow rate and input and output temperatures, cold water flow rate and input and output temperatures, electrical power output to the UAF grid, ORC unit working fluid (refrigerant) pump power consumption, and cold water flow pump power. The deduced parameters include ORC system performance parameters, estimated reductions in emissions and CO_2, and estimated economic parameters (e.g., payback period).

A.6.1 System Performance Parameters

This subsection discusses data reduction to estimate the values of system performance parameters, emissions and CO_2 reductions, and potential economic impacts of installing the 50kW ORC power unit.

Heat transferred ($Q_{HW,Su}$) from hot water to the working fluid in the evaporator of the ORC system is evaluated by,

$$Q_{HW,Su} = V_{HW} \bullet \rho_{HW} \bullet (h_{HW,in,P} - h_{HW,out,P}) \quad (A.1)$$

Density of hot water (ρ_{HW}), inlet enthalpy ($h_{HW,in,P}$), and outlet enthalpy ($h_{HW,out,P}$) of the hot water to power unit were obtained based on the evaporator hot water inlet and outlet temperatures [23]. ρ_{HW} is the average density of hot water obtained at the inlet and outlet of the evaporator. V_{HW} is the measured volumetric flow rate.

Heat transferred from the working fluid ($Q_{HW,Rej}$) to cold water in the condenser of the power unit is evaluated by,

$$Q_{CW,Rej} = V_{CW} \bullet \rho_{CW} \bullet (h_{CW,out,P} - h_{CW,in,P}) \quad (A.2)$$

Density of cold water (ρ_{CW}), inlet enthalpy ($h_{CW,out,P}$), and outlet enthalpy ($h_{CW,in,P}$) of the cold water to power unit were obtained based on condenser cold water inlet and outlet temperatures [23]. ρ_{CW} is the average density of cold water obtained at the inlet and outlet of the condenser. V_{CW} is the measured volumetric flow rate.

The system operating power output (P_{OP}), given in Eq. (A.3), was the power generated by the ORC system and uploaded to the university power grid. P_{Net} is the difference between the power generated by the screw expander (P_{SE}) and the power consumed by the working fluid pump of the ORC. $P_{Pump,CW}$ is the cooling water pump power consumption. In general, a stationary diesel

engine is equipped with a jacket water pump to dissipate heat to the atmosphere using air coolers. As stated in the introduction, many rural Alaskan diesel generators are equipped with jacket water heat recovery systems, which may have pumps already installed. Taking this into account, the electrical power consumed by the hot water pump ($P_{pump,HW}$) is neglected in P_{OP} calculation, assuming the already installed jacket water pump can be used to overcome the ORC power unit evaporator pressure drop. P_{OP} will be used in the annual diesel fuel saved, emissions reductions, and economic outcome calculations discussed in the following paragraphs. Here P_{Net}, $P_{Pump,P}$, and $P_{Pump,CW}$ are measured parameters, as explained above. Eq. (A.4) is used to estimate system operating efficiency (P_{OP}), which is the ratio of P_{OP} and $Q_{HW,Su}$.

$$P_{OP} = P_{Net} - P_{Pump,CW} \quad (A.3)$$

$$\eta_{OP} = P_{OP} / Q_{HW,Su} \quad (A.4)$$

Liters (or gallons) of diesel fuel saved per year ($F_{S/Y}$) was calculated using Eq. (A.5), which was based on a system operating power output (P_{OP}) of 363 power unit working days per year with 2 days of maintenance, and stationary diesel engine-specific fuel consumption (SFC). Stationary diesel engine SFC of 225.75 g/kWh (0.497 lb/kWh) [18, 19], considering a density of 835.3 kg/m^3, which is a reasonable SFC value for rural Alaska village diesel generator sets, gives a conservative estimate of fuel savings for most village generators. The dollar amount saved on diesel fuel per year ($F_{\$/Y}$) was calculated based on diesel fuel saved per year ($F_{S/Y}$) and a diesel fuel cost of $5.00/gal, which is a reasonable value for rural Alaska stationary diesel generator power plants.

$$F_{S/Y} = P_{OP} \bullet 363 \bullet 24 \bullet (835.3/0.225) \quad (A.5)$$

A.6.2 Reductions in Emissions and CO_2

Since the power generated by the ORC power unit comes from waste heat of a diesel generator set (i.e., free heating source), it would offset some of the power needs of the village and, in turn, reduce emissions. Annual emissions reductions were estimated based on the annual system power output and stationary diesel engine emissions (based on Tier-4 emissions standard [24]) given in Table A.2. Annual CO_2 reductions were based on liters (or gallons) of diesel fuel saved (2.66 kg of CO_2 generated per liter of diesel fuel [25]) per year ($F_{S/Y}$).

A.6.3 Economic Analysis

Economic feasibility was estimated based on payback period. The payback period is the time at which enough money has been accumulated at a given simple interest rate to offset the total

initial investment cost and annual maintenance/operation cost based on annual cost savings. Details can be found in the project final report [3].

A.7 Data Collection and Data Reduction

The ORC system experiment included both reliability and system performance tests.

A.7.1 Reliability Test

The reliability test lasted for 600hrs to determine the long-term endurance and performance of the unit. Reliability testing was limited to 600 hours in our test because of the limitation we had on cooling water supply at the current experimental site (the University of Alaska Fairbanks power plant). The system was operated under rated load (i.e., 50kW screw expander output or gross power), with input heating (hot water of 104.4°C (220°F) and 605.6 LPM (160 GPM)) and cooling (cooling water of 10°C (50°F) and 605.6 LPM (160 GPM)). Here LPM is liters per minute and GPM represents US gallons per minute. Table A.3 gives the results of the measured and derived parameters from the test. Measured parameters included hot water inlet and outlet temperatures, hot water flow rate, cold water inlet and outlet temperatures, cold water flow rate, ORC unit electrical power output, ORC working fluid pump power consumption, and cold water pump power consumption.

Table A.3 also gives reduced data of reliability test results for system performance, such as system operating output, power consumption of individual pumps, power supplied and released from the system, system efficiency, estimated emissions and CO_2 reductions, and payback period for operation of the ORC unit at rated load for 363 days a year with two days for maintenance. Cost information includes initial costs of component and installation costs of $191,348.52 and $89,000, respectively, and maintenance costs of $7,600 per year (mainly for travel and labor). Initial costs are based on data obtained from this experiment and maintenance costs are based on village maintenance for similar facilities used in villages, such as air conditioning and refrigeration systems (two days per year). Most of the operation cost results from the cold water pumping power consumption, which is provided by the ORC system's output power and need not be considered in payback calculations.

A.7.2 Performance Test

Table A.4 shows the hot water and cold water flow rate and temperature conditions under which the 50 kW ORC power unit was tested. From Table A.4 it can be inferred that the ORC power unit was tested under 150 different hot water and cold water supply conditions, 75 cases

for cooling water at 10°C (50°F) and 75 cases for 20°C (68°F). During the actual testing, for a cold water inlet temperature of 20°C, only one stable cold water flow rate was obtainable for each specific hot water temperature and flow rate. This stability problem was not fully investigated, but may have resulted from the performance characteristics of the two manual control valves of the cooling water loop. Therefore the ORC power unit was tested for a total of 100 cases (75 for cooling water at 10°C and 25 for 20°C) instead of 150 cases. The reduced number of test cases for 20°C cooling water temperature may not critically affect the importance and applicability of the experiment results to achieve the goal of this project, because the effect of cooling water flow rate on system performance is relatively less than that of the other input parameters (i.e., hot water temperature and flow rate and cold water temperature).

Based on the schedule listed in Table A.4 and above discussion, for cold water at a temperature of 10°C, performance data were measured and grouped into 5 sets (i.e., based on 5 different hot water temperatures), where each set contains 15 cases (i.e., combination of 5 hot water inlet temperatures and 3 cooling water temperatures). In order to limit the paper to an appropriate length, only one set of data for hot water temperature of 68.3°C (155°F) (cold water of 10°C) is given in Table A.5 (as an example). The reduced data is also shown in Table A.5. For cold water at 20°C, due to immateriality of the effect of cooling water flow rate, all the test results for 25 sets of data (5 hot water temperatures and 5 flow rates) are listed in Table A.6. All 6 sets of data (5 sets for 10°C and 1 set for 20°C) for different combinations of hot water and cold water temperatures and flow rates can be found in the project final report [3].

Reduced data for system performance are also given in Table A.5 and Table A.6 using equations given in the Data Reduction Methodology subsection.

A.8 System Performance

This section discusses the performance characteristics based on experimental data, and only characteristic curves which are related to the goals of this paper are presented. More performance characteristic curves can be found in the project final report.

A.8.1 Performance Data Reduction and Characteristic Curves

Based on measured and reduced data obtained from this project, performance characteristics curves are constructed and given in Figure A.3 through Figure A.8. Figure A.3 and Figure A.4 give the performance curves of heat supplied to and operating power output from the ORC unit for a cold water supply temperature of 10°C (50°F) and varying the other three parameters (hot

water temperature, flow rate, and cold water flow rate). Figure A.3 and Figure A.4 were plotted based on the average values of measured temperatures and flow rates of the hot and cold water supply, the power unit's electrical power output, the power consumption of the ORC working fluid pump and the cold water pump. The average values are obtained from data sampled at 30-minute intervals after the system reached a steady-state condition. Temperatures were sampled at a frequency of 1 second, electrical power data were sampled at a frequency of 30 seconds, and flow rates were noted manually from the flow meter display screen.

Figure A.5 through Figure A.8 give performance curves of the heat supplied by hot water, system operating power output, efficiency, payback period, and reductions in CO_2 emissions versus different hot water supply temperatures and flow rates for the cold water supply temperatures of 10°C (50°F) and 20°C (68°F). In each of the figures (Figure A.5 to Figure A.8), the top plot is for a 10°C cold water temperature and the bottom plot is for a 20°C cold water temperature. For a cooling water temperature of 10°C, the characteristic curves were constructed based on a cooling water flow rate of 605.6 LPM (160 GPM). The curves for other flow rates were not constructed to avoid confusion due to too many curves in a single figure. In addition, it has been observed that the effect of cooling water flow rate on performance was much less than that of hot water flow rate for the flow rate range (454.2 LPM (120 GPM) − 757.1 LPM (200 GPM)) used in this experiment (see item 4 of this subsection). For a cooling water temperature of 20°C, the flow rate used for each data point was the flow rate at which the cooling system operated under stable conditions (details in the Performance Test subsection). All four plots are presented on the same hot water supply temperature scale and with the same color-coding for each of deduced parameter readings.

A.8.1.1 Observations

This subsection presents the properties of the derived performance curves. The properties are divided into 5 items: items 1, 2, and 3 are related to the effect of the heating source; item 4 is related to the effect of the cooling source; and item 5 is related to the combined effect of both cooling and heating sources.

1. Effect of Heat Source: The ORC operating efficiency (i.e., $P_{OP}/Q_{HW, SU}$) varies little across a wide range of input. For example, for a heat source (i.e., hot water heat input in Figure A.3) of 627kW and 107.2°C (225°F), the highest heat input for this experiment, and a cooling source of 10°C, the ORC system operates with an output of about 47.7kW (Figure A.3) and

an efficiency of 7.6%. For a heat source of 257kW and 68.3°C (155°F) (the lowest heat input) and a cooling source of 10°C, the ORC system operating output is about 13kW (Figure A.4) with an efficiency of 5.3%.

2. For a given hot water supply temperature and cold water temperature and flow rate, in general, heat supplied by hot water ($Q_{HW,Su}$) to the power unit evaporator increased with the increase of hot water flow rate as shown in Figure A.3. For example, at a hot water supply temperature of 79.4°C (175°F) and cold water flow rate of 605.6 LPM (160 GPM), heat supplied by hot water increased from 327.4kW at a 454.2 LPM (120 GPM) flow rate to 380.7kW at a 1135.6 LPM (300 GPM) flow rate. However, for some cases, an irregular trend occurs due to occasional disturbances in the hot water supply temperature resulting from surges in the power plant's steam supply condition. A corresponding irregular trend is also observed in the power output curves in Figure A.4.
3. As hot water flow rate increased for a given hot water supply temperature, the heat input to the power unit reached an asymptotic condition (Figure A.3), i.e., for a given hot water supply temperature, the heat absorption by the working fluid in the evaporator reached a limiting value for higher hot water flow rates. The same trends were observed for system operating power output and efficiency (Figure A.5 and Figure A.6) as they reached asymptotic conditions for higher hot water flow rates. For example, it is observed that asymptotes exist for system operating output versus heat source flow rate curves (Figure A.5), and the values depend on the heat source temperatures. For example, for cold water at 10°C and hot water at 90.5°C (195°F), the system operation output has an asymptote of about 35kW, and system operation efficiency, about 7.4%. The reason for this asymptotic condition is that the ORC power unit evaporator reached its design capacity. There is another limitation from the ORC unit PLC software, which prevents the screw expander from generating more than the rated load of 50kW. The PLC software limitation, which limits the R-245fa flow entering the screw expander, is one of the many safety features which protect the screw expander from over-speeding.
4. Effect of Cooling Source: From Figure A.4, it is observed that, for a given hot water flow rate and hot water supply temperature, the effect of cold water flow rate on ORC system operation power output and, in turn, ORC system operation efficiency is minimal within the cold water flow rate range used in the experiment. For example, the system operating power

outputs at a hot water flow rate of 757.1 LPM (200 GPM), supply temperature of 90.5°C (195°F), and cold water temperature of 10°C, are 32.4kW, 32.9kW, and 33.2kW for cold water flow rates of 454.2 LPM (120 GPM), 605.6 LPM (160 GPM), and 757.1 LPM (200 GPM), respectively. Compared to the effect of hot water flow rate on system performance, the effect of cooling water flow rate may be negligible. Considering system efficiency, for cooling water at 10°C and hot water at 68.3°C (155°F) and 454.2 LPM (120 GPM), the ORC system operation outputs are 12.5kW, 12.8kW, and 12.4kW for cooling water flow rates of 454.2 LPM, 605.6 LPM, and 757.1 LPM, respectively.

5. Combined Effect of Heating and Cooling: The combined effect of heating source temperature and cooling source temperature was also observed. For hot water at 107.2°C (215°F), the ORC screw expander power outputs are 49.1kW and 44.7kW for cooling water at 10°C (50°F) and 20°C (68°F), respectively; the corresponding ORC net efficiencies are 7.5% and 7.4%. For hot water at 68.3°C (155°F), the ORC screw expander power outputs are 17.5kW and 12.3kW for cold water at 10°C and 20°C, respectively; the corresponding ORC net efficiencies are 5.9% and 4.4%. In Figure A.5 through Figure A.8, for cold water at 20°C, the results were presented only up to the maximum hot water supply temperature of 101.6°C (215°F) instead of 107.2°C (225°F), as for 10°C cooling water. This is because of the low saturated steam pressure in the power plant, which prevented the hot water supply temperature from reaching the expected maximum of 107.2°C during the test.

A.8.1.2 Example for Performance Estimate

This subsection describes how the experimental data could be used to estimate the performance of the ORC on a diesel power plant. The Power Cost Equalization (PCE) program data published by the Alaska Energy Authority for fiscal year 2011 [1] and available diesel engine data for a village, Galena, located in Central Alaska were used to evaluate diesel engine waste heat recovery for power generation using the present ORC system. Based on PCE data, the village's annual electrical load is 9,352,000kWh (1.068MW), and all of this power could be generated using a Caterpillar 1.5MW diesel engine. According to a communication with an engineer at the power plant, the fuel specific efficiency of the power plant is about 243.23 g/kWh of diesel, and jacket water temperature is about 85°C (185°F). According to these data, the diesel generator is, on average, operating at 71% of its rated load, of which the estimated exhaust temperature is about 400°C (752°F). Based on the low heating value of diesel fuel (36,372.47

kJ/liter (130,500 BTU/gal)), the engine efficiency is about 34%. If jacket water contains 20% and exhaust contains 36% of fuel energy, respectively, the available heat flux of the jacket water exiting the engine jacket water will be 628kW, and of the exhaust will be 1,131kW. Assuming that 757.1 LPM (200 GPM) of jacket water can be provided to the ORC system, available heat to the ORC system will then be about 404kW (from Figure A.3 for cooling water at 10°C). Due to the concern that low temperature of exhaust may cause corrosion of the exhaust system, it is not advised to absorb as much heat energy as possible from exhaust. Assuming that 50% of the exhaust heat can be captured by the coolant (e.g., water) through the exhaust to water coolant heat exchanger, the available exhaust heat to the ORC system will then be 565.5kW. The total combined heat of exhaust and jacket water is 1194 kW. Due to the power output limit of the screw expander, only about 618 kW (Figure A.3 for hot water flow rate of 757.1 LPM at 107.2°C (225°F) and cold water at 10°C) of the heat is absorbed by the evaporator for power generation.

To evaluate the ORC performance for waste heat recovery from the stationary diesel engine, two cases were simulated, the first being the jacket water heat recovery system only and the second being the combined jacket water and exhaust heat recovery. For both of the simulation cases, it was assumed that a water cooling source as heat sink is readily available at 10°C (50°F), which is about or above the year round groundwater temperature in the village.

Table A.7 gives the results for operating this ORC power system on waste heat from jacket water of the village generator. An exhaust temperature of 400°C (752°F) is well above the 107.2°C (225°F) required for the ORC to generate rated system operating power (based on this experiment). For the simulated case of combined jacket water and exhaust heat recovery system, if the heat recovery system is designed such that the jacket water from the engine is first passed through the exhaust heat exchanger, it is possible to achieve 107.2°C (225°F) or higher as hot water supply temperatures entering the ORC power unit evaporator. Table A.7 also gives the ORC power unit performance for combined jacket water and exhaust heat recovery systems installed together.

Table A.7 gives the system operating power output, efficiency, payback period, and CO_2 reductions obtained from Figure A.5 through Figure A.8. For combined jacket water and exhaust heat recovery, the system operating power output is about 45.7 kW (from Figure A.3 for hot water temperature at 107.2°C and flow rate of 757.1 LPM) with a payback period of 2.1 years for a 0% interest rate (from Figure A.7). The cost information used in the payback period

calculation includes the initial cost (component cost of $191,348.52, installation cost of $89,000) and maintenance costs of $7,600 per year. The initial cost is based on the cost of this experimental setup and maintenance is based on village maintenance (two days per year) of similar facilities (e.g., air conditioning and refrigeration systems). Travel accounts for a large portion of these costs. The major operation cost is the cold water pump power, which is provided by the ORC system, and so is neglected in payback period calculation.

Considerable reductions in emissions could be achieved, as listed in Table A.7. These reductions were calculated based on the EPA TIER-4 interim reduction standards discussed earlier.

A.9 Guidelines for Applying the ORC System in Rural Alaska

Major heat recovery applications in rural Alaskan villages include heating and power generation. For villages with fishing industries, cooling and refrigeration may also be important. For villages with small fishing industries, cooling and refrigeration are needed during the warm season and the amount of heat energy needed, in general, is not as much as that for space heating. Since the potential for fuel savings and economic impact for cooling and refrigeration system applications is minor, it is not further discussed in this paper. Based on performance data and characteristics of the 50kW ORC system discussed in the previous sections, this section presents guidelines for applying the ORC system to diesel generators in rural Alaska. Since individual villages may have different ORC installation and operation conditions (i.e., fuel cost, infrastructure, and village preference), the guidelines are in the form of proposed principles instead of step-by-step instructions. The presentation begins with an introduction of the difference between the applications of waste heat recovery for heating and waste heat recovery for power, which may be used to decide which type (heating or power) is more appropriate for an individual generator set. Then a discussion about guidelines is given for applying the 50kW ORC to the rural diesel generator sets. It should be noted that the focus of the discussion is on jacket fluid heat recovery.

A.9.1 Difference between Applying Waste Heat for Heating and Waste Heat for Power

This paragraph gives a comparison in benefits obtainable from applying heat recovery for heating and heat recovery for power. Assumed recoverable heat is 80% for jacket fluid heat (due to a variety of losses along piping and heat exchanger) and 50% for exhaust (due to piping heat loss and avoidance of low exit exhaust temperature to cause corrosion). In addition, considering

heat recovery for heating, the length of heating is assumed to be 7 months and boiler efficiency is assumed to be 80% (needed for fuel saving calculation). Additional assumptions for heat recovery for power include 6.8% (Figure A.6) of ORC efficiency and diesel generator efficiency of 40% (needed for fuel saving calculation). Fuel heating value is assumed to be 36,372.47 kJ/liter (130,500 BTU/gal). According to the assumptions mentioned above, every 1 kWh of jacket fluid heat may recover 4,066 kWh of heat annually for useful applications, which corresponds to potential diesel fuel savings of about 503.4 liters (133 gallons). For heat recovery for power, every 1 kWh of jacket water heat may generate 592 kWh power annually, which corresponds to potential diesel fuel savings of about 162.7 liters (43 gallons). If exhaust heat recovery is considered, the fuel savings for heat recovery for power may be improved due to the possible much higher temperature of the heat source, but the expected fuel savings for power generation alone (using the 50kW ORC system) may still be significantly lower than those of heat recovery for heating due to the limit of allowable heat source temperature to 115.5°C (240°F) (set by the manufacturer) for the ORC system.

Notes related to the two types of heat recovery:

1. Electrical power is more flexible to apply than heat energy.
2. The cost of infrastructure and installation for both applications is village-dependent and may become critical for economic benefit (e.g., for heat recovery for heating, the amount of arctic pipe needed, and labor cost may dominate; for heat recovery for power, the cooling system may become very important).
3. Costs of fuel for heating and power generation may differ.
4. For heat recovery using high temperature heat, the residual heat in the hot fluid (e.g., water) exiting the ORC may still have good quality (or temperature) and can be further recovered using a multi-stage heat recovery system, which may improve the effectiveness of heat recovery greatly.

A.9.2 Guidelines for Applying the 50 kW ORC System to Individual Diesel Generator Sets

Guidelines for applying the 50kW ORC to individual diesel generators may be divided into two categories. The first one is related to conditions associated with individual villages and the other is related to the performance of the ORC system. Since many parameters vary from village to village (e.g., fuel cost, infrastructure, cooling source), the guidelines presented here only serve as principles of how to effectively apply the ORC to rural villages.

A.9.2.1 Related to Individual Villages

Heating applications of rural Alaska villages include space heating (e.g., power plants, hospitals, schools, community centers, and libraries), city water temperature maintenance, and sewage heating. The heat quality (temperature) requirement for space heating is relatively high (76.6^{o}F (170^{o}F) or higher) in comparison with that of city water temperature maintenance and sewage heating.

A.9.2.1.1 Preference of Individual Villages

Village preference may not have much to do with technology and/or economy. Previous research has shown that some villages are reluctant to modify their diesel generators for heat recovery applications.

A.9.2.1.2 Existence of Heat for Heating System

If a village already has a heat recovery for heating system in operation and can efficiently use all the heat energy, then heat recovery for power can only be considered for summer applications after having been determined beneficial (use the procedure similar to the example given in the next section, "Match between the 50 kW ORC and a Diesel Generator Set").

If the amount of recoverable heat energy is noticeably more than that needed for applications, a 50kW ORC system may be adopted and considered for year-round usage, assuming that the leftover heat from heating is enough to operate the ORC and can benefit the village. If the leftover heat is enough for the need of more than one of the 50 kW ORC systems, a multi 50kW ORC or a larger ORC system (if available) may be used, assuming it is economically suitable. In general, larger ORC systems operate at a higher efficiency. If the temperature of the heating fluid exiting the ORC screw expander is high enough for other heat recovery usage, multi stage applications can be used, assuming economic suitability. It should be noted that for multi stage applications, the temperature of the jacket fluid exiting the last stage of the heat recovery loop (and reentering the engine jacket) needs to satisfy the temperature requirement of the diesel engine set up by the manufacturer. However, this does not have to apply to the exhaust heat recovery system if it includes an independent exhaust heating loop (no jacket fluid is mixed with heating fluid in the independent exhaust heating loop).

A.9.2.1.3 Nonexistence of Heat for Heating System

Economic benefit is the focused concern for choosing one technology over another (heating vs. power generation) as the major heat recovery system to serve the village. Economics for this

case may depend on many factors, such as the location of the power plant (e.g., distance between the power plant or heat source and the location of applications), preferences of the village, heat source type (jacket fluid and/or exhaust), cooling source type, costs of technologies needed for maintenance and operation, and infrastructure availability. Depending on the heat availability and other factors, the heat recovery applications may be for heating, power, or a combination of heating and power in different forms, such as heating and power in parallel or in series (as mentioned in the previous paragraph). Before any decision-making, an economic analysis is highly recommended.

A.9.2.2 Related to Performance of the ORC System

A.9.2.2.1 General Observation

The available space and details of existing utilities and heating/cooling sources are important for design and installation of the piping system of the ORC unit. The local codes, which may significantly affect the project cost, are equally important. For an isolated, small community, a careful purchase plan is also important in order to avoid long schedule delays and/or cost changes.

For this project, the installation and instrumentation (steam loop, hot water loop, cold water loop, electrical circuit, signal/monitoring/control circuits, data acquisition system) process was very smooth. In other words, the installation of the ORC system, in general, does not require complicated procedures if heat and cooling sources are readily available. Also, according to the experimental results, the system ran smoothly and no in-depth technologies were needed to operate the ORC. However, to claim reliability of the ORC system, longer term experimental test and/or field tests are needed.

A.9.2.2.2 Related to Heat Source

In this experiment the heating fluid used is water. It is believed that the performance characteristic would be similar, if water/glycol is use as heating fluid. Based on items 1, 2, and 3 listed in the section of "System Performance", the ORC system fits a wide range of diesel engine sizes, loads, and jacket water temperatures. The data related to items 1, 2, and 3 can help evaluate if the heat source of an individual diesel generator is appropriate for applying the ORC system. It is suggested to estimate the potential benefit that the ORC unit can bring to the individual diesel generator before purchasing.

The asymptotes mentioned in item 3 in the previous section may largely depend on heat exchanger design and power output limit of the ORC screw expander set by the manufacturer. If a heat source exceeds the asymptote of the expander output for a given hot water temperature, the screw expander may perform less efficiently (even if it generates more power). If the heat source is more than the requirement to generate 50kW from the screw expander, most likely, part of the heat energy will bypass the expander and not be used for power generation. For a given village diesel generator set, the asymptote information and the limit of screw expander output can be useful in determining appropriate waste heat flow distribution (either in parallel connection or in series connection) between the ORC and other co-existing heat recovery devices to keep the system from overfeeding and using heat energy ineffectively.

For the 50kW ORC, the asymptotes for different heating source temperatures are almost linearly dependent on the heat source temperature (Figure A.5) until the screw expander output reaches its limit of 50kW (i.e., operating output near 47kW) for the range of hot water temperatures used in this experiment (68.3°C to 107.2°C). This range is close to the temperature range given by the manufacturer (65.5°C (150°F) to 115.5°C (240°F)). Considering applications in rural Alaska, jacket water temperatures are most likely between 79.4°C (175°F) and 90.5°C (195°F) (based on log data of a few village diesel generator sets). It is suggested to use experimental data to predict the ORC performance for individual rural village generators.

According to this experiment, in which the heat source temperature ranges from 68.3°C to 107.2°C and flow rate ranges from 454.2 LPM (120 GPM) to 1135.6 LPM (300 GPM), the temperature of hot water exiting the ORC ranges from about 60°C (140°F) to 96.1°C (205°F). Plenty of relatively high quality heat energy still exists in the exiting hot water (i.e., residual heat). Furthermore, if the heat source temperature is 115.5°C (240°F) (for the case that involves exhaust heat recovery), the temperature of residual heat may be even higher. For these cases, the residual heat could be further used if other coexisting heat recovery facilities are available. When using residual heat, caution needs to be practiced if jacket water is involved. As mentioned before, the returning hot water entering the engine jacket needs to meet the minimum allowable temperature requirement set by the manufacturer. If the heat source is from exhaust only (i.e., a heating loop without engine jacket water), all the residual heat energy in the hot water is useful for further heat recovery. If independent exhaust heat recovery is used, corresponding pump power consumption needs to be considered as part of the operation costs.

A.9.2.2.3 Related to Cooling Source

There is no minimum cooling source temperature for the 50kW ORC (besides the freezing point of the cooling fluid). The maximum cooling water temperature is 43.3°C (110°F), set by the manufacturer.

From item 4 of the previous section, System Performance, the effect of the cooling water flow rate on system performance is minimal compared to that of the hot water flow rate for power generation. For 454.2 LPM (120 GPM) of cooling water flow, the measured pump power (parasitic power) requirement is around 1 kW. 1 kW is low in comparison with the level of the ORC output for jacket water heat application (between 20 kW and 40 kW). Therefore, use of 1kW as parasitic power for system performance and economic outcome evaluations may not cause significant error. However, it is always advisable to use measured performance data for system performance and economic evaluations, if measurements and data analyses are feasible. Related to Combined Effect of Heating and Cooling: From item 5 of the previous section, the results show that the cold water temperature has a greater effect on the ORC performance when the hot water temperature is low. Therefore, if the jacket water temperature is relatively low for a period of time (e.g., during summer), whether or not the application of the ORC system is economically beneficial needs to be carefully investigated.

In conclusion, the selection of a configuration of heat recovery application (i.e., for heating, for power, for combine both heating and power in parallel or in series, multiple power units, multiple stages) is village-dependent. To optimize the economic outcome, economic analysis may be needed and data from reliable sources is important. This section lists the factors which are important for selecting an appropriate heat recovery application configuration for individual village diesel power plants. It also outlines the underlying principles of how the 50 kW ORC system could be effectively adopted in rural Alaskan villages. The principles mentioned here may also be applicable to other ORC systems with similar performance characteristics.

A.10 Match between the ORC System and any Rural Diesel Generator Set

This section discusses how to determine whether or not a specific village generator will gain desired payback period from applying the 50kW ORC system. The major factors of concern include type (i.e., exhaust heat, jacket heat, or combination) and condition of heat source (e.g., year round temperatures and flow rates; availability of heat energy for the ORC operation), type and condition of cooling source (e.g., surface water, underground water, cooling tower, radiator,

conventional heat exchanger), willingness of the village to adopt the heat recovery system, installation and infrastructure costs, maintenance and operation costs, and interest rates. Due to the hot water temperature limits of the ORC system (65.5°C (150°F) to 115.5°C (240°F)), it is not able to take full advantage of very high hot water temperatures (higher than 115.5°C) resulting from using diesel engine exhaust heat. Therefore, the heat source (e.g., hot water) may come from jacket fluid alone or combined jacket fluid and exhaust for heat source temperatures under 115.5°C. For data obtained from this experiment, water is the jacket fluid.

A.10.1 Procedure

A proposed procedure is presented below to match the performance between the 50kW ORC and any individual diesel generator sets. An example follows:

1. Estimate fuel price, capital cost, interest rate, and desired payback period.
2. Use Figure A.9 for an interest rate of 10% (for a different interest rate, a similar curve can be easily developed using experimental data) to determine the minimum requirement of operating power output of the ORC that matches the desired payback period.
3. Estimate the availability of conditions (flow rates and temperatures) of heat and cooling sources available to the ORC application. The conditions may be as detailed as hourly data or as rough as yearly average data. More details may give more accurate predictions.
4. Estimate the parasitic power for operating the heat to power system. Sources of parasitic power may depend on the heating and cooling sources used for operation.
5. Use Figure A.5 (for cold water at 10°C and 20°C) to estimate the ORC operating output based on local hot water and cold water conditions available. If necessary, appropriate interpolation could be applied.
6. If estimated operation output of the system equals or exceeds the minimum required operation power output for the desired payback period (from step 2), the ORC system is recommended for the particular village power plant. If the amount of heat is much more than the minimum requirement for the payback period, a further study about how to more effectively use the waste heat (e.g., add more ORC systems, add a heat recovery system for heating, and select a different size of heat to power application) may be needed.
7. If the estimated ORC system operation output is less than the minimum required operation power output for desired payback period, applying the ORC system may not be beneficial.

A.10.2 Demonstration Example

An example that demonstrates the proposed procedure is given below.

Suppose a power plant has a hot jacket water flow of 454.2 LPM (120 GPM) and 85°C (185°F) and a cooling water source of 454.2 LPM and 10°C. We would like to determine the feasibility of using this 50kW ORC unit as its waste heat recovery system. Other known conditions are that the parasitic power for the cooling pump is about 1 kW for a flow rate of 454.2 LPM (the same as used in the experiment); the payback period is 10 years; the expected capital is $400,000; the interest rate is 10%; fuel cost is $5/gallon; and the system will operate year-round.

Based on the given hot water temperature and flow rate and cold water temperature, the system operating output power (from Figure A.5) is 25.5 kW (parasitic power has already been considered.). Based on the expected capital cost and interest rate, fuel cost, and desired payback period, the required minimum operating output power is about 24 kW (from Figure A.9). Comparing the system operating output power (25.5 kW) with the required power of 24 kW, it seems marginally feasible to adopt the 50kW ORC system for jacket water heat recovery for this power plant. Since this calculation is based on water as heating fluid, if the heating fluid is changed to 60/40 propylene glycol/water (which results in about a 10% reduction in power generation), the system operating output power needs to be modified accordingly. Then the application of the system may become marginally unfeasible at this power plant.

A.11 Potential Fuel Savings via Applying the 50 kW ORC System to Rural Alaska Villages

This section discusses the potential extra electrical power which could be generated if the 50kW ORC system would be adopted for all rural Alaska diesel generators that have the potential to generate 10kW or more from the ORC system. In addition, in this study, if the ORC unit generates an output of less than 10kW, the ORC will be shut off due to the assumption that a 10kW output brings no benefit to the village.

In rural Alaska, about 180 villages use off-grid diesel generator sets for their electrical power supply. The 2011 average electrical power usage of each of the villages is reported in the Statistical Report of the Power Cost Equalization Program for Fiscal Year 2011 published by the Alaska Energy Authority (AEA) in April 2012 [1]. Based on the diesel power data published, and assuming that engine efficiency is 40% (optimistic for engine efficiency and pessimistic for waste heat availability); the amount of jacket heat (assuming 20% of fuel energy) and exhaust

heat (assuming 30% of fuel energy) can then be calculated. Based on an estimate that only 80% of jacket heat source and 50% of exhaust heat can enter into the ORC system due to losses along the piping system and the concern of avoidance of exhaust system corrosion, the amount of heat source can then be evaluated and power generated by the ORC system can be calculated.

In this study, the heating fluid is assumed to be hot water, and the conversion efficiency from heat to power depends on the type of heat source (jacket heat or combined jacket and exhaust heat). If jacket water is the heat source, the temperature of the heat source can feasibly reach 90.5°C (195°F) and system operating efficiency is about 7% (Figure A.7); if combined jacket water and exhaust heat is used as the heat source, the temperature is assumed to be the maximum allowable heat source temperature (115.5°C) of the 50kW ORC system and the operating efficiency can be up to 7.5% or more (Table A.3). Additional assumption is that individual villages can use multiple ORC units, if heat sources are sufficient. Based on all the conditions mentioned above, only 26 village diesel generator sets are available, if jacket water alone is the heat source; 51 village diesel generator sets are available, if combined jacket water and exhaust are the heat source. Table A.8 lists all the villages for which the diesel generator sets are appropriate for installing the 50 kW ORC. Table A.8 also lists the calculated corresponding fuel savings for the respective villages, and fuel savings for all the rural Alaska villages as a whole for both cases of jacket water as heat source and combined jacket water and exhaust as heat source. According to Table A.8, applying jacket water heat alone, the potential total annual ORC power generation is 9,571 MWh, and annual diesel fuel savings is 2,587,859 liters (683,640 gallons) (based on a SFC of 225.75 g/kWh); applying combined jacket water and exhaust heat, the potential total annual ORC power generation is 23,005.9 MWh and annual diesel fuel savings is 6,220,495 liters (1,643,281 gallons).

Since capital, installation cost, fuel cost, emissions information is village-dependent, economic analysis was not considered in this example. If reliable data for a village is available, economic analysis can then be conducted following the procedure given in the "System Performance Parameters" section.

A.12 Conclusions

The major purpose of this study was to develop an experimental setup for a selected ORC system and obtain experimental data for deriving guidelines for effectively applying the system to rural Alaska village diesel generator sets. The selected ORC system for study, which was a 50

kW screw expander type system, was the only one available at the beginning of this project. Another goal of this study was to apply the data to estimate fuel savings that the ORC system could bring to each of the individual village diesel generator sets and to the rural Alaska diesel power industry as a whole. The study, therefore, needed to include the performance characteristics of the ORC system, from which guidelines could be concluded and fuel savings could be estimated. Fuel savings were used as an indicator of application effectiveness in this paper, owing to the fact that fuel and installation costs were village-dependent and not available for all villages. Instead in this paper an example has been used to demonstrate how to conduct a payback period analysis.

This paper included an introduction about the development of the heat to power industry for medium scaled (less than about 1 MW) diesel generator sets; short descriptions of the experimental setup, test schedule, and data obtained from the reliability test (600 hours) and system performance test (50 hours); brief reviews of the data reduction methodology and performance characteristics derived from reduced data; guidelines about how to effectively apply this system and estimates of potential fuel savings which could be brought to the rural villages.

Reliability and performance tests showed that the system was easy to install and operate. Based on this test results (from 650 hours' operation), maintenance may not cause critical concern. However, to claim system reliability, much longer time periods of experimental and testing are needed. One of the major reasons additional testing time is needed was that the system used a newly designed screw expander and no field data were available during the period of this test.

An example is given in the "System Performance" section of applying the experimental data to estimate the economic benefit and emissions reductions that the ORC system could bring to a particular village in Central Alaska. This example uses the data obtained from this test and operation data of the diesel generator of the village. It is found that the payback time can be 3.8 years for an interest rate of 0% and 4.4 years for an interest rate of 10%, assuming jacket water as a heat source and a fuel cost of $5/gallon. In addition, the initial cost is assumed to be $280,349 and the maintenance cost to be $7,600 per year.

Guidelines have been developed to recommend how to effectively apply the 50kW ORC system to rural diesel generator sets. The guidelines were divided into two categories: one based on village conditions and another based on ORC performance characteristics. Village condition-

based guidelines considered the preferences of the village, the existence (or nonexistence) of heat for heating systems in the villages, the amount of heat availability, and other related infrastructure and requirements. ORC performance-based guidelines considered general performance of the ORC system (e.g., reliability, potential economic benefit), heat source properties (e.g., jacket and/or exhaust, maximum heat source temperature, minimum power output requirements, quality and quantity of heat for multistage application, multi ORC unit applications, potential of using a different ORC system), cooling source properties (e.g., maximum cooling fluid temperature, cooling capacity), and the combined effect of heat source and cooling source (e.g., the importance of cooling temperature when heating temperature is low).

Since each village has unique conditions concerning the application of an ORC system (i.e., fuel cost, infrastructure, cooling source), the guidelines discussed in this paper are in the form of general principles of what needs to be considered in order to effectively apply this ORC system. All the guidelines are related to the outcome of economic benefit and the decision of whether or not to adopt this ORC system is most likely determined by economic impact. The guidelines may also be useful for other ORC systems which have similar performance characteristics. An example is presented in the Match between the 50 kW ORC and a Diesel Generator Set section to describe how to determine if the ORC system is beneficial to the village, for given local information (i.e., fuel cost, initial cost, interest rate, cooling source temperature).

The last section of this paper, Potential of Fuel Saving via Applying the 50kW ORC System to Rural Alaska, presents the potential fuel savings for each individual village in rural Alaska if the 50 kW ORC system is applied. Among 280 villages, only 26 villages can generate, on average, 10 kW or more of electrical power via applying the ORC system using only jacket water as a heat source. For the case of the heat source including both jacket water and exhaust, 51 villages will be able to generate 10 kW or more of electrical power. If 10 kW is considered the threshold for economic benefit and multiple units of the 50 kW ORC are allowed (this will be the case when the available heat energy of a village is more than the need of a single 50 kW ORC unit), the annual fuel savings for all of rural Alaska could potentially reach 2,587,859 liters (683,640 gallons). If both exhaust heat and jacket heat are used, the annual fuel savings would be 6,220,495 liters (1,643,281 gallons).

A.13 References

[1] Alaska Energy Authority, "Statistical report of the power cost equalization program for fiscal year 2011", 23rd Edition, April 2012.

[2] Avadhanula, V.K., Lin, C.S., and Johnson, T., "Testing a 50kW ORC at Different Heating and Cooling Source Conditions to Map the Performance Characteristics," SAE Technical Paper 2013-01-1649, 2013.

[3] Lin, C.S., "Optimizing Heat Recovery Systems for Power Generation in Rural Alaska," Final report prepared for Tanana Chiefs Conference and Denali Commission by the Alaska Center for Energy and Power, March 31, 2012.

[4] Holdmann, G., "The Chena Hot Springs 400 kW Geothermal Power Plant: Experience Gained During the First Year of Operation," Transactions of the Geothermal Resource Council, Vol.31, pp 509-514, Davis, CA, September 2007.

[5] Leslie, N.P., Zimron, O., Sweetser, R.S., and Stovall, T.K., "Recovered energy generation using an Organic Rankine Cycle system," ASHRAE Transactions # CH-09-024, Vol. 115, Part 1, ASHRAE Winter Conference, Chicago, 2009.

[6] Canada, S., Cohen, G., Cable, R., Brosseau, D., and Price, H., "Parabolic trough Organic Rankine Cycle solar power plant," presented at the 2004 DOE Solar Energy Technologies Program Review Meeting, Denver, Colorado, October 25–28, 2004.

[7] Bini, R., Schwarz, D.A., Gaia, M., Bertuzzi, P., and Righini, W., "Operational results of the first biomass CHP plant in Italy based on an Organic Rankine Cycle turbogenerator and overview of a number of plants in operation in Europe since 1998," Proceedings of the 2nd World Conference on Biomass for Energy, Industry and Climate Protection, Rome, Italy, pp. 1716 –1721, May10-14, 2004.

[8] Turboden ORC plants for Industrial Heat Recovery. Turboden press release URL: http://www.turboden.eu/it/public/downloads/11-COM.P-18-rev.4_HR_ENG.pdf. Accessed July 17th 2012.

[9] Yamamoto, T., Furuhata, T., Arai, N., and Mori, K., "Design and Testing of the Organic Rankine Cycle," Journal of Energy, Vol.26, pp. 239-251, 2001.

[10] Quoilin, S., "Experimental study and modeling of a low temperature Rankine cycle for small scale cogeneration," Master's Thesis, University of Liege, May 2007.

[11] Reid, A.D., "Low temperature power generation using HFE-7000 in a Rankine cycle," Master's Thesis, San Diego State University, July 2010.

[12] Leibowitz, H. and Mirolli, M., "First Kalina combined cycle plant tested successfully," Power Engineering, Vol. 101(5), pp. 45-48, 1997.

[13] Valdimarsson, P., "The Kalina power plant in Husavik – Why Kalina and what has been learned," Workshop on 10 Electricity Generation from Enhanced Geothermal Systems, Strasbourg, France, Sepetember 14-16, 2006.

[14] Knapek, E. and Kittl, G., "Unterhaching power plant and overall system," Proceedings of the European Geothermal Congress, Unterhaching, Germany, May 30 - June 1, 2007.

[15] Donald, C.E., "Refrigeration from Low Temperature Waste Heat," Chena Hot Springs Geothermal Conference, August 21, 2006.

[16] Hisham, E. and Ettouney, M., "Fundamentals of Salt Water Desalination," Elsevier, 2002.

[17] Mokkapati, V. and Lin, C.S., "Numerical study of an exhaust heat recovery system using corrugated tube heat exchanger with twisted tape inserts," International Communications in Heat and Mass Transfer, July 27, 2014.

[18] Raghupatruni, P., "Performance Analysis of Capture of Heat Energy from Diesel Engine Exhaust," Master's Thesis, University of Alaska Fairbanks, 2007.

[19] Raghupatruni, P., Lin, C.S., Witmer, D., Bargar, E., Schmid, J., Johnson, T., and Avadhanula, V.K., "An Experimental Feasibility Study of Using Diesel Exhaust for Space Heating in Alaskan Villages", Proceedings of the Tenth International Conference on Advanced Computational Methods and Experiments in Heat Transfer, Maribor, Slovenia, WIT Press, Vol.61, pp. 93-104, July 2008.

[20] Lin, C.S., "Capture of heat energy from diesel engine exhaust", Final report prepared for National Energy Technology Laboratory, DOE Award # DE-FC26-01NT41248, November, 2008.

[21] Alaska Energy Authority, "Optimizing Heat Recovery Systems for Power Generation in Rural Alaska-Task One Final Report", Prepared for the Alaska Energy Authority, August 25, 2009, Award#RSA 0925, http://www.akenergyauthority.org/PDF%20files/8-27-09_AEA-RSA0925TaskOneFinalReport.pdf. Accessed dated July 17th 2012.

[22] Alaska Department of Environmental Conservation, "Ground Water in Alaska", March 2005.

[23] Lemmon, E.W., Huber ML, and McLinden MO, "NIST Standard Reference Database

23: Reference Fluid Thermodynamic and Transport Properties-REFPROP," Version 8.0, National Institute of Standards and Technology, Standard Reference Data Program, Gaithersburg, 2007.

[24] U.S. Environmental Protection Agency, "Control of emissions of air pollution from non-road diesel engines and fuel," Rules and Regulations, Vol.69 (124), pp. 38980, June 29, 2004.

[25] U.S. Environmental Protection Agency, "Emission facts: Average carbon dioxide emissions resulting from gasoline and diesel fuel," EPA420-F-05-001, February 2005.

Table A.1 Thermodynamic properties and environmental date of R245fa

Safety	Vaporization Heat (1atm.)	Boiling Temperature (1atm.)	Critical Point	Saturation Slope	Ozone Depletion Potential (ODP)	Greenhouse Warming Potential (GWP) 100 year
Non-Flammable	197.5 kJ/Kg (355.5 Btu/lb)	14.6°C (58.3°F)	154°C (309.2°F) 36.4 bar (527.9psi)	Isentropic	0	1020

Table A.2 TIER-4 interim EPA emissions standards for non-road diesel engines

NO_x g/kWh (lb/kWh)	Particulate matter (PM) g/kWh (lb/kWh)	CO g/kWh (lb/kWh)	HC g/kWh (lb/kWh)	CO_2 kg/lit (lb/gal)
3.5 (0.0077161)	0.10 (0.0002204)	3.5 (0.0077161)	0.40 (0.0008818)	2.66 (22.2)

Table A.3 Reliability test results

Parameter	**Value**	**Uncertainty in measurement**
Average hot water supply temperature to power unit	104.2°C (219.7°F)	±1.1°C
Average hot water flow rate to power unit	604.9 LPM (159.8 GPM)	0.5%
Average cold water supply temperature to power unit	9.7°C (49.4°F)	±1.1°C
Average cold water flow rate to power unit	619.3 LPM (163.6 GPM)	0.5%
Power unit electrical power output	47.8 kW	0.5%
Power unit pump power consumption	3.61 kW	0.5%
Hot water pump power consumption	1.76 kW	0.5%
Cold water pump power consumption	1.76 kW	0.5%
System operating power output	46.04 kW	0.5%
Heat supply by hot water to power unit evaporator	610.4 kW	
Screw expander efficiency	8.4%	
Power unit efficiency	7.8%	
System operating efficiency	7.5%	
Diesel fuel saved per year	107757.4 liters (28466.5 gal)	
Dollar amount saved on diesel fuel per year	$142332.4/year	
Emissions reductions		
Oxides of nitrogen (NOX)	1394.8 kg/year (3075.1 lb/year)	
Hydrocarbons (HC)	159.4 kg/year (351.4 lb/year)	
Particulate matter (PM)	40 kg/year (87.9 lb/year)	
Carbon monoxide (CO)	1394.8 kg/year (3075.1 lb/year)	
Carbon dioxide (CO_2)	286670.4 kg/year (316 tons/year)	
Payback period		
Payback period @ 0% interest on capital	2.1 years	
Payback period @ 10% interest on capital	2.4 years	

Table A.4 Various hot water and cold water flow rates and temperatures at which the power unit was tested

Hot water temperatures, °C (°F)	**Hot water flow rate, LPM (GPM)**	**Cold water temperatures, °C (°F)**	**Cold water flow rate, LPM (GPM)**
68.3 (155)	454.2 (120)	10 (50)	454.2 (120)
79.4 (175)	605.6 (160)	20 (68) *	605.6 (160)
90.5 (195)	757.1 (200)		757.1 (200)
101.7 (215)	946.3 (250)		
107.2 (225)	1135.6 (300)		

*For a cold water inlet temperature of 20°C, only one stable cold water flow rate was obtainable

Table A.5 Performance results for HW Temp= 68.3°C; HW flow rate = 454.2 LPM to 1135.6 LPM; CW Temp 10°C and CW flow rate = 454.2 LPM, 605.6 LPM and 757.1 LPM

#	Hot water flow rate (LPM)	Hot water supply temperature (°C)	Cold water flow rate (LPM)	Cold water supply temperature (°C)	ORC net power (P_{Net}, kW)	ORC working fluid pump power ($P_{Pump,P}$, kW)	Cold water pump power ($P_{Pump,CW}$, kW)	Hot water heat input ($Q_{HW,Su}$, kW)	System Operating Power (P_{OP}, kW)	System operating efficiency (η_{OP}, %)
1	456.9	69.1	452.7	11.7	13.5	0.9	1.0	253.0	12.5	5.0
2	602.1	69.1	451.3	11.5	14.7	0.9	1.0	269.0	13.7	5.1
3	759.5	69.1	453.5	11.5	15.5	1.0	1.0	281.0	14.5	5.2
4	949.8	69.2	451.8	11.5	15.9	1.0	1.0	289.3	14.9	5.1
5	1138.5	69.2	454.0	11.5	16.4	1.0	1.0	300.4	15.3	5.1
6	456.5	70.0	595.5	11.5	14.6	0.9	1.8	257.5	12.8	5.0
7	602.5	70.1	600.0	11.3	15.7	1.0	1.8	272.8	13.9	5.1
8	763.6	69.2	622.5	11.7	15.4	0.9	2.0	272.0	13.4	4.9
9	953.1	70.5	593.7	11.2	17.9	1.1	1.8	302.7	16.1	5.3
10	1143.9	68.6	619.8	11.0	17.1	1.1	2.0	299.4	15.2	5.1
11	464.3	68.9	788.5	9.9	15.9	1.0	3.6	265.9	12.4	4.6
12	615.2	68.8	811.2	10.4	16.5	1.0	3.9	275.4	12.7	4.6
13	770.2	69.0	774.1	10.6	17.0	1.0	3.4	284.9	13.6	4.8
14	951.0	69.1	773.2	10.6	17.8	1.1	3.4	295.8	14.4	4.9
15	1136.2	69.4	774.4	10.6	18.4	1.1	3.4	306.7	15.0	4.9

Table A.6 Performance results for HW Temp= 68.3°C to 104.4°C; HW flow rate = 454.2 LPM to 1135.6 LPM; CW Temp 20°C and varying cold water flow rate

#	Hot water flow rate (LPM)	Hot water supply temperature (°C)	Cold water flow rate (LPM)	Cold water supply temperature (°C)	ORC net power (P_{Net}, kW)	ORC working fluid pump power ($P_{Pump,P}$, kW)	Cold water pump power ($P_{Pump,CW}$, kW)	Hot water heat input ($Q_{HW,Su}$, kW)	System Operating Power (P_{OP}, kW)	System operating efficiency (η_{OP}, %)
1	461.6	68.0	726.9	20.1	10.3	0.8	1.8	245.3	8.4	3.4
2	609.5	69.6	722.9	20.7	11.5	0.9	1.8	259.5	9.6	3.7
3	763.3	69.0	612.2	20.4	11.4	0.9	1.8	266.9	9.5	3.6
4	951.1	69.0	632.1	20.5	11.8	0.9	1.8	277.1	10.0	3.6
5	1139.1	69.0	639.2	20.7	12.3	0.9	1.8	285.5	10.4	3.7
6	466.1	80.1	1050.7	20.6	19.2	1.3	1.8	318.7	17.4	5.4
7	614.7	80.3	1018.2	20.7	20.2	1.3	1.8	331.6	18.3	5.5
8	761.2	79.9	1003.9	20.5	19.5	1.3	1.8	327.1	17.7	5.4
9	954.8	79.8	962.1	20.7	22.0	1.5	1.8	360.2	20.2	5.6
10	1140.8	79.6	988.4	20.5	23.0	1.6	1.8	374.5	21.2	5.7
11	466.4	90.8	815.4	20.8	28.2	1.9	1.8	410.4	26.3	6.4
12	608.4	90.8	761.4	20.5	30.3	2.1	1.8	442.7	28.4	6.4
13	769.0	90.9	854.1	20.4	32.2	2.3	1.8	466.4	30.4	6.5
14	946.9	91.0	857.2	20.6	33.3	2.4	1.8	485.5	31.4	6.5
15	1145.6	91.1	857.3	20.9	34.0	2.5	1.8	497.7	32.1	6.5
16	468.2	101.6	769.2	20.6	38.4	2.8	1.8	525.6	36.5	7.0
17	611.4	102.0	775.3	20.5	41.5	3.1	1.8	560.2	39.7	7.1
18	766.8	101.5	913.7	20.7	43.6	3.4	1.8	588.8	41.8	7.1
19	949.5	101.6	917.2	20.9	45.2	3.6	1.8	609.7	43.4	7.1
20	1137.8	100.7	932.0	20.7	45.8	3.7	1.8	624.2	43.9	7.0

Table A.7 Estimated ORC performance for operating on waste heat recovery from diesel engine

Parameter	Jacket water heat only	Jacket water + exhaust heat*
Hot water supply temperature to ORC power unit	85°C (185°F)	107.2°C (225°F)
Hot water flow rate to ORC power unit	757.1 LPM (200 GPM)	757.1 LPM (200 GPM)
Heat input to evaporator of ORC power unit	404.0kW	617.7 kW
System operating power output	27.0 kW (235.57 MWh/year)	45.7 kW (398.5 MWh/year)
System operating efficiency	6.7%	7.5%
Diesel fuel saved	68595.45 liters/year (18,121 gal/year)	116038 liters/year (30,654 gal/year)
Dollar amount saved on diesel fuel	$90,605/year	$153,270/year
Payback period @ 0% interest	3.8 years	2.1 years
Payback period @ 10% interest	4.4 years	2.4 years
Reductions in CO_2 emissions	182435 kg/year (201.1 short-tons/year)	308443 kg/year (340 short-tons/year)
Reductions in NO_X emissions	823 kg/year (1,817 lb/year)	1395 kg/year (3,075 lb/year)
Reductions in HC emissions	94.2 kg/year (207.7 lb/year)	159.4 kg/year (351.4 lb/year)
Reductions in CO emissions	823 kg/year (1,817 lb/year)	1395 kg/year (3,075 lb/year)
Reductions in PM emissions	23.5 kg/year (51.9 lb/year)	40 kg/year (87.8 lb/year)

*107.2°C (225°F) is the highest hot water temperature for testing; 115.5°C (240°F) is the highest hot water temperatures allowed for the ORC system.

Table A.8 Estimated fuel savings for rural Alaska villages via applying 50kW ORC system

Community	Annual diesel power (MWh)	*Average diesel power (kW)	**JW Heat (kW)	***Exhaust Heat (kW)	JW Heat Available (80%) (kW)	Exhaust Heat Available (50%) (kW)	(Exhaust + JW Heat) Available (kW)	ORC Power from JW (7%) (kW)	ORC Power from (JW + Exhaust) (7.5%) (kW)
Gambell	1941	221.6	110.8	166.2	88.6	83.1	171.7	0.0	12.9
Noorvik	1768	201.8	100.9	151.4	80.7	75.7	156.4	0.0	11.7
Savoonga	1801	205.6	102.8	154.2	82.2	77.1	159.3	0.0	12.0
Selawik	2362	269.6	134.8	202.2	107.9	101.1	209.0	0.0	15.7
Shishmaref	1610	183.8	91.9	137.8	73.5	68.9	142.4	0.0	10.7
Deadhorse	25601	2922.5	1461.2	2191.9	1169.0	1095.9	2264.9	81.8	169.9
Kotzebue	20882	2383.8	1191.9	1787.8	953.5	893.9	1847.4	66.7	138.6
Snake River	27837	3177.7	1588.9	2383.3	1271.1	1191.7	2462.7	89.0	184.7
Anaktuvuk	3421	390.5	195.3	292.9	156.2	146.4	302.7	10.9	22.7
Atkasuk	3214	366.9	183.4	275.2	146.8	137.6	284.3	10.3	21.3
Kaktovik	1844	210.5	105.3	157.9	84.2	78.9	163.1	0.0	12.2
Nuiqsut	4665	532.5	266.3	399.4	213.0	199.7	412.7	14.9	31.0
Point Hope	2861	326.6	163.3	244.9	130.6	122.5	253.1	0.0	19.0
Point Lay	3504	400.0	200.0	300.0	160.0	150.0	310.0	11.2	23.3
Wainwright	2598	296.6	148.3	222.4	118.6	111.2	229.8	0.0	17.2
Unalakleet	4144	473.1	236.5	354.8	189.2	177.4	366.6	13.2	27.5
Glenallen	14613	1668.2	834.1	1251.1	667.3	625.6	1292.8	46.7	97.0
Orca	20795	2373.9	1186.9	1780.4	949.5	890.2	1839.7	66.5	138.0
Kodiak	41633	4752.6	2376.3	3564.5	1901.1	1782.2	3683.3	133.1	276.2
Hydaburg	1506	171.9	86.0	128.9	68.8	64.5	133.2	0.0	10.0
Gustavus	1648	188.1	94.1	141.1	75.3	70.5	145.8	0.0	10.9
SW Balley	7448	850.2	425.1	637.7	340.1	318.8	658.9	23.8	49.4
Hoonah	6338	723.5	361.8	542.6	289.4	271.3	560.7	20.3	42.1
Kake	4145	473.2	236.6	354.9	189.3	177.4	366.7	13.2	27.5
Angoon	1965	224.3	112.2	168.2	89.7	84.1	173.8	0.0	13.0
Yakutat	8378	956.4	478.2	717.3	382.6	358.6	741.2	26.8	55.6
Nunapitchuk	2353	268.6	134.3	201.5	107.4	100.7	208.2	0.0	15.6
Togiak	2428	277.2	138.6	207.9	110.9	103.9	214.8	0.0	16.1
Aniak	2585	295.1	147.5	221.3	118.0	110.7	228.7	0.0	17.2
Bethel	41254	4709.4	2354.7	3532.0	1883.7	1766.0	3649.8	131.9	273.7
Cold Bay	3248	370.8	185.4	278.1	148.3	139.0	287.4	10.4	21.6
Illamna	2300	262.6	131.3	196.9	105.0	98.5	203.5	0.0	15.3
King Cove	3283	374.8	187.4	281.1	149.9	140.5	290.4	10.5	21.8
Kipnuk	1638	187.0	93.5	140.2	74.8	70.1	144.9	0.0	10.9
McGrath	2837	323.9	161.9	242.9	129.5	121.4	251.0	0.0	18.8
Naknek	20118	2296.6	1148.3	1722.4	918.6	861.2	1779.8	64.3	133.5
Dillingham	17483	1995.8	997.9	1496.8	798.3	748.4	1546.7	55.9	116.0
Sand Point	3942	450.0	225.0	337.5	180.0	168.8	348.8	12.6	26.2

Table A.8 continued…

St. Paul	3932	448.9	224.4	336.6	179.5	168.3	347.9	12.6	26.1
Unalaska	29474	3364.6	1682.3	2523.5	1345.8	1261.7	2607.6	94.2	195.6
Northway	1557	177.7	88.9	133.3	71.1	66.7	137.7	5.0	10.3
Tok	11559	1319.5	659.8	989.6	527.8	494.8	1022.6	36.9	76.7
Alakanuk	1548	176.7	88.4	132.5	70.7	66.3	137.0	0.0	10.3
Chevak	1829	208.8	104.4	156.6	83.5	78.3	161.8	0.0	12.1
Emmonak	2383	272.0	136.0	204.0	108.8	102.0	210.8	0.0	15.8
Hooper Bay	2404	274.4	137.2	205.8	109.8	102.9	212.7	0.0	16.0
Mountain Village	2472	282.2	141.1	211.6	112.9	105.8	218.7	0.0	16.4
St. Mary	2886	329.5	164.7	247.1	131.8	123.5	255.3	0.0	19.1
Galena	9352	1067.6	533.8	800.7	427.0	400.3	827.4	29.9	62.1
Ft. Yukon	2400	274.0	137.0	205.5	109.6	102.7	212.3	0.0	15.9
Denali	2014	229.9	115.0	172.4	92.0	86.2	178.2	0.0	13.4
Total (kW)								**1092.6**	**2626.2**
Total Annual MWh								**9571.0**	**23005.9**
Annual Fuel Saving with (14kWh/Gal)								**2,587,859 lit (683,640gal)**	**6,220,495 lit (1,643,281gal)**

*Engine efficiency assumed to be 40% of fuel energy. **Jacket coolant heat assumed to be 20% of fuel energy. ***Exhaust heat assumed to be 30% of engine heat.

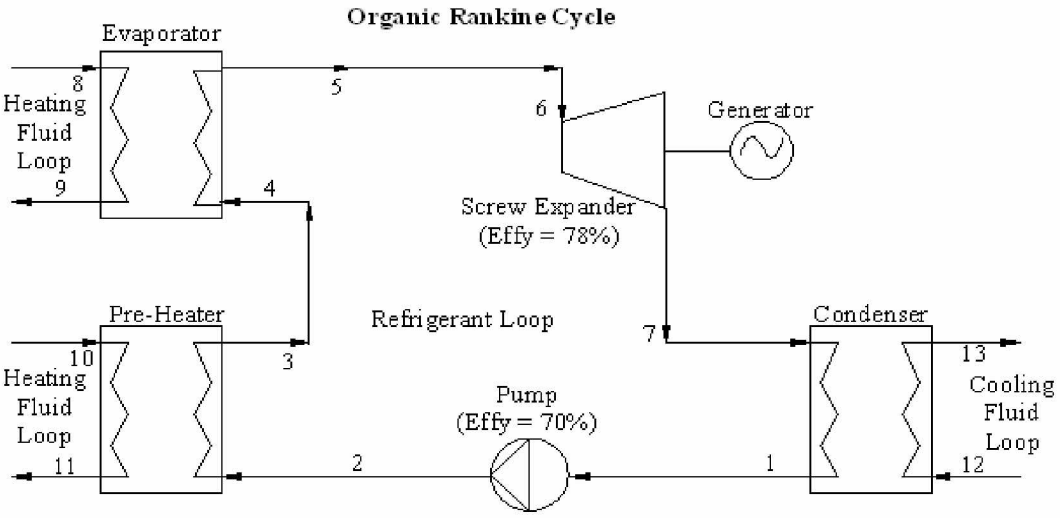

Figure A.1 ORC system line diagram

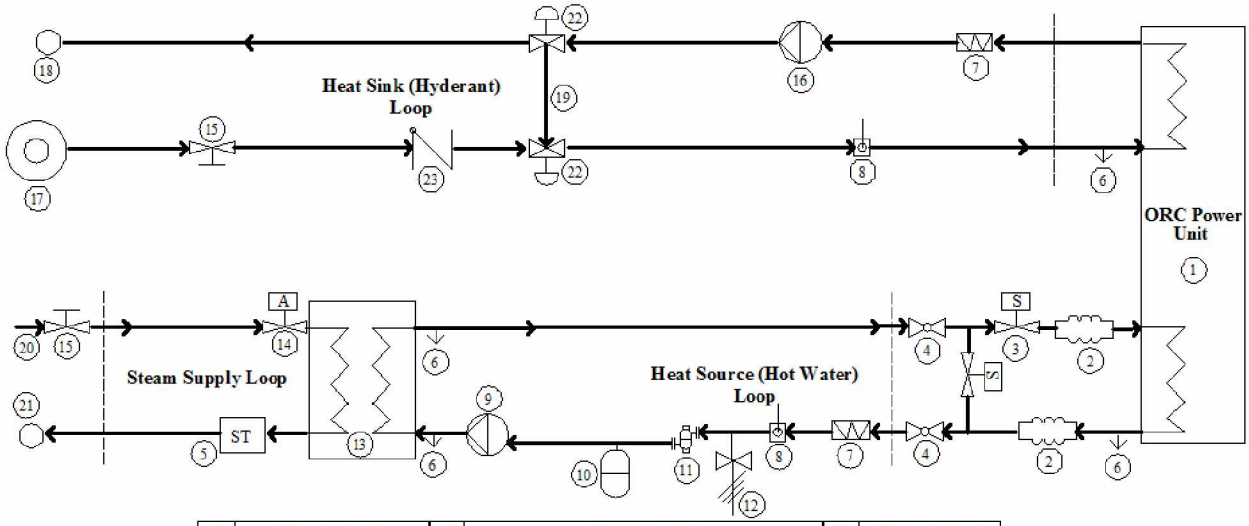

#	Component	#	Component	#	Component
1	ORC power unit	12	Pressure relief valve	23	Check valve
2	Expansions joints	13	Steam-to-hot water heat exchanger		
3	Solenoid valve	14	Steam control valve with actuator		
4	Ball valve	15	Manual control valve		
5	Steam trap	16	Pump (Constant flow rate)		
6	Drain	17	Hydrant source (Cooling water source)		
7	Temperature mixer	18	Cooling water from GM (Hydrant sink)		
8	Ultrasonic flow meter	19	By-pass for temperature control on coolant side		
9	VFD Pump	20	Steam inlet		
10	Expansion tank	21	Steam condensate outlet		
11	Rolairtrol air separator	22	3-way butterfly valve with actuator		

Figure A.2 Design line diagram of the testing system

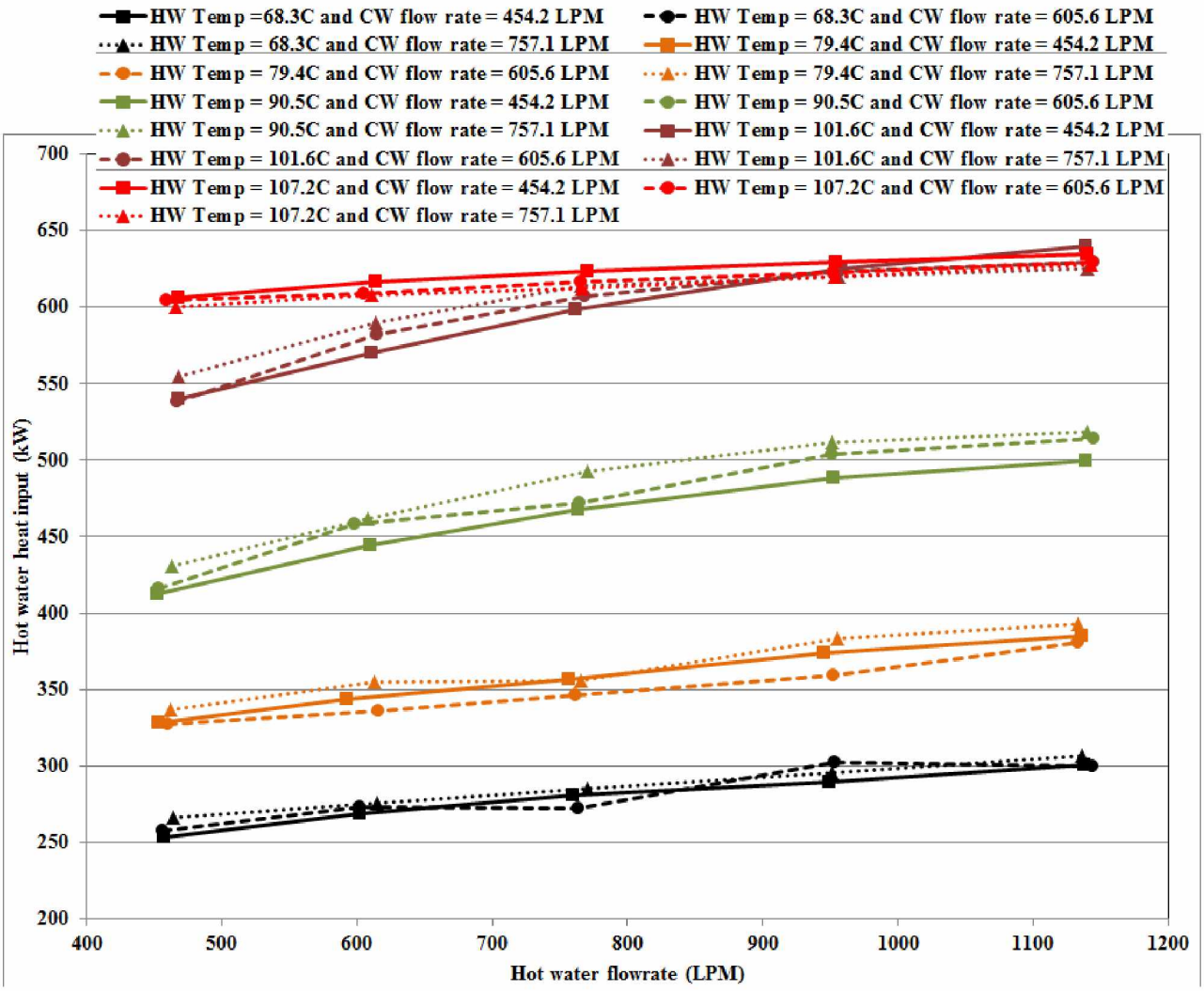

Figure A.3 Heat input to power unit evaporator vs. hot water flow rates at different hot water supply temperatures and cold water flow rates (10°C (50°F) cold water temperature)

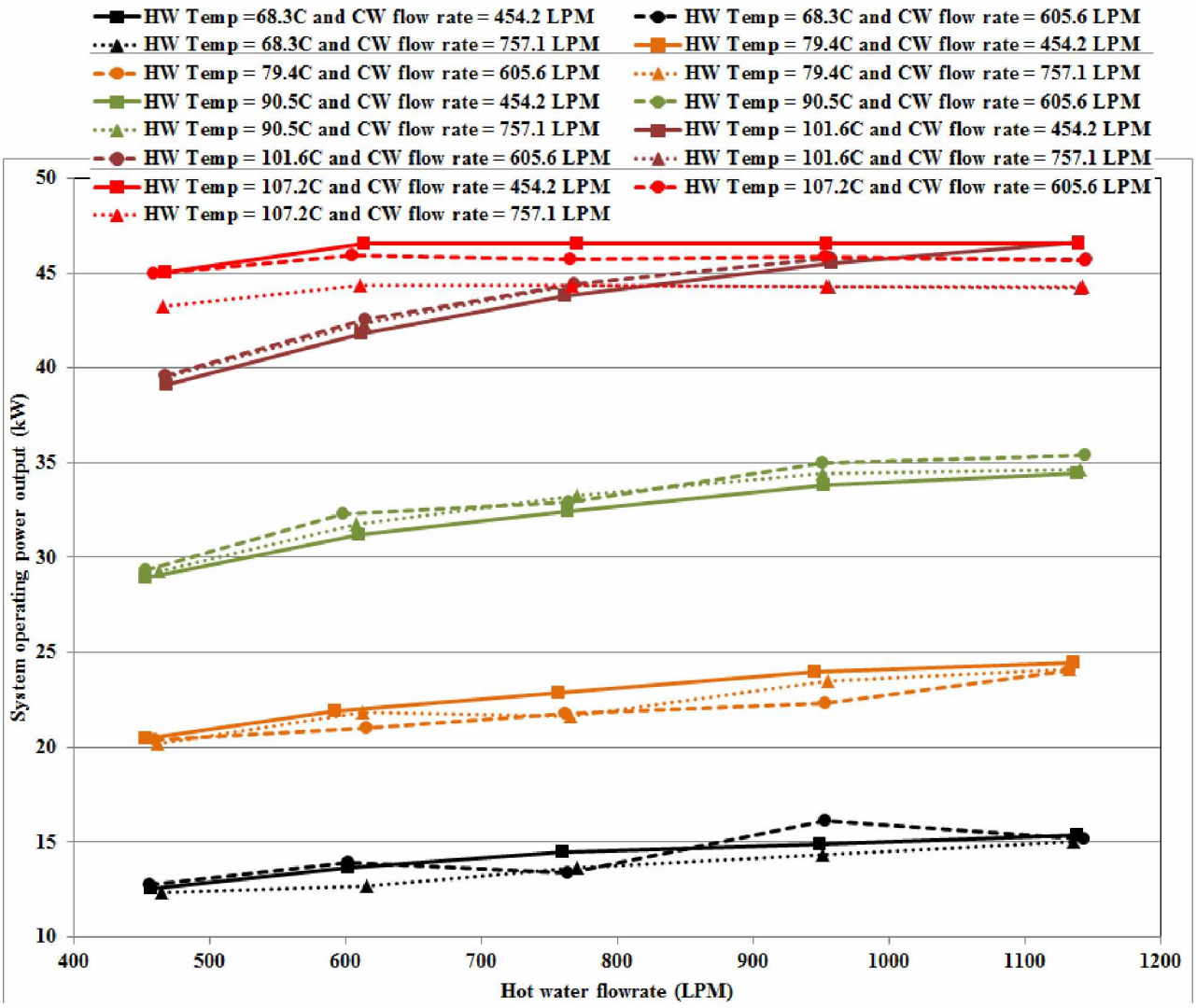

Figure A.4 System operating power output vs. hot water flow rates at different hot water supply temperatures and cold water flow rates (10°C (50°F) cold water supply temperature)

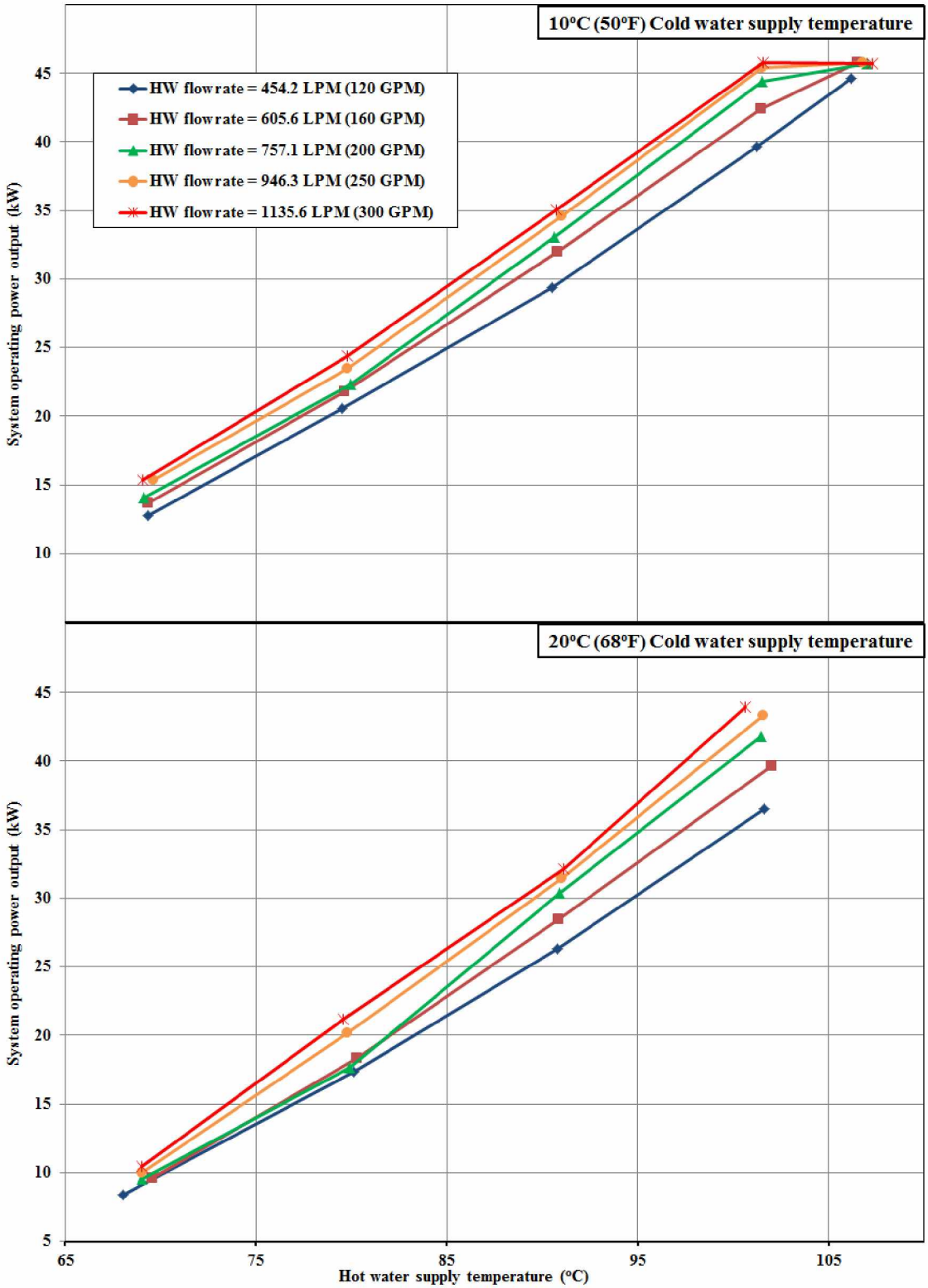

Figure A.5 System operating power output vs. hot water supply temperature (Neglect the effect of cooling water flow rate)

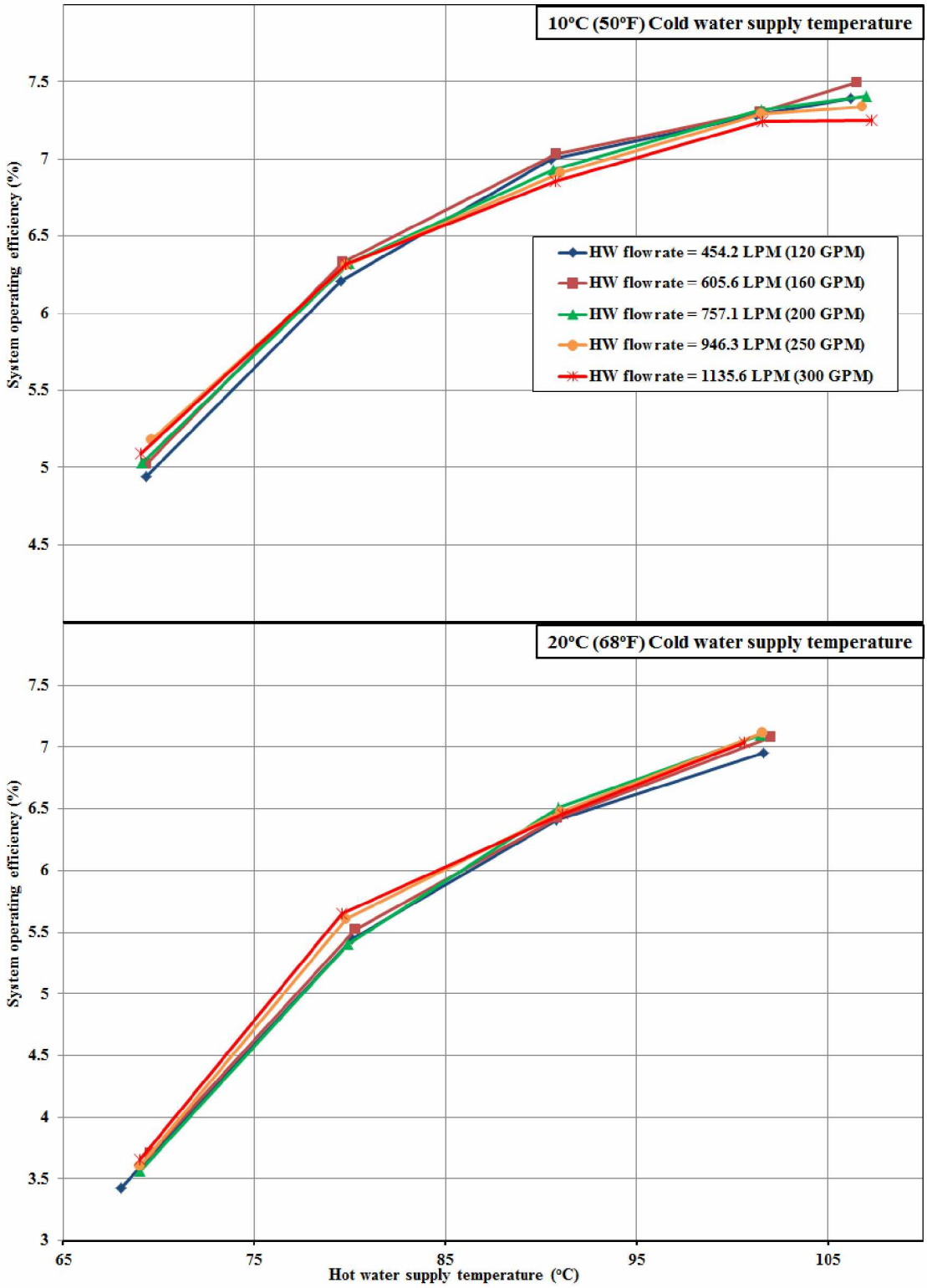

Figure A.6 System operating efficiency vs. hot water supply temperature

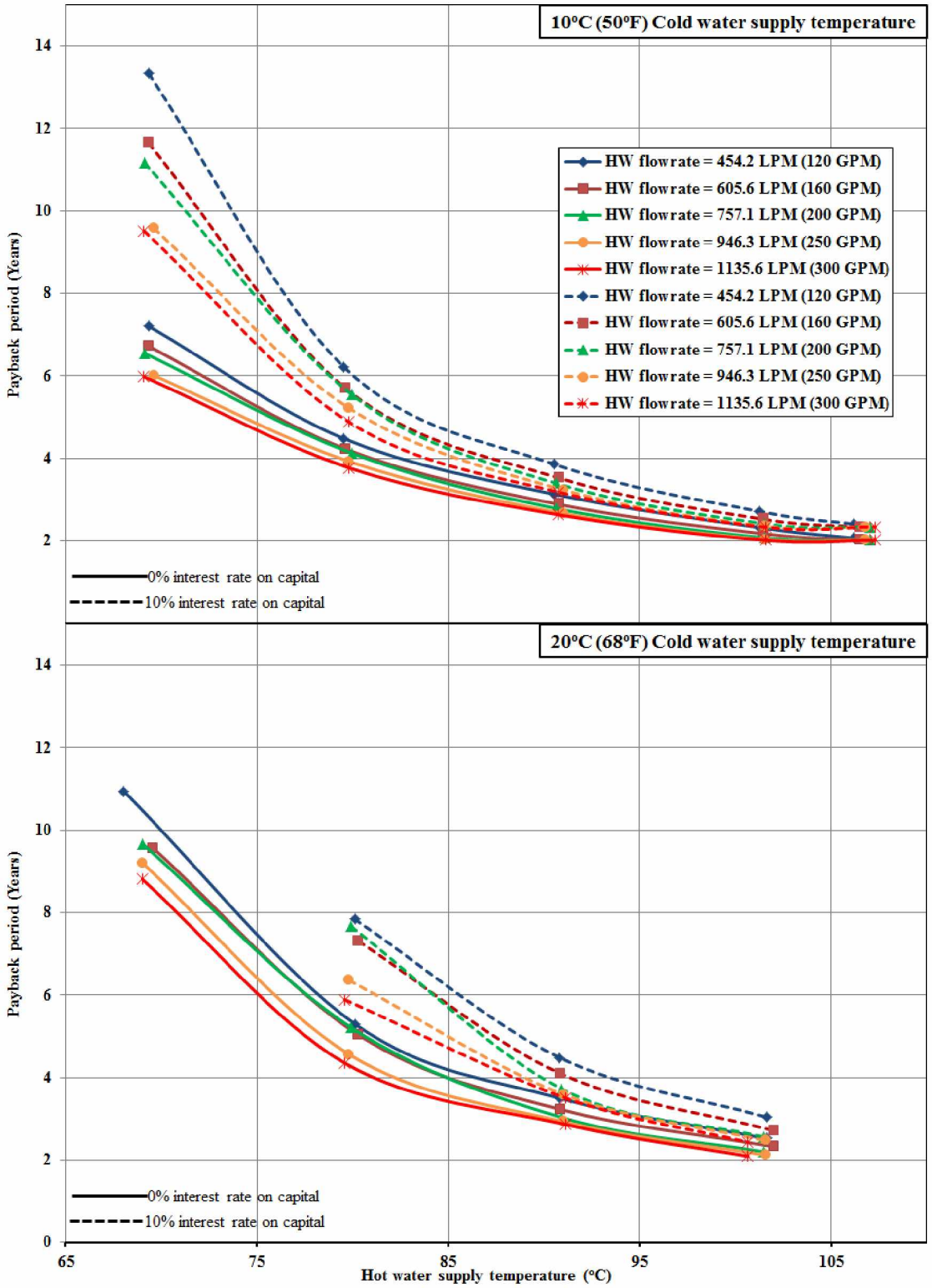

Figure A.7 Payback period vs. hot water supply temperature

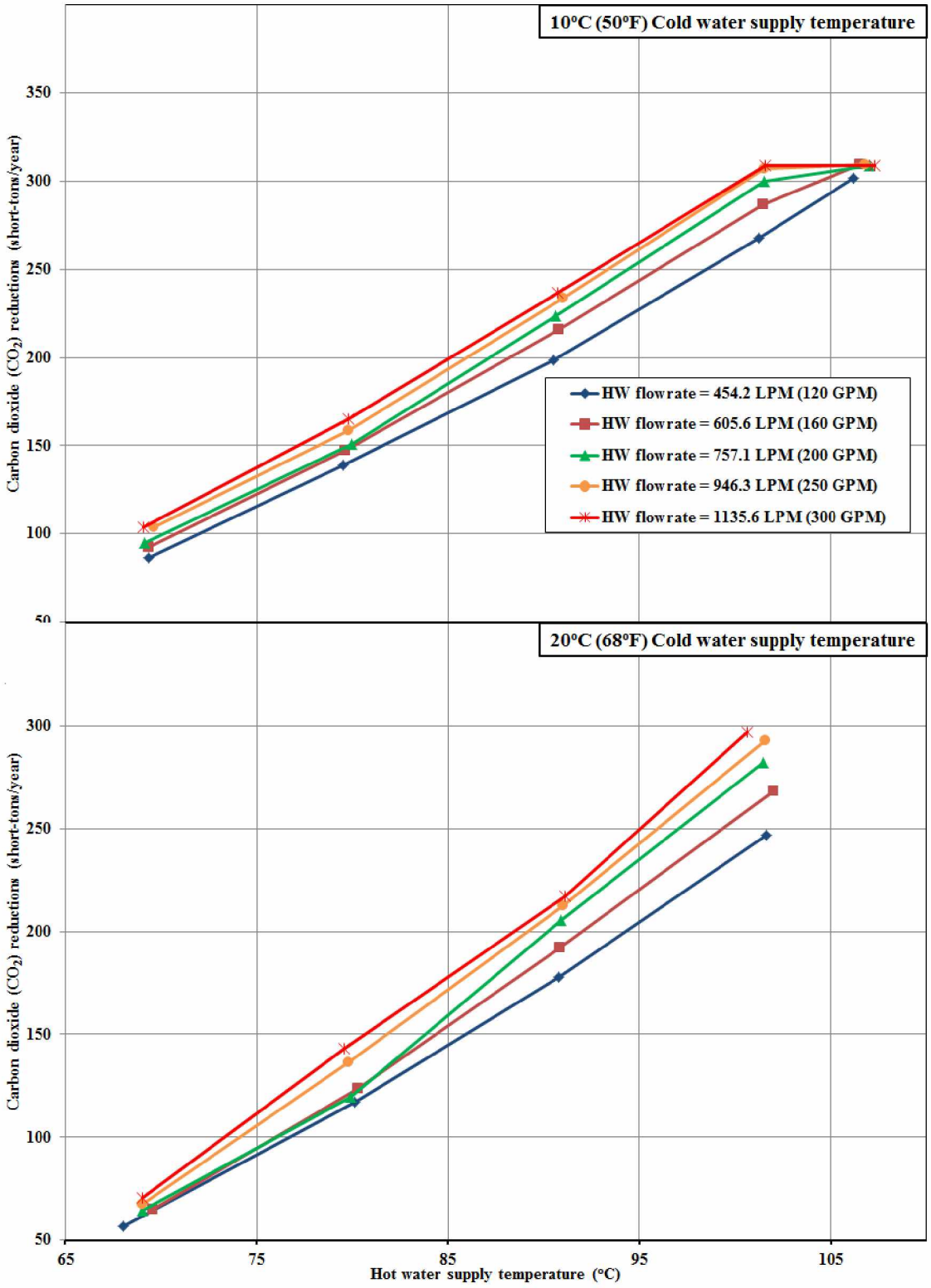

Figure A.8 CO_2 reduction vs. hot water supply temperature

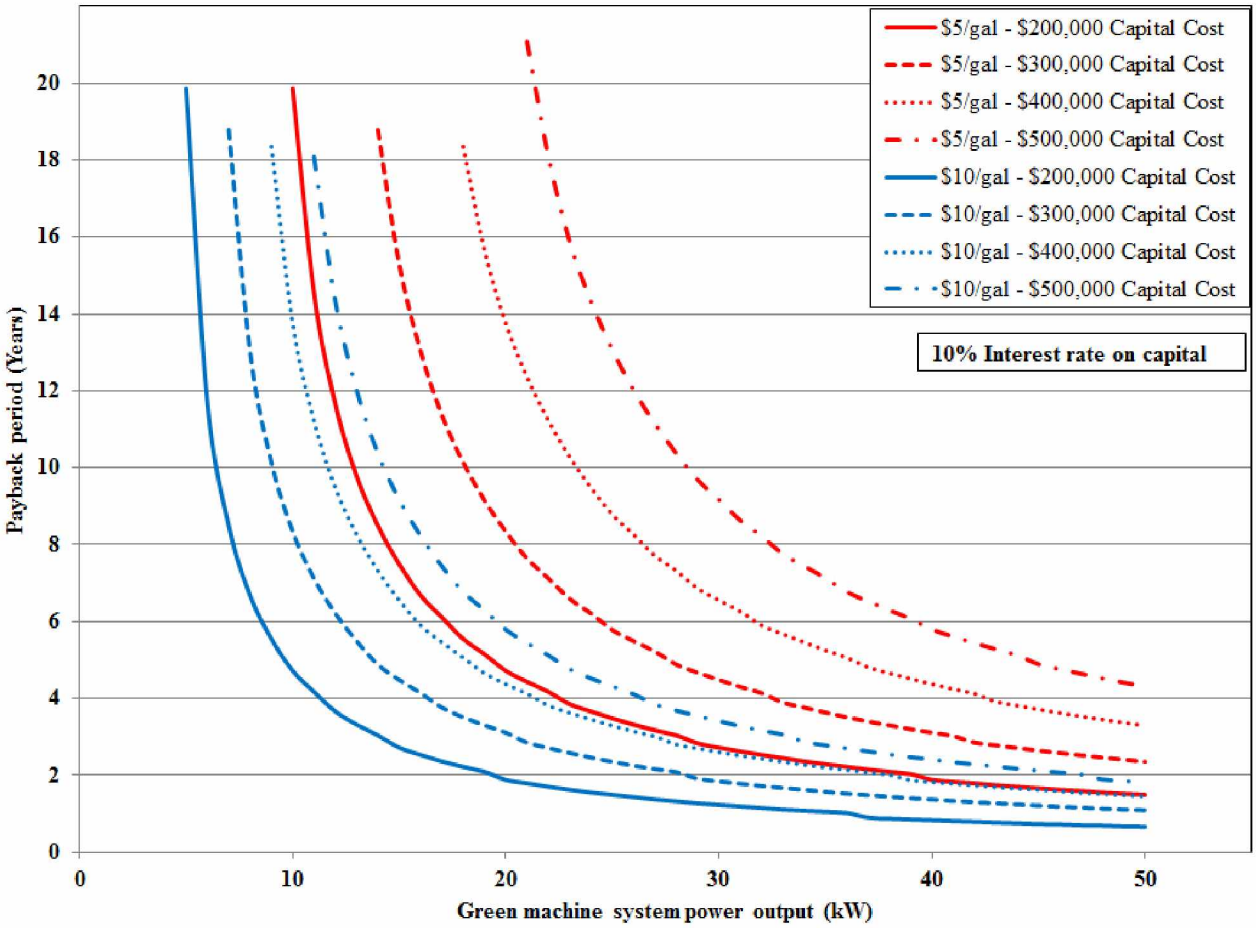

Figure A.9 Payback period at 10% interest rate on capital for different ORC power output, fuel pieces, and capital costs